A Novel Blend, CARSOXY, as a Working Fluid for Advanced Gas Turbine Cycles

By

ALI IBRAHEEM MOHAMMED AL-DOBOON

B.Sc. Mechanical Eng. & M.Sc. Mechanical Eng.

A thesis submitted to Cardiff University in Fulfilment of Requirements for the Degree of Doctor of Philosophy in Mechanical Engineering

CARDIFF UNIVERSITY
SCHOOL OF ENGINEERING
Cardiff, United Kingdom

January 2019

DECLARATION

This work has not been submitted in substance for any other degree or award at this or any other university or place of learning, nor is being submitted concurrently in candidature for any degree or other award.

Signed …… (candidate) Date…….03/01/2019……

STATEMENT 1

This thesis is being submitted in partial fulfilment of the requirements for the degree of PhD.

Signed …… (candidate) Date…….03/01/2019……

STATEMENT 2

This thesis is the result of my own independent work/investigation, except where otherwise stated, and the thesis has not been edited by a third party beyond what is permitted by Cardiff University's Policy on the Use of Third Party Editors by Research Degree Students. Other sources are acknowledged by explicit references. The views expressed are my own.

Signed …… (candidate) Date…….03/01/2019……

STATEMENT 3

I hereby give consent for my thesis, if accepted, to be available online in the University's Open Access repository and for inter-library loan, and for the title and summary to be made available to outside organisations.

Signed …… (candidate) Date…….03/01/2019……

STATEMENT 4: PREVIOUSLY APPROVED BAR ON ACCESS

I hereby give consent for my thesis, if accepted, to be available online in the University's Open Access repository and for inter-library loans **after expiry of a bar on access previously approved by the Academic Standards & Quality Committee.**

Signed …… (candidate) Date…….03/01/2019……

“*The more I study science the more I believe in God.*”

Albert Einstein

“*Science knows no country, because knowledge belongs to humanity, and is the torch which illuminates the world.*”

Louis Pasteur

ACKNOWLEDGEMENTS

*First and foremost, I would like to praise and thank **GOD** for helping me to complete this thesis.*

*I would like to express a great debt of gratitude to my supervisors, **Professor Philip J Bowen and Doctor Agustin Valera-Medina** for their guidance, immense support and patience throughout my studies and for providing endless answers to questions. I would like to thank **Professor Nick Syred, Dr Richard March** and all the **Combustion Research Group** for supporting this study.*

*I also would like to thank the whole staff of the School of Engineering. Special recognition to all technicians in the Mechanical Engineering Workshop for their support with my experimental work. My sincere thanks to **Mr Malcolm Seaborne**, whose technical knowledge helped in the successful completion of the experimental stage of the study. My deepest appreciation for those whom I always remember **(Gina Goddard, Chris Lee, Jeanette Whyte and Aderyn Reid)**. I extend my thanks as well to my colleagues for their assistance and support.*

*Exceptional thanks to my sweetest half, my lovely wife **Mayada,** for her endless love and support; without you I could not have achieved this work. Special thanks to my fabulous sons **Alhussein** and **Mohammed** for being my two amazing angels who help me to overcome the hardest times in my studies. I hope I will be the husband and father that you will always be proud of.*

*Finally, I would like to dedicate this work to my late **mother** and **father**, without whom I could not be the person that I am today.*

ABSTRACT

Fossil-fuel-fired gas turbines continue to be the most reliable and cost-effective power production method. Turbines running with natural gas are considered to be one of the cleanest fossil-fuel-based engines in terms of carbon emissions. Nevertheless, CO_2 and other pollutants emitted from this type of power generation contribute to global environmental deterioration. This has led to the development of innovative and efficient approaches to producing energy through fossil fuels. The main challenge when implementing these new technologies is providing the equivalent performance to current systems running with conventional methods while reducing harmful emissions.

Carbon Capture and Storage (CCS), Oxyfuel (OF) combustion, humidified gas turbines and closed cycles running with inert gases are the most well-known of these technologies. The novel approach proposed in this study is to combine the above methods to attempt to produce a gas blend consisting of Co_2, ARgon, Steam and OXYfuel (CARSOXY) that could replace conventional air as a working fluid.

This study employs theoretical methods, which include Gaseq, Minitab and Chemkin-Pro, to identify the optimum novel blend. Then, a bespoke numerical simulation test of the feasibility of running the novel blend in a real industrial gas turbine is conducted. The performance of the proposed cycle is also numerically examined using Aspen Plus. A central diffusive burner is utilised for experiments to demonstrate the applicability of the optimum blend in industrial gas combustors.

Findings indicate that CARSOXY could be used as a realistic replacement for air as a working fluid in gas combustors because it has similar characteristics and produces higher efficiency while eliminating NO_x and recycling CO_2 in the combustion process. From a practical point of view, the combustion process when running the proposed blend is shown to be more stable than when running air, with lower emission levels.

Table of Contents

Index of Figures

Index of Tables

Nomenclature

Symbol	Definition	Unit
D_1	Density of the gas at the working conditions	kg/m^3
D_2	Density of a blend	kg/m^3
c_p	Specific heat at constant pressure	kJ/kg.K
$\bar{c}_{p\ air\ (1-2)}$	Averaged value of air specific heat through compression	kJ/kg.K
$\bar{c}_{p\ gas-air\ (3-4)}$	Averaged value of gas specific heat through expansion	kJ/kg.K
G	Gibbs free energy	J
G_i^o	Molar free energy at atmospheric pressure	-
h_{fuel}	Specific enthalpy of fuel at combustion chamber inlet	kJ/kg
L_c	Specific work of compression	kJ/kg
LHV	Lower heating value	kJ/kg
L_T	Gas turbine specific work	kJ/kg
M	Cooling air distribution factor	-
$\dot{m}_{fuel}$	Fuel mass flow rate	kg/s
$\dot{m}_2$	Air mass flow rate	kg/sec
nSp	Species n	-
p	Pressure	Pa
q_{in}	Amount of input heat	kJ/kg
q_{v1}	Volume flow rate of the gas at the working conditions	m^3/sec
q_{v2}	Volume flow rate of a blend	m^3/sec
R	Universal gas constant	J/mole. K

r_{air}	Cooling air mass flow and compressor inlet mass flow ratio	-
T	Temperature	K
T_0	Ambient temperature	K
T_1	Inlet compressor temperature	K
T_2	Outlet compressor temperature	K
T_{3t}	Inlet turbine temperature	K
x_i	Equilibrium number of moles of species i	-
ϕ	Equivalence ratio	-
η_{CC}	Efficiency of a combustion chamber	-
η_{GT}	Gas turbine plant efficiency	-
η_m	Mechanical efficiency	-
η_{pC}	Polytropic efficiency of a compressor	-
η_{pT}	Polytropic efficiency of a turbine	-
Π_C	Compressor pressure ratio	-
Π_T	Turbine pressure ratio	-
η	Cycle efficiency	-
FAR	Fuel-air ratio	-
$\Delta H_{Reaction,25^0C}$	Standard enthalpy change of the combustion reaction	kJ/kg
$\Delta H_{products}$	Enthalpy of products	kJ/kg
$\Delta H_{reactant}$	Enthalpy of reactants	kJ/kg
H_u	Net heating value	kJ/kg

CHAPTER ONE

Chapter 1 Introduction

This chapter examines the background to the environmental problems connected with energy generation. It looks at attempts to address these issues and introduces this study's initial focus on an oxyfuel-based approach in regard to this area.

First, the background of energy dependence and generation is provided. Then, the development of renewable energy and the current widespread use of fossil fuels are described. The necessity for gas turbines running with natural gas as a main means of meeting current electricity demand is then discussed, along with the environmental problems created by gas turbine emissions.

Next, the potential pathways to decarbonising power production are considered, leading to the introduction of the concept of oxy-combustion and Carbon Capture and Storage (CCS) technology. A summary of the chapter's main ideas is then given. Finally, the structure of this thesis is outlined and related published output is detailed.

1.1 Energy dependence

The prosperity of modern societies and communities is considered to be one of the major drivers of growth in energy demand, especially from the perspective of social accomplishment and economic development. In the earliest civilisations, either human or animal muscle power was used, representing a simple form of energy to perform mechanical work. Thermal energy was also needed for the onset of sedentary domestication and the source of this type of energy was burning biomass fuel.

In pre-industrial societies, available forms of energy stayed at minimal and stable levels of consumption for many centuries. In contrast, the twentieth century was connected with a significant rise in total energy demand in comparison with the entire preceding millennium.

The great expansion in global population from 1900 to 2000, when it increased approximately six-fold, was the reason for this dramatic increase in energy use. In addition, the evolution of the technology of modern society, such as that used for electricity generation, industrial, residential, and transportation purposes, has been an essential driver of increased energy consumption [1].

The results of the 2015 World Population Prospects Revision indicate that the world's population will continue to grow and will reach around 10 billion by the middle of the twenty-first century [2]. Additionally, according to the International Energy Outlook 2016 (IEO 2016) projection, the global demand for energy will increase by 48% from 2012 to 2040. Figure 1.1 shows world energy consumption in quadrillion British thermal units (Btu) from 1990 to 2040. This energy is consumed by both the Organisation for Economic and Cooperation Development (OECD) countries and non-OECD countries. In terms of energy consumed, electricity has experienced the fastest-growing global demand for decades [3].

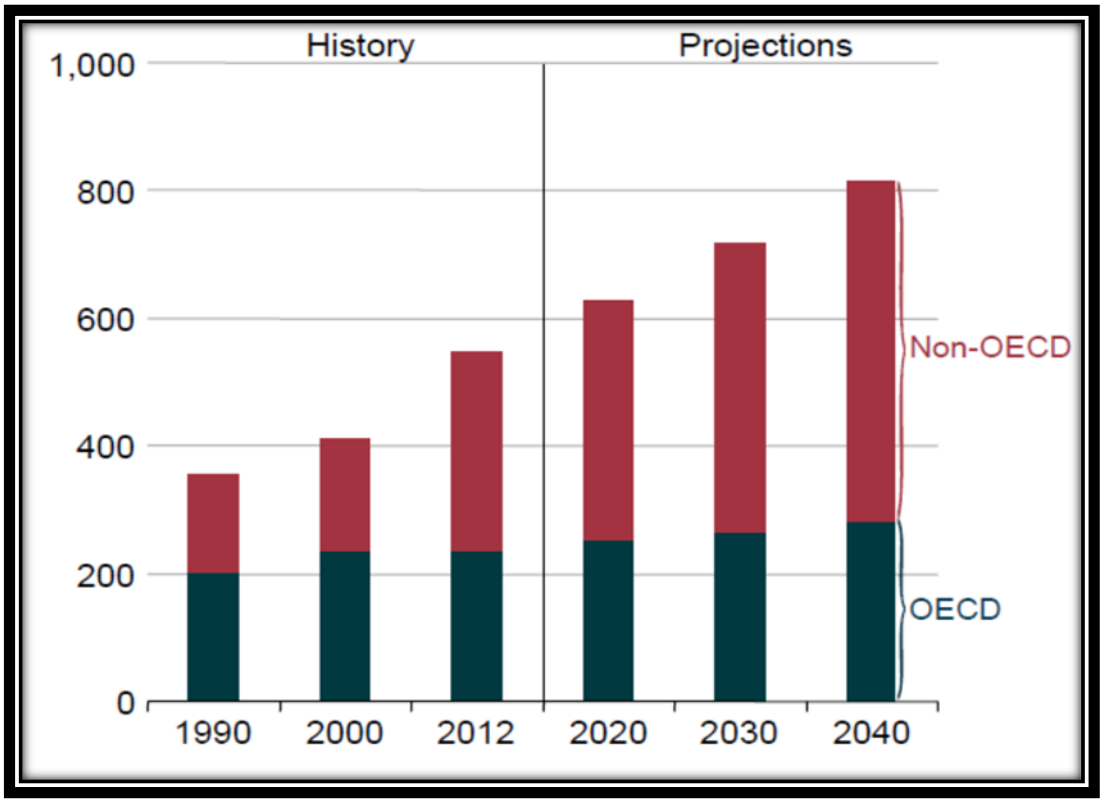

Figure 1.1 Global energy consumption [3]

1.2 Electricity generation

Economic growth, as measured by gross domestic product in modern social communities, is underpinned by the reliability and cost-effectiveness of the electrical power generation sector [4, 5]. Approximately 70% of generated electricity is consumed by three main categories of consumer, which are: industrial, residential and lighting services, as shown in Figure 1.2 [6].

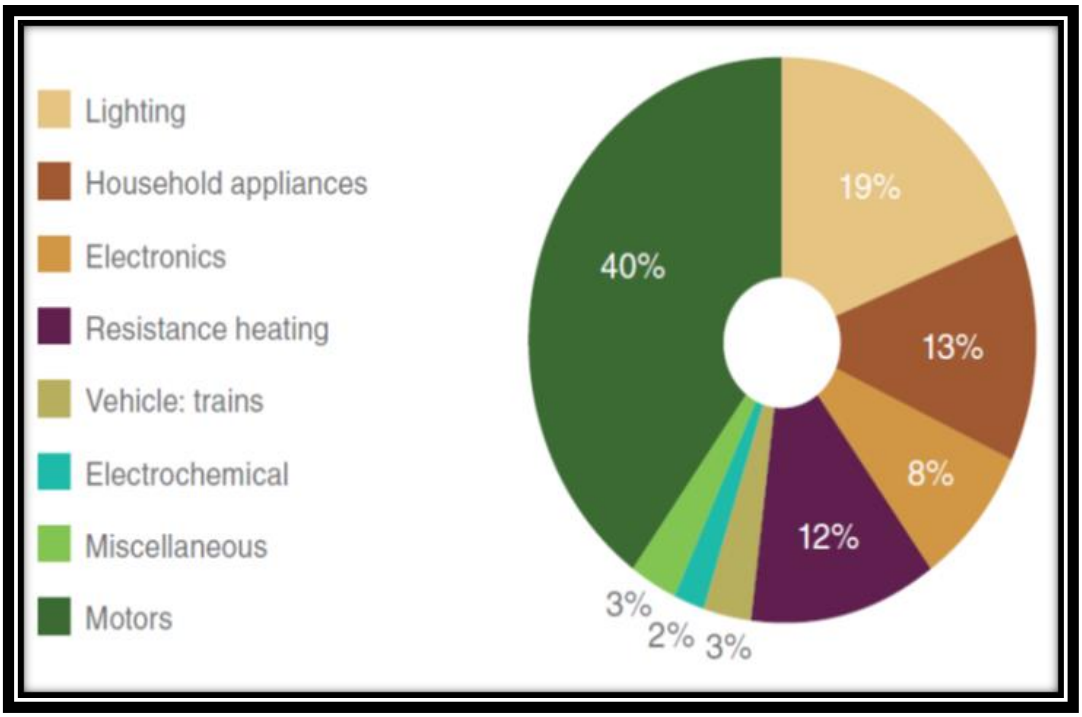

Figure 1.2 Global electricity demand by sector [6]

Global electricity generation is projected to increase by 69% between 2012 and 2040. Figure 1.3 shows the growing generation of electricity using a range of resources over this period [3, 7]. Although many different technologies can be used to generate electricity from various sources, they can be classified into two main categories: renewable and non-renewable energy.

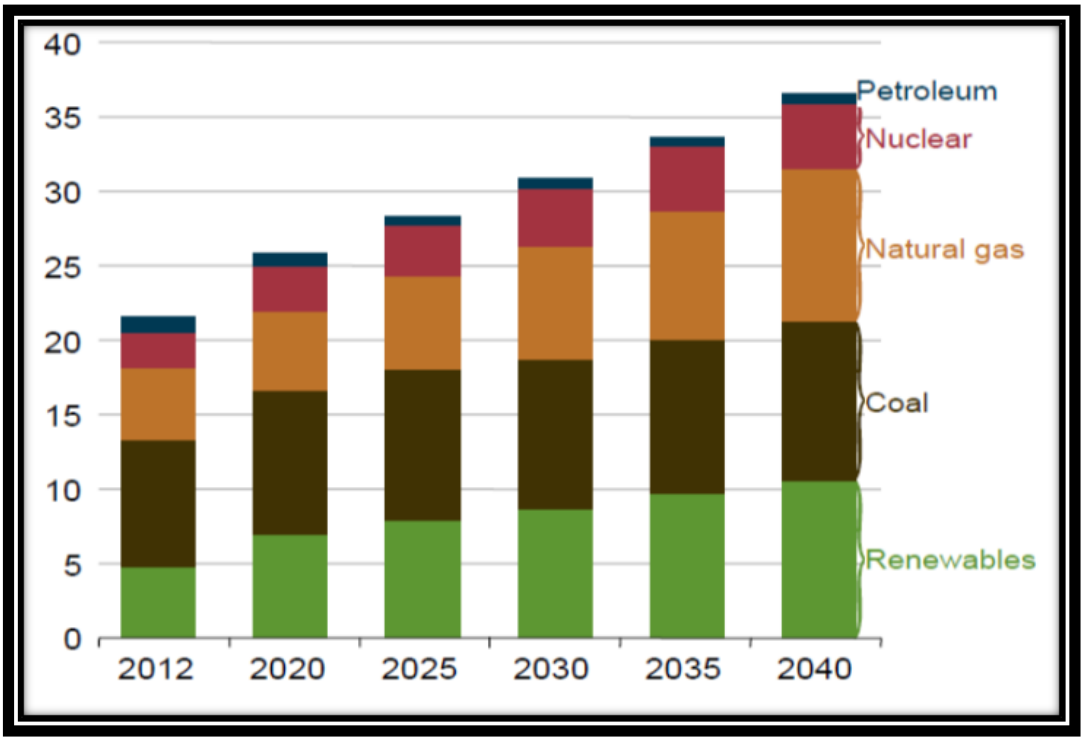

Figure 1.3 World net electricity generation by resources 2012–2040 (in trillion kilowatt-hours) [3]

1.3 Renewable energy

Renewable energy is a term that is used to describe energy obtained from natural and sustainable sources that can be replenished in a human lifetime. The most abundant and permanent sources of renewable energy originate from the sun. Solar energy is obtained directly from this sustainable source of energy.

Other sources, such as wind, tidal, hydropower and biomass, are indirectly derived from the sun. All of these renewable energy resources provide clean and environmentally-friendly energy, with a 16% share of global energy consumption, as shown in Figure 1.4 [6, 8]. Thermal solar energy uses invisible infrared radiation emitted by the sun to heat a working fluid, such as air and water.

This technology is considered to be a simple technique compared with other complicated approaches, such as the photovoltaic model using solar radiation as a source of light to

produce electricity [9]. These methods represent energy resources derived directly from the sun. However, the following sources of power are also indirectly obtained from solar radiation:

The wind is air in motion caused by a rise in air pressure gradient. This differential in air pressure is created by a temperature difference above land and water due to solar radiation [10]. Tidal energy uses the regular rise and fall of sea levels, known as tides, which occur due to the effect of gravitational forces exerted by the moon and the sun on the earth's surface. The moon's force has a greater impact on the earth than the sun's force because the former is closer to the earth than the latter [11].

Hydropower is also known as hydroelectric power and it harnesses the energy in falling water streams into useful power, which is then utilised to spin a turbine to generate electricity. The falling water is either diverted naturally from a waterfall or it is caused by constructing a dam to provide the height of water level that is needed to create the required driving force [12].

Biomass is an organic material that can be obtained from either living or recently living plant matter, such as wood or crops. The heat required for electricity generation can be directly produced by burning these biological materials. Gasification, which is one of the new technologies, uses heat and air to convert biomass material to generate a synthetic gas (syngas) which consists of carbon monoxide, hydrogen and methane.

Therefore, the gasification process can be considered as one of the renewable energy sources that can be used to generate syngas that could be used instead of natural gas in power plants [8].

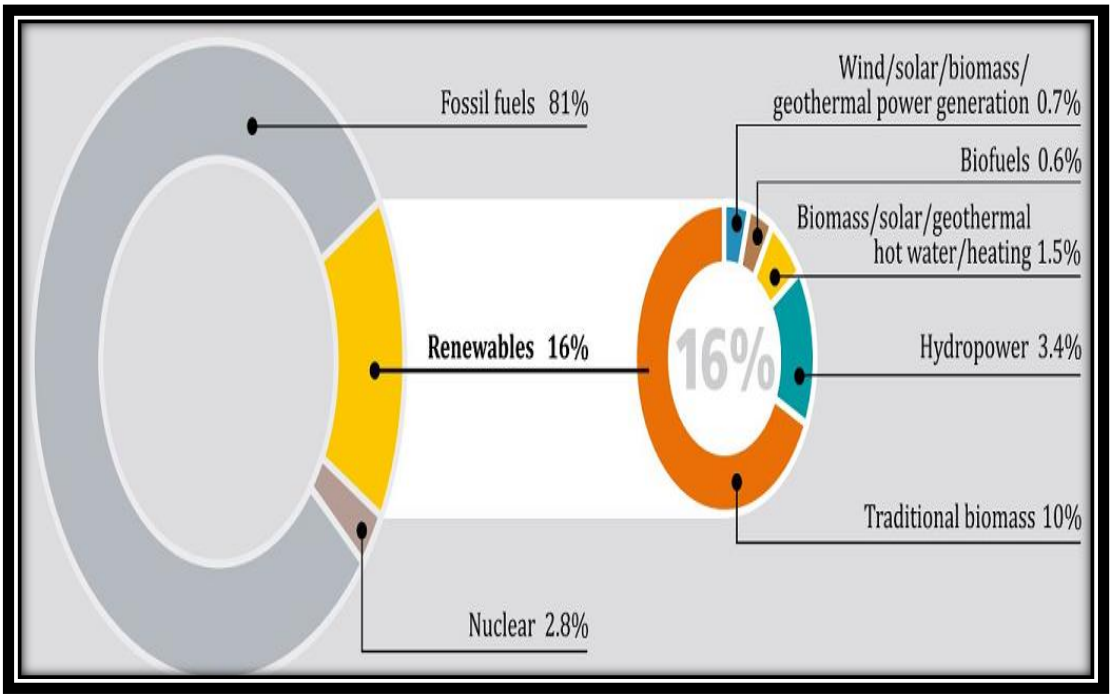

Figure 1.4 Renewable energy share of world energy demand, 2009 [13]

The availability of non-depletable environmentally-friendly energy resources can be used to provide clean and sustainable electricity. However, the main challenges facing renewable energy technologies are their high initial cost, low efficiency and intermittency. These drawbacks are considered to be some of the reasons why all combined renewable energy resources are projected to make up only around 30% of world net electricity generated in 2040, which is almost the same percentage that natural gas (NG) is predicted to provide [3, 13].

1.4 **Fossil fuels**

The term non-renewable refers to the energy that comes from the decomposition of buried ancient organisms and plants. Fossil fuels are a product of this decomposition process.

Hydrocarbons are derived from NG, fuel oil and coal, which are the main products of fossilisation. Fossil fuels are ultimately finite, which means that they are depletable and cannot be replenished in a human lifetime. Fossil fuels are still major energy resources and

the electrical generation sector is reliant on them, with a share of approximately 68% of global electricity generation in 2010 compared to other energy resources; as shown in Figure 1.5 [13, 14].

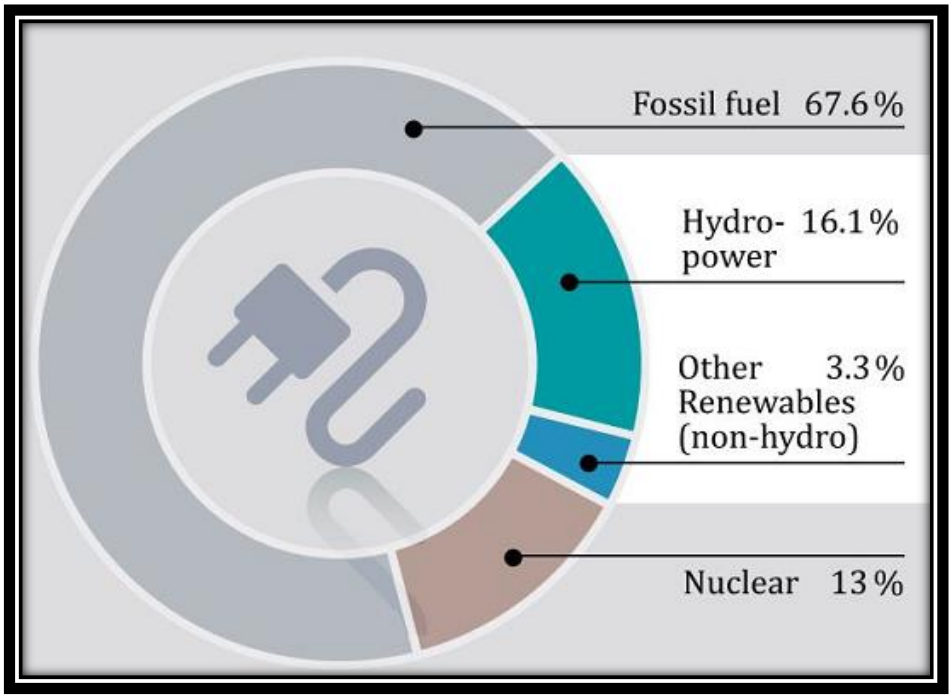

Figure 1.5 Renewable energy share of world energy demand, 2010 [13]

Nevertheless, fossil fuels are the largest source of CO_2 emissions and, in comparison with other energy resources, they have a negative impact on the environment. However, NG has a lower carbon content and is often considered to be the cleanest fossil-based fuel [15].

1.4.1 **Natural gas**

NG is a fossilised product that consists mainly of methane, with a mixture of gases comprising the remaining percentage [16, 17], as shown in Table 1.1

Table 1.1 Chemical composition of NG [17]

Chemical component	Typical analysis (vol%)	Range (vol%)
Methane	94.9	87.0-96.0
Ethane	2.5	1.8-5.1
Propane	0.2	0.1-1.5
Isobutane	0.03	0.01-0.3
n-Butane	0.03	0.01-0.3
Isopentane	0.01	Trace up to 0.14
n-Pentane	0.01	Trace up to 0.14
Hexane	0.01	Trace up to 0.06
Nitrogen	1.6	1.3-5.6
Carbone dioxide	0.7	0.1-1.0
Oxygen	0.02	0.01-0.1
Hydrogen sulphide	Trace	Trace up to 0.02

NG production requires several different techniques depending on its resource type and characteristics. Figure 1.6 demonstrates the distribution of NG resources depending on their size, location, ease of extraction and cost, showing that higher quality NG reservoirs provide reliable, less effort-intensive, cheaper and higher concentrations [18]. NG-fired gas turbine stations are now being employed more widely than other types of turbines due to their availability, feasibility and the versatility of their capacity.

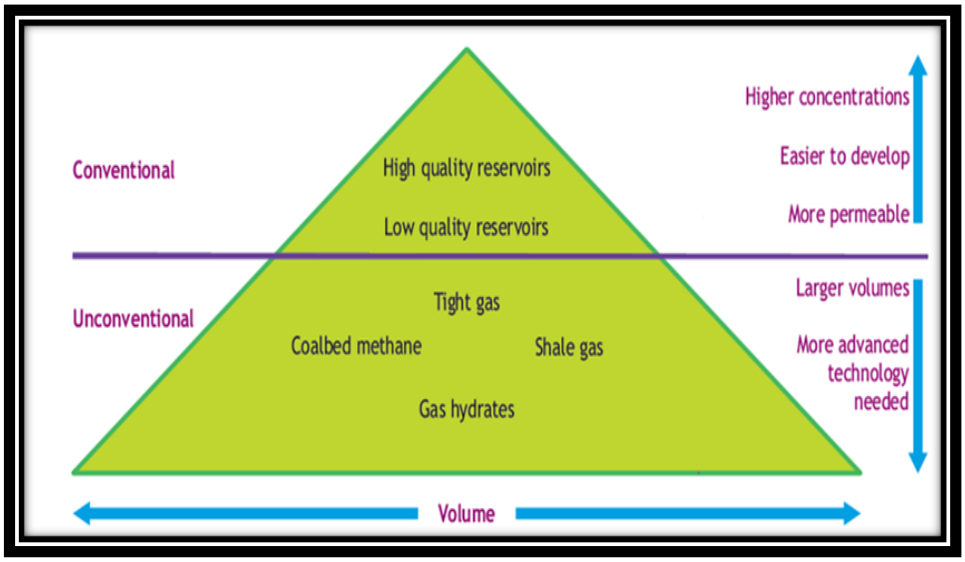

Figure 1.6 Typology of NG resources [18]

These turbines are also able to be combined with more than one system, leading to improved gross efficiency, lower costs, shorter-term installation and longer-term NG supply [19]. Thus, reliance on NG fuels is projected to increase to cover more than 60% of all new demand for electricity generation between 2025–2040. Moreover, NG is predicted to satisfy 31% of all electricity demand by 2040, as shown in Figure 1.7 [20].

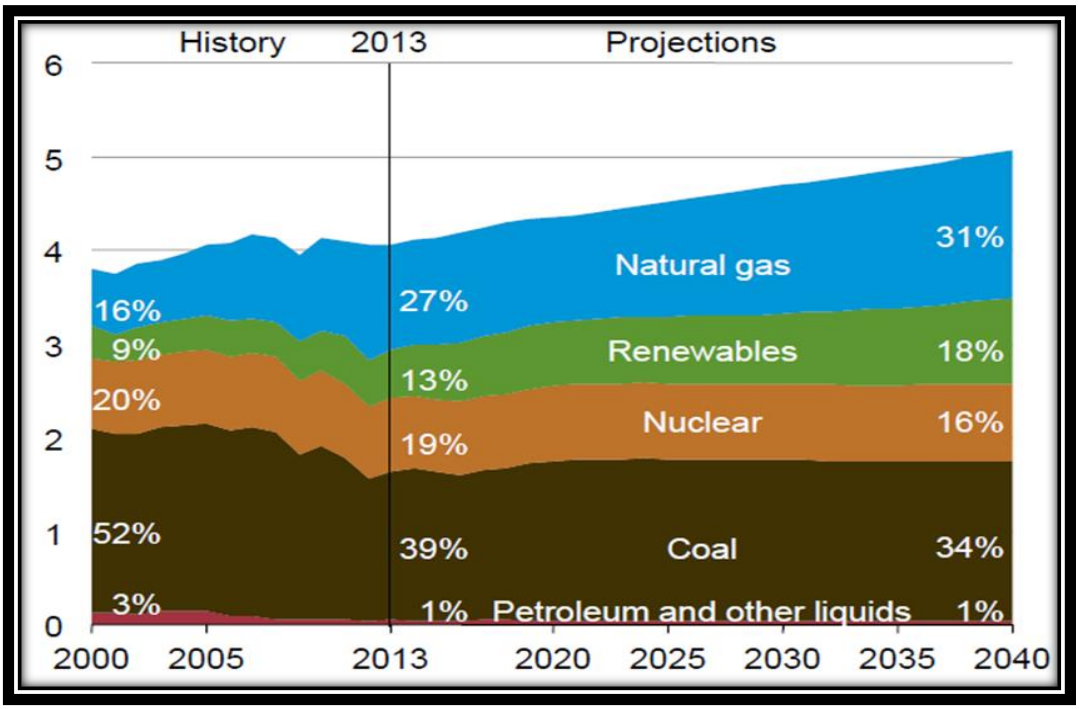

Figure 1.7 Electricity generation by fuel, over four decades (in trillion kilowatt-hours) [20]

1.5 Gas turbines

Turbine is a Latin term that describes a spinning machine that converts fluid which flows through blades attached to a rotor into rotational work. Although the steam turbine was first defined in 150 BC, the modern gas turbine was pioneered by John Barbar in 1790. The combined model of a gas turbine, which includes an axial compressor driven by an axial turbine and a built-in combustion chamber with a regeneration unit to reheat the recovery system, was first built in 1900 [21, 22].

The principles of the gas turbine are similar for both the land stationary type, as used by power plants, and the thrust type, as used for aircraft engines. A major difference between these configurations is the use of a reciprocating compressor in the land stationary type, which is able to provide the high power needed for electricity generation, as shown in Figure 1.8 [23]. Meanwhile, a centrifugal compressor is used in aircraft engines to provide mass and acceleration.

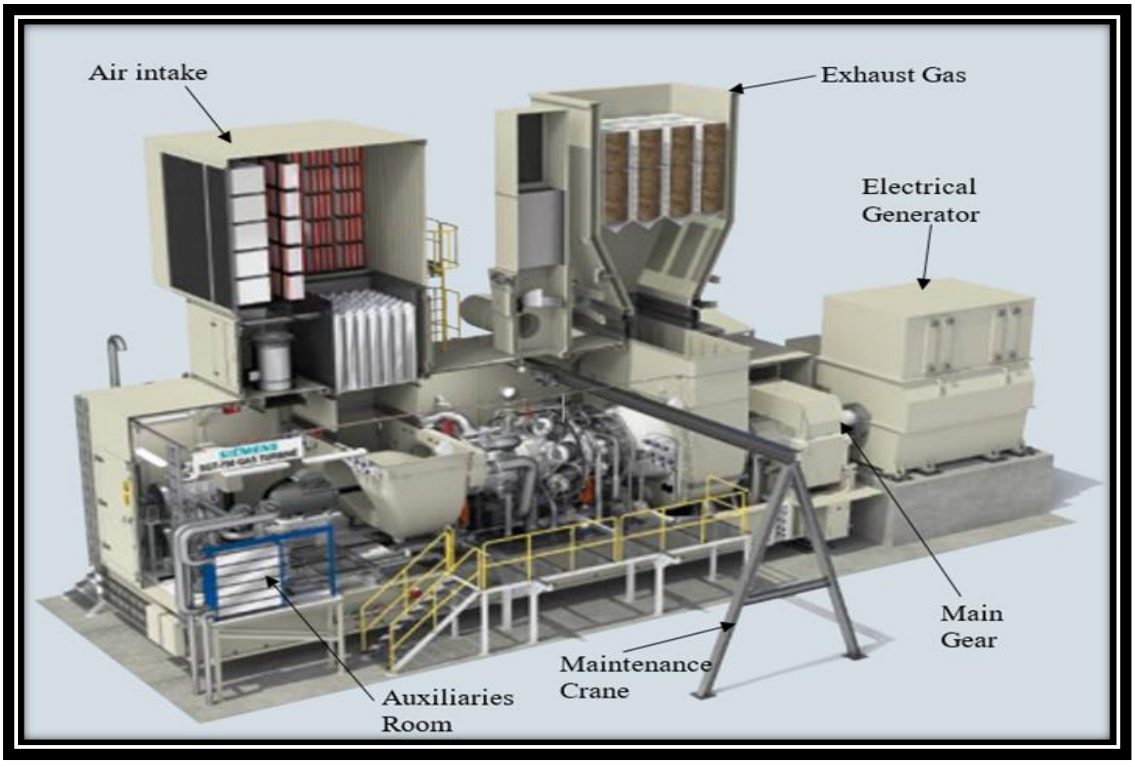

Figure 1.8 Siemens 37 MWe STG-750 gas turbine [24]

Figure 1.9 demonstrates an aero engine, where intake air is compressed by the spinning of blades attached to the shaft of the compressor. Next, fuel is burned with the compressed air in a combustor and a jet of hot gases is forced backwards through a nozzle after the expansion process. This creates the thrust that pushes an aircraft forward [16].

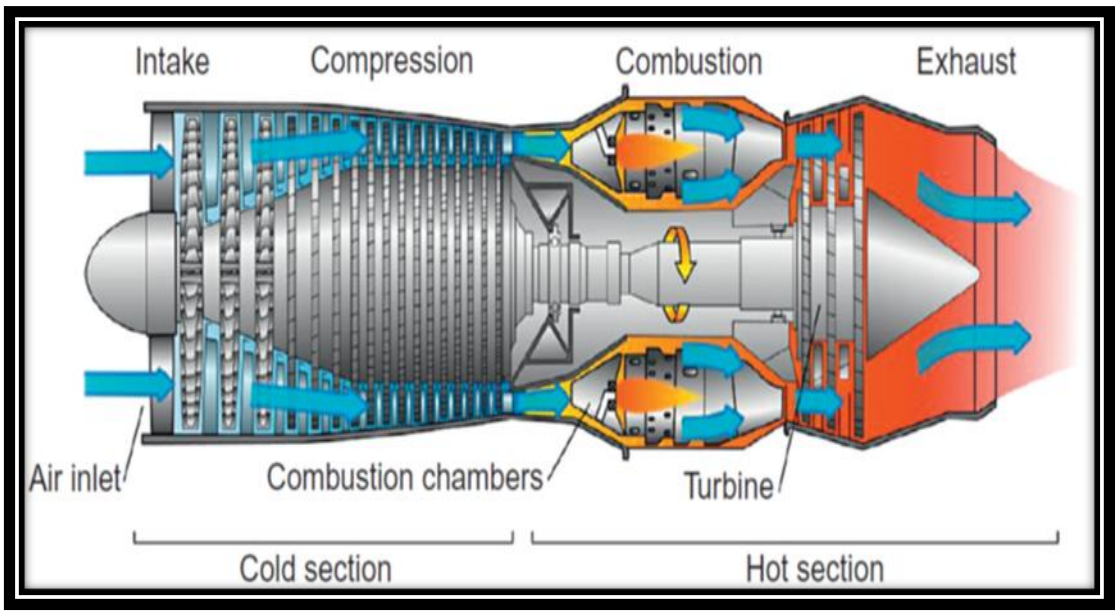

Figure 1.9 Schematic of a jet gas turbine [16]

1.6 Ideal gas turbine cycle

The air standard Brayton constant pressure closed cycle is the basis of the cyclic gas turbine power plant. This cycle has four processes: starting with the (1-2) compression adiabatic process involving negative work in the system (W_C). Then, in the process (2-3), heat is added (Q_{in}) from the combustion chamber at a constant pressure.

The adiabatic expansion process (3-4) involves positive work (W_T) produced by a turbine. Finally, in the process (4-1) heat is rejected (Q_{out}) into the atmosphere at a constant pressure. Figure 1.10 represents temperature-entropy, which is a thermodynamic quantity representing the unavailability of a system's thermal energy for conversion into mechanical work, and

pressure-volume for the Brayton cycle. The turbine drives both the compressor and a generator, delivering electrical energy [25, 26].

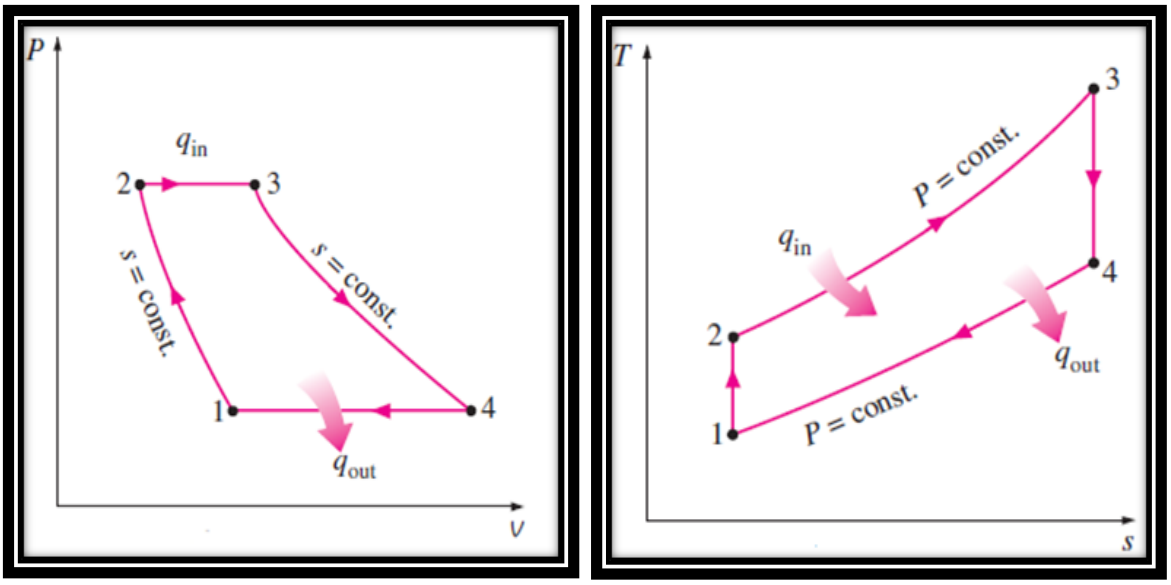

Figure 1.10 Brayton cycle on P-V and T-S diagrams

Gas turbine power plants can operate with either an open or closed configuration. Exhaust gas from a turbine in the open system is directly discharged to the atmosphere, whereas in the closed configuration the exhaust gas is passed through a heat exchanger.

Figure 1.11 represents an open gas turbine cycle where the air is compressed by a compressor. The compressed air is then routed to a combustion chamber and mixed with fuel in a combustion process. The combustion products, which represent the working fluid with a high pressure and high temperature, are then directed to a turbine where the expansion process occurs and useful mechanical work is produced. This work is used to run an electrical generator to provide energy and residual work is driven by the compressor. Finally, the exhaust gas is discharged directly to the atmosphere with lower pressure and temperature [25, 27].

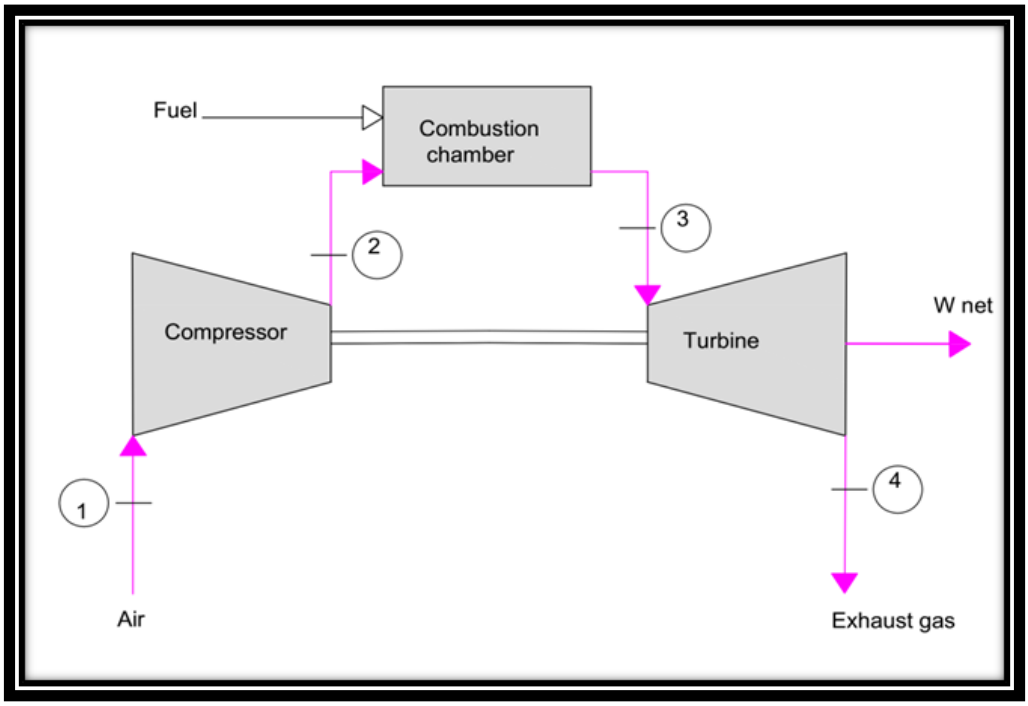

Figure 1.11 Open cycle gas turbine [25]

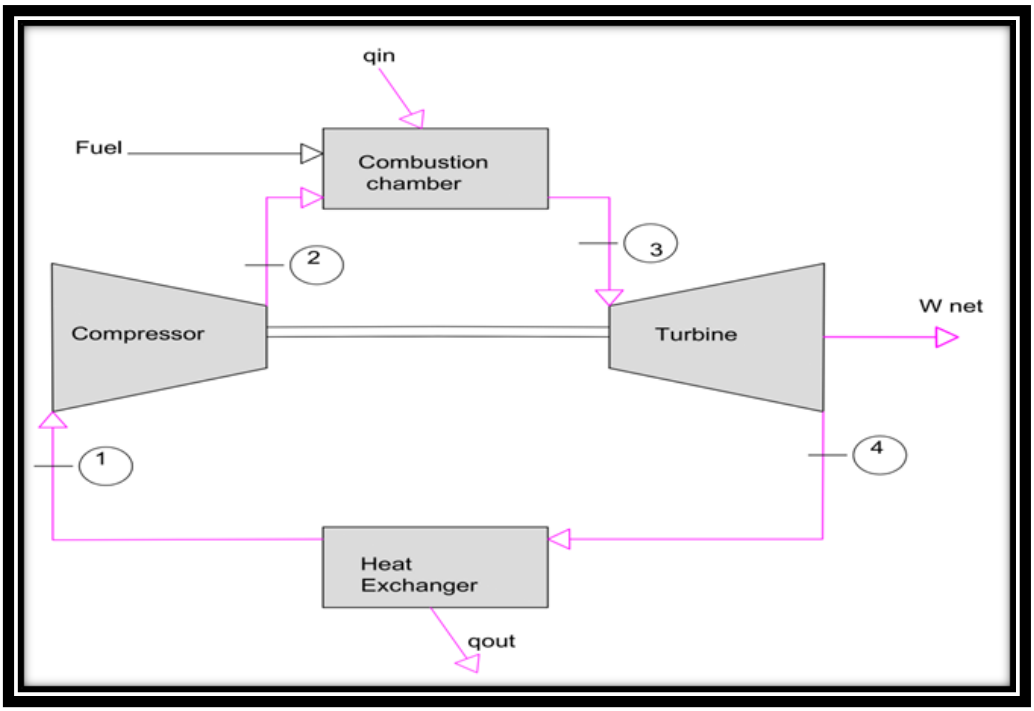

Figure 1.12 Closed cycle gas turbine [25]

In a closed gas turbine cycle, the system follows the same processes as in the open configuration, with one exception: the exhaust gas in this system is directed from the turbine exit to a heat exchanger where heat rejection occurs. The exhaust gas is recycled to exchange

heat in this system to improve the performance of the cycle and reduce contamination, as shown in Figure 1.12 [27]. Practically, a gas turbine power plant operates an open system, which cannot be represented as a thermodynamic cycle. Therefore, the equivalent closed cycle can be used as a theoretical model to assess cycle efficiency.

1.7 **Pollutants from gas turbines**

Anthropogenic pollutants emitted from industrial combustion processes and, more specifically, from gas turbine combustors contribute considerably to the deterioration of the global environment. Emissions from stationary gas turbines can be classified into two categories: the first category, whose main species consist of carbon dioxide (CO_2), water vapour (H_2O), oxygen (O_2) and nitrogen (N_2) and the second category, whose minor species include carbon monoxide (CO), unburned hydrocarbons (UHC), particulate matter (C), oxides of sulphur (SO_x) and oxides of nitrogen, which are nitric oxide (NO) and nitrogen dioxide (NO_2), commonly referred to as (NO_x) [28, 29].

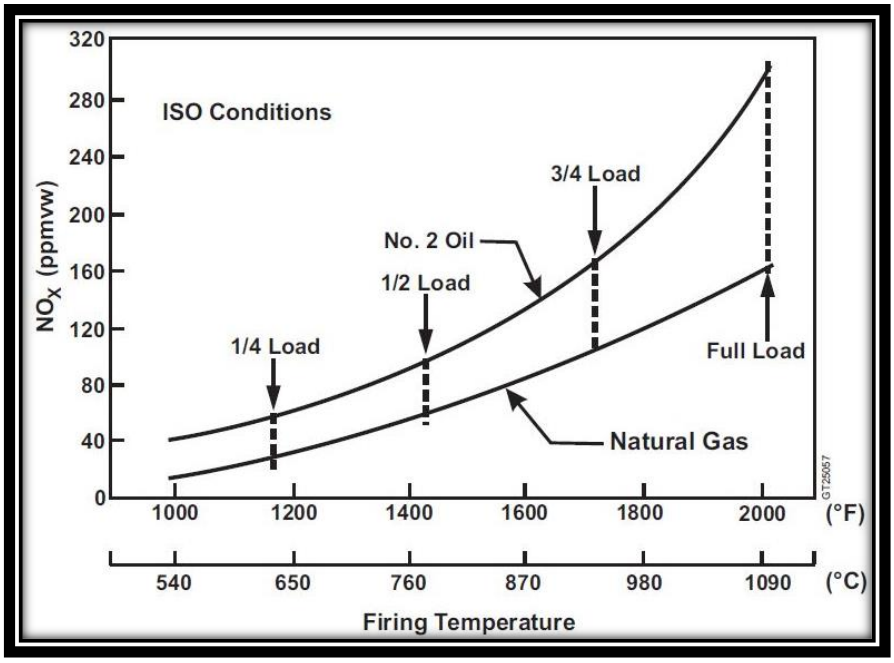

Figure 1.13 Firing temperature vs. NO_x products for combustor burning conventional fuels [28]

Among the pollutants in the second category, thermal NO_x concentration in exhaust gases is the most highly affected species by firing temperature [30]. Figure 1.13 shows that the level of wet particles of produced NO_x measured by volume exponentially heightens with increases in the temperature of a combustor burning two types of conventional fuels. This combustor temperature is elevated to match the typical requirements of high-power operational conditions, leading to higher levels of emitted NO_x. Thus, different technologies have been investigated to reduce harmful NO_x emissions from gas turbine combustors.

1.8 NO_x abatement technologies

Different mechanisms have been utilised in the combustion process of a gas turbine with the aim of controlling the firing temperature, which contributes directly to increased NO_x in its exhaust gases. One of these techniques essentially involves the initial mixing of a fuel with a concentration of dry air that is typically three times higher than the amount of air required for complete combustion. The excess air then works as a cooling fluid that reduces the combustion temperature, resulting in better controlled NO_x emissions [31]. In the second mechanism, which is known as wet control, steam or water is injected into gas combustors, thus decreasing the firing temperature. The injected steam heightens the performance of the turbine by increasing the mass flow rate through the system. The steam also controls thermal NO_x formation in the combustion chamber, leading to a low level of emitted NO_x [32, 33].

However, gas turbines combustors developed to utilise the above-mentioned control techniques to lower NO_X emission levels have encountered serious technical issues that raise the cost and reduce the reliability of these gas turbines in industrial applications. The challenges connected to employing these sophisticated combustors include: pressure oscillations in the combustion chamber, flame instabilities and additional energy requirements to generate steam. Using a wet mechanism to reduce the combustion

temperature for the purposes of controlling NO_x formation also leads to a significant increase in CO emissions, as shown in Figure 1.14.

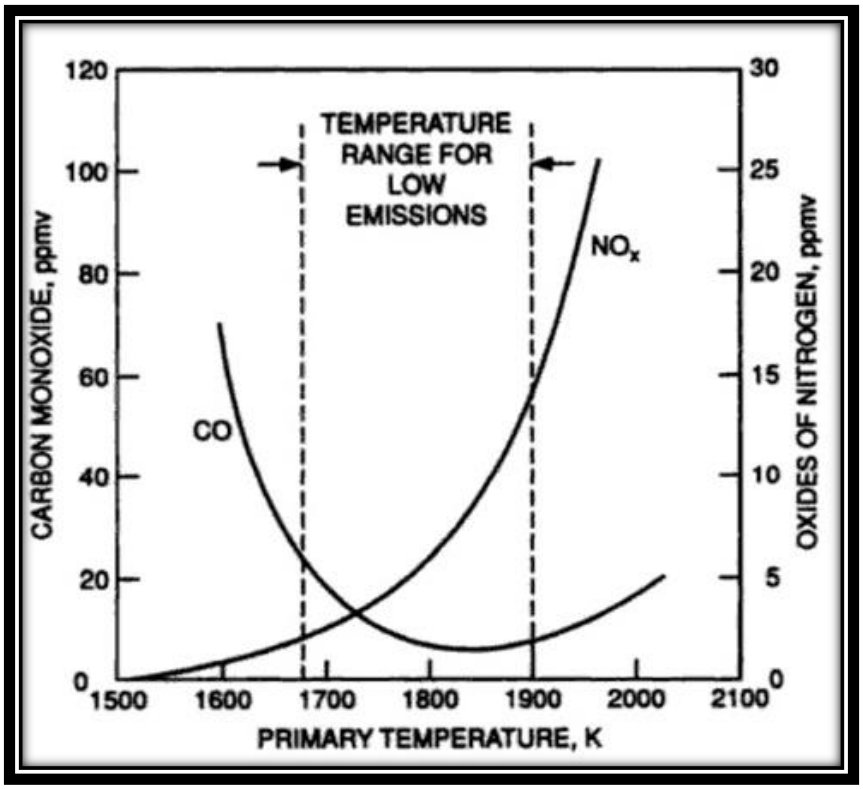

Figure 1.14 Influence of firing temperature on CO and NO_x emissions [33]

1.9 Climate change and global warming

Climate change is a global average change over a long timescale to weather patterns, such as temperatures, precipitation, humidity and wind. An increase in the earth's average temperature over this period is known as global warming [34], as shown in Figures 1.15 and 1.16.

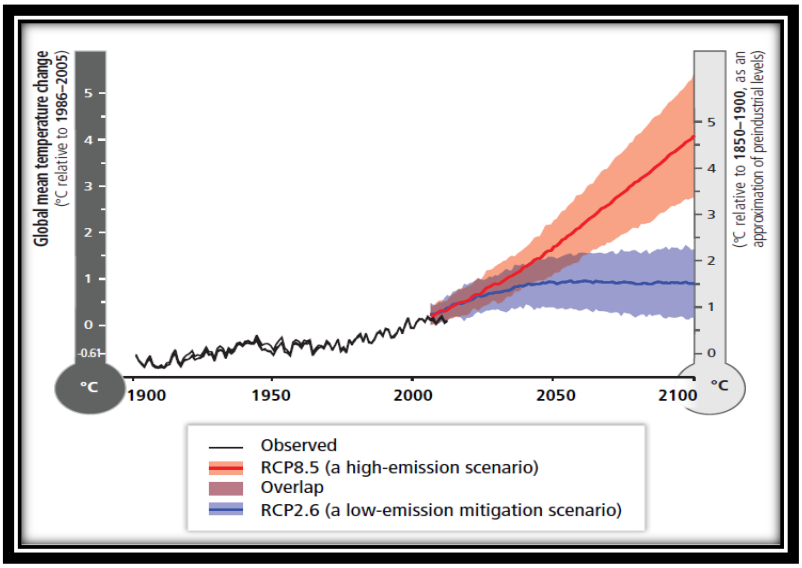

Figure 1.15 Global perspective on climate-related risk [35]

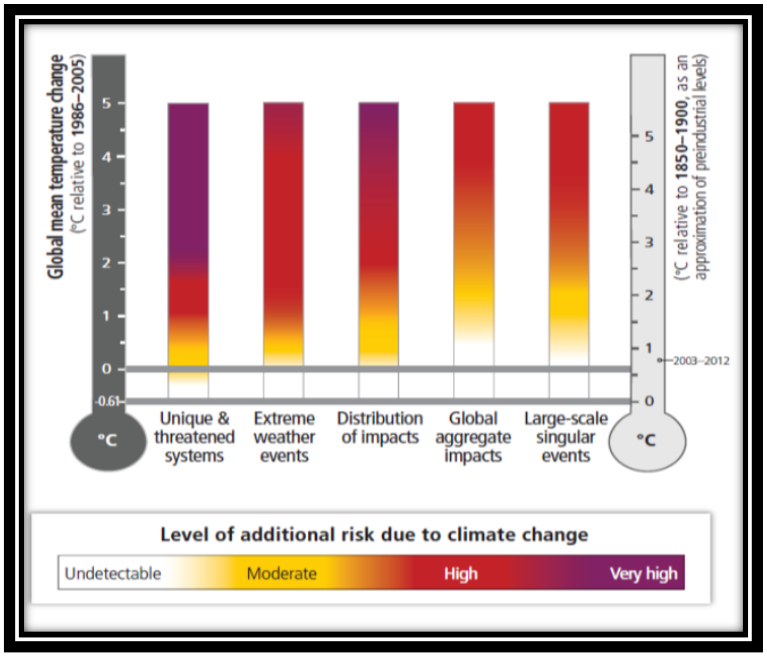

Figure 1.16 Risk associated with reason for concern [35]

This has been one of the greatest problems facing human beings since the mid-twentieth century. Anthropogenic gases, such as NO_x and CO_2, emitted into the atmosphere have been the main cause of this problem, directly affecting the global environment, which in turn impacts on humans and other creatures on the planet, as shown in Figure 1.17.

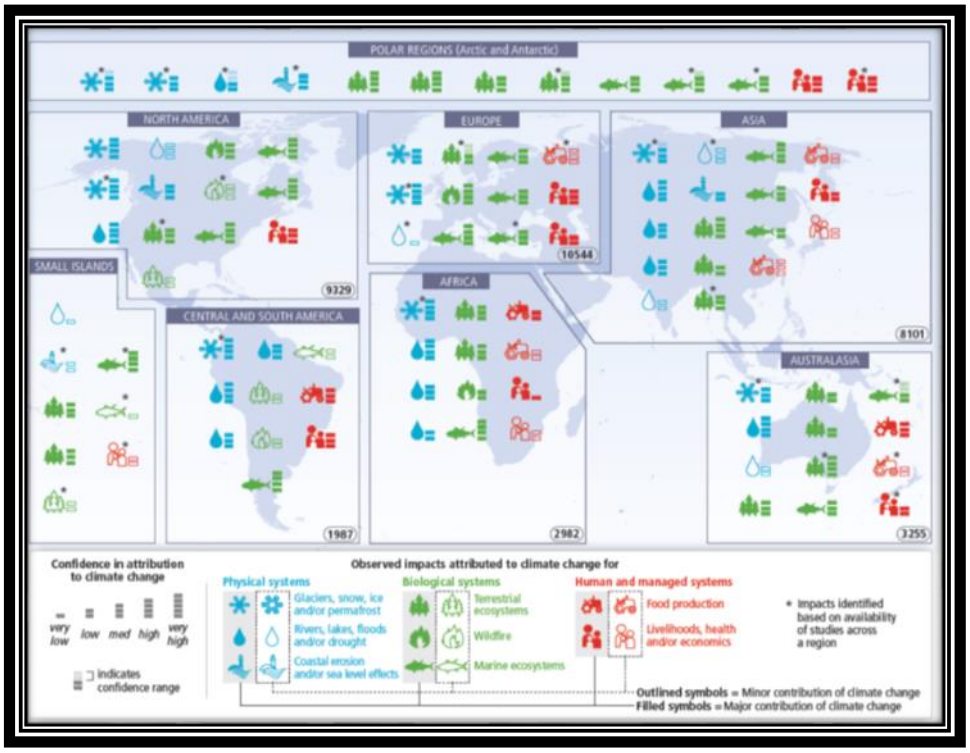

Figure 1.17 Impact of climate change, with minor and major contributors [36]

1.10 **Greenhouse gas effect**

About half of the total amount of radiant energy reaching the earth's atmosphere from the sun is reflected back to space. The other half is solar radiation in the form of visible rays with a short wavelength and high heat energy, which are absorbed by land and oceans. This energy is converted into infrared as it hits the earth, with a long wavelength and less heat energy.

This invisible heat radiation is re-emitted by the planet and is trapped and reflected back in different directions by the atmosphere, which is a combination of Greenhouse Gases (GHGs) surrounding the earth. This sequence of absorption and re-emission of infrared radiation sustains heat energy in the earth's atmosphere, which helps to keep it warm. The process is similar to the natural process called the greenhouse effect.

The earth's temperature is maintained at a value that ensures the existence of life. Without this process, Earth would be a lifeless rocky planet because it would be considerably cooler. Some of the GHGs, such as water vapour and N_2O, absorb infrared heat radiation due to the complicated arrangement of their molecules. Others, such as CO_2 and CH_4, have a different mode of rotation and vibration movement which enables their molecules to trap and re-emit this long wavelength of heat energy to the earth [37].

The greenhouse effect is being intensified as gases such as CO_2 and NO_x are released into the atmosphere by human activities, leading to incremental increases in the planet's temperature. This causes catastrophic global consequences, such as chronic water shortages, coastal flooding and more frequent hurricanes [38].

Since 1950, CO_2 concentration in the atmosphere has been measured accurately and the findings have shown a dramatic rise in the proportion of atmospheric CO_2. The level of CO_2 molecules in the atmosphere emitted by industrial processes has increased by around 30% in the last five decades. This has led to an increase in the interception of outgoing long-wave radiation, thereby retaining additional heat and feeding the global warming phenomenon. CO_2, in particular, is considered to be one of the anthropogenic greenhouse gas emissions that has the most critical influence on the earth's climate, intensifying global warming by around 64 %. This is known as the enhanced greenhouse effect [39].

1.11 **The predicament of CO_2 emissions**

Figure 1.18 shows how CO_2 emissions have dramatically increased since the Industrial Revolution, from almost zero until their values reached over 32 $GtCO_2$ in 2011.

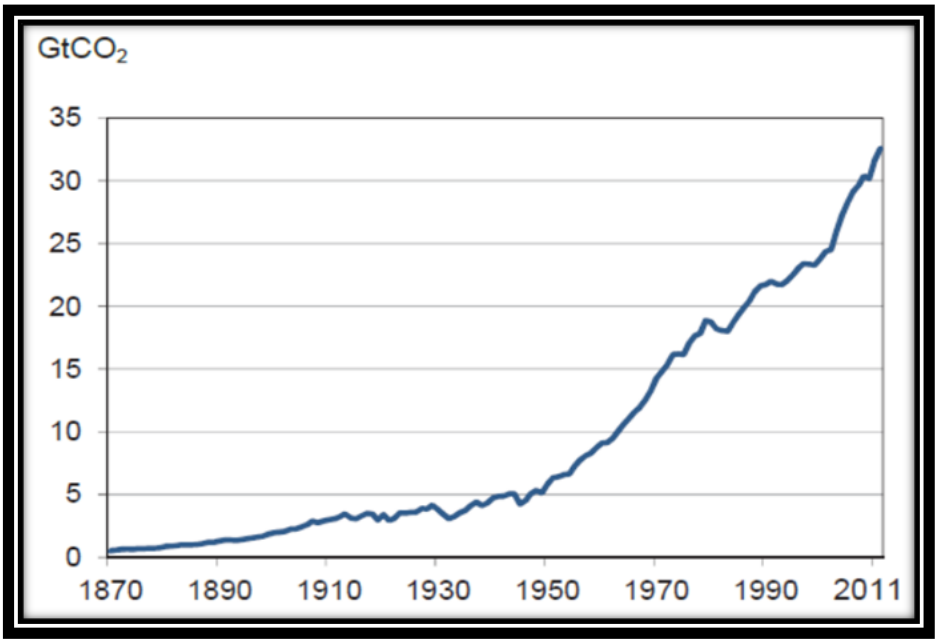

Figure 1.18 Trend in CO_2 emissions from fossil fuel combustion [40]

The electricity and heat generation sector is by far the largest emitter of CO_2, and in 2013 it produced 42% of all worldwide CO_2 emissions, as shown in Figure 1.19. This means that this sector has had a primary role in causing global warming, climate change, and ecosystem degradation [40].

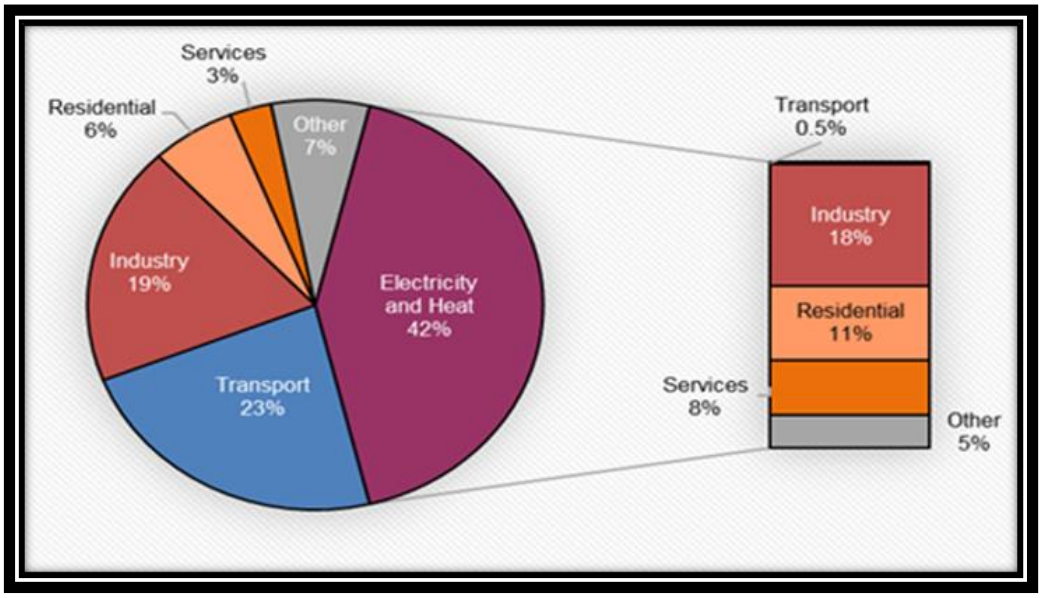

Figure 1.19 World CO_2 emissions by sector, 2013 [40]

The concentration of CO_2 will continue to increase, reaching a worst-case estimate of approximately 500-700 ppm in 2100, which is potentially almost double the value in 2010, as shown in Table 1.2 [41].

Table 1.2 Atmospheric CO_2 concentrations [41]

Decade	Carbon dioxide concentration ppm
1700	270-280
1900	293
1940	307
1960	326
1980	339
1990	354
2000	369
2010	390
2050	400-500
2100	500-700

1.12 **Road map to decarbonising power production**

Energy and the environment are now the main global concerns leading to international and intergovernmental initiatives and programs to combat environmental deterioration. Climate change has become the principal reason why policy makers have focused on reducing emissions of GHGs.

Internationally, efforts have been made to decarbonise power systems and produce low-carbon sources of energy, such as establishing the Intergovernmental Panel on Climate Change (IPCC), operating under the management of both the World Meteorological Organisation and the United Nations Environment Programme (UNEP) [42].

The Kyoto Protocol, which is a treaty agreed under the United Nations Framework Convention on Climate Change (UNFCCC), is another attempt to achieve this goal. These measures aim to monitor and set binding obligations to reduce anthropogenic GHG emissions. This includes emitted CO_2, which represents the main contributor to climate change [43].

Despite these attempts, the International Energy Agency (IEA) states that fossil fuels, considered the source of most man-made GHG emissions, remain the main source of global energy production, exactly as it was 25 years ago [44]. NG, which is the least carbon-intensive of fossil-based fuels, generates 22% of global power demand and is the only fossil fuel whose proportion of energy consumption is projected to grow [45].

1.12.1 **World energy trilemma**

For ongoing global power generation, stable and sustainable energy systems require a balance in the three dimensions of what is known as the energy trilemma. This model was created by the World Energy Council (WEC) in partnership with Oliver Wyman, and it represents energy security, energy equity and environmental sustainability, as shown in Figure 1.20.

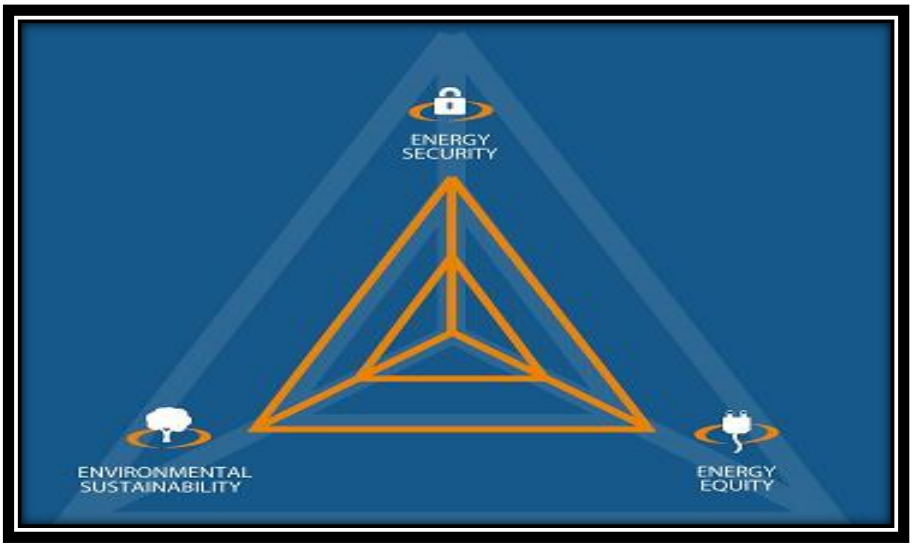

Figure 1.20 World energy trilemma [46]

Energy security refers to the effective management of supplying reliable and diverse primary energy sources. This means utilising energy infrastructures that are able to produce power while diversifying energy resources to match the expanding demand for electrification at the speed needed to cover world population growth.

Accessible and affordable modern energy services, as represented by energy equity, are also necessary for local populations. These trends, coupled with the third dimension of environmental sustainability, focus on reducing anthropogenic emissions from the energy sector [46, 47].

One of the key low-carbon technologies designed to support environmental sustainability by reducing emitted CO_2 from power generation plants is CCS. In this technology, CO_2 is separated from exhaust gases emitted from abundant industrial sources, such as power generation stations.

The captured CO_2 is then processed and finally deposited into geologic storage with a monitoring system. Oxyfuel (OF) combustion is another new technique, which involves burning a fuel in an almost pure domain of oxygen. OF can be combined with CCS technology to create a hybrid system recycling CO_2 emitted from power plants [48].

1.13 **Novel idea: Oxy-combustion with other working fluids**

The popularity of NG-fired gas turbine power plants is predicted to continue to rise as they become more widely used in electricity generation (as previously mentioned). However, the CO_2 emitted from gas turbines in these stations is considered to be a major contributor to climate change. Consequently, many different innovative approaches have been employed in turbines to reduce these emissions. One such method is based on CO_2 recycling in gas

combustors. Nevertheless, reduction in performance and reliability are still major obstacles to using this recirculation approach in gas turbines.

This study proposes the use of a combination of concepts in the combustion process for gas turbines, the main features being CCS technology integrated with OF combustion with the recycling of a high concentration of CO_2. Water also needs to be added in this approach to enhance turbine performance. A novel aspect of this research is that it uses the inert gas Argon with a CO_2-water mixture to improve the thermodynamic properties of this mixture, which can be used as a working fluid in gas turbines.

The following paragraphs provide a guide to the process through which the concept for the novel blend CARSOXY was generated and developed during this study, along with the relevant literature that made a contribution to this process. Specifically, they illustrate the way in which the combination of concepts from the technologies and techniques was studied by the researcher led to the development of the idea for this novel blend, which was proposed as a reliable and feasible replacement for air as a working fluid in the combustion process in industrial gas turbine.

The main aim of this novel idea is to develop a blend that could be used as a replacement working fluid for conventional air in industrial gas combustion systems to help reduce emissions of CO_2 and NO_x from power plants, which are contributing to the deterioration of the global environment, by producing lower levels of these emissions than those produced by these systems when using air. A connected objective is for the use of CARSOXY in industrial gas combustors to achieve similar performance to that obtained by conventional air gas turbines, which will make it a practical replacement in terms of not increasing costs or requiring modifications to existing equipment. As a result, it is essential here to detail each of the investigative approaches and technologies that were reviewed during the course of this study, each of which formed a crucial component in developing the idea of combining

a range of technologies and approaches to generate this novel blend for use in the proposed cycle. It is also useful to detail these contributing approaches and ideas here because they helped to inform and practically guide the methodology of this study in investigating and developing the novel blend itself.

The techniques and approaches highlighted here all contributed to the development of the idea for the novel CARSOXY blend because foundational concepts from each formed a component of the overall concept. Thus, all the highlighted approaches or techniques reviewed during this study and presented here are conceptually linked. OXY, an abbreviation which forms the 'OXY' part of the CARSOXY acronym, comes from the oxyfuel technique that was focused on in this research to reduce CO_2 emissions in the combustion products of industrial gas turbines, and thus their environmental impact. An important feature of this technique is recirculation of CO_2 in the combustion process, the main motivation for which is to control the flame temperature of the combustion process while reducing CO_2 emissions [49]. A review of this approach led to the concept of including CO_2 in the developing novel blend, which led to the addition of the 'C' in the CARSOXY acronym for carbon.

This guided the literature survey towards CCS technology, which is one of the most widely-used techniques for the recirculation of CO_2 [50]. However, installing CCS technology in power plants has been shown to result in a direct decrease in the overall efficiency of the cycle because of the CO_2 capture and compression processes in comparison to a conventional natural gas turbine conventional power plant running without CCS [51]. Therefore, another innovative approach was required to be combined with oxyfuel integrated with CO_2 recirculation to preserve the potential benefits while avoiding any reduction in system efficiency. Consequently, humidified gas turbine cycles, which have been demonstrated to enhance the overall performance of gas turbine cycles through their use of steam injection into the combustion process, were studied as a potential solution to this issue.

The concept of employing water vapour, which is represented by the 'S' as in 'steam' in CARSOXY, was combined with the other established component concepts of recirculating CO_2 in an oxyfuel gas combustion process [52, 53]. This followed the goal of reducing harmful emissions because both CO_2 and NO_x combustion products could be reduced due to water injection, which reduces the formation of NO_x in the combustion process while producing equivalent power to the existing traditional gas turbine cycle.

Although the steam injection technique has been shown to enhance cycle performance, this enhancement is limited because the addition of water vapour in the combustion process presents the increasing likelihood of a flame blowout as the amount of steam in the system is increased. Thus, gains to cycle performance improvement are necessarily limited when using this technique as there is a restriction on the amount of water vapour that can be used [54].

This led to the investigation of possible alternative working fluids to air to find alternative means to further improve the performance and while trying to ensure that the proposed blend would work in a similar way to a conventional blend in practical applications, especially in closed cycles as this type of cycle is used for the recirculation process. Thus, the use of inert gases, such as CO_2 and helium, each of which is used in some existing systems, was reviewed with the aim of exploring alternative approaches to further enhancing gas turbine performance [55, 56].

The focus then moved to consideration of the physical properties of other inert gases that had not previously been used in industrial gas turbine combustion processes, specifically argon. This is due to its relatively high concentration in air and other potentially useful properties for system performance, such as its specific heat ratio and its molecular weight, which suggests that it is a potential practical alternative in terms of not requiring system

modifications for use [57]. As a result, Ar constitutes a novel component of the proposed blend, and is represented by the 'AR' in CARSOXY.

In summary, a novel concept of using Argon as one component of a proposed blend alongside CO_2, steam and oxygen (CO_2-Argon-Steam), integrated with OXYfuel combustion (CARSOXY) can potentially provide an emission-reducing and feasible replacement for air as a working fluid in industrial gas combustors was developed.

In this thesis, the optimum CARSOXY blend is theoretically identified. This is achieved through the use of Gaseq software, which generates a large number of blends (120) to provide as wide a blend range as feasible for the purpose of testing the blends' thermodynamic properties and indicate which blend possesses a balance of characteristics that are most similar to those of air and combustion products required for recirculation in the proposed cycle.

Empirical data is used to identify the 16 blends from the 120 generated blends that have the most similar characteristics to air in terms of thermodynamic properties and required combustion products for recirculation. Chemkin-Pro is then used to test the flame velocity of these 16 selected blends to make a comparison with air at the same running conditions. Finally, following this flame velocity investigation, blend number 58 is identified as the optimum blend because it possesses equivalent thermodynamic properties and almost matching product outlet temperature to air under the same investigative conditions

The optimum blend is then investigated in the proposed cycle, as shown in Figure 1.21, to examine its performance in comparison with a conventional air cycle to demonstrate the applicability of the proposed cycle, which is detailed in Chapter Five, in the power sector. The aim is to reduce emissions by recycling a high proportion of emitted CO_2 from exhaust gases while producing equivalent efficiency to that of a conventional air cycle. Additionally,

the novel blend is experimentally tested in a 20-kW generic burner to show its feasibility in terms of providing flame stability as a practical replacement for air as a working fluid in an industrial gas combustor.

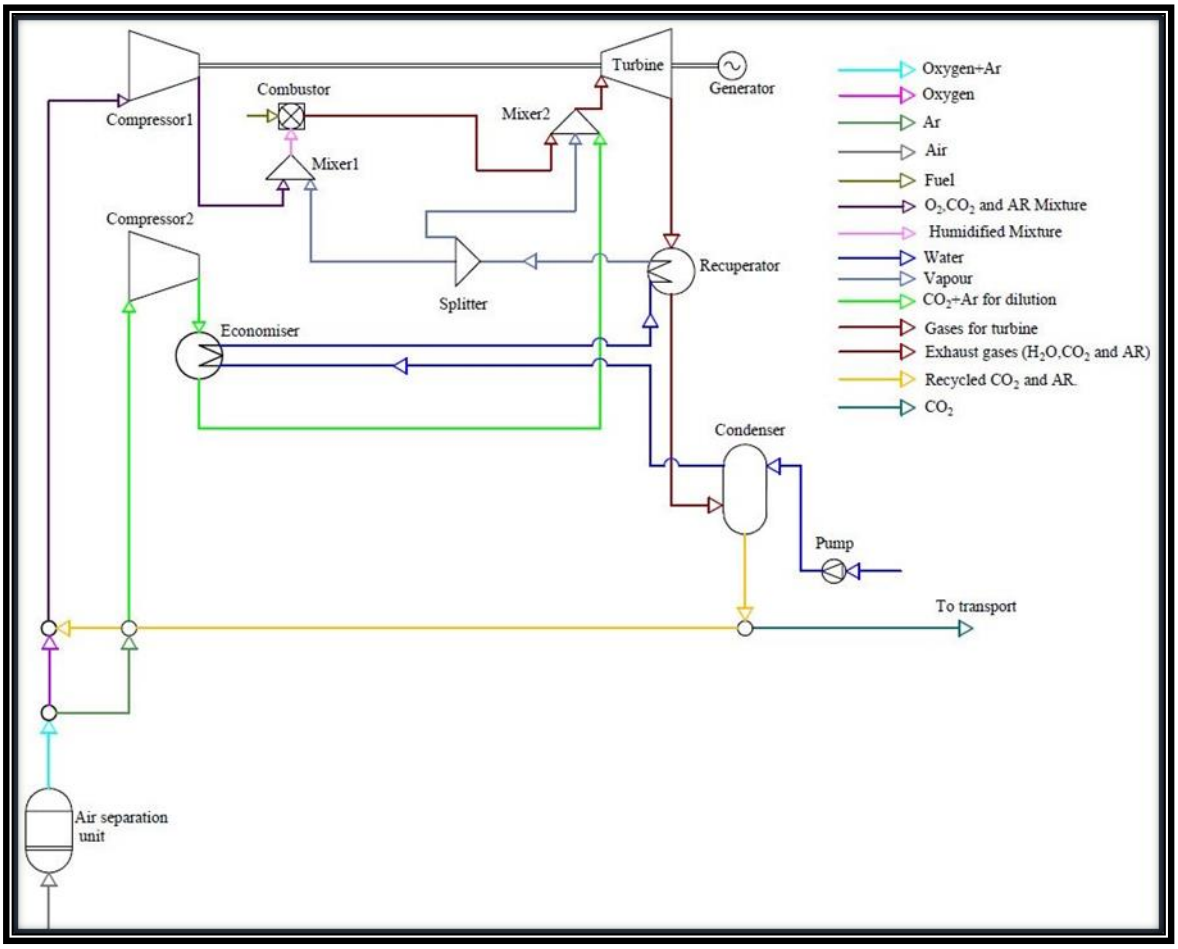

Figure 1.21 CARSOXY cycle

1.14 **Aim and objectives**

The aim of this thesis is to infer, through theoretical and experimental investigation, an optimal balance of component gases for the proposed novel CARSOXY blend to be used in industrial gas combustors as an alternative to air in the proposed cycle to reduce harmful CO_2, and NO_x emissions while maintaining the feasibility of use in terms of overall cycle efficiency and flame stability.

Following this aim, the below objectives are pursued in this study:

- Theoretically investigate the thermodynamic properties (i.e. combustion product outlet temperature, specific heat ratio and heat capacity), and CO_2 and H_2O combustion products of a wide range of relative proportions of CARSOXY blend components. The aim is to find an indication of the optimal blend combination that closely matches the thermodynamic characteristics of air while providing the required amounts of CO_2 and water vapour combustion products for the proposed cycle.
- Theoretically investigate the flame speed of the potential CARSOXY blend combinations to identify the closest possible match to that of air and provide an indication of the optimal selection in terms of combustion conditions for ensuring flame ignition and stability.
- Experimentally investigate the indicated optimum blend's combustion product outlet temperature compared to air under the same running conditions in the same representative combustion system to consider how the data's trends compare to this study's computational data on its use in comparison with air, in terms of feasibility of use as a replacement.
- Experimentally investigate the indicated optimum blend's combustion products CO, NO_x and H_2 compared to air under the same running conditions in the same representative combustion system to consider how the data's trends compare to this study's computational data on its use in comparison with air in terms of reduction of harmful emissions and indication of combustion process efficiency.
- Using the same fuel (i.e. methane) with the same mass flow rate of fuel and a similar mass flow rate of working fluid, for air and the indicated optimum blend, experimentally investigate whether the blend provides flame ignition for further

investigation of self-excitation of the flame under the same running conditions as air in the same representative combustion system.

- Experimentally investigate heat release at self-excitation running conditions for the indicated optimum blend in the same representative combustion system to find an indication of flame stability compared with the values for air under the same running conditions.

1.15 **Summary**

This chapter has presented the significant role of power production in modern life and the fact that the huge demand for electricity consumption has led to rising anthropogenic greenhouse gas emissions.

This has had a direct impact on climate change, with its inherent global environmental consequences. In the next few decades, natural gas-fired power stations are predicted to take the lead in terms of generation of required electrical power. However, CO_2 and NO_x emissions from gas turbines in power plants are considered to be the main contributors to deterioration of the world's environment.

CCS technology integrated with the OF technique is proposed as one path towards finding solutions to this specific problem. Following a survey of the relevant literature, the novel concept in this thesis is that it combines the aforementioned integrated techniques with humidification of the combustion process and the addition of argon in order to propose a novel blend – CARSOXY – which could be used as a replacement for air as a working fluid in industrial gas turbines and reduce harmful emissions while maintaining system performance and requiring no system modifications for use. This study's main aim and related theoretical and experimental investigative objectives are presented in terms of investigating the proposed blend's potential for use in this way. This proposed approach

could be used to establish a permanent basis for a three-dimensional triangular model, through which reliable and achievable energy can be produced while maintaining a clean atmosphere. The next chapter will describe CCS technology and OF combustion, and their application in gas turbine cycles, in more detail.

1.16 **Thesis structure**

This thesis is organised into seven chapters, with the following structure:

Chapter 1. Introduction

The growing demand for energy and the problems of CO_2 emissions are presented in Chapter One. In addition, a novel idea to help address this issue is proposed, utilising the combined concepts of CCS technology integrated with the OF technique in humidified gas turbine cycles with argon in gas combustors.

Chapter 2. Literature review

CCS is defined in this chapter, with its three main techniques. One of these techniques, OF combustion integrated with gas turbine cycles, is then explained, along with its main obstacle to commercial power production use. Evaporative gas turbines (EvGT) could be considered as one solution to this problem, through their use of water injection into gas turbine combustors.

Chapter 3. Methodology

Approaches used to ascertain the optimum CARSOXY blend, measure the CARSOXY cycle's performance in comparison with a conventional humidified air cycle and to perform experimental tests using the blend using a generic burner are discussed from theoretical and experimental points of view in this chapter.

Chapter 4. Inferring the optimum blend through data analysis

The optimum CARSOXY blend is indicated in this chapter through the generation of a huge number of Ar, H_2O and CO_2 blends with oxygen and methane as reactants. This optimum blend was inferred by its indicated superior thermodynamic properties and flame speed values which approximately match those of air and, thus, could be used to replace air as a working fluid in conventional cycles**.** Additionally, the blend produces higher efficiency and power output compared to NG/air.

Chapter 5. Efficiency of CARSOXY cycle

The Aspen Plus program is employed as an effective tool in this chapter to simulate the performance of the proposed CARSOXY cycle in comparison with a conventional humidified air cycle running at the same operating conditions.

Chapter 6. Experimental work

The diffusive burner setup procedure for using the proposed blend as an oxidiser in a combustion process, to be compared with air, is presented in this chapter. Preliminary experimental data and analysis also indicate the feasibility of using the novel blend in a gas combustor in terms of emissions reduction and flame stability.

Chapter 7. Conclusions and future work

The main objectives of this study are briefly summarised in this chapter. A summary of the theoretical and experimental methods used to achieve these aims is given and significant findings are presented again in concise form with overall conclusions. Finally, future work connected to this study is suggested.

1.17 **Published output**

Through the direct and supporting contributions of this thesis, A journal paper has been published, a further journal paper is under review and four conference papers have been produced, three of which were presented at the conferences. The fourth conference paper is going to be presented in Tokyo, Japan in August 2019. Details follow below.

1.17.1 **Journal publications**

[1] A. Al-Doboon, M. Gutesa, A. Valera-Medina, N. Syred, J.-H. Ng, and C. T. Chong, "CO2-argon-steam OF (CARSOXY) combustion for CCS inert gas atmospheres in gas turbines," *Applied Thermal Engineering*, vol. 122, pp. 350–358, 2017.

[2] Odi Fawaz Alrebei, Ali Al-doboon, Bowen, Philip, Agustin Valera-Medina, "CO2-Argon-Steam Oxy-Fuel Production for (CARSOXY) Gas," *Journal of Thermal Science and Engineering Applications-ASME, Under review.*

1.17.2 **Conference publications**

[1] Alrebei O, Aldoboon A, Bowen P, Valera-Medina A, "CARSOXY combined with Ammonia Production for Efficient, Profitable CCS cycles," INTERNATIONAL GAS TURBINE CONGRESS (IGTC) 2019 Tokyo, Japan.

[2] A. I. M. Al-Doboon, A. Valera-Medina and M, Gustesa " Improving the Performance of a Gas Turbine Cycle Using CO_2-Argon-Steam-Oxyfuel (CARSOXY) as a Working Fluid in the Combustion Process." 13th Conference on Sustainable Development of Energy, Water and Environment Systems – SDEWES, 2018, Palermo- Italy. September 30- October 04, 2018.

[3] N. Syred, M. V. Gutesa, A. Al-Doboon, A. Valera-Medina and P. J. Bowen, "CARSOXY (CO_2-Argon-Steam-OF) Combustion in Gas Turbines for CCS Systems.". 55^{th} AIAA Aerospace Sci-Tech Forum, Grapevine, Texas, 9-13 January 2017.

[4] A. I. M. Al-Doboon, A. Valera-Medina, N. Syred, and J. H. Ng, "CO_2-Argon-steam OF (CARSOXY) combustion for CCS inert gas atmospheres in gas turbines.". CHISA 2016 PRAGUE, 19^{th} Conference on Process Integration, Modelling and Optimisation for Energy Saving and Pollution Reduction, PRESS 2016, Prague, Czech Republic, 27-31 Agust 2016.

CHAPTER TWO

Chapter 2 Literature review

This chapter is structured in the following way, as guided by relevance to the novel idea presented in Section 1.13. Regarding carbon capture technology, this chapter details this approach and the techniques that it makes use of. It also examines the use of oxyfuel combustion in gas turbines and looks at how these concepts could be combined to provide a means to address the problem of harmful gas turbine emissions.

First, CCS technology is detailed and explained, along with the systems involved in the process of CO_2 capture, which is presented as a means to capture CO_2 for recirculation in the gas combustion process. The oxyfuel (OF) technique is considered next, as one of the technologies by which CO_2 can be recirculated in gas combustors, which are also defined in this chapter along with a definition of flame zones. Among the most important components in the OF approach are air separation units (ASU), which are considered both as a requirement for this technique and a challenge, as these units require extra power from the system. In this chapter, an explanation of all three main air separation methods used in these units is given.

Due to the reduction in efficiency caused by both the recirculation of CO_2 in the combustion process and the additional power required by the ASU, some means to enhance system performance is required. This can be achieved by adding another component to the blend: water vapour or steam. Thus, humidified gas turbine cycles are detailed in this chapter, with a specific focus on EvGT. However, the use of water in these cycles is limited due to the flame blowout restrictions,

Consequently, alternative gases as a working fluid, such as in the Allam cycle that uses CO_2, are considered here for the purposes of presenting means to avoid the flame blowout restrictions while increasing overall cycle performance. As such, helium and other inert

gases are also considered, with a main focus on argon. Combustion modes and their definitions, along with their relative benefits and drawbacks, are then presented, with consideration of premixed and non-premixed combustion. Non-premixed combustion is the focus here because CARSOXY does not include nitrogen, which eliminates NOx emissions, thus providing increased stability.

Next, the potential and means for recycling captured CO_2 are discussed. Descriptions of gas combustion turbine systems and combustor types are then provided, along with the benefits of using mixed combustion, particularly non-premixed, techniques in these systems. Subsequently, the use of swirling flows in burners is explained, together with the related challenge of blowout in the system. The OF process in gas turbines is then outlined through a description of the systems and processes involved in air separation for oxygen production.

The Allam and humidified gas turbine cycles are then presented, followed by an examination of the use of alternative gases as working fluids in gas turbines. The concept of evaporated gas turbines used in combination with OF combustion is then detailed. Next, formulae for calculating system outputs and efficiencies for gas turbine cycles are presented. Finally, a chapter summary is provided.

2.1 CO_2 capture system

CO_2 has been identified as one of the most readily available forms of carbon resource and it is considered as nontoxic, abundant and economic. However, the activation and utilisation of CO_2 as a chemical feedstock raw material is still limited to a few industrial processes, such as the synthesis of urea, salicylic acid and cyclic carbonates as CO_2 is considered to be thermodynamically stable and/or kinetically inert when used in transformation approaches. Therefore, the process for the transformation of CO_2 into other chemicals typically requires a considerable consumption of energy [58, 59].

Table 2.1 shows the emissions and number of sources of CO_2 from different industrial processes, such as electricity stations that burn fossil fuels or biomass, major CO_2-emitting factories, NG production, synthetic fuel stations and fossil fuel-based hydrogen production plants. Practically, to match the large size of contemporary power plants, many studies have highlighted approaches that have the potential to scale up the recovery of CO_2. These approaches require an extensive integrated unit at energy generation stations requiring CO_2 capture, transportation and a CCS system with safe storage [60].

Table 2.1 CO_2 emissions from industrial processes exceeding 0.1 Mt CO_2/year [61]

Process	Number of sources	Emission ($MtCO_2\ yr^{-1}$)
Fossil Fuels		
Power	4,942	10,539
Cement production	1,175	932
Iron and steel industry	638	798
Refineries	269	646
Petrochemical Industry	470	379
Oil and gas processing	Not available	50
Other sources	90	33
Biomass		
Biomass and bioenergy	303	91
Total	7,887	13,466

In terms of measures that can be taken to achieve the Energy Technology Perspective (ETP) BLUE MAP Scenario's ambitious goal of a 50% reduction in GHG emissions from the energy sector by 2050, CCS systems are predicted to be responsible for about 20% of all emissions reductions required to meet this target, as shown in Figure 2.1. Employing CCS technology as part of the approach to decreasing GHG emissions represents the least expensive approach to tackling the problem of harmful emissions.

Otherwise, the capital cost of meeting this target by 2050 without CCS systems would be 70% higher than when using CCS technology [62].

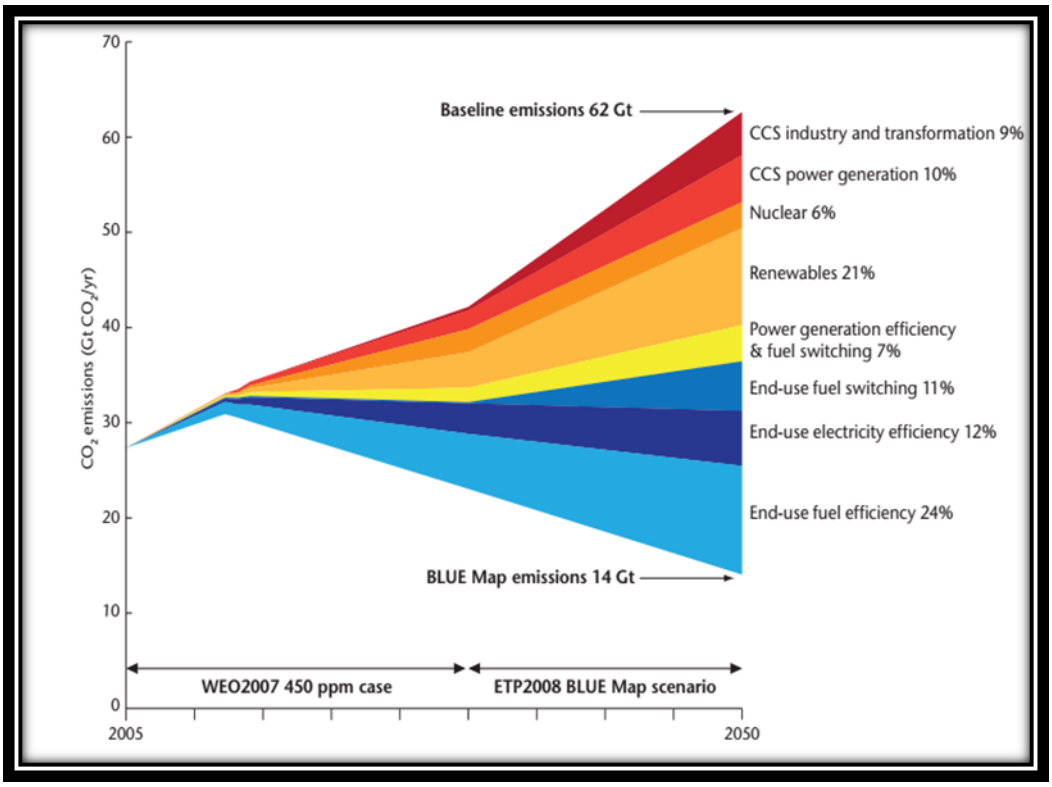

Figure 2.1 Percentages of ETP BLUE MAP 2050 emission reduction target by approach [63]

Currently, there are three main CCS techniques: post-combustion capture, pre-combustion capture and OF combustion capture; as shown in Figure 2.2. All of these categories can be commercially integrated as CO_2 capture techniques within power production plants and in industrial processes [61].

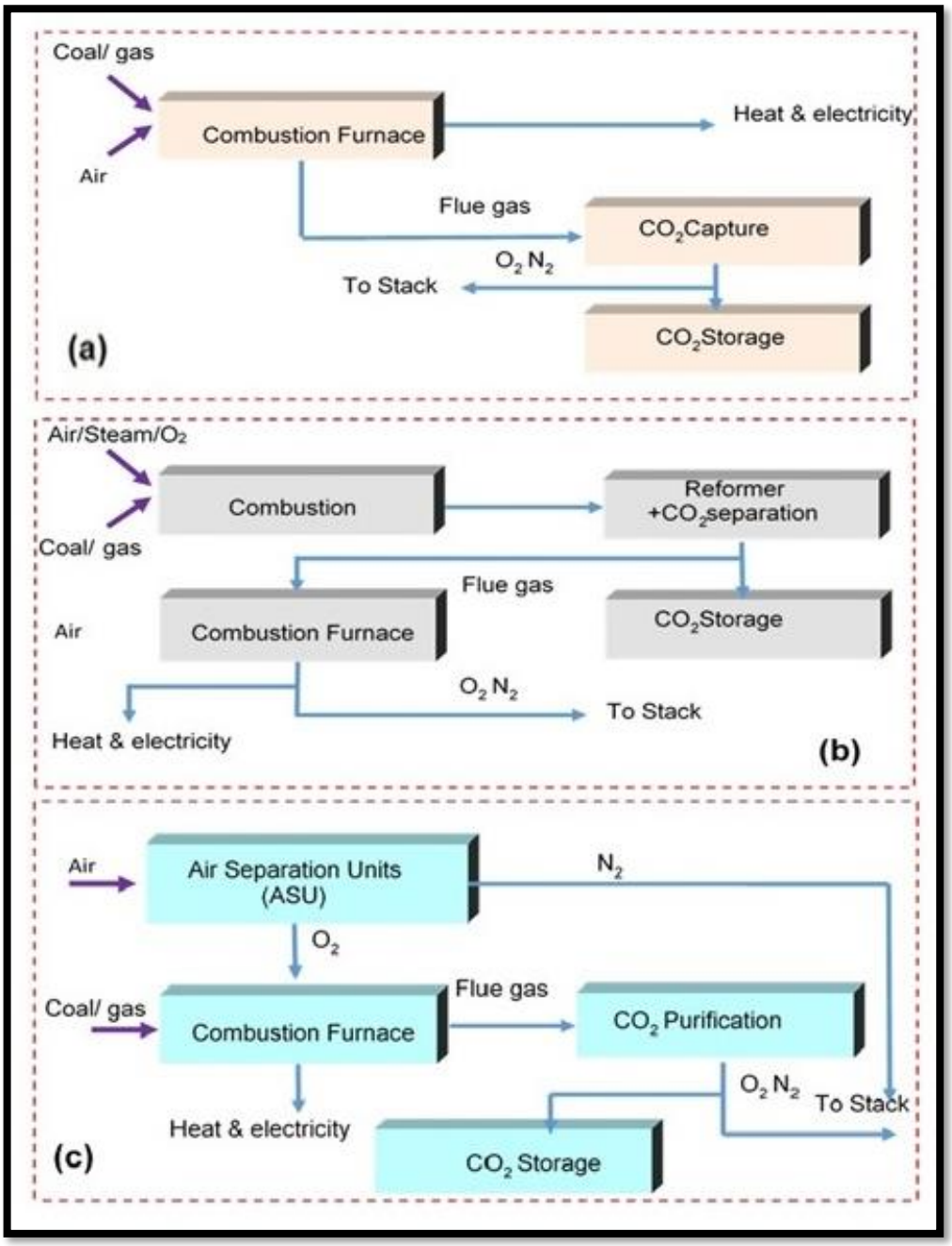

Figure 2.2 Three main systems installed for capturing CO_2 (a) post-combustion, (b) pre-combustion and (c) OF combustion [64]

2.2 Carbon capture and storage technology

CCS is one of the most promising technologies to allow the continued use of fossil-fuelled power generation plants while mitigating climate change by significantly reducing CO_2 emissions into the atmosphere [65, 66].

Briefly, CCS is a process that captures CO_2 from abundant sources, such as gas turbine power plants or industrial processes, and then deposits it safely and securely into an appropriate site, such as underground, to maintain a clean atmosphere [67, 68]. Figure 2.3 demonstrates how CO_2 is captured from large industrial sources that have a high density of CO_2. This is then transported and deposited into safe and secure sites to keep the atmosphere clean.

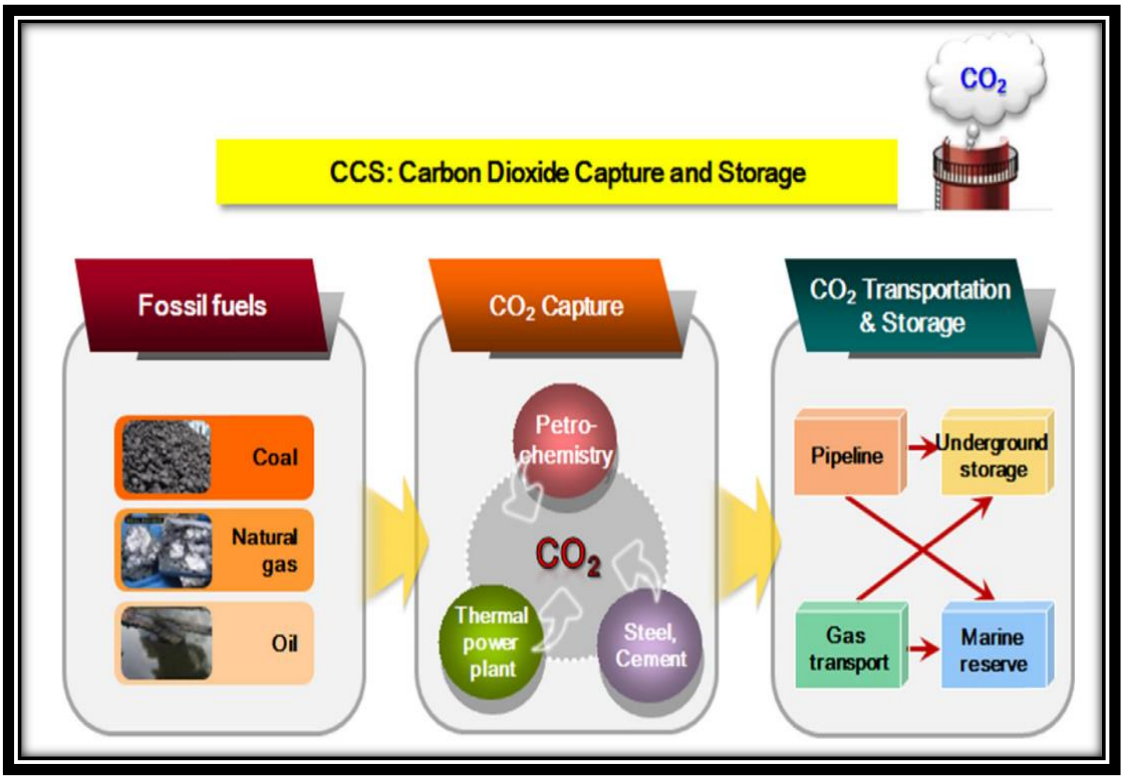

Figure 2.3 Concept and summary of CCS [64]

2.2.1 **Post-combustion capture**

In this technique, CO_2 is captured from flue gas streams produced by the combustion of fossil fuels and/or biomass in the air. A chemical sorbent, either in liquid or solid form, is used to separate CO_2 from the flue gas.

After it has been compressed, this fraction of the captured CO_2 is fed to a storage reservoir. Finally, the residual flue gas is discharged into the atmosphere. Figure 2.4 shows the classification of the applied technologies for post-combustion capture of CO_2 [68, 69].

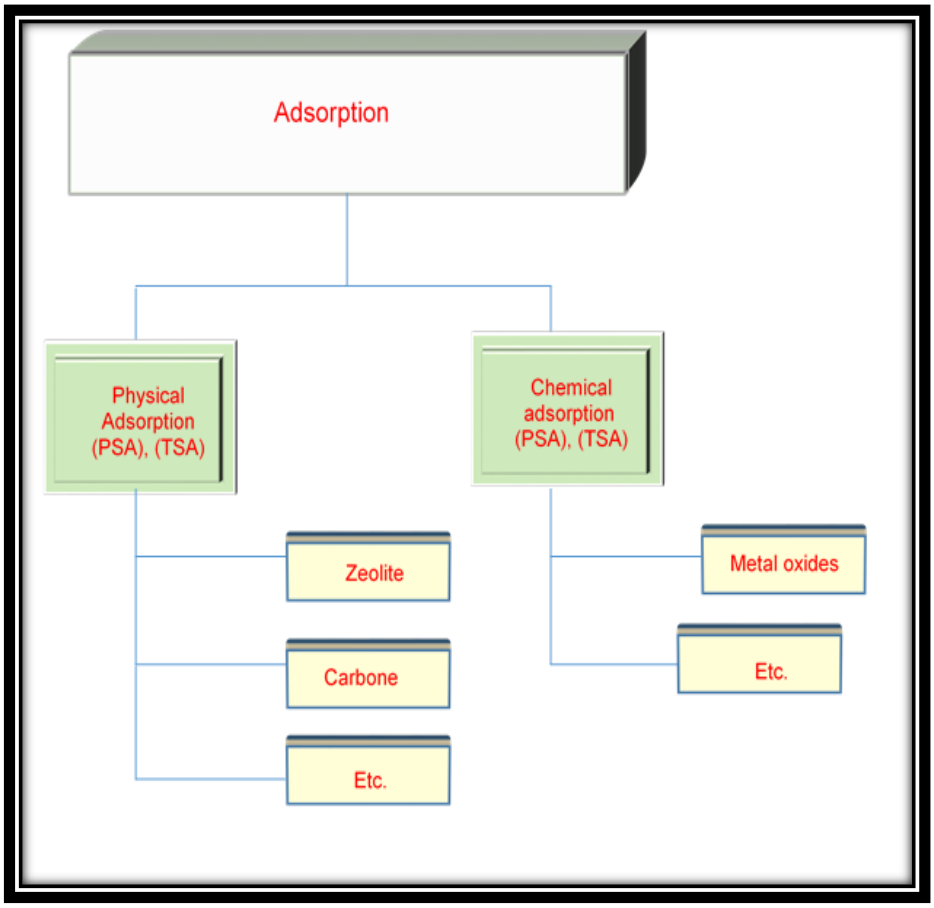

Figure 2.4 Post-combustion techniques for capturing CO_2 [64]

Figure 2.5 shows a schematic diagram of a power generation unit integrated with this technology and employed to capture CO_2. This approach can be installed in different power stations, which run with various types of fossil fuels, such as oil, coal, or NG [70].

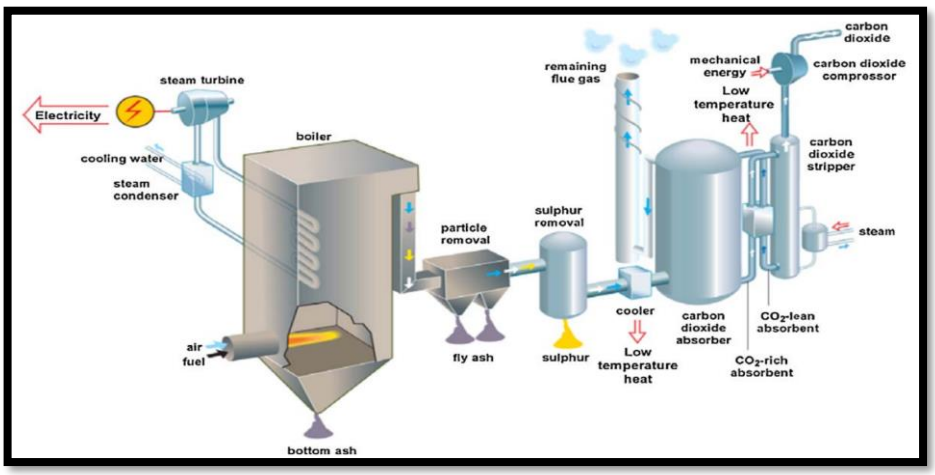

Figure 2.5 Schematic of post-combustion CO_2 capture system for power plants [70]

2.2.2 OF combustion system

The main idea behind this combustion technique is to burn the fuel in an almost pure domain of oxygen, which prevents CO_2 from mixing with nitrogen. This makes the process of capturing CO_2 from exhaust gases much less complicated. The exhaust from this process consists of high concentrations of CO_2 and water vapour. The CO_2 can be captured without difficulty after condensing the water vapour using traditional systems [71, 72].

2.2.3 Pre-combustion system

The pre-combustion system is preferred for use in integrated gasification combined cycles (IGCC). In IGCC power plants, a fuel with oxygen or air and/or steam is gasified and converted to syngas. Syngas is normally composed of carbon monoxide and hydrogen with small proportions of carbon dioxide, water vapour, hydrogen sulphide, ammonia, and other gases, and is used for energy production in a combined cycle [73].

In an IGCC plant, CO_2, with a high concentration and high pressure, is captured by utilising physical or chemical absorption processes. However, the system is restricted because of its significantly high investment cost and because of problems with the storage of physical solvents [74, 75].

2.3 Global electricity demand and gas turbines

The IEA states that the global demand for energy has been growing and will continue to grow steadily until 2030 due to an annual incremental increase in electricity consumption of 1.7% (as mentioned in the previous chapter). The power sector's dependence on NG will also become higher. Thus, this period of time may be considered to be a golden age for NG [76].

The fourth assessment report of the IPCC found that in 2030 fossil fuels will be the main source for 80% of world energy production. Of the systems using such fuels, gas turbine cycles have good potential to be used in a wide range of energy production industries. Therefore, these types of engine have a major role to play in the power sector [77].

Gas turbines have been employed to supply the continuously increasing demand for electricity, including those employing combined cycles and diesel engines [78]. Consequently, it is necessary to focus on increasing the output power and efficiency of gas turbines utilised for power production while maintaining the ability to service global demand for electricity and complying with legislation designed to help protect the environment. Mixing techniques for combustible blends in gas turbine combustors can play a significant role in this by improving the performance of gas turbines and reducing the emission of combustion products that can damage the global environment.

2.3.1 **Combustors in gas turbines**

Gas turbines, which are versatile engines used for stationary and aviation applications, commonly incorporate the following main components: compressors, shaft, combustion chamber and turboprop or turboshaft. The fundamental geometry of these parts, with their functional use in the Brayton cycle, as described in Chapter One (see Section 1.6).

The main function of the combustion chamber is to add heat to the gas turbine cycle by burning a fuel with compressed air to produce a hot gas stream at a high temperature of around 1100^{o}C. The hot products flow to the turbine, where the heat energy is converted to mechanical work by the turbine blades [29, 79]. Figure 2.6. provides a schematic diagram of this conceptual process in a gas turbine combustor.

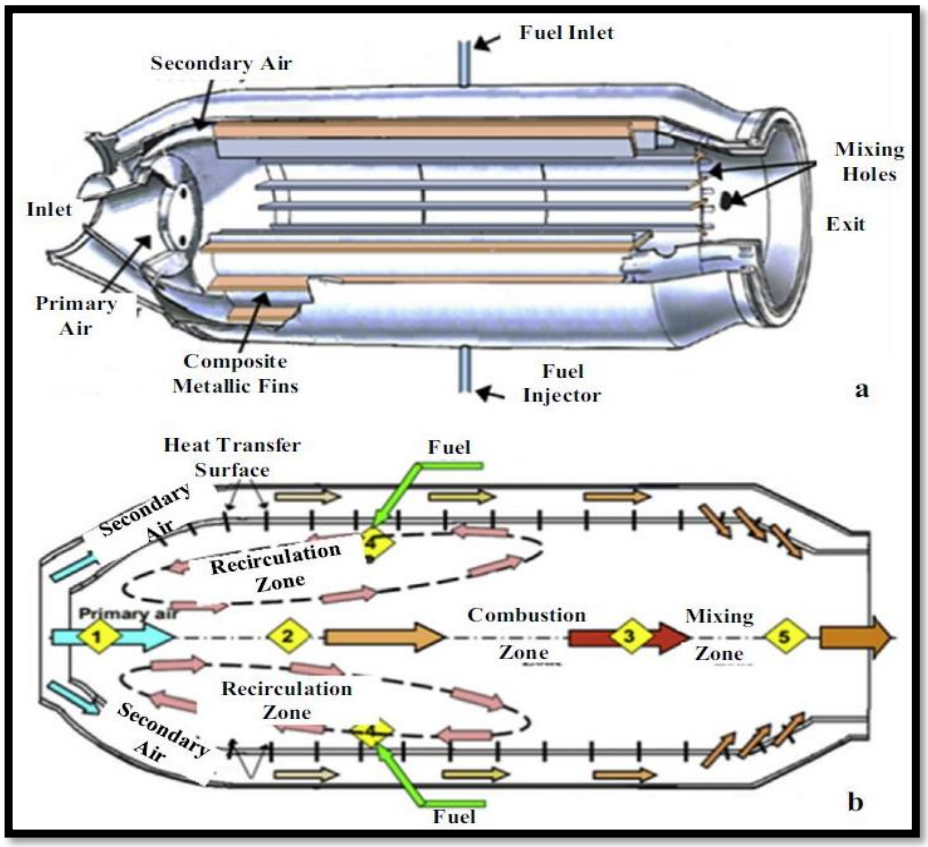

Figure 2.6 Schematic of gas turbine combustor [80]

(a) A cut-section of a combustion chamber and (b) main zones of a conventional combustor

2.3.1.1 **Combustor requirements**

The functions of the diverse combustor types available, such as annular, tube-annular and multi-can combustors (as shown in Figure 2.7) are to fulfil the following requirements that are essential for gas combustors to cover a wide range of applications effectively and efficiently [81]:

- High combustion efficiency with complete burning of a fuel-air mixture
- Combustion product temperature within the turbine design limit
- Minimising pressure loss and producing a low level of emissions
- Cost-effective with ease of maintenance procedures

2.3.1.2 **Requirement to work under diverse operating conditions**

In addition to meeting the requirements detailed in Section 2.3.1.1, the combustors are required to run under various conditions, such as running at ambient conditions, running with a range of fuel/air ratios and running with different types of fuel.

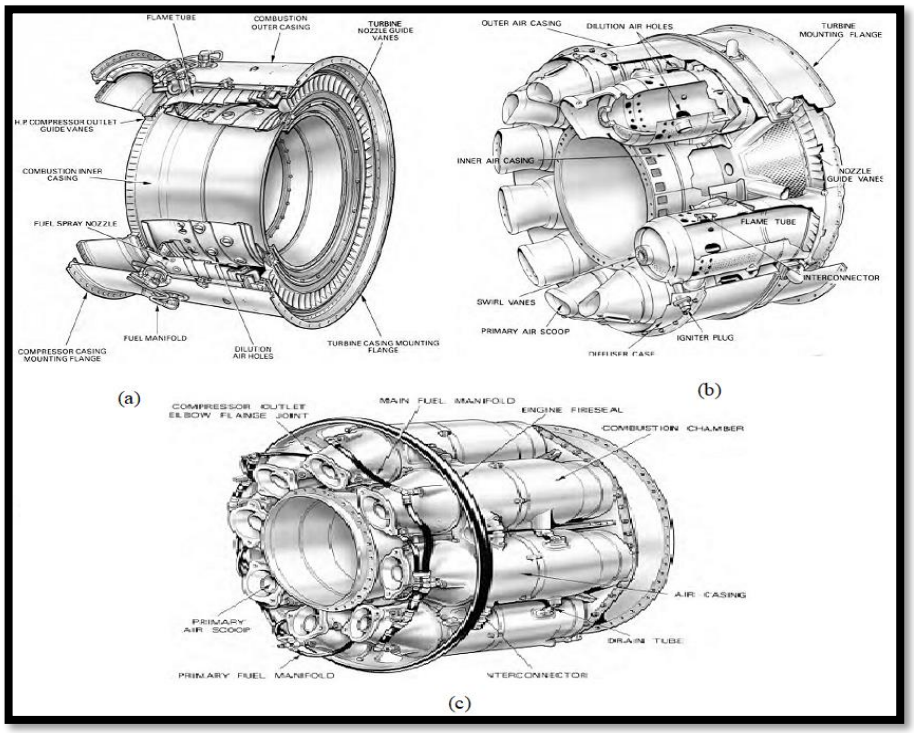

Figure 2.7 Different configurations of combustors [23] (a) annular, (b) tube-annular and (c) multi-can

2.3.1.3 **Combustion zone characteristics**

The geometries of gas turbine combustors are diverse, depending on their applications and operating conditions. A conventional gas combustor generally includes three distinctive zones, which are primary, secondary and dilution zones, as shown along with their common characteristics in Figure 2.8.

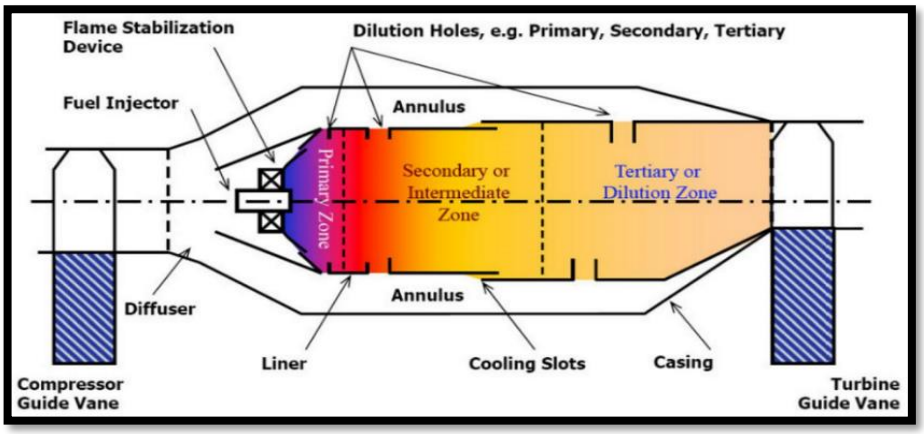

Figure 2.8 Main components of conventional combustor [82]

2.3.1.3.1 Primary zone

This zone aims to ensure achievement of complete combustion by providing the required conditions, such as adequate time, optimal temperature and correct amount of fuel-air mixture. In this way, a stable flame with low NO_x emissions is attained. Although different patterns, such as swirl configuration, can be utilised to achieve this goal, the main characteristic of the primary zone is an increased level of turbulence through the formation of a reversal of toroidal flow, which helps a portion of the burned gas to be recirculated. Consequently, the recirculation of the hot gas provides the conditions necessary for ignition of the unburned combustible mixture [82, 83].

2.3.1.3.2 Secondary zone (intermediate zone)

The function of this zone in the combustion process is to reduce primary zone temperature from a high level, at which dissociation reactions leading to the appearance of significant unwanted amounts of CO and H_2 occur, to an intermediate level by adding a small quantity of air. This additional air increases the efficiency of the combustion process by facilitating the complete burning of CO and other unburned hydrocarbons. This lessens the formation of pollutants and reduces their potential negative effects in the dilution zone by reducing the possibility of such pollutants passing from the secondary to the dilution zone [82, 83].

2.3.1.3.3 **Dilution zone**

The primary role of the dilution zone is to control the combustion temperature to ensure that its output stream provides the turbine with combustion products that fall within an acceptable temperature range, which is a known pattern factor. An additional role of this zone is to allow through air that remains after combustion and wall-cooling requirements have been fulfilled. In a conventional combustor, a diluted air stream enters the zone through holes that are designed and distributed to optimise penetration of air jets that enhance the mixing process with the mainstream, which helps to obtain high combustor performance [83].

2.3.2 **OF process in gas turbines**

OF combustion has attracted the attention of several power generation plants and research centres due to its potential to mitigate CO_2 emissions. Another benefit of this combustion technique is that it produces practically zero emissions of nitrogen oxides (NO_x).

In this technique, fuel is burned in an enriched oxygen domain that is devoid of nitrogen. However, this combustion process, which is almost at stoichiometric conditions, increases the combustion temperature and this can exceed the limit that major parts of the gas turbines, such as the nozzle guide vane, the turbine blades and their rotor, can withstand. Therefore, a mixture of H_2O and CO_2, which comprises the highest proportion of the exhaust gas, is recycled as a working fluid to limit the flame temperature, which affects the turbine inlet temperature (TIT) by keeping it within the level imposed by the turbine design. Compared with air, which is used in a conventional air combustion process and includes a high percentage of N_2, this mixture (H_2O and CO_2) has a higher heat capacity. Although the conventional combustion process produces high levels of NO_x products, this mixture has zero NO_x emissions. The water in this mixture can be extracted from the exhaust gas by a

condensation process, while a portion of the CO_2 in the exhaust gas can be recycled. The residual CO_2 could either be stored or transported [66, 84, 85].

OF combustion is one of the leading techniques integrated with the CCS system to capture CO_2 from gas turbines in power generation plants. To produce the oxygen required for the combustion process in this application, O_2 is obtained by an ASU, where nitrogen is separated from air using, for example, cryogenic or membrane-based processes. In addition to the CO_2 processing unit (CPU), the ASU could be considered the main additional energy consumption requirement for these plants. This energy could be required to be provided by the power plant, thus reducing the total efficiency of the power cycle [86, 87].

2.3.2.1 **Air separation unit for oxygen production**

The oxygen for the OF combustion process can be generated by an ASU, either by non-cryogenic systems, which are based on pressure swing adsorption (PSA) and membrane technologies or by cryogenic systems, as shown in Figure 2.9 [88].

The cryogenic system has the potential to produce a large amount of oxygen with the highest levels of purity. Nevertheless, argon cannot be separated in this process. Non-cryogenic systems are employed to produce lower quantities of the products, generally with minimal purities [89].

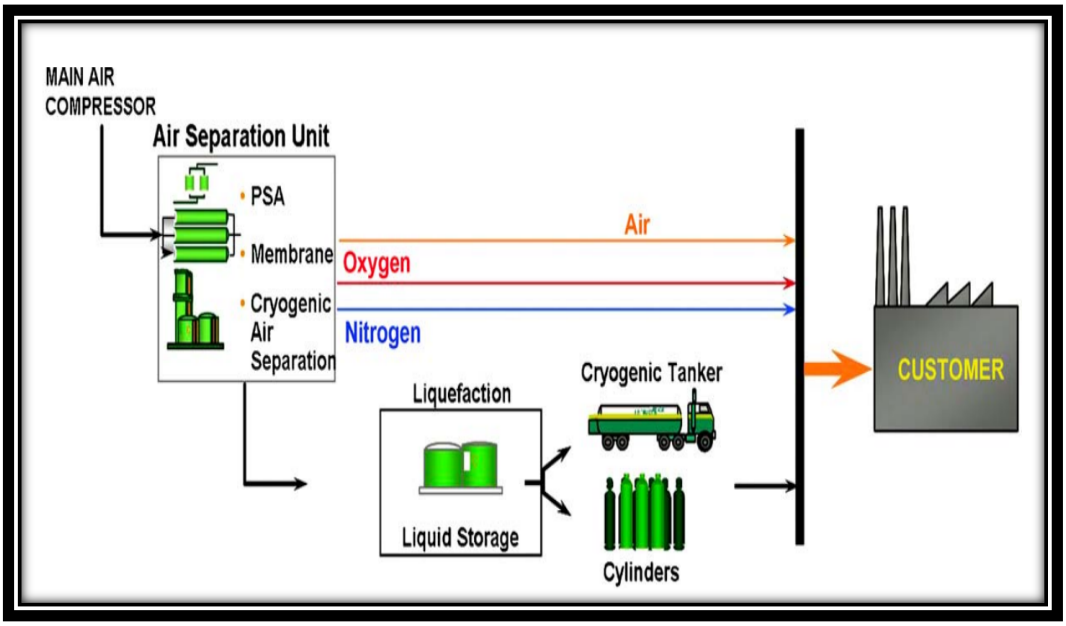

Figure 2.9 Three main systems for oxygen production [88]

2.3.2.1.1 Cryogenic industrial process

In this process, air components are separated using a condensation unit at a low temperature, which is obtained using a refrigeration system. Figure 2.10 shows that the cryogenic process uses two distillation columns. First, ambient air is compressed to 6-bar and pre-cooled through the main heat exchanger using the products of oxygen and both nitrogen and argon, which are considered as waste from this process [90]. The pressurised air is subsequently throttled, which decreases the air temperature to the liquefaction point of oxygen. This stream, consisting of liquid oxygen and gaseous nitrogen, is then directed to the first distillation vessel, which is called a high-pressure column (HPC). Nitrogen is boiled and discharged through the top of the HPC to the second distillation vessel, which is known as a low-pressure column (LPC), while the oxygen settles in the bottom of the HPC. Finally, the oxygen is depressurised and fed to the LPC, where large quantities of oxygen with around 99% purity accumulate with a low percentage of argon [91, 92].

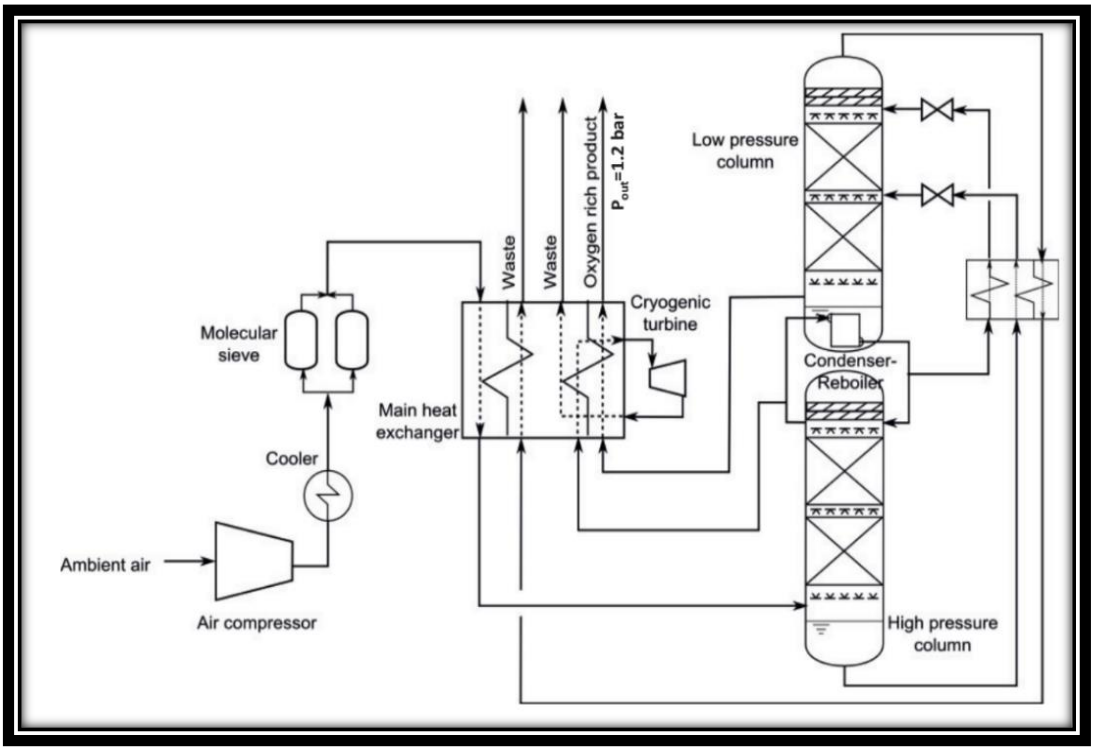

Figure 2.10 Schematic of cryogenic distillation ASU with two columns [90]

2.3.2.1.2 **Membrane systems**

Generally, membrane modules can be operated in four-end or three-end modes. In the first, which is called a high-temperature membrane air separation unit (HTM-ASU), a flue gas consisting of a high concentration of CO_2 is recycled and used as a sweep gas on the permeable (porous) side. Meanwhile, a vacuum pump is placed on the permeable side because there is no sweep gas process, as shown in Figure 2.11. This pump provides the differences in oxygen pressure through the membrane, which are necessary for the oxygen transport process in the three-end type [93, 94].

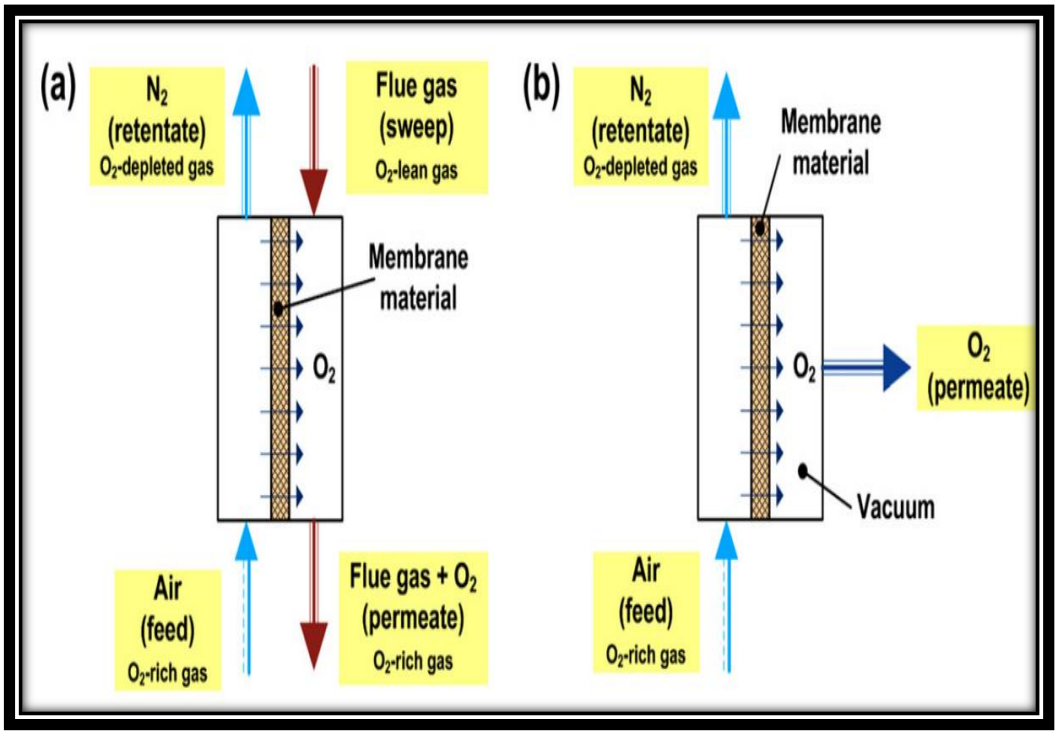

Figure 2.11 Membrane module in (a) four- and (b) three-end operation modes [93]

2.3.2.1.3 Pressure swing adsorption process

The PSA process is an established technique that is used to separate gas mixtures, such as nitrogen from air, using the differences in adsorption capacities between air components. In this process, ambient air is first compressed and is later fed to one of the two bed systems employed for the adsorption process [95], as shown in Figure 2.12.

Because oxygen is more strongly adsorbed than nitrogen, this leads the oxygen to pass through the bed, where it is then collected as a product. When the absorbent becomes saturated with the oxygen in this process, the second bed is pressurised to form the flow. Then, the feed of compressed air is stopped, which reduces the total pressure in the first bed and removes most of the adsorbate to re-pressurise it for reuse. Other technologies could be used for the separation of oxygen with high purity, such as temperature swing adsorption and vacuum swing adsorption (VSP) [96, 97].

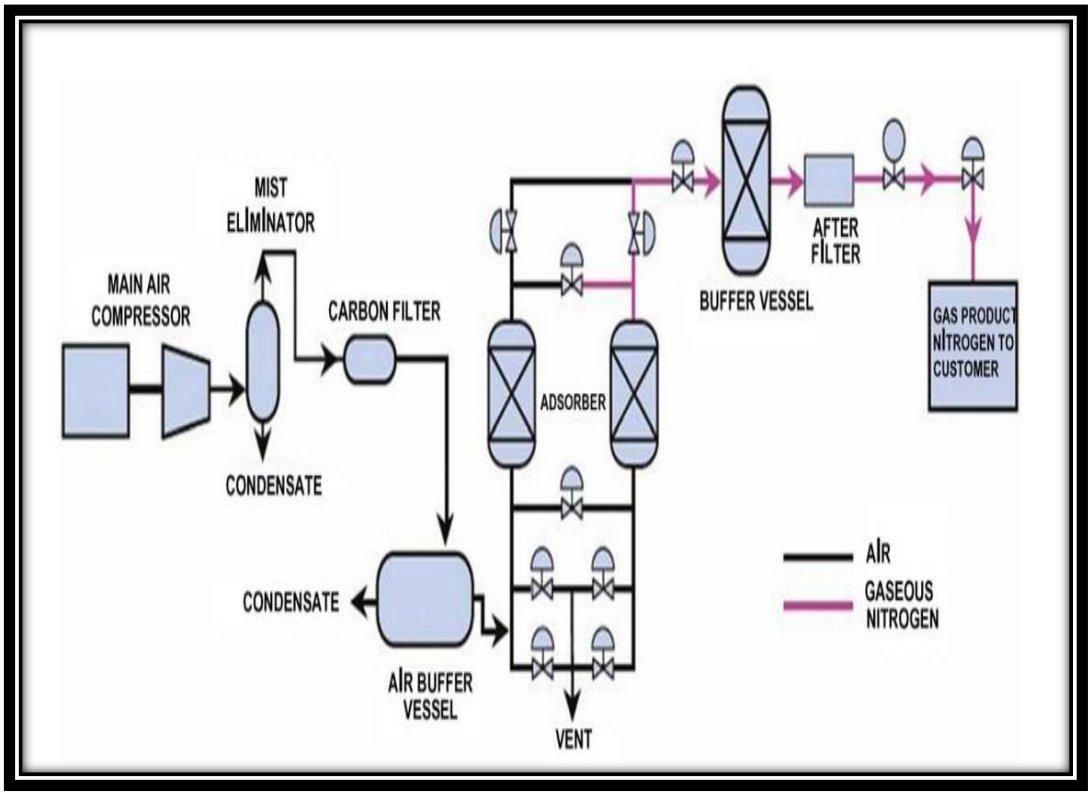

Figure 2.12 Nitrogen production process [88]

2.3.3 **Humidified gas turbine cycle**

The humidified power cycle is a new generation of a gas turbine. This configuration of the gas turbine consists of an intercooled compression process, heat recovery from the exhaust air, and a water recovery system. The basic concept of humidified gas turbines (HGTs) is that a water-air mixture is used as a working fluid in these cycles. This increases the mass flow rate in the cycle while the compressor work remains the same [98].

HGTs allow a rise in both the specific output power and the total efficiency to be achieved. Additionally, the injection of hot humid air into the combustion chamber reduces the NO_x emissions that have a direct impact on environmental deterioration. The capital cost of HGT cycles is comparable with the cost of gas/steam cycles. In addition, the efficiency of these cycles can be improved by humidifying the compressed air [99, 100]. However, this improvement in the overall performance of gas turbine cycles is limited due to the challenge

of a flame blowout with its system shutdown consequences [101]. The HGT cycle has several different configurations, such as a humid air turbine (HAT) or EvGT, and a gas turbine with water injection.

2.3.3.1 **EvGT**

The principle of the EvGT, which is a type of HAT, is that water is injected into the combustor where, due to the evaporation process, it increases the mass flow rate through the turbine. Therefore, the specific power output of the turbine rises while the compressor work remains constant.

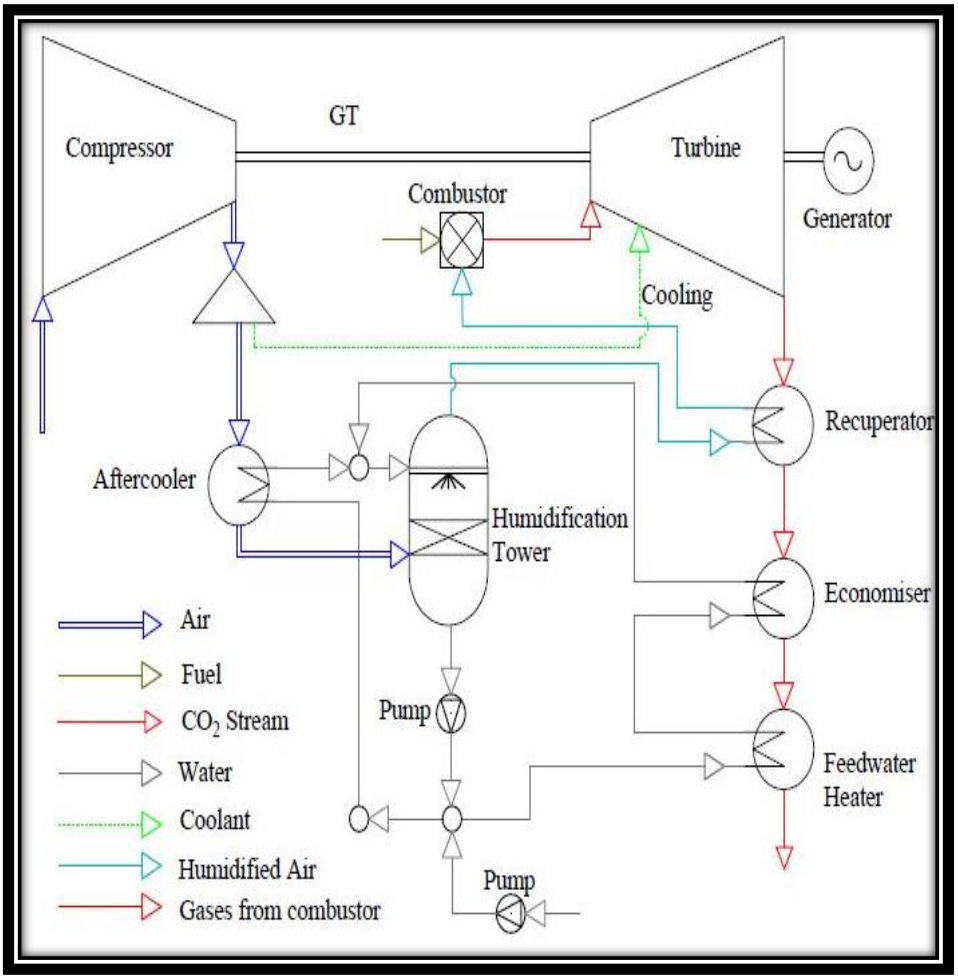

Figure 2.13 Schematic diagram of EvGT cycle [102]

As illustrated in Figure 2.13, the temperature of the water is increased to near saturation point by the exhaust gas passing through both an economiser and feed water heater on one

side, and by compressed air crossing through an aftercooler on the other side. This heated water flows in a counter-current to the compressed air in a humidification tower and heat exchange between both currents occurs. Consequently, part of the water is evaporated (correlating to the partial pressure of the water in the mixture) by the heat released when the hot water is cooled at the bottom of the tower. Meanwhile, the compressed air is heated and humidified at the upper end of the tower [103, 104].

2.3.4 **Use of alternative gases as working fluids**

Gas turbines operate on the Brayton cycle (as presented in Section 1.6) to produce mechanical work. These engines can be classified according to the path of gases in: (a) an open cycle, (b) a closed cycle and (c) a semi-closed cycle. NG is considered to be the cleanest type of fossil fuel and it will likely continue to be one the main heat sources for all gas turbine cycles, particularly closed cycles where the exhaust gas is recirculated. Therefore, innovative technologies have started to utilise alternative gases as working fluids, such as supercritical-CO_2 (S-CO_2), helium or other noble gases, to replace the air in the combustion process of closed cycle gas turbines with the goal of improving efficiency. The closed Brayton cycles (CBC) running with one of these alternative gases as a working fluid are characterised by their high efficiency achievement in comparison with a conventional air cycle at a high inlet temperature. Additionally, these closed cycles can be run with a high-pressure range similar to an open gas turbine cycle, which usually runs with a smaller pressure ratio [105].

2.3.4.1 **CO_2 Allam cycle**

The Allam cycle uses CO_2 at a high percentage (around 95%) as a working fluid in a gas turbine cycle to reduce the capital cost of clean electricity production from fossil fuels. This cycle employs the integrated OF combustion technique with high-pressure S-CO_2 as a working fluid. In this combustion process, both fuel and oxygen make up only 5% of the

mass flow rate in the combustor while CO_2 is a recycled product and makes up the highest percentage. The CO_2 stream restrains the combustion temperature within acceptable levels and produces significant amounts of heat, which is recovered in the cycle.

Thus, there is less need for oxygen and its requirements, such as a cryogenic ASU, in the combustion process. By overcoming the main obstacle to using OF in electricity generation plants, the Allam cycle provides a practical and feasible technique for using the OF process in the power industry while producing approximately zero CO_2 emissions [106].

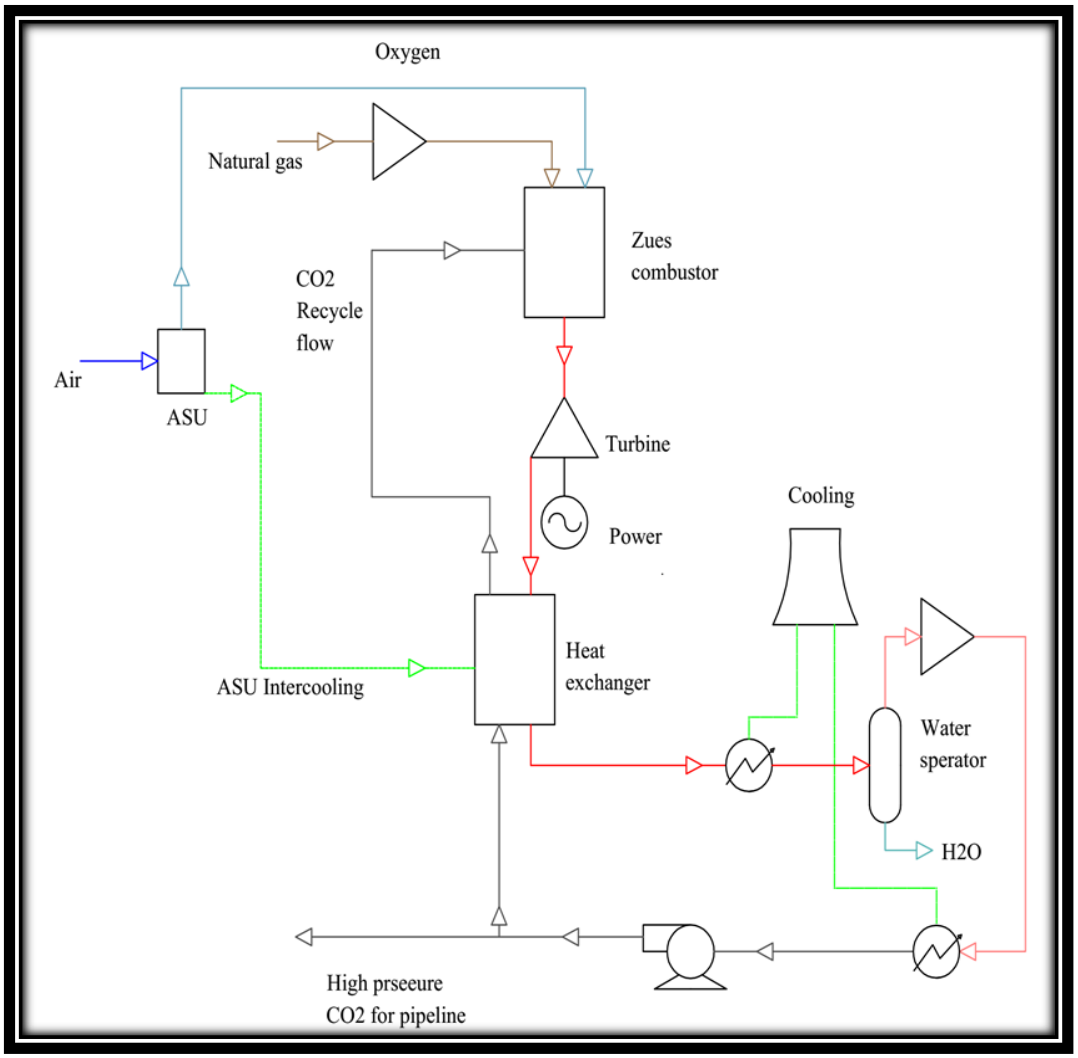

Figure 2.14 Allam cycle with NG

The schematic diagram in Figure 2.14 shows that the Allam cycle uses NG as a fuel. First, the high proportion of CO_2 at high pressure and temperature directed to the combustion

chamber serves to dilute the combustion products that dominate the TIT. Next, the turbine exhaust gas passes through an economiser where heat is exchanged between the exhaust stream and CO_2, which is retained in the cycle. The exhaust gas is then cooled by air- or water-cooling system while the water separator unit extracts water from hydrogen or moisture. Finally, the remaining stream contains approximately 90% CO_2. This is then compressed to the required high pressure and again passed to the economiser, where the CO_2 stream is heated to the required high temperature. The stream is then recycled [107, 108]. However, using S-CO_2 as a working fluid in gas turbines leads to a greater corrosion problem than with inert gases. In addition, components developed specifically for the gas turbine cycle are required and limited innovative designs are available to work at the required operating conditions of the cycle [105].

2.3.4.2 **Helium**

Practically, helium has been considered to be a desirable working fluid due to its specific heat ratio (1.667), which is higher than air (1.4). This leads to the achievement of considerably higher efficiency in power generation plants based on CBC as a replacement for a conventional air open cycle. Use of the non-corrosive inert gas helium in the CBC also enhances the heat exchange process through the cycle due to its heat transfer coefficient, which is also higher than air. Therefore, a range of CBC configurations of power conversion units utilise helium as a working fluid, as indicated in Figure 2.15, instead of air in such applications [55, 109].

Compressed helium with a high temperature flows from the reactor core and enters the turbine to produce mechanical work that is used to drive a generator which produces electricity for a grid.

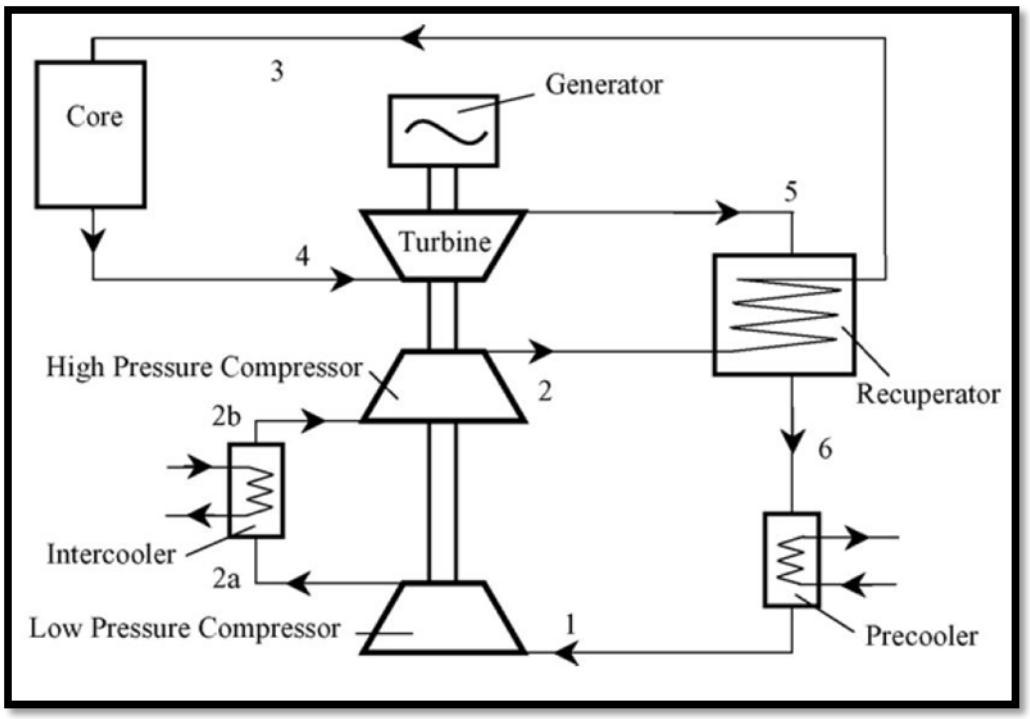

Figure 2.15 Schematic layout of CBC running with helium [110]

A low percentage of this work produced by the turbine is also used for the helium compression process through the compressors. The high-pressure helium from a high-pressure compressor (2) exchanges heat with exhaust helium expanded in the turbine. Therefore, the temperature of this low-pressure exhaust helium is reduced after passing through the recuperator and the precooler. This low-pressure and low-temperature helium is then compressed by two intercooled compressors to produce high pressure-low temperature helium that enters the recuperator to be preheated.

This high-pressure and high-temperature helium then flows to the reactor core to be heated and used in the turbine and the thermodynamic cycle is repeated [110]. However, using helium as a working fluid in the CBC leads to a high TIT, which could cause damage to turbine parts. Consequently, a new turbomachinery design that provides a high-temperature limit is required. Additionally, the low molecular weight of helium, which is 4.002g/mole, results in unique requirements in terms of the design characteristics of helium gas turbines, such as a short blade height with a high number of stages in comparison with a conventional

air turbine. Consequently, this intensifies the leakage problem through the CBC, leading to overall efficiency reduction [109, 111].

2.3.4.3 **Argon**

The inert gas argon has one of the highest relative concentrations in air, after nitrogen (78.09%) and oxygen (20.95%), with a proportion of 0.93 % by volume. As mentioned in Section 2.3.2.1.1, argon is generated through the cryogenic unit used to separate oxygen from air due to its condensation temperature of 87.3 K being very close to that of oxygen, which is 90.18 K, at atmospheric pressure. Thus, the production process for argon is considered comparatively inexpensive compared to production processes for other noble gases, such as helium. In addition, the temperature flame limit with argon is notably lower than with helium and the molecular weight of argon, which is 39.94 g/mole, is considerably higher than helium. Therefore, modification of turbomachinery is not required in the case of using argon as a working fluid [57, 112].

2.4 Combination of OF technologies

2.4.1 EvGT with OF combustion with recycled exhaust

A system diagram of the EvGT cycle integrated with the OF technique is shown in Figure 2.16. Practically, the recycled exhaust gas system has two different configurations. The dry system includes a condenser and is represented as being more stable than the second system, which does not use a condensing unit. In the second system, water vapour is condensed as an exhaust gas is directed to it. Consequently, CO_2 in the exhaust is separated from the water vapour. A portion of the CO_2 at the exit of the condenser is sequestrated for storage purposes while the greatest fraction is recycled, mixed with oxygen, and then compressed. The compressed stream is next divided into two unequal fractions.

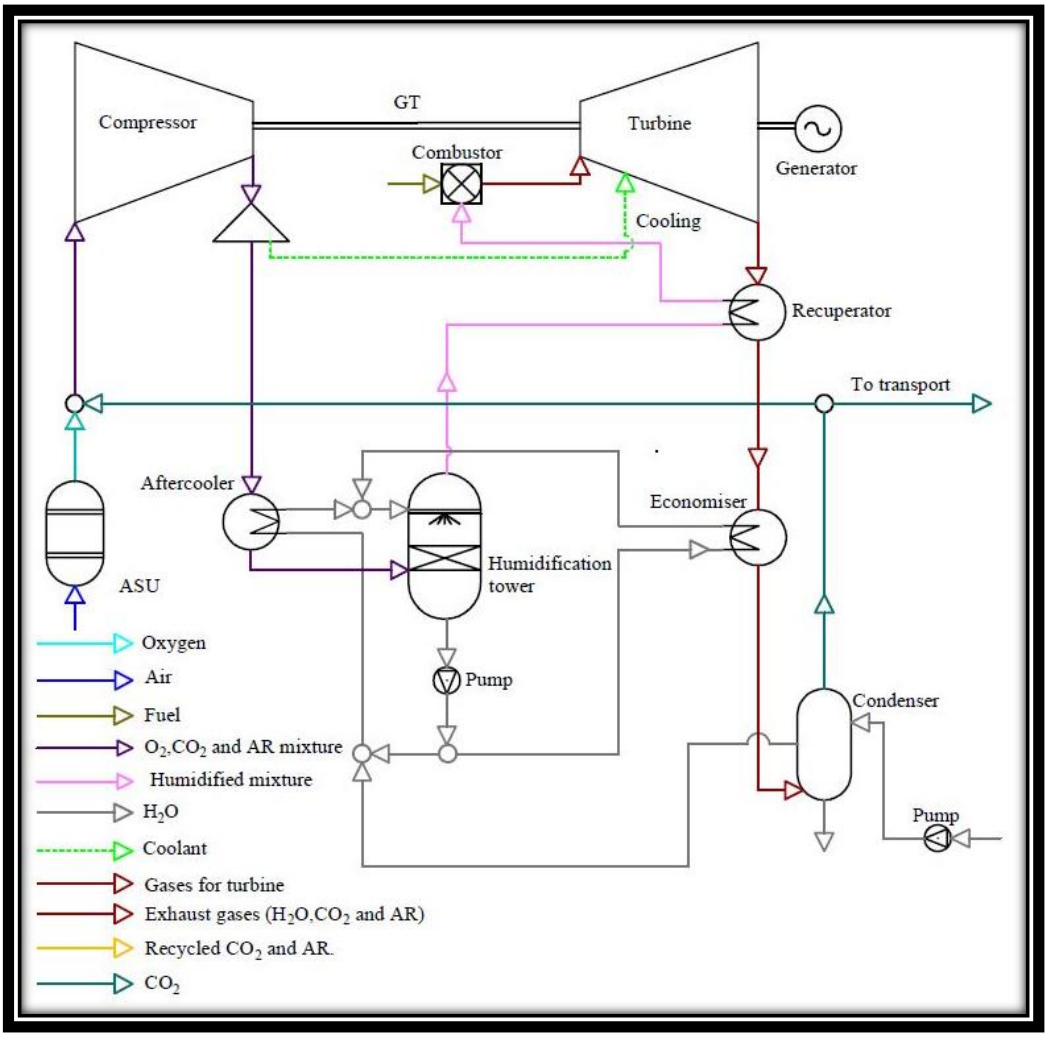

Figure 2.16 Schematic of the EvGT integrated with OF combustion [102]

A smaller fraction is used for turbine cooling, while the larger fraction is first routed to the economiser to exchange heat with the exhaust gas. It is then humidified in a humidification tower and is finally heated further in a recuperator before being fed into the combustor [17, 102].

2.4.2 EvGT OF with Ar

As previously discussed, much progress has been made in improving NG-fired turbine efficiency through the use of alternative gases as working fluids. Due to its inherent advantages compared to air, including a higher specific heat ratio and a higher heat transfer coefficient, helium has been the main focus of research and development as a working fluid.

However, there are issues inherent to the use of helium in the industrial gas turbine combustion process that result in its use remaining problematic, including high TIT potentially causing damage to system parts and its low molecular weight requiring system design modifications.

Using argon as an alternative working fluid has the potential to maintain or exceed the efficiency gains achieved through the use of helium, while avoiding its main problems. First, argon's relatively high concentration in air, together with its very similar condensation temperature to oxygen, makes it cheaper to produce than helium. Second, its significantly lower temperature flame limit compared to helium reduces the potential for damage to system parts. Finally, argon's molecular weight is significantly higher than that of helium, which means that the time, expense and other issues connected to modifying the system's turbomachinery are avoided. Despite these clear potential advantages, argon has not yet been investigated as an alternative working fluid for an industrial gas turbine. As a result, this study proposes using argon as part of its novel combined approach to the cycle.

Figure 2.17 illustrates the cycle that is proposed to run with the novel blend CARSOXY as a working fluid with methane. This novel gas mixture represents a combination of technologies, using CO_2, Ar, H_2O and the OF technique to replace air as an oxidiser in a conventional humidified cycle.

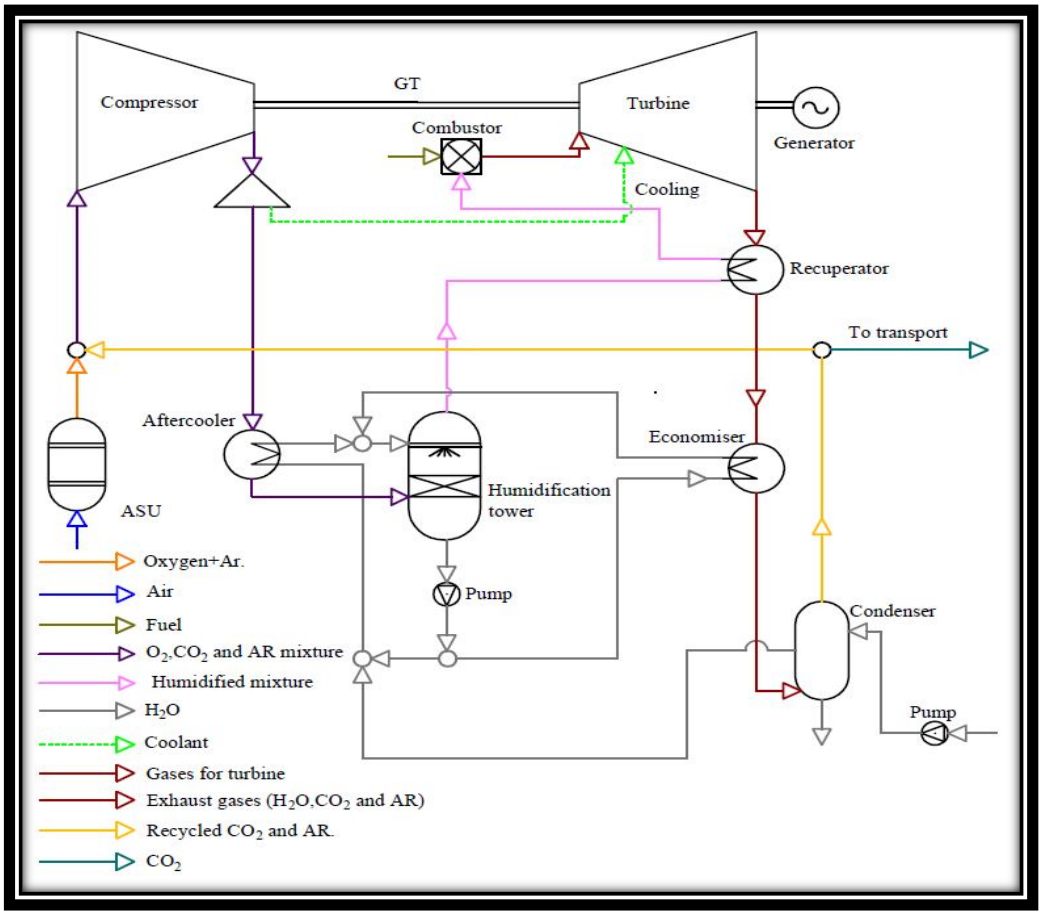

Figure 2.17 Diagram of proposed EvGT integrated with OF and recycled argon with CO_2 [113]

Oxygen and argon, which are generated from the ASU, are compressed with CO_2, which is recirculated from the condensation process of exhaust gas. A low portion of water vapour is injected into a gas combustor to increase the mass flow rate, which enhances gas turbine performance. A higher portion of water vapour is used for the cooling process. The inert gas argon, which is also recirculated with CO_2, is used with this combined mixture due to its specific heat ratio, which is higher than air [113].

2.5 Combustion modes

2.5.1 Combustion mixing techniques

In general, the combustion mixing process in gas turbine burners can be divided into two main types:

2.5.1.1 **Premixed flame**

In this type, the gaseous fuel and oxidiser are molecularly mixed at ambient temperature before the unburnt mixture is delivered to the flame zone, with the aim of improving the mixing process between the oxidiser components. A chemical reaction occurs as the unburnt mixture approaches the flame front, which gradually heats the mixture adequately by conduction and radiation.

Consequently, the structure of the premixed combustion mode and flame speed, which is the critical factor in the combustion process utilising this flame mode, can be influenced by balancing the heat transfer in the reaction zone with the chemical reaction. The major problem is that the flame propagation speed can exceed desired levels, even the local speed of sound in some cases, resulting in an explosion in the system [114, 115].

2.5.1.2 **Non-premixed or diffusion flames**

In this type, the gaseous fuel and oxidiser are injected from separate nozzles into the reaction zone, where the reactants are mixed at the level of molecules by convection and diffusion before burning takes place. Therefore, diffusive flames can be characterised by their high stability compared to those produced using the premixed approach described above, which is due to the burning rate depending on the injection and mixing process rather than on chemical kinetics.

Additionally, in the diffusive burning mode, the fuel and oxidiser are not initially mixed before burning and thus the risk of explosion due to unexpected combustion is minimised. Due to the greater stability and safety provided, a non-premixed burning mode is utilised in a wide operating range of industrial and commercial gas turbine combustors, such as those used by aircrafts and spacecraft [116-119]. However, soot particles emitted from non-premixed systems, where there is an inadequate concentration of oxygen in the oxidiser flow

to burn the fuel completely, have been identified as a major undesirable combustion product that increases man-made emissions into the atmosphere [120-122].

Adding CO_2 to the fuel or the oxidiser has been shown to reduce the formation of soot particles in several studies [123, 124]. Oxyfuel combustion, which employs CO_2 to control the combustion temperature, has been proposed as one of the developed techniques that could be used in non-premixed burning modes to lessen soot by recycling it in the diffusion flame and eliminating NO_x products due to the absence of nitrogen from the oxidiser [85, 125].

The non-premixed flame mode has been employed in the gas turbine combustor by some well-known studies to prevent unstable flames and other complex undesirable phenomena. One such phenomenon is known as a flashback, which represents the main drawback of premixed systems. This occurs when the velocity of the flame is higher than the velocity of the flow, which could propagate the flame upstream to the premixing zone from the combustion region, causing the engine to explode [126-128].

2.5.1.3 **Swirl burners**

Swirl is a technique that is widely employed in burners to stabilise the flame in the combustion process of fossil fuels used by diverse industrial applications, such as gas turbine combustors, petrol and diesel engines, boilers and furnaces. In brief, the mechanism provides a swirling flow that aerodynamically creates a Central Toroidal Circulation Zone (CRZ), which helps to accelerate heat transfer and recirculate active chemical species close to the exit of the nozzle.

This increase flame stability in gas combustors while reducing emissions. Figure 2.18 illustrates the CRZ formation mechanism in a swirling flow regime. By contrast, indirect burners, which are also known as tangential burners, the fuel and the oxidiser flow in parallel

with each other. Owing to the swirling mechanism, swirl systems are characterised by their relatively low velocity, which leads to flame stability and addresses the flashback issue in premixed systems by allowing matching of local flow velocity to flame speed. In addition, in the non-premixed technique, the swirling flow significantly increases the flame stability limit and greatly increases blowout limit in some cases. NO_x has also been demonstrated to be reduced using swirl technology [129-131].

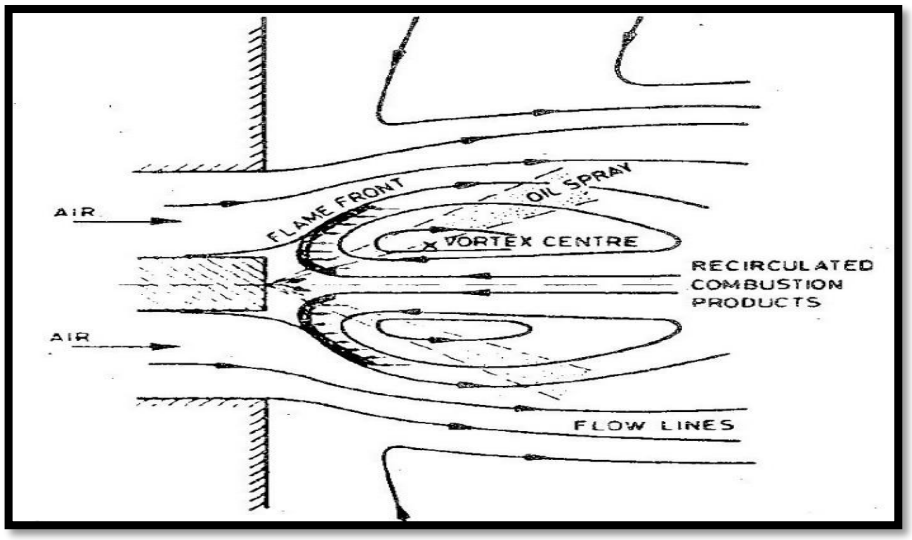

Figure 2.18 Formation of CRZ in swirl burner [132]

Various swirl configurations and their characteristics are indicated in Table 2.2.

Table 2.2 Characteristics of different swirl configurations [133]

	Vaned		Tangential		
Type	Straight	Profiled	with radial entrance	Moveable block	Scroll
1	Ease to manufacture and install	Difficult blades to manufacture	Ease to manufacture	Ease to varied	Ease to manufacture
2	Low efficiency	High efficiency 70%	High efficiency 70%-80%	High efficiency 60%-70%	Efficiency= 47%
3	High loss coefficient	Low loss coefficient	Low loss coefficient	Low loss coefficient	Low loss coefficient

Combustion instabilities in this type of burner are considered to be one of the major problems that could cause enormous damage to burners used in a variety of gas turbines, as shown in Figure 2.19, or in other combustion systems in diverse applications, such as liquid or solid rocket engines, boilers and furnaces.

This problematic phenomenon occurs inside a combustion chamber when pressure fluctuation and heat release rate are in phase. Flame blowoff, or flashback, and low-lifetime combustor reliability represent the main consequences of the instability phenomenon [134].

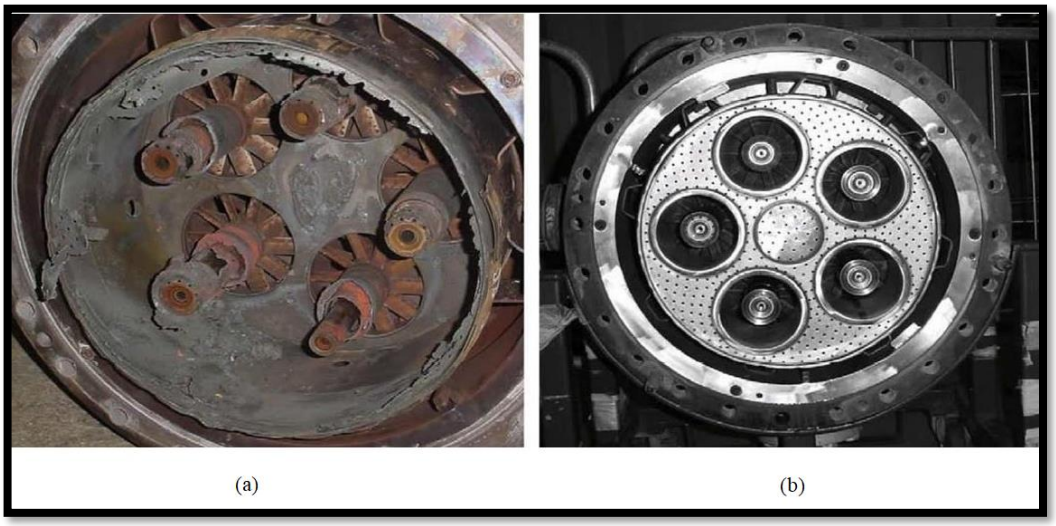

Figure 2.19 Comparison of two gas burners: (a) damaged burner (b) newly-assembled burner [135]

Flame instability in these burners is caused by an unsteady flow which could generate a high magnitude of pressure waves inside the combustion chamber. This then interferes with the heat release rate, which causes velocity fluctuations, thus closing the feedback loop [136, 137], as depicted in Figure 2.20.

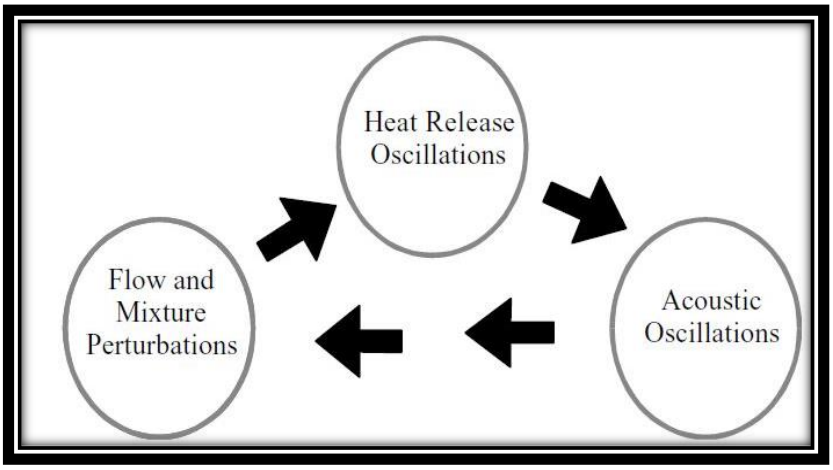

Figure 2.20 Illustration of feedback loop responsible for combustion instabilities [138]

Blowoff, which is also known as lift-off, represents one of the combustion characteristics that can directly impact on flame stability in swirl combustors working under different operating conditions. Blowoff is a phenomenon which occurs due to a mechanism present in both non-premixed and premixed systems. This mechanism results from an imbalance between heat released by reactants and supplied to the unburned reactants from the CRZ [139-141].

A similar phenomenon has been identified in a non-premixed flame, where the local flow velocity is higher than the local flame speed. This leads to the flame physically detaching from the bluff-body mouth and stabilising downstream. The distance between the base of the lifted flame and the mouth of the burner rim is known as lift-off height, as indicated in Figure 2.21. Additionally, lift-off velocity is described as the velocity at which blowoff occurs. Lift-off height increases and the flame moves further downstream when the flow velocity value attains its highest value. Consequently, the flame is extinguished in a phenomenon that is known as a blowout situation [142-144].

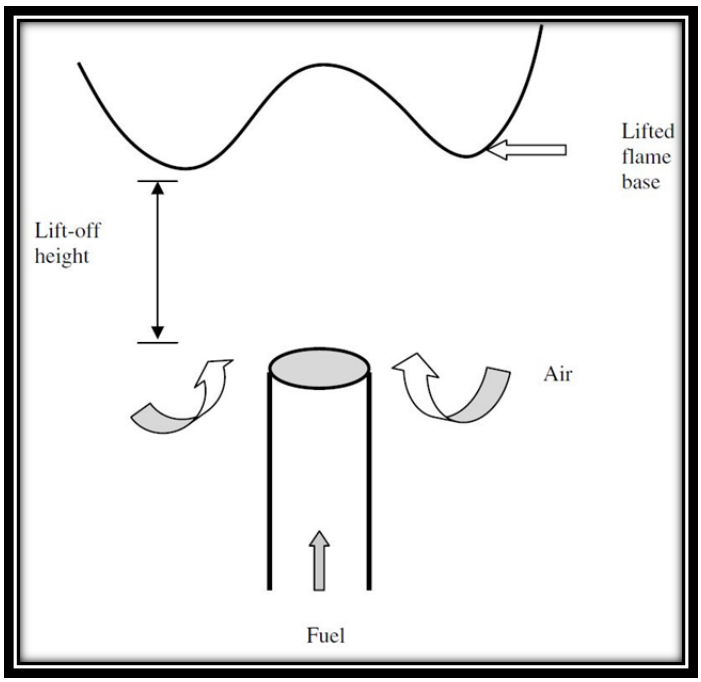

Figure 2.21 Lifted flame in non-premixed mode [145]

Experimental and theoretical studies have shown that blow off is influenced by different parameters. For example, lift-off height correlates linearly with increasing lift-off velocity. However, this distance is inversely affected by heightening flame speed, which also depends on fuel type.

Other research has shown that non-premixed flame modes running with an oxygen-enriched atmosphere extend the flammability boundaries and heighten the chemical reaction rate, which increases the flame velocity. Therefore, flames produced in oxyfuel burners are characterised by higher stability compared with those produced in a conventional air environment. In addition, oxyfuel-produced flames remain attached to the burner mouth [146-148].

2.6 Efficiency of gas turbine cycle

The formulae that are used to calculate and model the relevant outputs and efficiencies in gas turbine power plants are presented in Appendix 1, which contains the equations that are

used to calculate the output power and efficiency of a gas turbine. It also shows the calculations for heat capacity and the specific work required for the compressor [25, 149]. These equations were used in the new numerical model to calculate the gas turbine's efficiency and to compare the air and the proposed CARSOXY blend processes.

2.6.1 **Air standard efficiency**

For air standard analysis, $m_1 = m_3$, as shown in the Appendix 1, whereas in an actual cycle

$m_3 = m_1 + m_f$, in open gas turbine

Where the fuel's calorific value is CV, heat is added in air standard cycle

$Q_{in} = m_1 . (h_3 - h_2)$, Whereas $Q_{in} = m_f \times CV$ for an actual cycle

Network = $W_T - W_C$ Eq. (2.1)

$$W_{net} = \{m_3(h_3 - h_4) - m_1(h_2 - h_1)\} \quad \text{Eq. (2.2)}$$

Air standard efficiency for a Brayton cycle:

$$\eta_{Brayton} = \frac{W_{net}}{Q_{in}} = \frac{m_1\{(h_3 - h_4) - (h_2 - h_1)\}}{m_1(h_3 - h_2)} \quad \text{Eq. (2.3)}$$

$$\eta_{Brayton} = \left\{1 - \frac{(h_4 - h_1)}{(h_3 - h_2)}\right\}$$

as, $(h_4 - h_1) = C_p (T_4 - T_1)$ and $(h_3 - h_2) = C_p (T_3 - T_2)$

$$\eta_{Brayton} = \left\{1 - \frac{(T_4 - T_1)}{(T_3 - T_2)}\right\}$$

$$\frac{T_2}{T_1} = \frac{T_3}{T_4}$$

$$\frac{T_4}{T_1} = \frac{T_3}{T_2}$$

$$\frac{T_4 - T_1}{T_1} = \frac{T_3 - T_2}{T_2} \equiv \frac{T_4 - T_1}{T_3 - T_2} = \frac{T_1}{T_2}\left(\frac{\frac{T_4}{T_1} - 1}{\frac{T_3}{T_2} - 1}\right) = \frac{T_1}{T_2}$$

$$\frac{T_4 - T_1}{T_3 - T_2} = \frac{T_1}{T_2} = \left(\frac{P_1}{P_2}\right)^{\frac{(\gamma-1)}{\gamma}}$$

Making substitution for Brayton cycle efficiency:

Making substitution $\left\{\frac{(T_4-T_1)}{(T_3-T_2)}\right\}$ for Brayton cycle efficiency:

$$\eta_{Brayton} = \left(1 - \frac{T_1}{T_2}\right) = 1 - \left(\frac{P_1}{P_2}\right)^{\frac{(\gamma-1)}{\gamma}} = 1 - \frac{1}{\left(\frac{P_2}{P_1}\right)^{\frac{(\gamma-1)}{\gamma}}} = 1 - \frac{1}{r^{\frac{(\gamma-1)}{\gamma}}}$$

$$\eta_{Brayton} = 1 - \frac{1}{r^{\frac{(\gamma-1)}{\gamma}}} = \quad \text{Eq. (2.4)}$$

As a result, it can be seen from the expression above that the efficiency depends only on pressure ratio (r) and specific heat ratio (gas nature) (γ).

For a particular gas, its efficiency value is heightened with increasing pressure ratio and for the unity pressure ratio the efficiency equals zero. Figure (2.22) illustrates the variation of efficiency with the pressure ratio for both air ($\gamma = 1.4$) and argon as a monatomic gas ($\gamma = 1.667$).

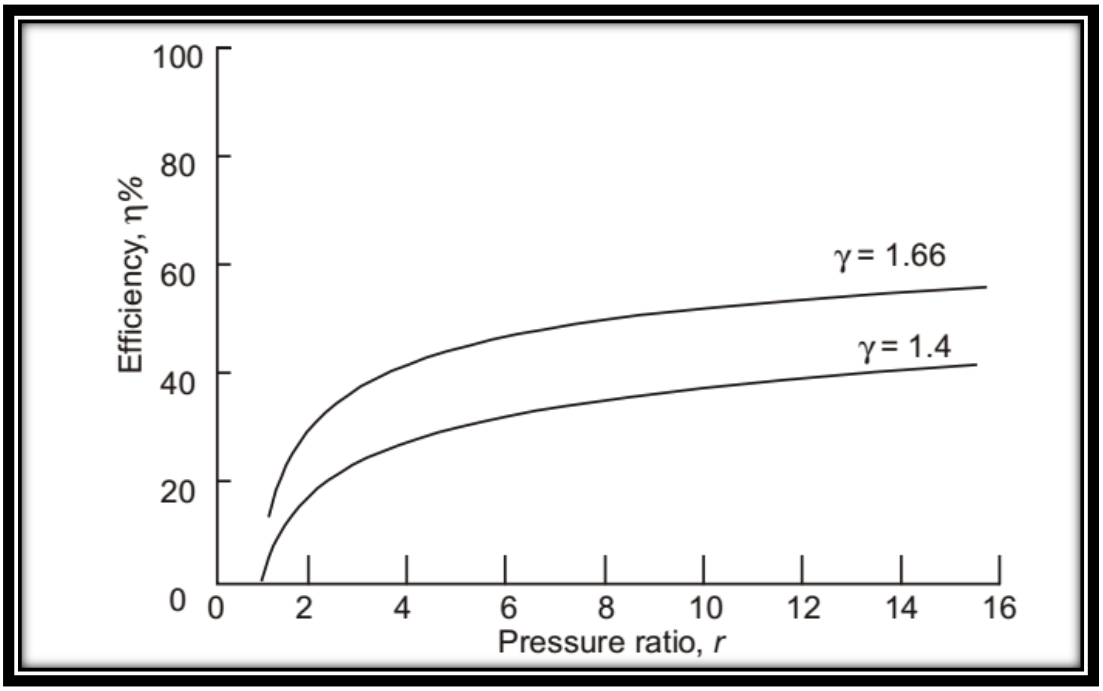

Figure 2.22 Efficiency vs. pressure ratio in simple cycle [149]

2.7 Summary

This chapter has described how CCS is one of the most promising technologies to address the problem of CO_2 being emitted from power generation stations that burn fossil fuels. The basic concept of this technology is that CO_2 is captured from abundant sources and deposited into a secure repository, such as underground, to maintain a clean environment. As NG dependency increases, the importance of gas turbines to the power sector also continues to rise. Therefore, it is necessary to develop approaches which reduce gas turbines' emissions of harmful pollutants and improve their performance while allowing them to fully service the increasing demand for electricity. Development and use of an alternative mixture of gases as working fluids - notably for this study, argon - and mixing of combustion techniques have been shown to be effective or potentially effective paths towards achieving this aim.

In terms of mixed combustion techniques, non-premixed systems utilising swirl burners have been demonstrated to be safer and more stable than premixed alternatives. However, the

likelihood of encountering blowoff and blowout situations represent a significant drawback to the use of such approaches. The use of OF combustion, which can be combined with CCS to enhance the combustion efficiency for the power cycle, has been shown to help significantly in addressing this issue.

In this method, fuel is burned in a high proportion of oxygen, and the exhaust gas, consisting of high concentrations of CO_2 and H_2O, can be recycled. This technique may be employed in gas turbine cycles that are used in the power production sector to mitigate CO_2 emissions. NO_x emissions are also reduced and this helps to prevent the damage that is currently being caused to the global environment. However, the main challenges of using this approach are the added energy consumption in the ASU and its effect on the flame temperature. These two issues reduce the efficiency of the gas turbine, which is considered a disadvantage of employing OF in gas turbines.

Therefore, water injection into the combustion process is needed to control the flame temperature. The EvGT cycle is proposed as one of the categories of the HAT cycles that can be integrated with both OF combustion and the recycling of CO_2 first proposed in the Allam cycle. In such an integrated cycle, a water-air mixture is used as a working fluid to enhance the turbine performance by maintaining the flame temperature within tolerance levels and increasing the mass flow rate.

This could provide a short-term solution for mitigating CO_2 emissions while using fossil fuels in the power industry, while providing improvements in output, efficiency and stability. The next chapter will describe the methods utilised to set up the specific theoretical and experimental work necessary to this study.

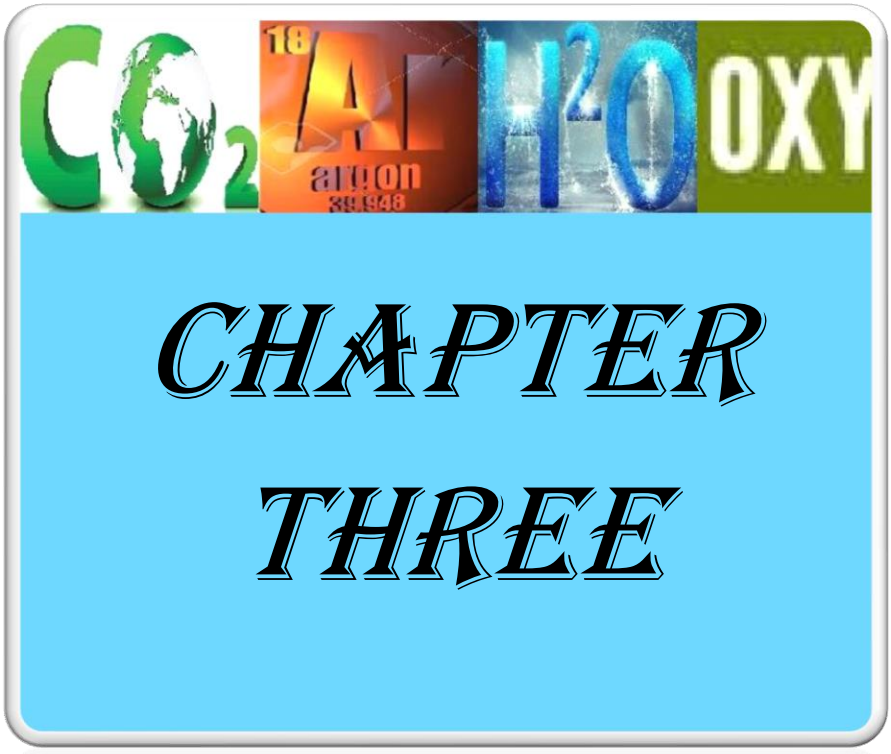

CHAPTER THREE

Chapter 3 Methodology

This chapter presents the theoretical and experimental methods that have been used in this study, taking into account the relevant literature from the review. This chapter will describe the procedures for the theoretical methods that are used to guide the investigation towards indicating the optimum CARSOXY blend. The experimental procedure that was employed to investigate the proposed blend's potential use as a reliable and feasible replacement for air as a working fluid in an industrial gas combustor is also illustrated. The data gathered from the procedures outlined in this chapter will be presented and analysed separately in Chapters Four, Five and Six.

This chapter is divided into four main sections: theoretical setup, new numerical model, Aspen Plus setup and experimental setup. In the first section, all of the software programs (i.e. Gaseq, Minitab and Chemkin-Pro) that were used to generate 120 potential blends to identify the optimum blend possessing similar characteristics to air as a working fluid for use as an alternative to air in industrial gas combustors are detailed and their use in this study is explained. The second section describes the numerical approach that is used to calculate the performance of an industrial gas turbine running with the proposed novel blend, which enables a comparison with the performance of air as a working fluid under the same conditions.

The third section details and explains the use of Aspen Plus to simulate the performance of the proposed cycle using CARSOXY as a working fluid for comparison with the conventional air cycle and to calculate the efficiency for both cycles to simulate employment of the CARSOXY blend as a working fluid compared with air in a gas turbine combustor in the proposed cycle. The experimental rig, measurement instruments and the procedures for installing and using them are then detailed in the fourth section. Some experimental testing was vital, both to ascertain that the novel blend provides flame ignition and to experimentally

measure emissions of exhaust gases and flame stability, which enables a comparison with the conventional air flame at the same running conditions. Next, chemiluminescence analysis and its relevance to this study are detailed, along with the devices and instrumentation necessary for providing chemiluminescence and emissions data. Finally, a summary of the study's research methodology is provided.

3.1 Theoretical setup

3.1.1 Details of the computer programs used for blend selection

3.1.1.1 Gaseq

The Gaseq chemical program, which can be used on Windows 2000 and XP, was created using the method defined by Gordon and McBrige for NASA to calculate compositions at equilibrium conditions. The Gibbs free energy equation for *n* species is included here because chemical reaction products in the Gaseq program were calculated according to this equation Eq (3.1) [150]:

$$\frac{G}{RT} = \sum_{i=1}^{nSp} \left(\frac{x_i \, \mathrm{G}_i^o}{RT} + x_i \ln \frac{x_i}{\sum x_i} + x_i \ln p \right) \qquad \text{Eq. (3.1)}$$

This program was used to generate blends consisting of argon, water, and CO_2, with pure oxygen and methane as a reactant. The combustion outlet temperature, specific heat ratio and heat capacity were calculated. The mole fractions of both CO_2 and H_2O were also determined.

This program can be employed to calculate composition and thermodynamic parameters at specific conditions, such as constant pressure, constant volume and adiabatic compression or expansion. Gaseq can also be utilised in defining blends and used as a single component.

The Gaseq program also includes several features that provide reliability and flexibility in the treatment of species and thermodynamic data. The first feature is a new species, which means that each radical can be utilised in a thermodynamic calculation if its elemental species is specified, in addition to enthalpy and entropy at 298K and heat capacity (C_p) at different temperatures. The second feature is that every reactant can be considered as temperature independent. The third feature is that the concentration of the radicals can be entered in mass units, as well as mole fractions. The final feature is that the interface with Excel enables the results to be saved in separate Excel sheets, allowing for representation in graphs.

Gaseq was previously used as one of the numerical tools in an investigation of flame stabilities and calculation of combustion products in a gas combustor using ammonia and methane blends as fuel [151]. In another study on flame characteristics, the program was utilised to determine the mass flow rate of the exhaust gas from a combustion process in a swirl burner for an industrial gas turbine [152].

A numerical simulation has been used to study the behaviour of alternative fuels that were utilised in a gas combustor. The results that were obtained from a mathematical model were then compared with values that were also calculated with Gaseq in adiabatic equilibrium conditions [153]. The program was also employed as one of the tools in a further study of water/steam injected with the fuels in a combustion process to determine the mole fractions of composition products, which were compared with those obtained from their thermodynamic model [154].

3.1.1.2 **Minitab**

The Minitab software package was designed to provide reliable results for statistical analysis. One of the features in this program is Design of Experiment (DOE), which is used in this study to quantify the correlation between the reactants and combustion products.

Figure 3.1 demonstrates the available designs in Minitab that can be used according to factor numbers. At this stage of this investigative approach, the DOE was employed to save the time, expense, and effort of traditional experiments by reducing the number of test configurations.

The matrices obtained from this approach can translate the experimental results and, therefore, provide reliable decisions for the blend component proportions. The system requirements for Minitab version 17.0, which is the version used in this study, are Windows XP, 7.0 or Windows 10 with 1 GB RAM. The DOE feature was utilised similarly in other studies to optimise operating conditions or reduce emissions in gas turbines [155-157].

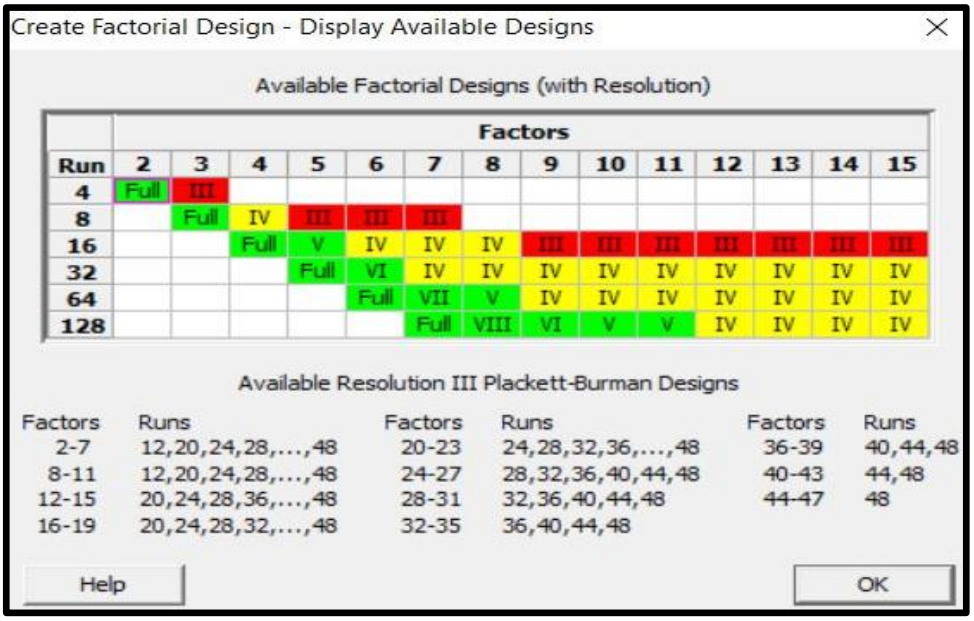

Figure 3.1 Available designs in Minitab

3.1.1.3 **Chemkin-Pro**

The Chemkin-Pro program incorporates advanced standards with robust and flexible functionality to simulate chemical reaction flows. It can provide optimal and accurate models for a wide range of applications, such as turbine combustion systems, chemical and material processing equipment and refining units.

This program can define three types of species: gas- phase, surface and bulk. In addition, it can ideally simulate the gas-phase species inflow or stagnation states, which can provide a precise solution for many of the problems in these applications [158]. Additionally, this program applies the GRI-Mech 3.0 chemical kinetic reaction mechanism and it is able to give reliable results by providing different critical species for a one-dimensional combustor model.

The Gas Research Institute (GRI) provides a list of basic chemical reactions with associated rate constant parameters. Most of the listed reactions have been experimentally investigated with measurement of most of the rate constant parameters. GRI-Mech 3.0 is an optimised mechanism that is created to model natural gas combustion, including NO formation and reburn chemistry. The optimization process is designed to provide sound basic kinetics along with reliable combined modelling predictability of basic combustion properties [159, 160].

However, there is a lack of references available on the use of this mechanism with the diluents investigated in this study (Ar, CO_2 and H_2O). Nevertheless, the outlet temperature and combustion products of the proposed blends calculated at a specific equivalence ratio employing this mechanism provide similar results to those determined using Gaseq, which represents another program that simulates a gas combustor. Thus, this mechanism is used in this study to test the novel blend as a working fluid because it can provide reliable results when used to calculate combustion products in combination with Gaseq. The results obtained from Gaseq were initially compared with those for air as a working fluid at the same running conditions.

A Perfectly Stirred Reactor (PSR) is one of the reactor models in Chemkin-Pro, inside which thermo-chemical properties are considered to be homogenous in turbulent stirring conditions. In this study, a partial premixing approach is assumed to simulate the real mixing process for the particles. The PSR can be also be used to model a jet flame network, which represents a practical application of the program. The PSR network can also model the combustion process in a gas turbine in an industrial application [161].

3.1.1.3.1 **Model description: Assembling the network**

The burner reactor model that was used in this study consists of two clusters, as shown in Figure 3.2. The first cluster is called the PSR, which represents the region around the flame and which consists of three distinct zones. The first zone is called the mixing zone, in which fuel is partially premixed. The second zone is the flame region, which connects directly to the first zone. The third zone is the Central Recirculation Zone (CRZ), where the products of the combustion process are recirculated. The second cluster uses a Plug Flow Reactor (PFR) for post-flame operation, which takes place along a 0.1 m duct between the flame and the turbine. This model can be used in the design and optimisation of a process. Numerically, the flame speeds for the final selected blends were simulated in this PSR-PFR model, which is usually referred to as a PSR network. This cluster is equivalent to a gas turbine combustion chamber.

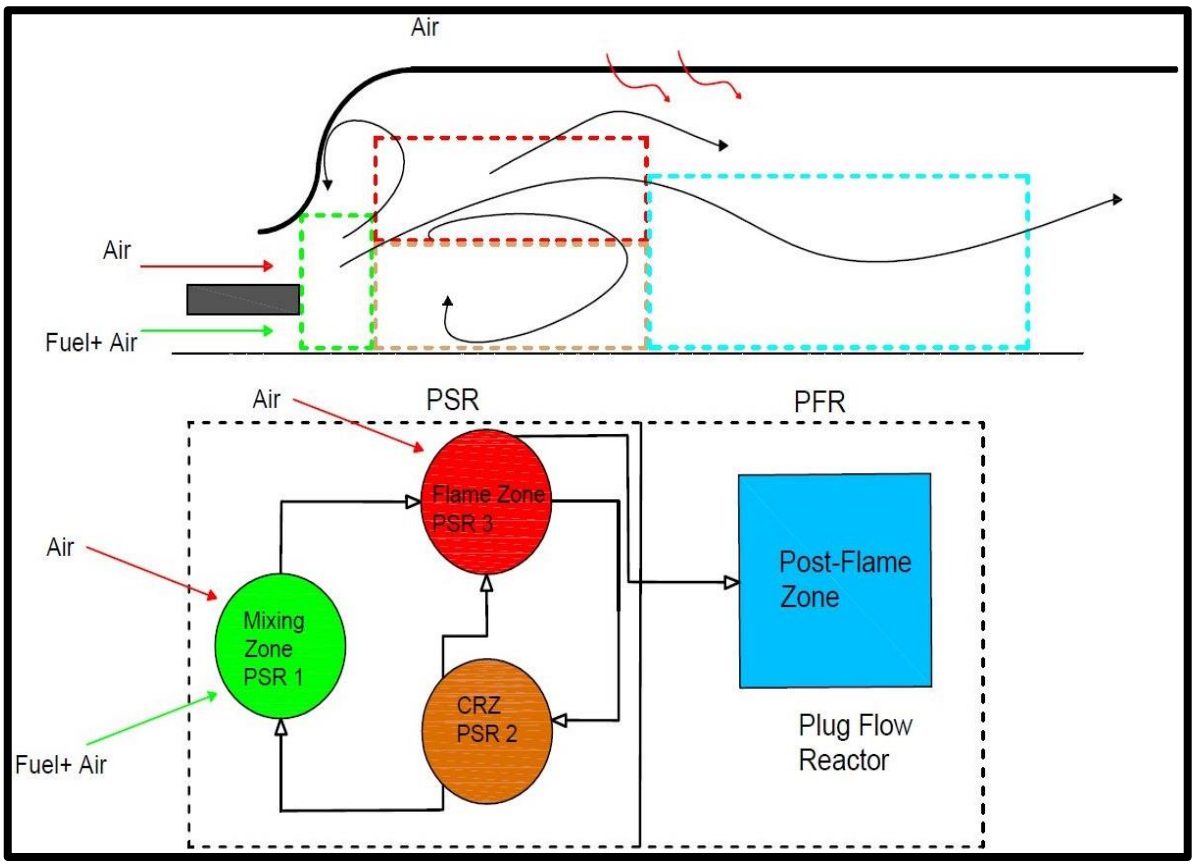

Figure 3.2 PSR-PFR schematic

A PSR-PFR network in Chemkin-Pro was used to simulate the mixing process and flow characteristics to find the effect of the variable geometry of the gas combustor on its performance while reducing NO_x/CO emissions [162]. A PSR-PFR model has also been employed in a separate study to investigate the effect of exhaust gases recirculated in a gas combustor on the reduction of NO_x formation [163]. Chemkin-Pro was developed for another numerical simulation that was conducted in an experimental study to find the lean blowout limits of the combined annular pilot burner and premixed gas combustor while maintaining NO_x emissions within the typical range [164]. A Chemkin-Pro network model was also used as a significant tool to provide details about NO_x formation levels in a gas combustor that runs with various compositions of fuels working at different operating conditions [165].

3.1.2 Contribution of software to CARSOXY blend optimisation

A four-step theoretical investigation was used to identify the optimum blend for the working fluid in a combustion process. The air in the gas combustor can then be replaced by this blend. The aim is to generate equivalent power and efficiency to that of current systems while reducing emissions and pollutants.

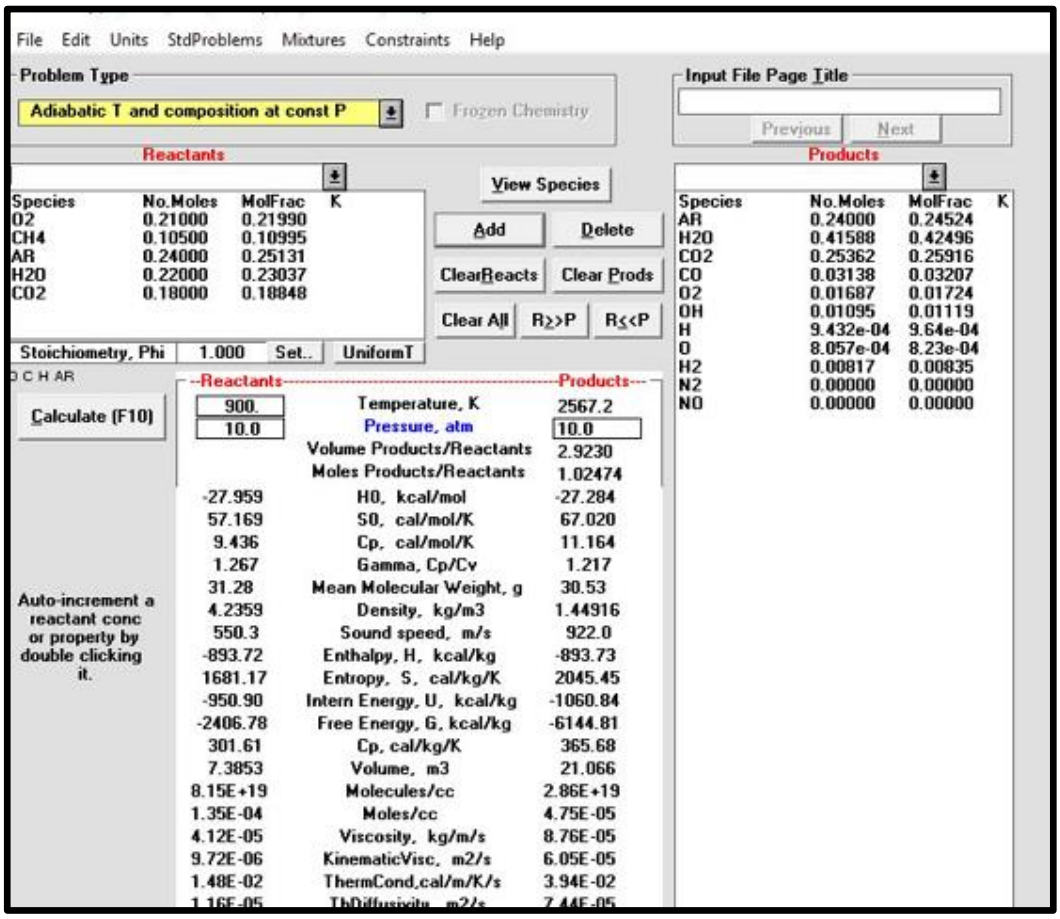

Figure 3.3 Using Gaseq software to generate 120 blends

This investigation started by using chemical equilibrium software with Gaseq, as shown in Figure 3.3, to generate a large number of blends—120 blends—to provide as wide a range as reasonably as possible within the time and resource constraints of this study to select the optimum blend in terms of its similar characteristics to air. Theses 120 blends of argon, water, and CO_2, with pure oxygen and methane as a reactant. In these blends, the outlet temperature and thermodynamic properties (e.g. specific heat ratio and heat capacity) were

calculated using Gaseq program. The mole fractions of both CO_2 and H_2O were also determined. The first step in the use of Gaseq for the generation of the 120 blends was to delete N_2 as an air component in the reactant field, to be replaced with a new species (including Ar, CO_2 and H_2O) with different mole fraction proportions of the species for each run. The adiabatic temperature with constant pressure was set to consider the combustion process as an adiabatic process.

Then, 10 bar and 900 K inlet temperature were specified to simulate conventional operation conditions for a gas combustor. Next, a range of equivalence ratios between 0.667 and 1 was selected for each blend. Finally, outlet temperature, thermodynamic properties with CO_2 and H_2O products were calculated. Every blend was represented by its number and an acronym (X, Y, Z) where X stands for the molar fraction of Ar, Y for H_2O, and Z for CO_2.

The empirical data was then used to compare the blends' properties obtained from the 0-D simulation model in Gaseq with a conventional fuel-air mixture, which was used as a reference under the same operating conditions. The aim of this comparison was to narrow down the number of blends by selecting those with approximately similar characteristics to the reference. To achieve this target, the maximum and minimum values were then selected for each property and for the product concentration of these blends. These values were then divided into four equal intervals. Each interval was given (+, −) signs, according to their direction from the reference.

Next, the DOE technique was employed to statistically quantify the cause and effect correlation between inputs and outputs. The inputs in this study represented the blends' components, which were argon, water and CO_2. The outputs in this study represented the outlet temperatures, the thermodynamic properties, and CO_2 and H_2O as products, all of which were from the gas combustor. Minitab software was employed as a tool for the DOE to examine how each component affects these outputs in terms of both the direction and the

magnitude of the effect. The first step in applying the DOE process to this study was to define the type of design. Due to the number of inputs, a two-level full factorial design was selected to provide a linear correlation between each blend component and the outputs, giving a reasonable theoretical indication of these effects. Using Minitab, it is possible to select one of two types of full factorial design, which is a design that allows the researcher to be able to measure responses at all factor level combinations.

The two design types available in Minitab are: first, 2-level full factorial designs, which contains only 2-level factors; and second, general full factorial designs, which contain factors with in excess of two levels [166, 167]. A 2-Level factorial design is used to create an experimental design to study the effects of 2−15 factors. A 2-level factorial design, as in shown Figure 3.4, was selected for this study because it can help the researcher to identify important factors, which can then become the focus for further experimentation.

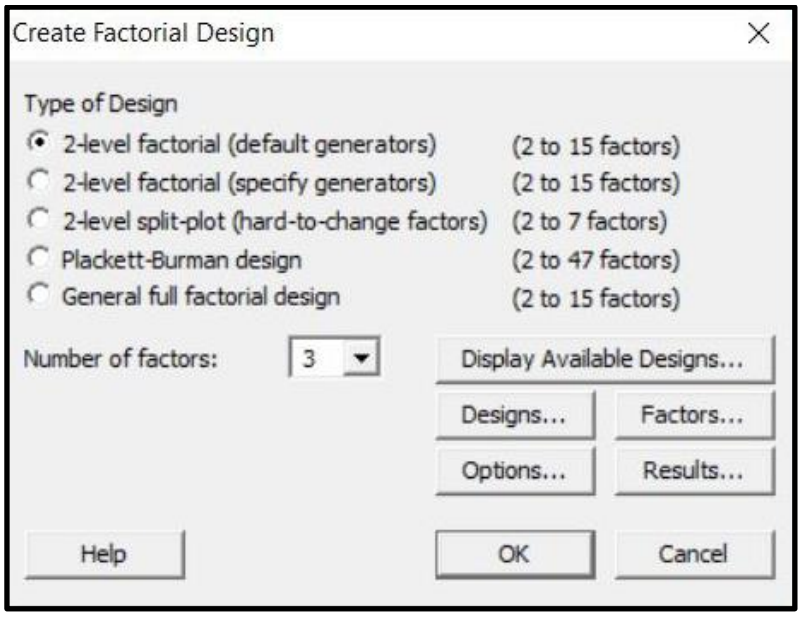

Figure 3.4 Creating a factorial design in Minitab

The next step in this two-level full factorial design process is to define the factors' names, which are Ar. H_2O and CO_2, and then the default set, which allows Minitab to run with a randomised design. Randomisation in Minitab allows the program to run with the Taguchi

model allowing all type of designs, including 2-level designs, 3-level designs, 4-level designs, 5-level designs, and mixed-level designs. Additionally, a randomised design helps to minimise the impacts of investigative factors that are not included in the study and ensure that certain statistical assumptions are met by the experiment. Consequently, eight random combinations of these blends' components were generated with Minitab.

Then, using these eight combinations, the Gaseq program was used to calculate the required characteristics of the products of the combustion process, along with the mole fractions of CO_2 and H_2O as products—according to the design of the experimental model generated by the Minitab program, as shown in Figure 3.5. Then, according to this 2-level factorial design and the eight generated combinations, Minitab was used to show the correlation between the blends' components and the products and characteristics that had already been calculated by Gaseq.

File Edit Data Calc Stat Graph Editor Tools Window Help Assistant

orksheet 2 ***

C1	C2	C3	C4	C5	C6	C7	C8	C9	C10	C11	C12	C13
StdOrder	RunOrder	CenterPt	Blocks	Ar	H2O	CO2	Product T	Prod Cp, J/mole.K	Prod Gamma, Cp/Cv	H2O_1	CO2_1	
3	1	1	1	0.2	0.30	0.16	2530.85	47.60	1.209	0.497443	0.239558	
8	2	1	1	0.4	0.30	0.23	2363.39	44.30	1.230	0.398608	0.251355	
7	3	1	1	0.2	0.30	0.23	2441.05	48.50	1.205	0.470178	0.293146	
1	4	1	1	0.2	0.16	0.16	2679.48	46.80	1.216	0.407466	0.259826	
2	5	1	1	0.4	0.16	0.16	2587.45	42.80	1.246	0.336144	0.219338	
6	6	1	1	0.4	0.16	0.23	2491.97	43.09	1.238	0.319983	0.271947	
4	7	1	1	0.4	0.30	0.16	2447.44	43.50	1.236	0.418337	0.204750	
5	8	1	1	0.2	0.16	0.23	2577.20	47.60	1.209	0.384269	0.321336	

Figure 3.5 Structure of DOE worksheet in Minitab

3.1.3 **Pareto charts and main effects plots in Minitab**

Minitab uses Pareto charts to represent these correlations in terms of the magnitude—but not the direction—of their effect on each thermodynamic property and product, as well as CO_2 and water as products. A Pareto chart is a graphic designed to show the absolute values of the standardized effects, running from the most significant to the least significant effect. These standardized effects are test statistics (known as 't-statistics'). A t-statistic is a random variable that has been calculated from sample data and is used to test whether the null hypothesis (that the effect is 0) can be rejected.

The Pareto chart also plots a reference line (see the red line in Figure 3.5) to provide an indication as to which effects are statistically significant [166, 167]. In a 2-level design—such as the one used in this study—Minitab uses Lenth's pseudo standard error (PSE) method to draw a statistical significance reference line because unstandardized effects can be calculated and shown for this design type. The PSE method uses the assumption that the variation in the least significant effects results from random error (this is known as the 'sparse effects' concept). Minitab uses this approach to calculate PSE and plot 2-level statistical significance reference lines, as follows: first, the absolute value of the effects is calculated. S, which represents 1.5 * median of the effects in Step 1. Next, the median of the effects that are less than 2.5 * S is calculated. Finally, PSE, which represents 1.5 * the median calculated in Step 3, is calculated.

Because Pareto charts display the absolute value of the effects of each blend component on the products, it is possible to determine which effects are large—the magnitude of the effects—but not to determine the direction of the effects (i.e. which effects increase or decrease the response). Figure 3.6 provides an example of this type of standardized effects Pareto chart, showing the magnitude of the effect from largest to smallest but not the effects' direction.

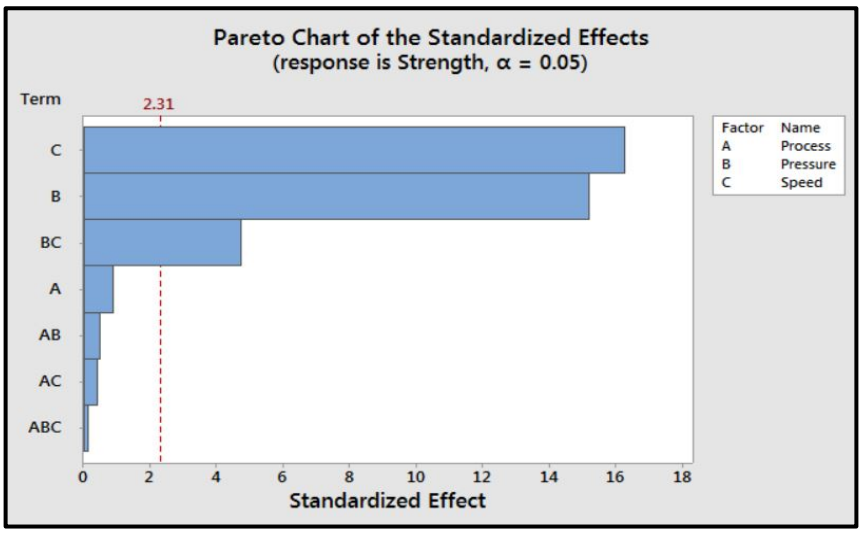

Figure 3.6 Example of Pareto chart of the standardised effects

Therefore, it was also necessary to employ main effects plots in this study to present the data in Figures 4.11–4.15. These charts indicate the mean of the response variable for each level of a factor each level of blend component property investigated in this study. Minitab plots the response mean for each blend's component level and it then links the points for each factor. A reference line is then drawn at the overall, also known as grand, mean. Thus, the main effects can be visualised by the line linking the factor levels. Only the main effects plots for factors considered significant according to the effects and coefficient table from the analyse factorial design should be viewed. A main effect can be considered to be present when a significant change in the mean response across the levels of a factor can be seen [167, 168].

The Pareto charts representing the results obtained in terms of the magnitude of the effects and the main effects plots generated to show the direction of the effects using the Minitab DOE will be provided and analysed in Chapter 4.

3.1.4 Using Chemkin-pro for flame speed calculation

The final inspection in this theoretical study was to use the Chemkin-Pro program to simulate a combustion process in a gas turbine combustor. This programme was used to calculate the

flame speed for the final 16 blends selected using empirical data with 1-bar, 288K and 10-bar, 900K as operating conditions. The flame speeds for the final selected blends in a gas turbine combustor were determined using this model. These values were then compared to those obtained using air as a working fluid under the same running conditions. These mixtures were simulated through PSR and PFR clusters.

3.2 New numerical model

A simulation model was used to calculate the performance operating regimes. Meanwhile, a simulation model of a 3.9 MW Rolls Royce Allison 501-KB5 industrial gas turbine was used for comparison. This numerical model is considered new in several aspects. The first is that it introduced variable polytropic gas turbine efficiency as a function of mass flow rate of the combustion products, consistent with the gas turbine plant reference data. The next is the calculation of heat supply according to combustion chamber energy balance. The final aspect is the introduction of a 'b' coefficient to incorporate fuel enthalpy into the numerical model of a physical cycle to simulate flow behaviour, heat transfer and energy transformation; this coefficient was used in this study's calculations [169].

This model works with a pressure range of around 10-bar, which is similar to the operating conditions used in the calculations for the optimum blend investigative approach, which are considered to be conventional industrial operating conditions. In this numerical model, Equation 3.2 was first used to calculate the specific compression work. Then, the outlet temperature for compressed air was determined by employing Equation 3.3.

The heat capacity, which is a variable dependent upon the ambient temperature, was then calculated using Equation 3.4. Next, b, which represents a new approach to calculating fuel/air mass flow rate ratio—and is the reason this approach is considered a new numerical model to calculate gas turbine performance—was determined from Equation 3.5. In the next

stage, Equation 3.6 was utilised to calculate the specific work produced by the industrial turbine. Finally, both heat supplied and the efficiency of the gas turbine were determined sequentially using Equations 3.7 and 3.8.

The model was first used in this study to calculate the specific output power and the efficiency working with natural gas/air (NG/air). The results were then correlated to those obtained from a real turbine running an equivalent fuel-air mixture. The operation conditions were considered under design (100% load) and off-design (10%–90%) for this correlation method.

The optimum CARSOXY blend, blend 58, as selected using the above-mentioned programmes and procedures, with oxygen and methane as reactants, was inputted into this numerical model. The obtained data was then compared to the data gathered from NG/air running under stoichiometric working conditions, calculated using the same computational model. The model uses the following required equations to calculate the specific output power and the efficiency of the turbine [29, 113]:

$$L_c = \bar{c}_{p\,air\,(1-2)} . T_1 \left(\Pi_C^{\frac{1}{\eta_{pc}} \cdot \frac{R_{air}}{\bar{c}_{p\ air(1-2)}}} - 1 \right) \qquad \text{Eq. (3.2)}$$

$$T_2 = T_1 . \Pi_C^{\frac{1}{\eta_{pc}} \cdot \frac{R_{air}}{\bar{c}_{p\,air(1-2)}}} \qquad \text{Eq. (3.3)}$$

$$\frac{c_p(T)}{R} = \sum_{K=1}^{12} c_k . \left(\frac{T}{1000} \right)^{k-6} \qquad \text{Eq. (3.4)}$$

$$b = \frac{\dot{m}_{fuel}}{\dot{m}_2} = \frac{\bar{c}_{p\ gas\ (0-3)} \cdot (T_{3t} - T_0) - \bar{c}_{p\ air\ (0-2)} \cdot (T_{2t} - T_0)}{\eta_{CC} \cdot (LHV + h_{fuel}) - \bar{c}_{p_{gas\ (0-3)}} \cdot (T_{3t} - T_0)} \quad \text{Eq. (3.5)}$$

$$L_T = \bar{c}_{p\ gas-air\ (3-4)} \cdot \frac{(1-r_{air}).(1+b).T_3 + r_{air}.M.T_2}{(1-r_{air}).(1+b) + r_{air}} \cdot \left(1 - \Pi_T^{\eta_{pT} \cdot \frac{R_{gas-air\ (3-4)}}{\bar{c}_{p\ gas-air\ (3-4)}}}\right) \quad \text{Eq. (3.6)}$$

$$q_{in} = \frac{1}{\eta_{CC}} . (1 - r_{air}) \left[(1 + b) . \bar{c}_{p\ gas-air\ (0-2)} . (T_{3t} - T_0) - \bar{c}_{p\ air\ (0-2)} \cdot (T_{2t} - T_0) - b \cdot h_{fuel}\right] \quad \text{Eq. (3.7)}$$

$$\eta_{GT} = \frac{L_T \cdot \eta_m - L_C}{q_{in}} \quad \text{Eq. (3.8)}$$

3.3 **Aspen Plus**

Aspen Plus is a market-leading simulation package that is used to provide a process design facility integrated with appropriate selection of thermodynamic properties to calculate, monitor and optimise a system's performance [170]. Therefore, Aspen Plus is used to model a wide range of complex processes including the production of power, chemicals, petrochemicals, polymers and minerals within the metal industries [171, 172].

In a previous theoretical study, Aspen Plus was used to model a combined cycle gas turbine power plant integrated with capturing and recirculation of CO_2. Data obtained from the investigative simulation showed that the performance of the combined cycle gas turbine improved with recirculation of exhaust gas [173]. Aspen Plus was used in another study to evaluate the performance of a modified NG combined cycle power plant running with

O_2/CO_2 and using the cryogenic technique for CO_2 capture from inert gases. Their results showed that the efficiency of the O_2/CO_2 cycle was higher than that of a system using a conventional chemical-based approach to CO_2 capture [174].

Aspen Plus was also employed in a theoretical investigation of performance optimisation for a conventional gas turbine combined cycle in comparison with one integrated with a CO_2 capture unit. The results from this simulation approach showed that the integration of a CO_2 capture unit enhanced the performance of the combined cycle [175]. In a further study, a pressurised oxyfuel combustion cycle was modelled in Aspen Plus to investigate the performance of the cycle. The results obtained from the simulation process showed that the total specific power and thermal recovery power of the pressurised combustor were higher than for the combustor working on atmospheric pressure [176].

Consequently, Aspen Plus has been employed in this study to model the CARSOXY cycle to calculate cycle efficiency. The performance of the CARSOXY cycle was then compared with that of a conventional humidified air cycle. The results obtained from Aspen Plus simulation both cycle running with CARSOXY as a working fluid and conventional air humidified cycle were compared with results determined using the new numerical model. The same mathematical equations as described in Section 3.2 were employed to calculate output power and work required for compression. Therefore, the comparison approach focused on the cycle components, such as compressor, mixers and turbine.

3.4 Aspen Plus setup

As discussed, Aspen Plus is the program which was used to simulate the combustion process using CARSOXY as a working fluid. The simulation process was started by creating a new file. Then, gas processing with metric units was chosen for this model. Next, the components

in this model were specified as follows: methane as fuel, CARSOXY or air as a working fluid and anticipated combustion products (most of which are NO_x and CO_2).

The anticipated products CO_2, H_2O, NO_2, N_2O, H_2 and CO were then entered. All this data was obtained from the software's database and they were renamed using acronyms for each chemical species. The next step was to set the calculation method for the physical properties for fuel, CARSOXY, air and combustion products. The Peng–Robinson equation of state is used as the default for Aspen Plus, which was selected for this simulation because it provides acceptable results for nonpolar components [177-179] (i.e. those which share electrons equally and are considered electrically neutral), such as fuel, CARSOXY and air. Once the components and the method had been selected, the simulation stage followed.

3.4.1 **Creating a flow sheet for simulation**

The simulation process was begun by setting up the worksheet by selecting the blocks from the Model Palette. These blocks are initially named by letters with numbers but can be renamed to identify their function (e.g. B1 can be renamed 'comp1'). The combustion process for the proposed cycle was represented by the following blocks: compressor, mixer, combustor and turbine.

These blocks were then connected with the material flow streams. There are two types of material streams: pointing into or out of this equipment (e.g. the red arrow pointing into the compressor indicates a required input data, representing stream and thermodynamic conditions). Moreover, work or heat arrows can be selected from the material flow stream and the direction of these arrows indicates whether the process is exothermic or endothermic. After all of the required data for these blocks was input, as shown in Figure 3.7, the 'Flow Sheet complete' statement appeared and the run button could be pressed.

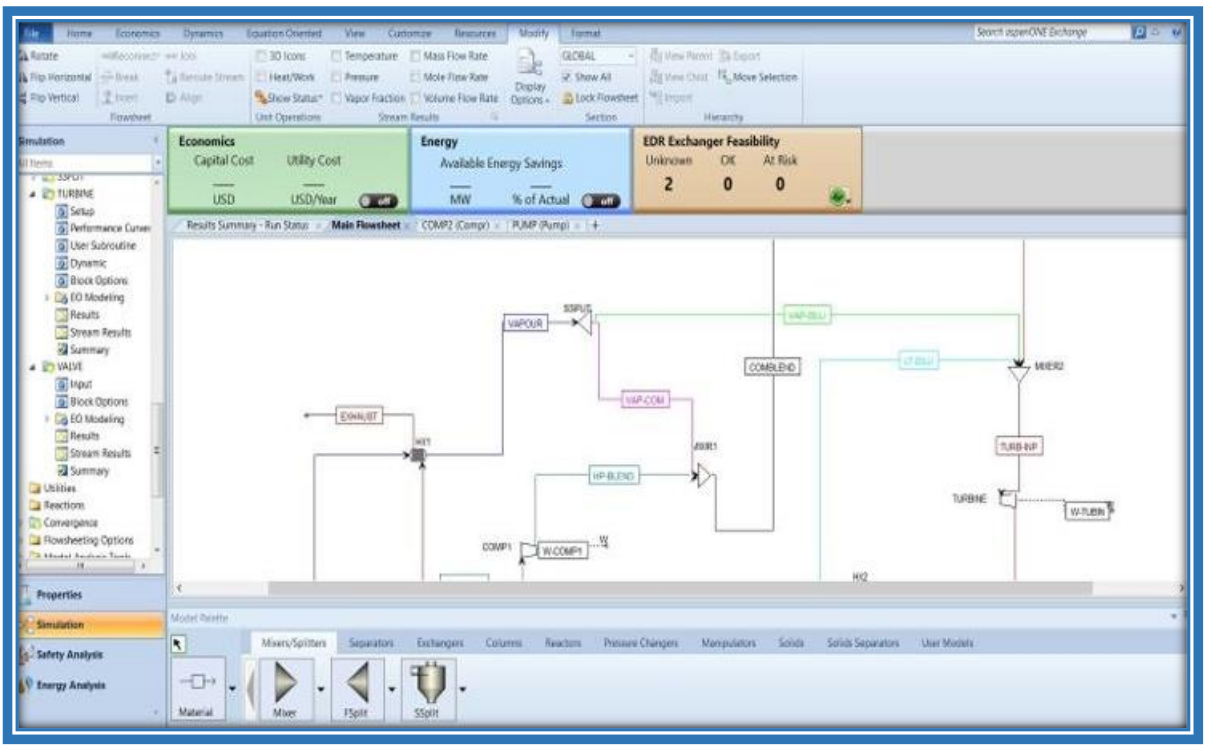

Figure 3.7 Using Aspen Plus to simulate CARSOXY cycle

3.5 Experimental rig

3.5.1 Burner design and fabrication

A 20-kW generic burner was used to investigate the proposed blend in comparison with air as a working fluid, as in conventional gas turbine systems. The objective of this procedure was to compare the proposed blend with conventional air as a working fluid through measurement of stability and emissions to investigate the feasibility of using the blend practically as a more stable, lower-emitting replacement for air.

The rationale for the use of this rig is as follows: an experimental rig set up to be representative of industrial combustion device conditions was needed to explore the use of the novel blend in a swirl burner system in order to ascertain and demonstrate the practicability of employing this alternative working fluid in industrially representative combustion devices. The aim was to experimentally analyse CARSOXY's feasibility for use

in such systems in three significant ways: in terms, first, of emission reductions, in terms, second, of providing flame ignition and, finally, in terms of flame stability by determining its feasibility for combustion purposes in terms of emissions reductions.

The ultimate aim is to employ the blend, coupled with CCS, in a non-premixed injection system for large-scale power generation. This is because non-premixed burners provide more stable flames in industrial contexts (see Section 2.5.1.2), such as in gas turbines and jet engines, thereby reducing the risk of flashback phenomena, which is considered the main drawback of premixed systems (see Section 2.5.1.1). Thus, a non-premixed burner was used in this study's experimental procedures. A further reason for the installation of a diffusive burner in this rig is that CARSOXY does not include N_2, so no premixing is required (see Section 2.5.1.2).

The burner consisted of the following main parts (which are shown in a 2-D schematic diagram in Figure 3.8): main body, fuel intake connected directly to the injector, metal base (shown in Figure 3.9); diffusive injector (photo shown in Figure 3.10); working fluid intake (see Figure 3.11); swirling base (shown in Figure 3.12); and rig frame, transparent confinement cylinder and a pilot (shown in Figure 3.13).

The first specific feature of the experimental setup that was essential to this study was to link a fuel intake directly with the diffusive injector. A diffusion type of burner is usually used instead of a premixed type, which is used to reduce emissions, when preventing system shutdown is the main concern. As highlighted above, in this study's experimental investigation, the diffusive type of burner was installed because the working fluid does not contain N2 and, therefore, there are no NOx emissions from the combustion process.

As mentioned in Section 2.5.1.2, the diffusive mode of combustion provides greater stability for the flame than the premixed type and it reduces the risk of flashback phenomena, which

is considered the main drawback of the premixed mode. The second feature of the rig was to employ a metal base of appropriate height to install the quartz confinement cylinder. This was essential to ensure chemiluminescent visibility of the flame signature to the High-Speed Camera (HSC). The third feature was to consider the reliability and flexibility of the rig when replacing air as a working fluid with the proposed blend, which ensured the ease of the exchange process and prevented any leakage by using a single working fluid intake.

3.5.1.1 **System elements**

Figure 3.8 shows the main parts of the rig, with the diffusive injector positioned centrally to provide a stable flame inside the nozzle. In addition, the injector is connected directly to the fuel line.

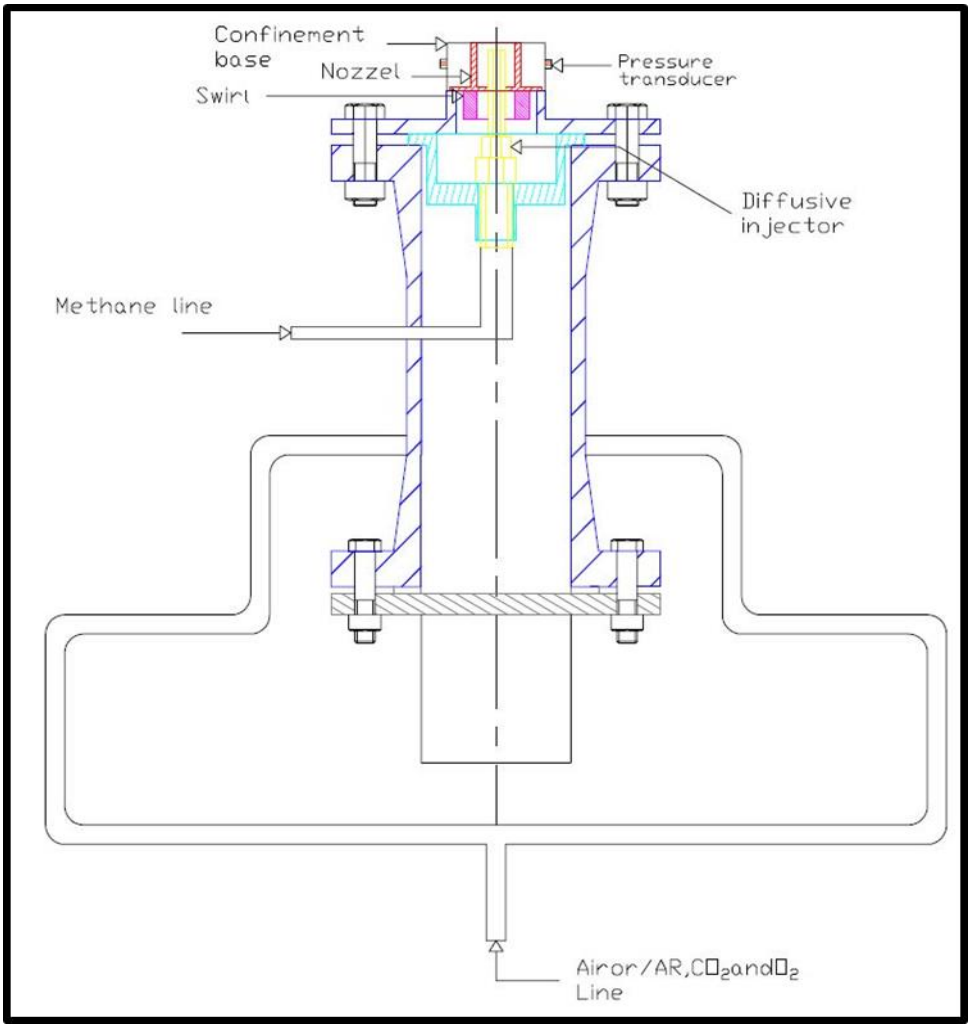

Figure 3.8 2-D cross section of burner

Figure 3.9 shows the main body of the burner and the metal base, which is used to install the cylindrical quartz confinement that is used for flame protection and visibility.

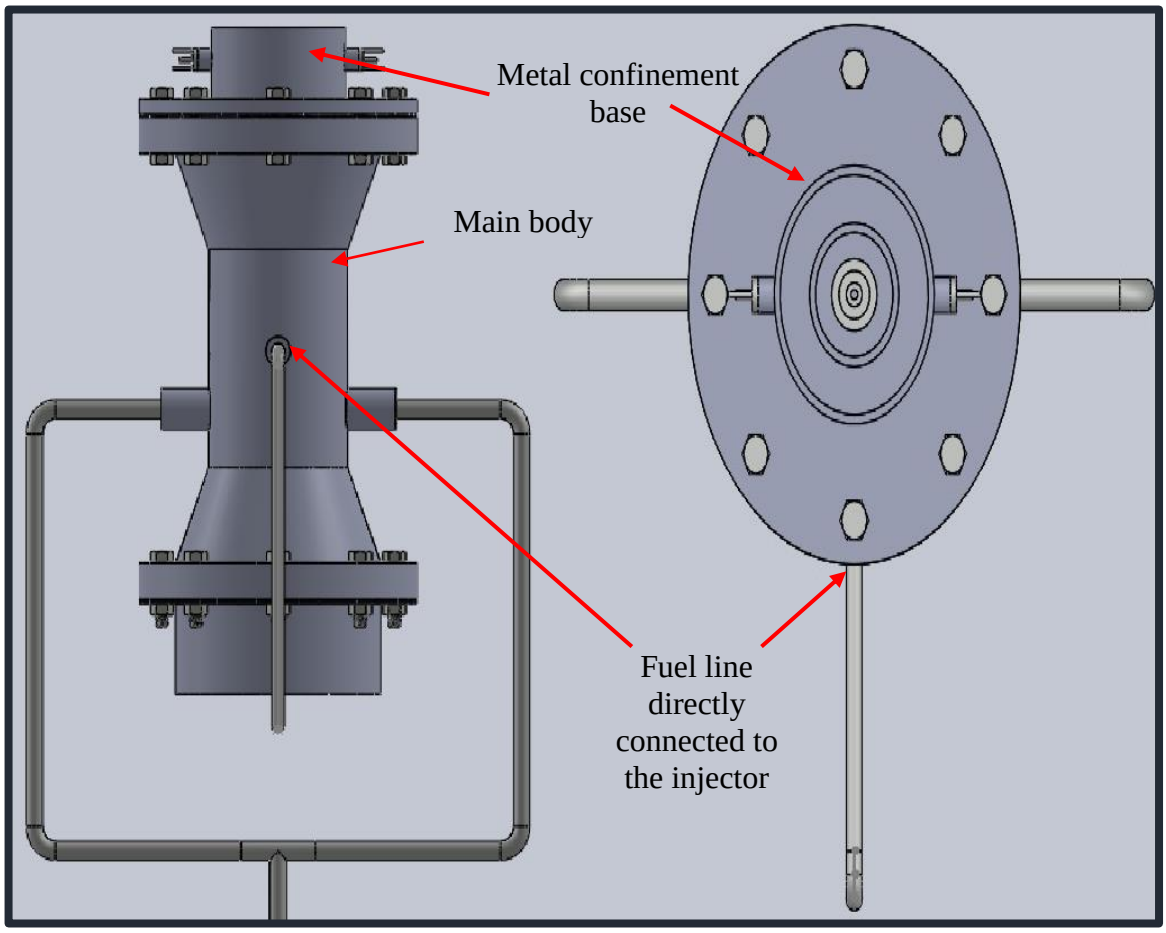

Figure 3.9 Front and top view of rig

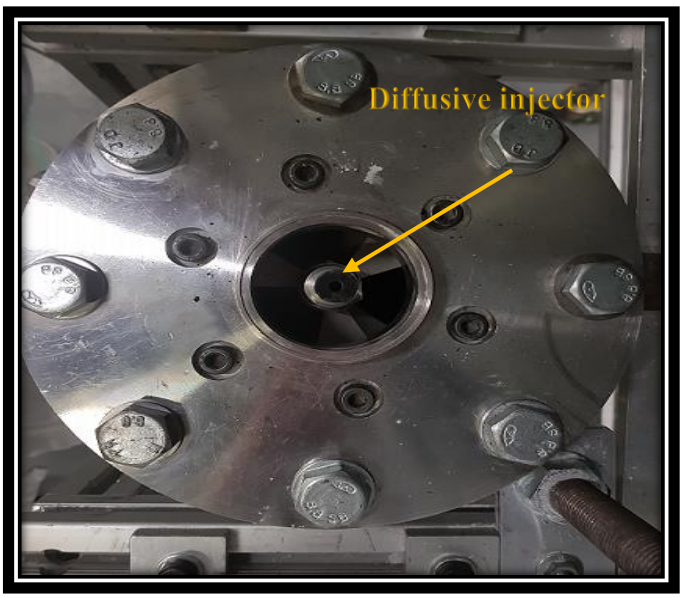

Figure 3.10 Actual diffusive injector

Figure 3.10 is a photo of the specific diffusive injector used in this study's experimental investigation, which was positioned in the centre of the burner. Figure 3.11 shows the working fluid and fuel lines connecting to the burner. The former supplies either air or the proposed blend the system, thereby ensuring that no premixing occurs while providing flexibility for switching between the two working fluids. The details of the blend cylinder with the regulator fitted, which is connected to the working fluid line, are presented in Table 3.1.

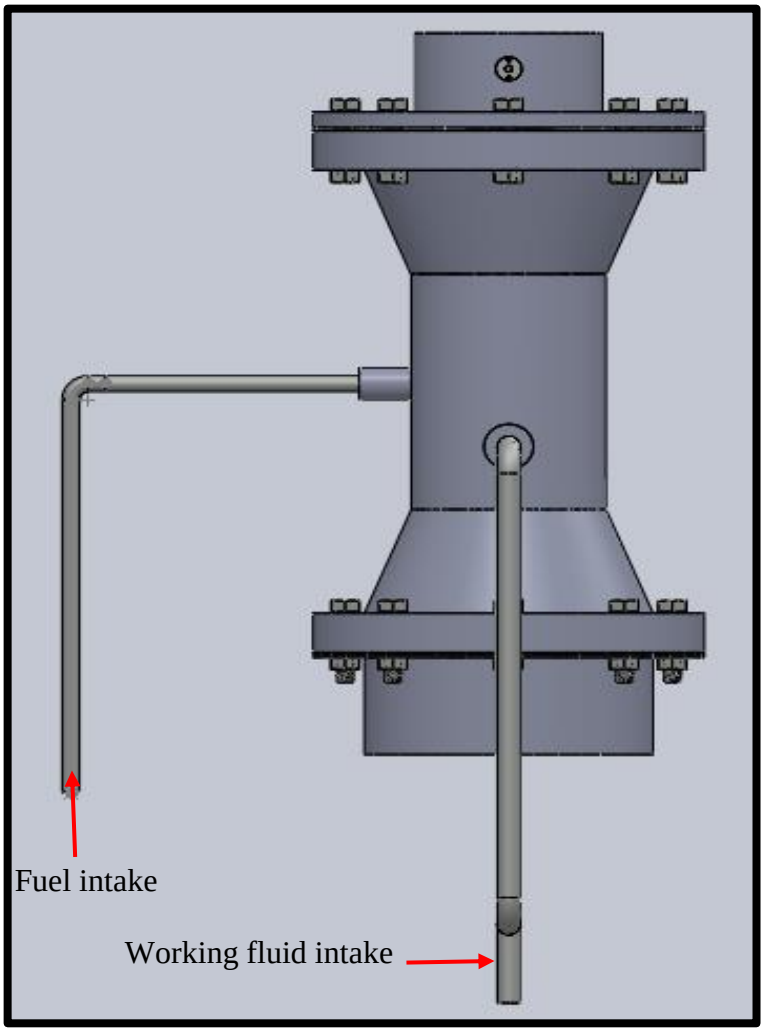

Figure 3.11 Side view of burner

A 3-D schematic diagram can be seen in Figure 3.12. This shows the whole system, including the position of the pipelines supplying the fuel and working fluids, the central injector and the swirl base where the nozzle is installed to simulate a conventional industrial burner.

Table 3.1 Blend cylinder with regulator

S/N	Blend cylinder	
1	Cylinder size	AV (680mm x 181mm - 10 liquid litre capacity)
2	Pressure (bar)	179
3	Valve outlet	BS3
	Two Stage Regulator	
1	Material Description	C106X/2S.7BAR-BS3-1/4NPTF 230BAR
2	Max. Inlet Pressure	300 bar (X)
3	Outlet Pressure Operating Range	0 - 7 bar
4	Outlet Gauge Range	-1 – 14
5	Flow Rate	Cv = 0.1
6	Inlet Connection	BS3
7	Outlet Connection	1/4” NPTF
8	Suitable for use with	(in molar percentage) 29% Carbon Dioxide/32% Oxygen/balance Argon

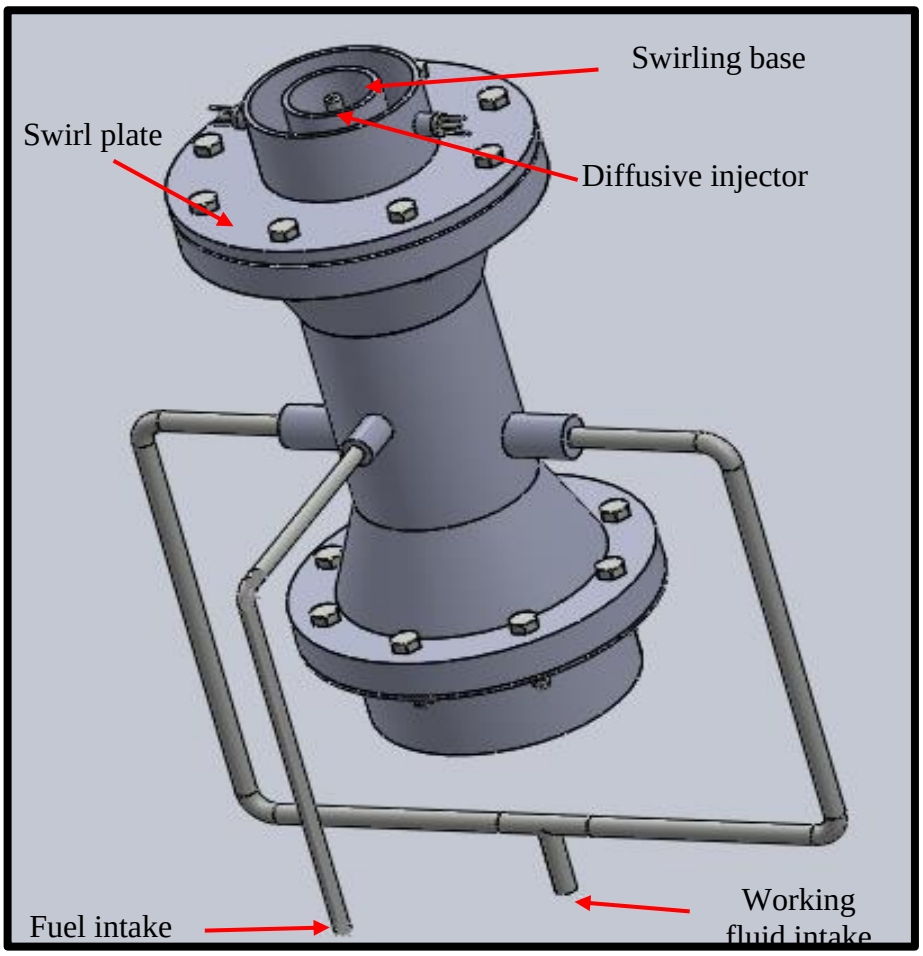

Figure 3.12 3-D schematic of rig

Figure 3.13 shows the rig frame for the burner setup, including the quartz confinement cylinder that is 8 cm in diameter and 40 cm in height to protect the flame from influence by ambient air, while still providing visibility of the flame to be captured by a HSC for CH* investigation. The pilot is installed at a position and distance from the burner that ensures stable ignition while preventing system shutdown due to the pilot blowout.

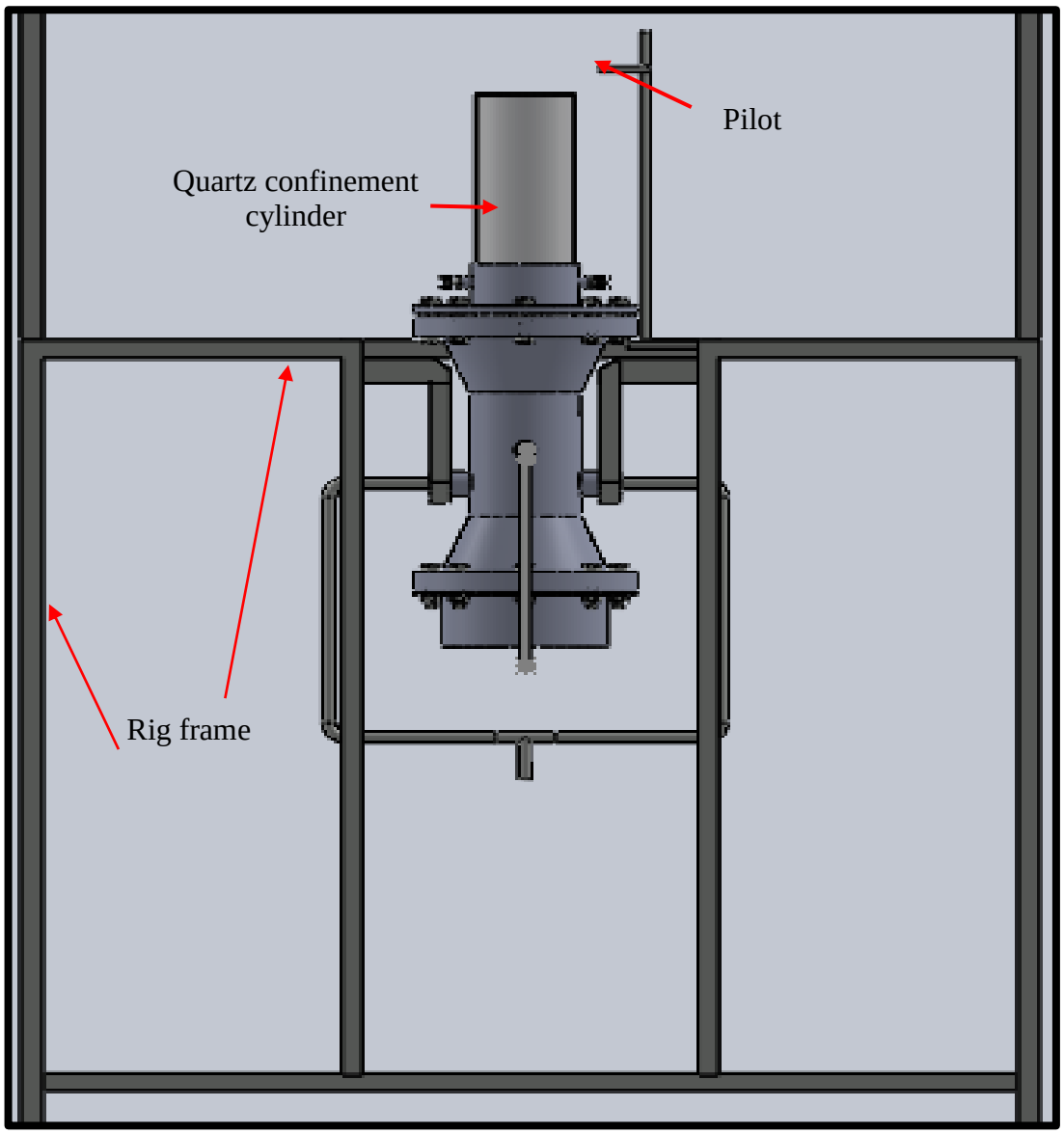

Figure 3.13 Front view of rig

3.5.1.2 **Injector installation procedure**

The following steps describe the injector installation process for the burner. The first step was to set up the swirl configuration, which consists of nine tangential vanes (as shown in Figure 3.14) fitted to the swirl plate.

Figure 3.14 Tangential swirl configuration

Then, the nozzle (2.8 cm, 3 cm) with a 90^{o} divergent angle was attached and locked in position using a metal cover (see Figures 3.15 and 3.16).

Figure 3.15 90-degree nozzle

Figure 3.15 Metal cover

After locking the parts in position, the diffusive injector was fitted in the centre of the configuration at a distance of 5 mm from the top of the nozzle, as shown in Figure 3.17.

Figure 3.16 Diffusive injector centrally positioned in configuration

Figure 3.17 Fuel pipeline installed in burner

Following these steps, the main body of the burner was drilled to make a hole. This hole was then used to install the fuel pipeline to directly connect it to the injector, as shown in Figure

3.18. Finally, a fitting was used to link the fuel pipeline with the fuel supply and prepare the burner to be used for the experiments, as can be seen in Figure 3.19.

Figure 3.18 Fitting linking fuel pipeline with supply

3.6 Chemiluminescence (flame spectral analysis)

Chemiluminescence is a term which describes the light emitted through a chemical reaction. This visible electromagnetic radiation is emitted by electrons moving towards a new energy state. In the hydrocarbon flame front in the combustion process, excited radicals, such as OH^*, $CH^*$and C_2^* emit chemiluminescence when they move from a high energy state to a lower state. Thus, chemiluminescence analysis represents a unique and feasible diagnostic approach to investigate a chemical reactive flow in a combustion process for fundamental research and practical applications [180, 181].

The chemiluminescent emissions can be measured at separate characteristic wavelengths. These wavelengths occur within specific spectral ranges: OH^* at 283-309nm, CH^*at 387-431nm and C_2^* at 513-516nm. The same principle has been experimentally used to indicate a specific optical signature for a flame in a combustion process. A chemiluminescent flame signature is used to look for correlations with other flame characteristics, such as temperature, heat release fluctuations and fuel-air ratio [182-185].

This principle can also be used to detect emitted NO_x pollutants from industrial combustion processes. NO_2, which is produced as a reaction result of this emitted NO_x encountering ozone (O_3), produces infrared light that can be detected chemiluminescently [186, 187]. The infrared light spectrum for this emitted NO_2 is between 600- 2800 nm [188]. However, this type of measurement is not recommended practically in industrial units because it requires time for data processing rather than providing direct and accurate readings from specifically designed measurement devices.

Testo 360 XL is a practical and specifically designed device that has been proven to reliably detect the emissions from industrial systems. Consequently, Testo 360 XL, which is defined in Section 3.7.1.2, is employed in this study to measure emissions in the exhaust gases under a range of different combustion operation conditions.

3.7 Instruments

3.7.1.1 High Speed Camera (HSC)

As mentioned in the previous section, observation of chemiluminescence can be used to detect the flame signature, which indicates its characteristics. A Photron FASTCAM APX-RS HSC was used to visually capture chemiluminescent flame signature (as shown in Figure 3.19 a and b). The HSC has a C-MOS imaging sensor, the sensor resolution is 1024×1024 pixels and a 105 mm, 1:2.8 Nikon lens was used in an F mount. The frame rate of the HSC can be set to any external synchronic signal of 50 Hz to 25000Hz. The Photron FASTCAM APX-RS is connected with a DC power supply fed from an AC power adapter connecting to a 100VAC power line, as shown in Figure 3.19 b [189]. Figures 3.20 (a) and (b) show a Hamamatsu C9546-03 image intensifier and a photo of the actual intensifier used, which was connected to the HSC.

(a) **(b)**

Figure 3.19 a) Front view of Photron FASTCAM APX-Rs HSC - b) Rear view of Photron FASTCAM APX-Rs with DC power connection [189]

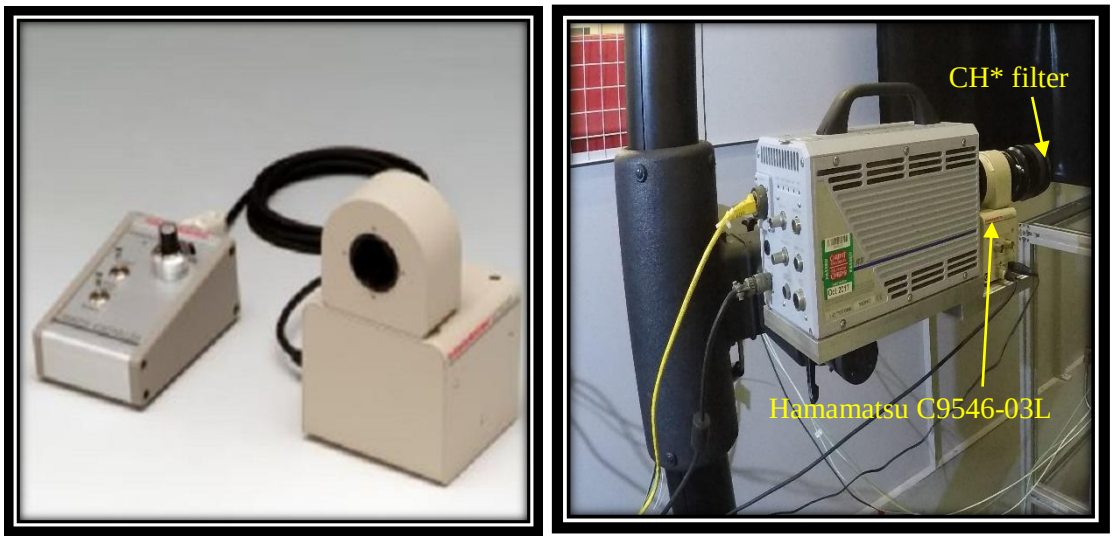

Figure 3.20 (a) Hamamatsu C9546-03L image intensifier with its controller [190] (b) Photo of actual Hamamatsu C9546-03L image intensifier connected to Photron FASTCAM APX-Rs HSC

High-speed gating of 3 ns for the Hamamatsu C9546-03 image intensifier provides intensified images at high gain with electronic shutter operation, which allows capture of instantaneous images occurring in extremely short time periods. Additionally, the image intensifier has a remote controller for adjustment of image intensifier gain, along with a built-in protection circuit that protects the device from damage by excessive light input. In this image intensifier, luminous photocathode sensitivity is 230 µA/lm and the photocathode effective diameter is 17 mm.

3.7.1.1.1 Chemiluminescence experimental setup

A Hamamatsu C9546-03 image intensifier was connected to the lens to amplify the chemiluminescence emitted from CH* radicals from the flame that pass through the CH* filter, which is installed on the lens. The optical wavelength of the bandpass CH* filter used to measure CH* radicals was centred at 430nm (15 nm FWHM). A Bentham wide-spectrum light source and a Macam fibre optic spectroradiometer were used to measure the bandpass width and transmissivity of the CH* bandpass filter. A previous study found that the maximum transmissivity of the CH* filter is around 100% at the wavelength tested [191].

A photocathode in the image intensifier converts the incident light emitted from the flame to photoelectrons and then passes them to a microchannel plate where the electrons are amplified. The amplified electrons are then reconverted by a phosphor screen into light with a high intensity. Finally, the HSC captures the intensified light as CH^* images. Photron FASTCAM Viewer PFV software, as shown in Figure 3.21, was used to illustrate the images and thereafter a MATLAB 2017-b code was utilised to process the obtained images.

The HSC setup involved the following steps: first, the camera was physically positioned to provide a centred image of the burner. Then, the HSC was calibrated using zero gain from the intensifier and after that, the CH* filter was removed.

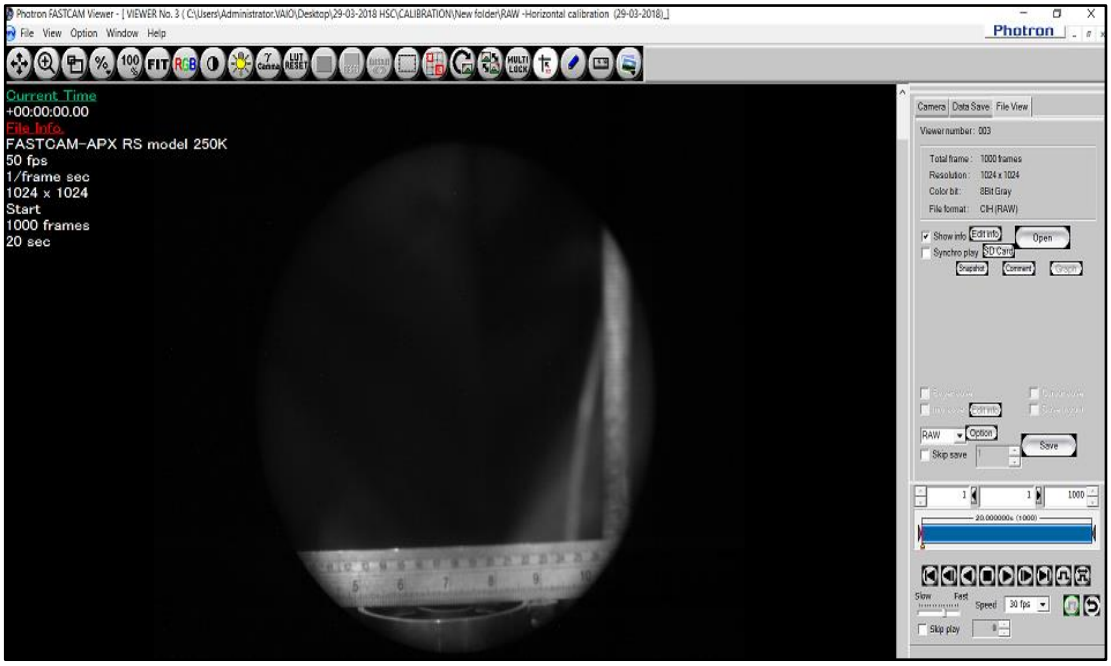

Figure 3.21 Photron FASTCAM Viewer PFV software used with HSC

A frame speed of 50 fps was selected, which was set through the pragmatic considerations, to provide the highest light intensity for calibration. Then, images using a ruler for reference were captured to check the position of the flame. After calibration, the CH* filter was reinstalled and the shading process was carried out. Next, the flame was lit and the gain of the intensifier was manually set to a specific value for each set of operating conditions. This

was achieved using the remote controller by gradually increasing the gain to the required value to visibly capture the flame using the CH* filter, while protecting the HSC from flame glare.

3.7.1.2 **Testo 350 XL portable gas analyser**

A Testo 350 XL portable gas analyser instrument is used to measure products temperature and detect emissions from exhaust gases in industrial engineering processes. The emissions are detected using six sensors that can test carbon monoxide, oxygen, nitrogen monoxide, sulphur dioxide, carbon dioxide, hydrogen sulphide and hydrocarbons (such as ethane, methane and propane).

This device tests carbon dioxide with an infrared sensor, while the other five sensors, which are used to measure other gases, are electrochemical. This instrument consists of two units: the main part is the analyser unit and the small part is the control unit. The control unit can be detached from the analyser unit to measure humidity and differential pressure.

Figure 3.22 Testo 350 XL including analyser unit, control unit and gas probe

This unit also includes filters, which can become discoloured when they need to be replaced. This main unit has a condensation trap to accumulate water that condenses from water vapour in exhaust gases. This water trap can be drained after the water reaches an unacceptable level and the device should be switched off.

In addition, the main unit has a power plug, data bus, air rinse, trigger for the alarm and an input for the temperature probe and a flue gas socket with a differential pressure socket. The display unit also has a data bus input, flue probe and differential pressure socket.

The thermocouple is set at the end of the standard probe, which ends with a probe handle that connects to the probe shaft and gas tubes via a thermocouple line. The control unit is integrated with the main gas analyser that connects directly with the gas probe, as shown in Figure 3.22.

The display unit shows the page number at the top right-hand side of the screen while in the top left-hand side, the measurement-programming icon is shown. Each page includes six measurement parameters. The pump flow rate and the ambient temperature can be shown on one of these pages. The control panel, which is placed below the display, includes the control function buttons, including start and pause for the pump, memory and print function [192]. Studies have used the Testo 350 XL portable emission analyser to measure the exhaust gas temperatures and quantify the level of products, such as CO_2, NO_x and CO, emitted for various practical applications [193, 194].

This device was installed to measure outlet temperature and combustion product emissions. In terms of installation, the end of the probe was placed inside the quartz confinement cylinder at the cylinder's open end. This placement ensured that the probe measured combustion outlet temperature and not flame temperature, so there was no contact with a direct flame, which also helped to protect the analyser itself; as shown in Figure 3.23.

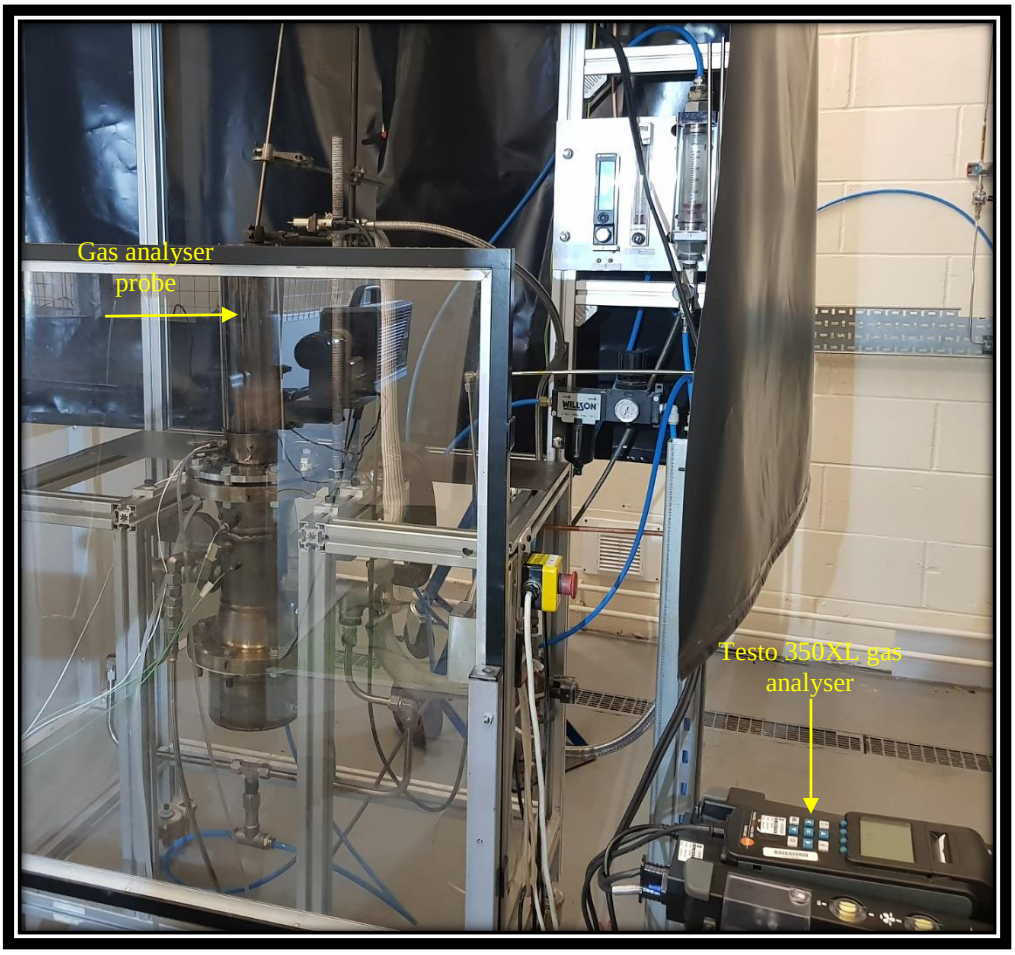

Figure 3.23 Installing Testo 350XL gas analyser in the 20-kW generic burner

Additionally, it ensured that combustion products were not diluted with ambient air, which could have resulted in unreliable data. These setting variables were considered for all cases of measurement running with air as a working fluid and with the novel blend. To provide consistent and repeatable measurement, all of the measurements were taken after a certain time period (i.e. 1 minute), which was established using the pragmatic procedure as the time interval that provided a stable reading for the measured parameters.

The technical characteristics of the Testo 350XL gas analyser are indicated in Table 3.2. The temperature measurement range of Testo350XL is -40 --1200^{o}C with accuracy of ±0.5 % of mv (+100----+1200 ^{o}C) and + 0.5 ^{o}C (-40 -- +99^{o}C) with resolution of ±0.1^{o}C (-40 -- +1200 ^{o}C).

Table 3.2 Testo 350XL gas analyser technical data

Probe type	CO (H_2Compensated)	CO low measurement (H_2Compensated)	NO measurement	NO low measurement	NO_2 measurement
Meas. range	0…+10000 ppm CO	0…+500 ppm CO	0…+3000 ppm NO	0…+300 ppm NO	0…+500 ppm NO_2
Accuracy±	±5 % of mv (+100…+2000 ppm CO) ±10 of mv (+2001...+10000 ppm CO) ±10 ppm CO (0…+99 ppm CO)	±5 % of mv (+40…+500 ppm CO) ±2 ppm CO (+0...+39.9 ppm CO)	±5 % of mv (+100…+1999.9 ppm NO) ±10 of mv (+2000...+3000 ppm NO) ±5 ppm NO (0...+99 ppm NO)	±5 % of mv (+40…+300 ppm NO) ±2 ppm NO (0...+39.9 ppm NO)	±5 % of mv (+100…+500 ppm NO_2) ±5 ppm NO_2 (0...+99.9 ppm NO_2)

3.8 Summary

This chapter has detailed and described this study's theoretical and experimental approaches, along with all the relevant tools used. The computer programs employed to identify the novel blend CARSOXY, which were Gaseq, Minitab and Chemkin-Pro, were presented under the theoretical setup heading, which represents the first section.

A new numerical model was then presented, which is used in the next chapter to compare the performance of an industrial gas turbine using the optimum CARSOXY blend as a working fluid and methane as fuel with air and NG as a fuel at equivalent operating conditions.

In the third section, Aspen Plus was introduced and described. The aim of using Aspen Plus is to study the performance of the CARSOXY cycle and to compare its performance with that of the conventional air humidified cycle under certain operating conditions.

The fourth section detailed the design and fabrication of the burner used for the experimental investigation in this study. This section also included the installation procedures for the instrumentation and measurement devices that were used for the experiments, along with a

description of how chemiluminescence can be used to observe and measure gas combustor flame stability in this study's experimental investigation.

The next chapter will describe how the optimum blends were inferred.

CHAPTER FOUR

Chapter 4 Inferring the optimum blend through data analysis

This chapter details the theoretical investigation of a large number of blends comprising, CO_2, argon and steam with OF combustion (CARSOXY), with the aim of discovering the optimum blend possessing similar thermodynamic properties to air while allowing CO_2 recycling and emitting zero NO_x. It also presents a mathematical software-based comparison of industrial gas turbine output power and efficiency when running the optimum blend with oxygen and methane, compared with NG/air. A theoretical evaluation of the use of atmospheres comprising argon, water, and high CO_2 concentrations to achieve OF combustion in multi-burner combustors, with the aim of improving efficiencies and power outputs while controlling inlet/flame temperatures and enabling CO_2 storage, is then described.

First, this study's investigative approach to gathering the data used to infer the optimum blend is outlined. An 0D-Chemical reaction analysis using the Gaseq program is then provided, showing outlet temperatures and thermodynamic properties compared with a conventional methane-air mixture to identify the blends that have the closest characteristics to those of air. Next, the DOE method is presented, showing analysis of the gas components' effects on combustion characteristics and products, and identifying the gas component that has the greatest effect. A numerically modelled overall comparison of the optimum blend with NG/air is then provided, followed by a chapter summary.

In brief, this chapter's investigation and analysis indicate that the optimum blend for this study's aims out of the 120 investigated blends can be inferred to be blend number 58. The efficiency of the numerical model of the gas turbine running with this blend is shown to be higher than that of air as a conventional working fluid.

4.1 Investigative approach

First, the Gaseq program was applied to generate 120 blends (see Appendix 2), formulated as detailed in Section 3.1.2. This number is high enough to provide as wide a variety as possible of blend component concentrations, including the high proportions of CO_2 and H_2O required for recycling in the combustion process of the CARSOXY cycle proposed in this study, while remaining feasible for investigation within the study's time and resource constraints. These blends were investigated to indicate which blend could be selected as the optimum in terms of its possession of similar characteristics to air, to then be used as an alternative in the combustion process for gas turbines.

It was also necessary to investigate a relatively large range of blend component concentration combinations to increase the probability of producing combinations whose characteristics closely matched the multiple balance of properties necessary for use in the proposed cycle, as follows: producing similar outlet temperatures to air as a working fluid to avoid modifications to existing turbomachinery design; possessing similar thermodynamic properties so as not to reduce overall efficiency levels compared to those when running with air; and, for recycling in the proposed cycle, producing a higher concentration of CO_2 and water as products compared to air.

Therefore, to balance the need for a high number of generated blend component combinations with the likelihood of generating combinations possessing the desired characteristics outlined above, this study focused on blend component concentrations generated within the following range: Ar – highest proportion: 0.34, lowest proportion: 0.02; H_2O – highest proportion: 0.30, lowest proportion: 0.05; and CO_2 – highest proportion: 0.41, lowest proportion: 0.09. This resulted in the generation of blends numbered from 1 to 120 with random blend component proportion combinations, within the chosen range.

Thus, the blends consisted of the following components in varying proportion combinations: Ar, CO_2 and H_2O in an oxygen atmosphere with methane as a reactant. Next, 10-bar pressure and 900 K temperature were set because they are considered equivalent to industrial operating conditions. Outlet temperatures and products for all blends were calculated using Gaseq and compared with air, which was used as a reference running at the same operating conditions.

Empirical data taken from results gathered from Gaseq was then utilised for comparison of these blends against the reference data for air (see Appendix 2). The maximum and minimum values for each property and CO_2 and H_2O as products were chosen for these blends to divide these values into equal intervals. In this method, four intervals were taken for each property.

The DOE was devised and employed in this stage of the investigation to quantify the cause and effect relationship between the blends' components, which were represented by argon, water and CO_2 against both the thermodynamic properties and CO_2 and H_2O as products. They were calculated by the Gaseq program according to the design of the experimental model.

Following these investigative steps, the eight selected blends were simulated with Chemkin-Pro to calculate the flame speed in a gas turbine combustor running with methane as fuel and those selected mixtures as a working fluid. Finally, the flame speeds were compared with values obtained from air under the same working conditions.

4.2 Results and discussion

4.2.1 0-D chemical reaction analysis

In order to show the outlet temperatures, thermodynamic properties and combustion products for the 16 blends, five blends were chosen as a representative sample. For reasons

of clarity when graphically representing the resulting data at this stage because there would be substantial overlap between some blends' results, which could make the charts' information unclear, it was necessary to select a smaller representative sample for analysis. This representative selection (blends 27, 58, 79 and 109) was based on the flame speed data for the 16 selected blends compared to air as a reference, while blend 18 was also included here as a representative of the remaining blends rejected as a result of the Chemkin-Pro investigation, as detailed in Section 4.2.3. The results obtained from the Gaseq program show the outlet temperatures and thermodynamic properties with CO_2 and H_2O as products for each blend. All of these characteristics were determined against a range of equivalence ratios and compared with the conventional methane-air mixture, which was used as the reference.

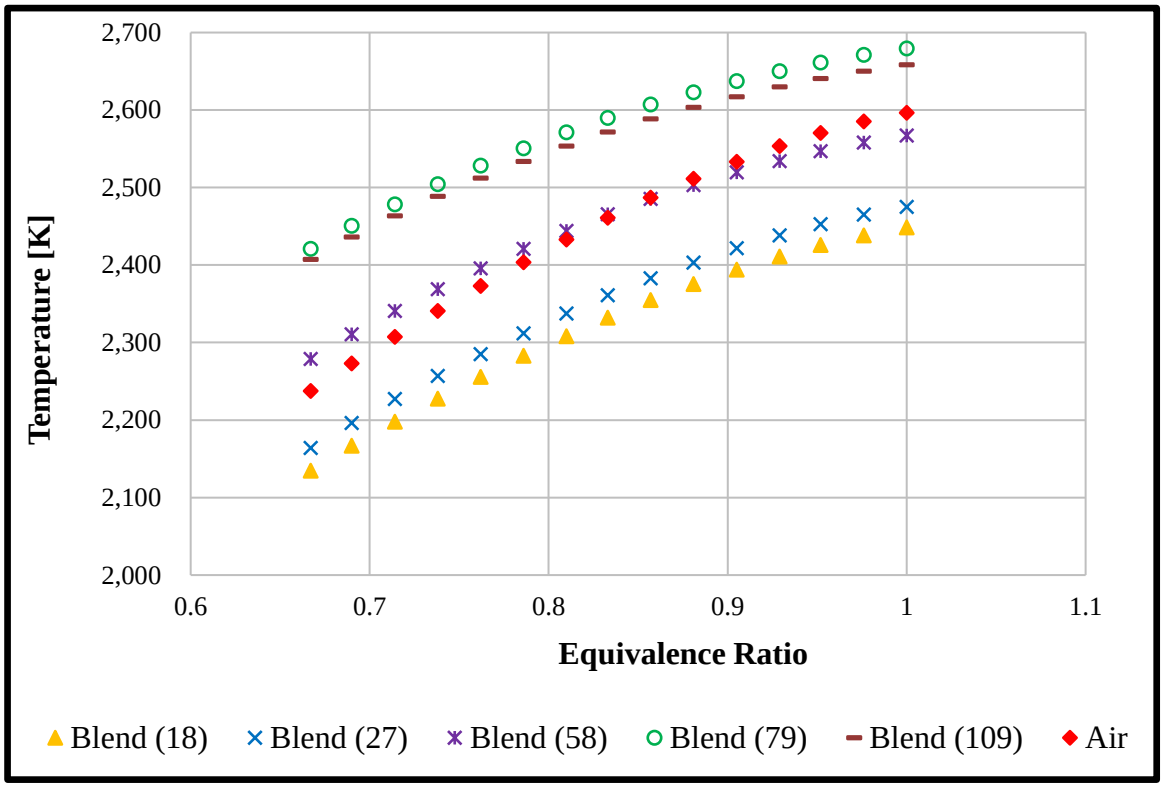

Figure 4.1 Outlet temperatures for selected blends compared with air

As shown in Figure 4.1, the outlet temperatures indicate that blends 79 (24-19-19) and 109 (20- 7- 24) are about 100 degrees higher than the reference. However, blends 18 (32-28-20)

and 27 (30-24-16) are lower than the fuel-air mixture by almost the same number of degrees. In one case only were there approximately similar temperatures to those obtained from the reference; that is, blend 58 (25, 23, 19). Regarding the values for specific heat ratio, the results for the blends are lower by only around 2-4% compared to the values obtained from air running at the same conditions, which was used as a reference. Figure 4.2 shows that blend 58 was located around the middle of the group of selected blends.

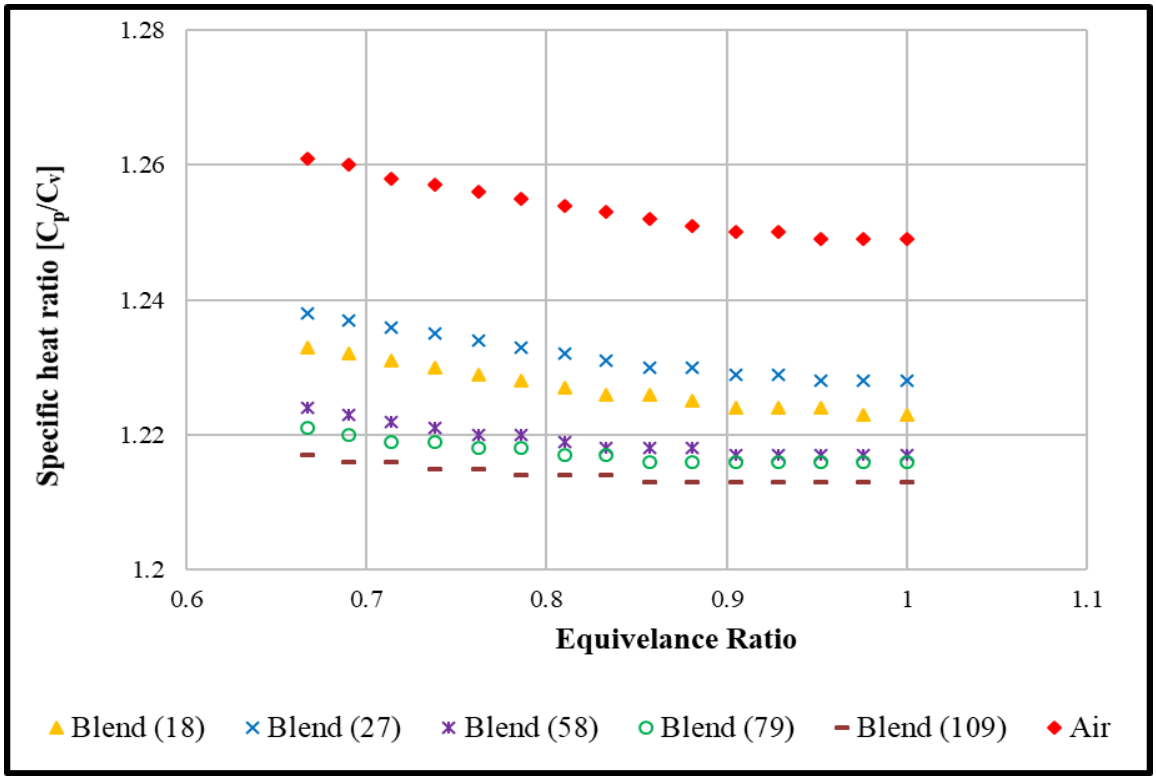

Figure 4.2 Products of specific heat ratio for selected blends compared with air

In comparison with levels for air as a working fluid, as shown in Figure 4.3, the heat capacities show an improvement of about 3-7 J/ mole. K for all of the gas mixtures. Blend 58 is again located in the middle of these blends.

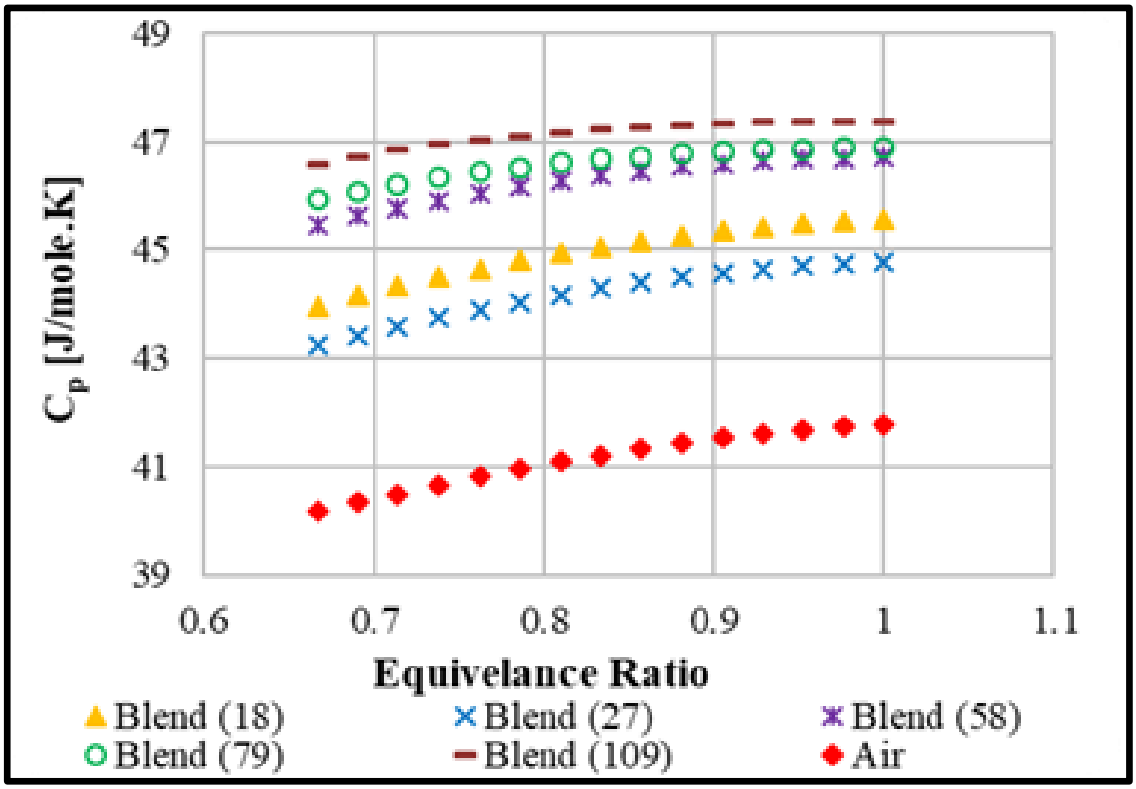

Figure 4.3 Products of heat capacity for selected blends compared with air

In terms of complete combustion products, Figure 4.4 demonstrates that all five blends produce about 30-40% of CO_2 as products compared with only approximately 10% produced by air as a reference. These higher molar fractions for CO_2 as a product could be essential for recycling a higher portion of CO_2 with argon, while the residual CO_2 can be treated.

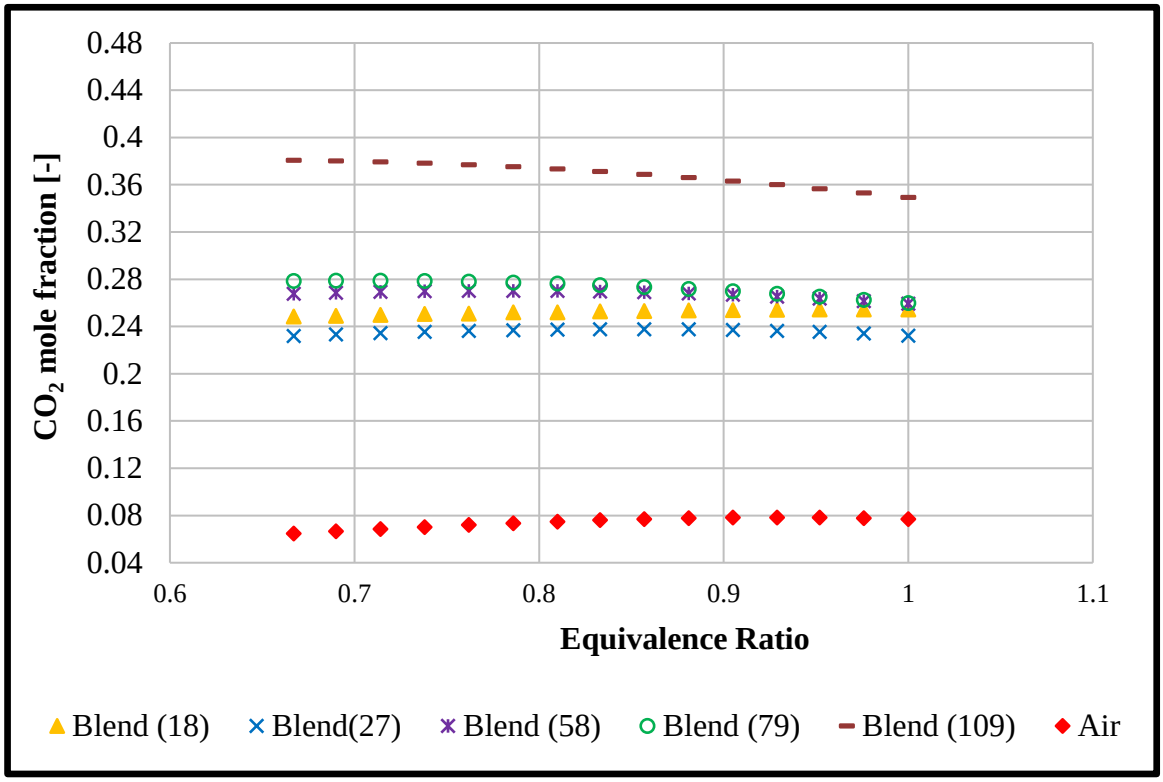

Figure 4.4 CO_2 as a product for selected blends compared with air

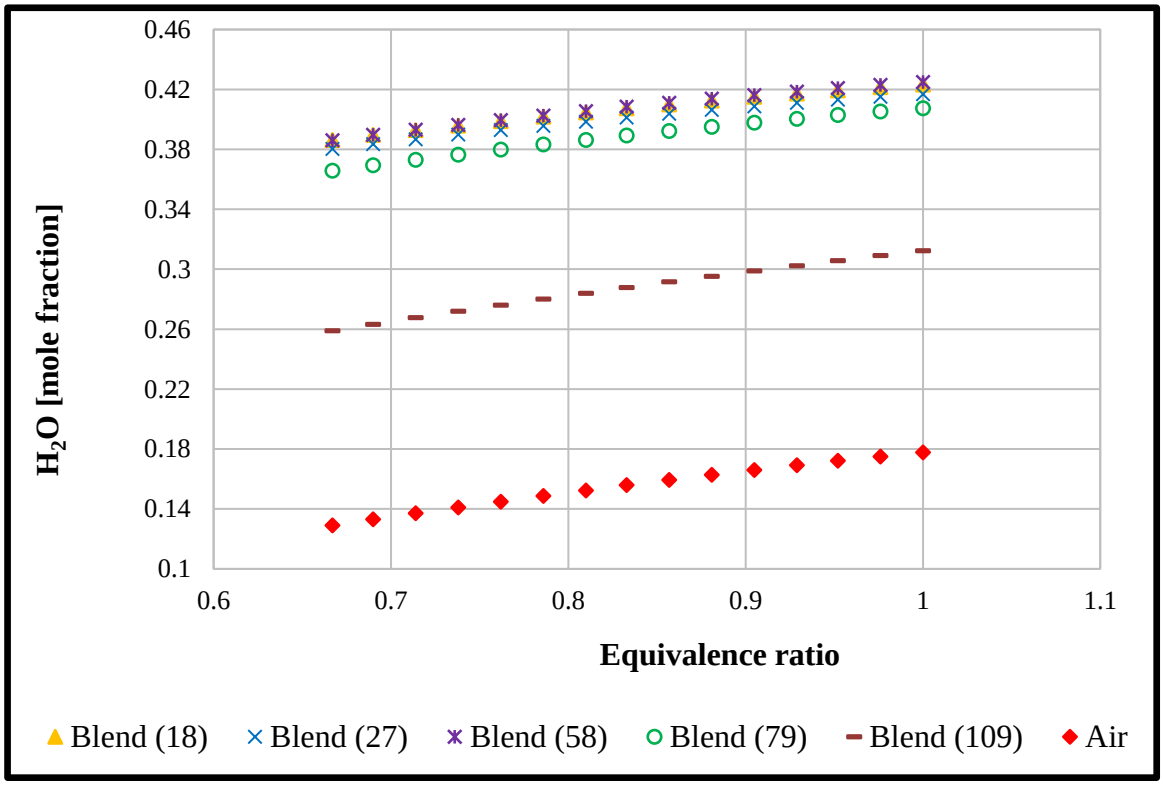

Figure 4.5 H_2O as a product for selected blends compared with air

Regarding water as a product of complete combustion, Figure 4.5 shows that blend 58 has the highest values for mole fraction of water, approximately matching the values for both blends 18 and 27. This amount of water in exhaust gases might be used in a water recovery system.

The matrix shown in Table 4.1 represents the optimal 16 blends out of all of the generated blends, selected for further analysis. These 16 blends were selected by the researcher according to the following five parameters: outlet temperature, heat capacity (Cp), specific heat ratio (gamma), H_2O combustion product and CO_2 combustion product. This matrix was created using empirical data resulting from the utilisation of Gaseq software. In this matrix, each thermodynamic property and the mole fractions of CO_2 and H_2O as products for all generated blends were compared with their equivalents produced by air as a working fluid.

The 120 blends were then narrowed down to the 16 blends that were shown empirically to have the closest balance of properties to air as a working fluid in terms of the parameters outlined above, with a specific emphasis on outlet temperature to avoid design modifications, as detailed previously, while also producing increased levels of CO_2 and H_2O combustion products.

This number of blends was selected at this stage for reasons of time constraints; as can be seen in Appendix 2, where the 16 selected blends are highlighted in yellow, two additional blends with properties almost as well-balanced with those of air (case numbers 16 and 31, highlighted in blue) were considered for selection at this point but rejected in favour of not expanding the selection number above 16.

In Table 4.1, column 1 represents the blend's number, and columns 2−4 sequentially show the mole fractions of Ar, H_2O, and CO_2 for each blend. Following that, columns 5−7

represent the outlet temperature and thermodynamic properties for these blends. The last two columns, 8 and 9, signify mole fractions of H_2O and CO_2 products.

Table 4.1 The optimum selected blends, using empirical data

Case	Ar [Mole fraction]	H_2O [Mole fraction]	CO_2 [Mole fraction]	T(K)	C_p [J/mole. K]	Gamma [Cp/Cv]	H_2O [Mole fraction]	CO_2 [Mole fraction]
Air				2596.4	41.766	1.249	0.177607	0.076828
4	0.244	0.271	0.199	− −	++	− −	+++	++
5	0.262	0.271	0.181	−	++	− −	+++	++
6	0.271	0.271	0.172	−	++	− −	+++	++
18	0.287	0.251	0.179	−	+	− −	+++	++
20	0.239	0.248	0.221	−	++	− −	+++	++
26	0.343	0.231	0.154	−	+	−	+++	+
27	0.307	0.244	0.163	−	+	-−	+++	++
32	0.246	0.229	0.246	− −	++	− −	+++	++
33	0.292	0.237	0.182	−	+	− −	+++	++
34	0.264	0.237	0.210	−	++	− −	+++	++
49	0.226	0.188	0.188	− −	++	− −	+++	++
58	0.251	0.230	0.188	0	++	− −	+++	++
59	0.265	0.208	0.227	−	++	− −	+++	++
69	0.255	0.182	0.273	− −	++	− −	++	++
79	0.239	0.191	0.191	+	++	− −	+++	++
109	0.242	0.084	0.290	0	++	− −	++	+++

0: Same as reference; +: Greater than reference; ++: Considerably greater than reference; +++: Far greater than reference; −: Lower than reference; − −: Considerably lower than reference; − − −: Far lower than reference.

Additionally, the signs (−, +) were used in this matrix to indicate whether, and by how much, outlet temperature, thermodynamic properties, and the concentration of products are higher or lower than the reference. The single, double, and even triple numbers for these signs indicate how far from or close to the reference value these characteristics and products are. These references are indicated in the second row of Table 4.1.

4.2.2 **DOE analysis**

The DOE method is able to identify which of the gas components, inert gas, H_2O, and CO_2, has the greatest effect on one or more of the characteristics and products among all of the components. This calculation is performed using t-statistics to test the null hypothesis, as explained in Section 3.1.3. As highlighted in the same section, the following Pareto charts do not indicate the direction of the response of these properties towards the blends' components, only the magnitude of these effects.

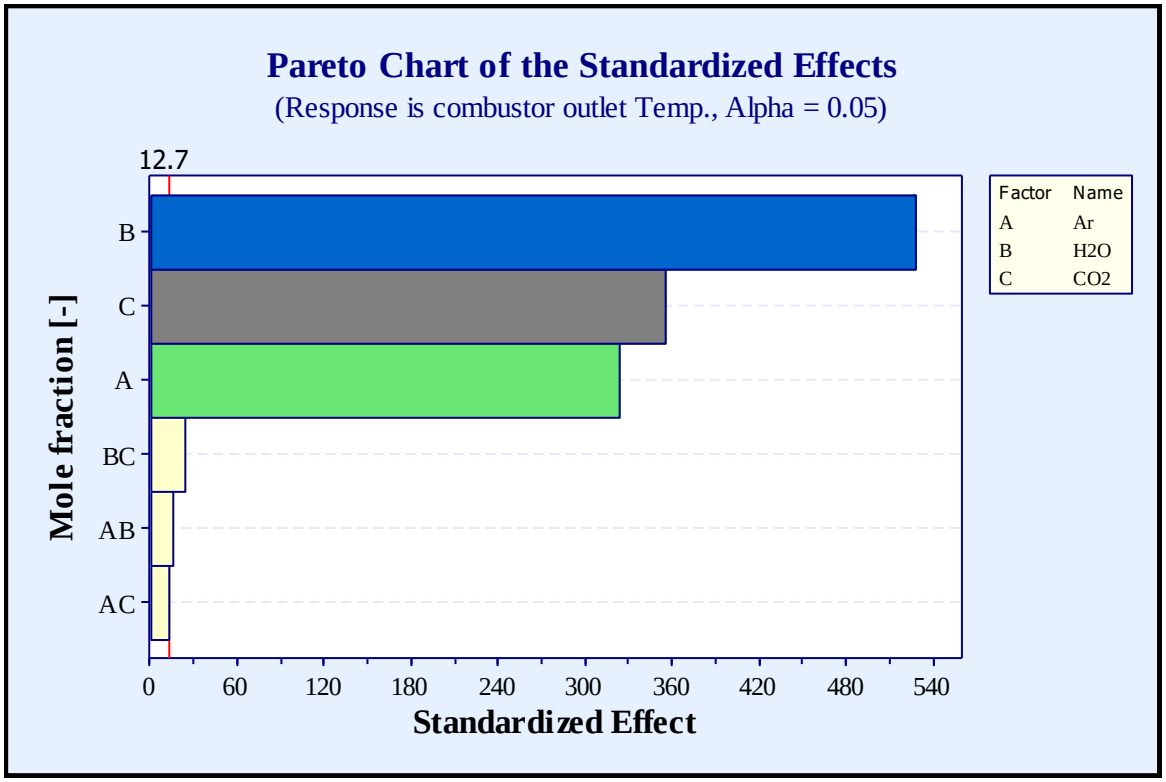

Figure 4.6 Pareto chart of blend components' effect on outlet temperature

The t-value, which is represented on the x-axis of the Pareto graphs, presents the standardized effect (which is the coefficient divided by its standard error) and shows the predicted significance of the effect of the investigated parameter – in this case, the components of the proposed blend (Ar, H_2O and CO_2) - on the response. As mentioned above, the response in this section represents a thermodynamic property or gas combustor product. The t-values can vary between the graphs presented.

It is evident that water as a blend component has the greatest effect on combustor outlet temperature in comparison with Ar and CO_2, which are shown in Figure 4.6 to have a very similar magnitude of effect on temperature value. Water has the most significant effect, which is likely to be due to its propensity to cause a flame blowout and which has a significant effect on outlet temperature. Support for this explanation can be found in Figure 4.11, which shows that the directions of all blend components' effects are negative, most significantly that of water.

This indicates that a blowout is being caused. In terms of specific heat ratio of the combustion products, Argon (which has gamma =1.66) has the most significant effect on this property; as indicated in Figure 4.7. A probable explanation for this is that Ar possesses a higher specific heat ratio than the other components. Therefore, this gas as a blend component has by far the greatest effect on this thermodynamic property of the combustion products. In comparison with Ar, the other gas components—with their lower specific heat ratios—have less impact on the value of this property. Thus, it can be seen that water, which has a comparatively slightly higher specific heat ratio than CO_2, affects this property in a slightly more significant way.

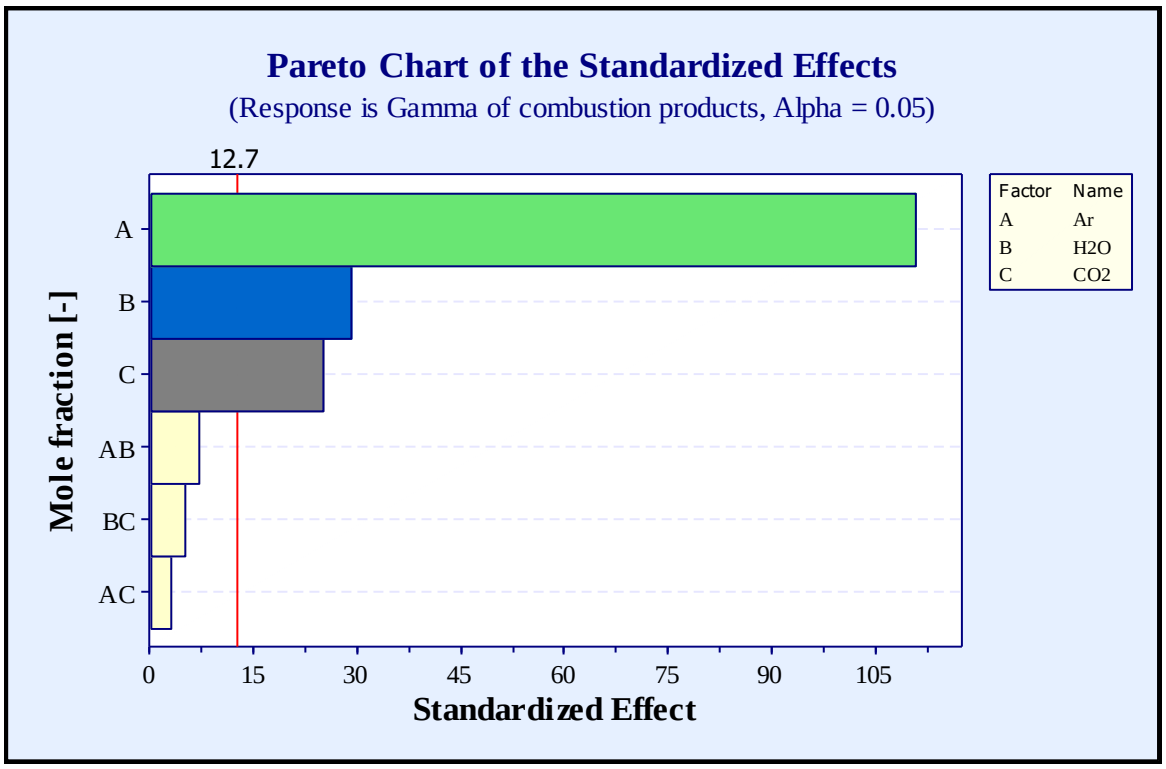

Figure 4.7 Pareto chart of blend components' effect on specific heat ratio

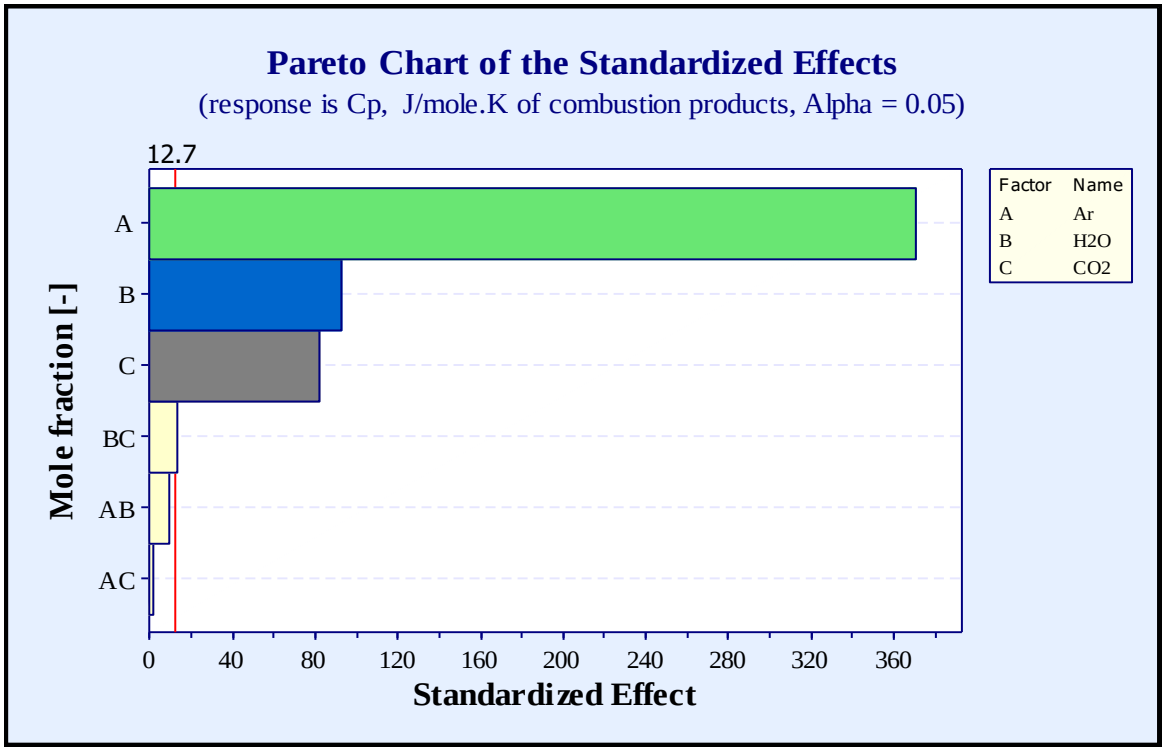

Figure 4.8 Pareto chart of the blend components' effect on heat capacity

Additionally, Ar has the highest effect on heat capacity among all blend components, as shown in Figure 4.8. A possible explanation for this is that Ar has the lowest heat capacity

of the blend components, taking into consideration that the standardized effect Pareto chart shows magnitude of effect but not whether this effect is positive or negative. Thus, it is necessary to consult Figure 4.13 to find the direction of this effect (i.e. whether it is an increase or a decrease). In fact, Figure 4.13 shows that increased Ar concentration in the blends' components results in a decrease in heat capacity in the combustion products, while higher CO_2 and H_2O positively impact this property.

Figure 4.9 indicates that water as a blend component has the greatest impact on water vapour in the combustion products. This can be attributed to the fact that an increase or decrease in the amount of water in the combustion process should directly correlate to an increase or decrease in its concentration because water vapour in the combustion products will result. This is evidenced in the main plot chart in Figure 4.14, which demonstrates an increase in water vapour as a combustion product.

This figure also shows that increased Ar concentration in the blend components has an inverse impact on water vapour concentration in the combustion products. Ar has slightly less effect on H_2O as a product than water as a gas component. However, CO_2 has very little impact on this.

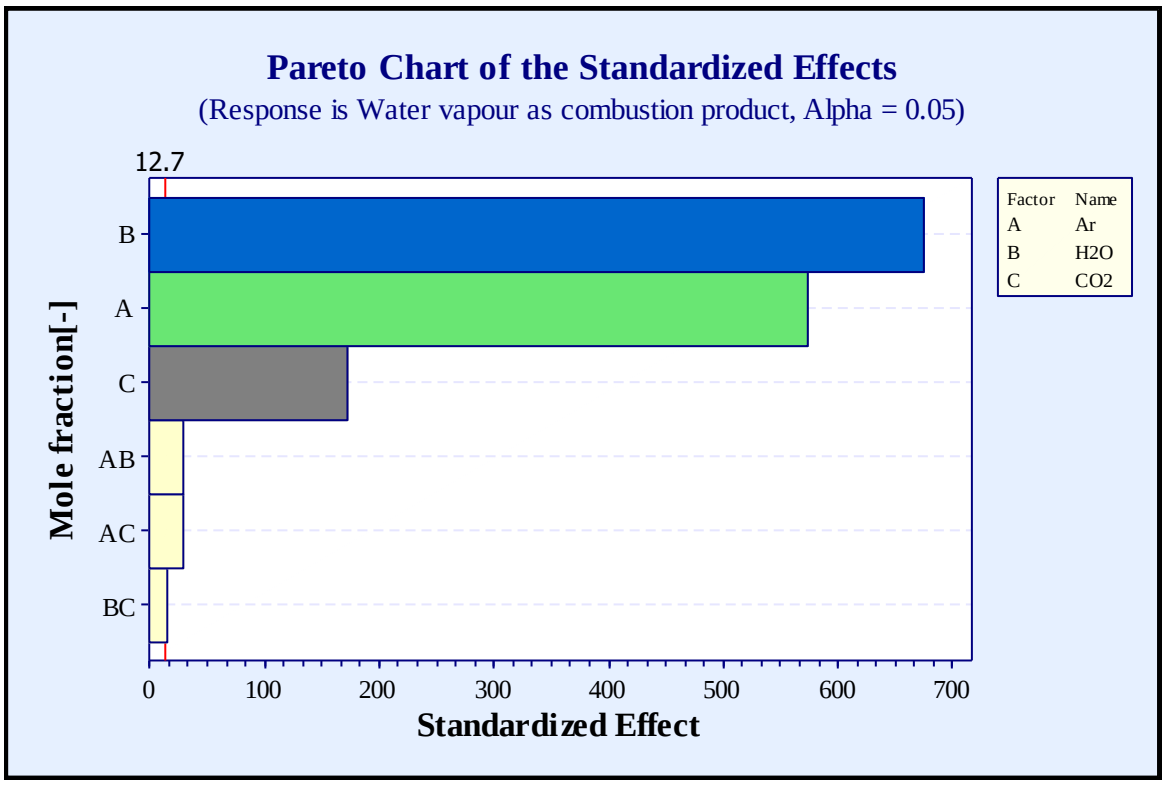

Figure 4.9 Pareto chart of the blend components' effect on H_2O vapour as a product

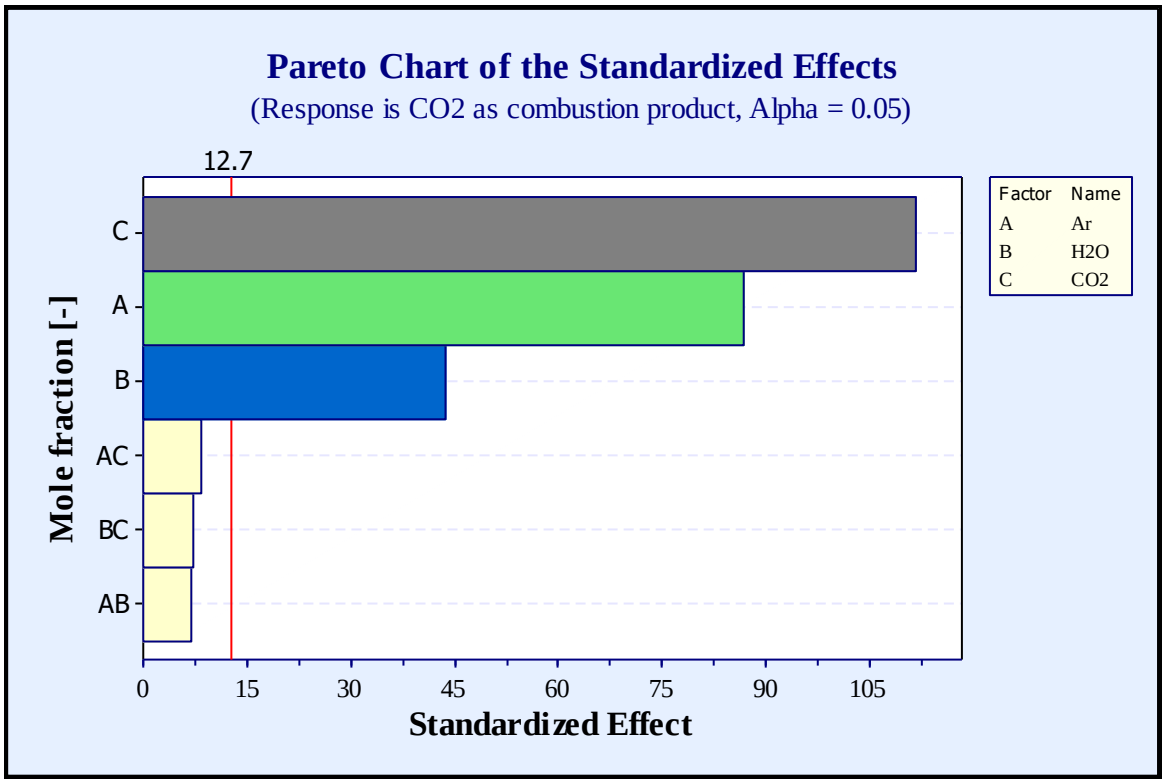

Figure 4.10 Pareto chart of blend components' effect on CO_2 as a product

Another combustion product is CO_2, as shown in Figure 4.10. The mole fraction of this product is impacted the least by water. In contrast, CO_2 as a gas component has the greatest effect on this product, slightly higher than that of Ar. In the same way as with water in the previous figure, this can be attributed to the fact that if the amount of CO_2 in the combustion process rises or falls, then a direct rise or fall in its concentration in the combustion products should result. This is supported by Figure 4.15, which shows that increased CO_2 concentration as a blend component has a positive impact on its level as a combustion product. However, increases in the proportion of water and argon as blend components are shown to have a negative impact on their proportions as combustion products.

Additionally, all of these figures are verified by another parameter, the (probability value) P-value shown in Table 4.2, which is calculated by the Minitab program. A smaller P-value for any gas component (Ar, H_2O, and CO_2) means that this gas has a greater impact than the other components on a specific thermodynamic property or product.

Table 4.2 P-value for blend components

Case	Product	P-Value		
		Ar	H_2O	CO_2
1	Temperature	0.002	0.001	0.002
2	Specific heat ratio	0.006	0.022	0.025
3	Heat capacity	0.002	0.007	0.008
4	H_2O	0.001	0.001	0.004
5	CO_2	0.007	0.016	0.006

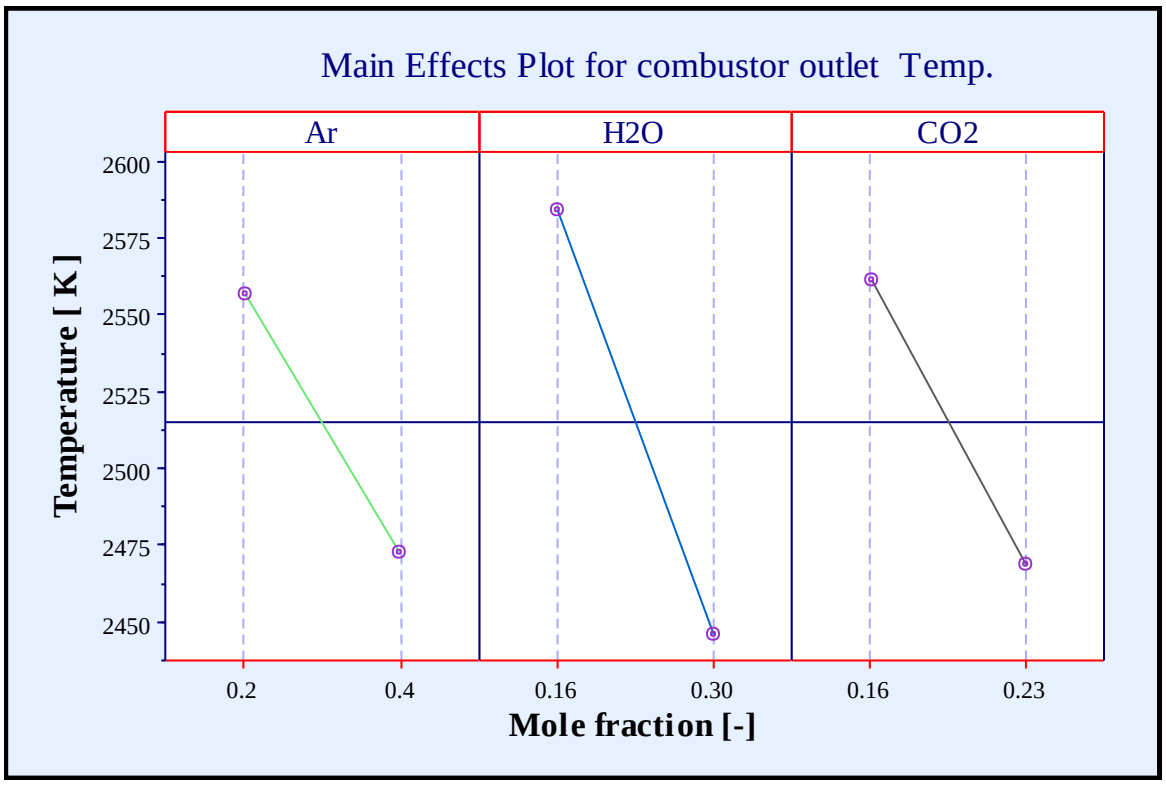

Figure 4.11 Main effects plot of combustion outlet temperature response towards each blend component

As mentioned previously, the Pareto charts only provide information about which of the gas components has the greatest impact on the characteristics of the products and they do not provide information on the direction of this impact. Therefore, the DOE approach was used to provide the following findings, which indicate the positive or negative effect of these gas components on the previously mentioned properties and products.

Figure 4.11 shows that increasing all of the gas components (i.e. Ar, H_2O, and CO_2) decreases the combustion product outlet temperature. The reduction in this outlet temperature is significantly affected by a rise in the proportion of H_2O.

This can be explained by the fact that injecting a significant amount of water vapour into the combustion process directly cools the combustion chamber, which leads to a reduction in the products' temperatures. In some cases, this could lead to the serious problem of system shutdown [101]. This figure also shows that increased CO_2, while having a smaller effect

than water, also noticeably reduces combustion product temperatures. This can be explained by the physical properties of this gas, which contribute to flame extinguishment [57].

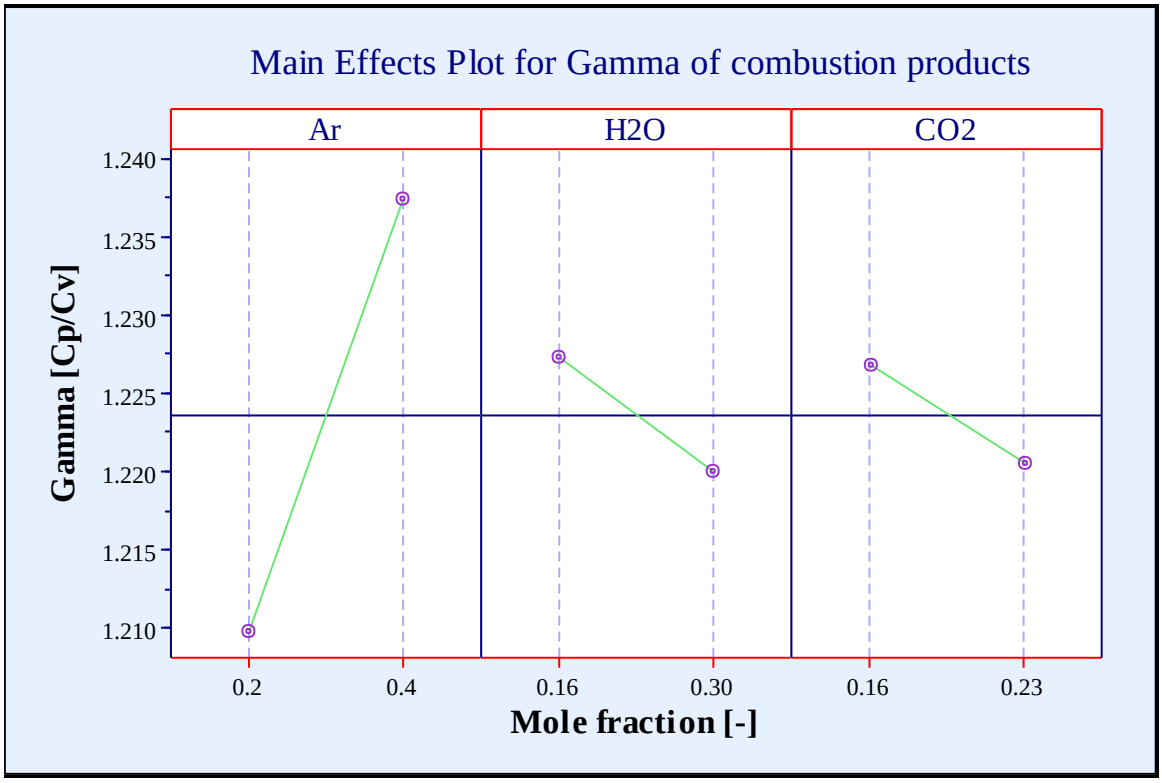

Figure 4.12 Main effects plot of specific heat ratio response towards each blend component

Figure 4.12 shows that the specific heat ratio responds positively to an increase in Ar. Coupled with the data from Figure 4.7, it can be seen that an increase in Ar concentration in the blend components has a significant effect on this thermodynamic characteristic in terms of increasing the specific heat ratio of combustion products, which may directly enhance turbine efficiency; as previously shown in Figure 2.22.

However, increases in the concentrations of CO_2 and H_2O in the blend components have a direct impact in terms of reducing combustion product temperature and, likely due to these components' comparatively lower specific heat ratios than Ar, they have a negative effect on this property in the combustion products [57, 59].

In the case of the property of heat capacity, increasing H_2O and CO_2 has a positive impact on its value while a rise in Ar reduces heat capacity, as shown in Figure 4.13.

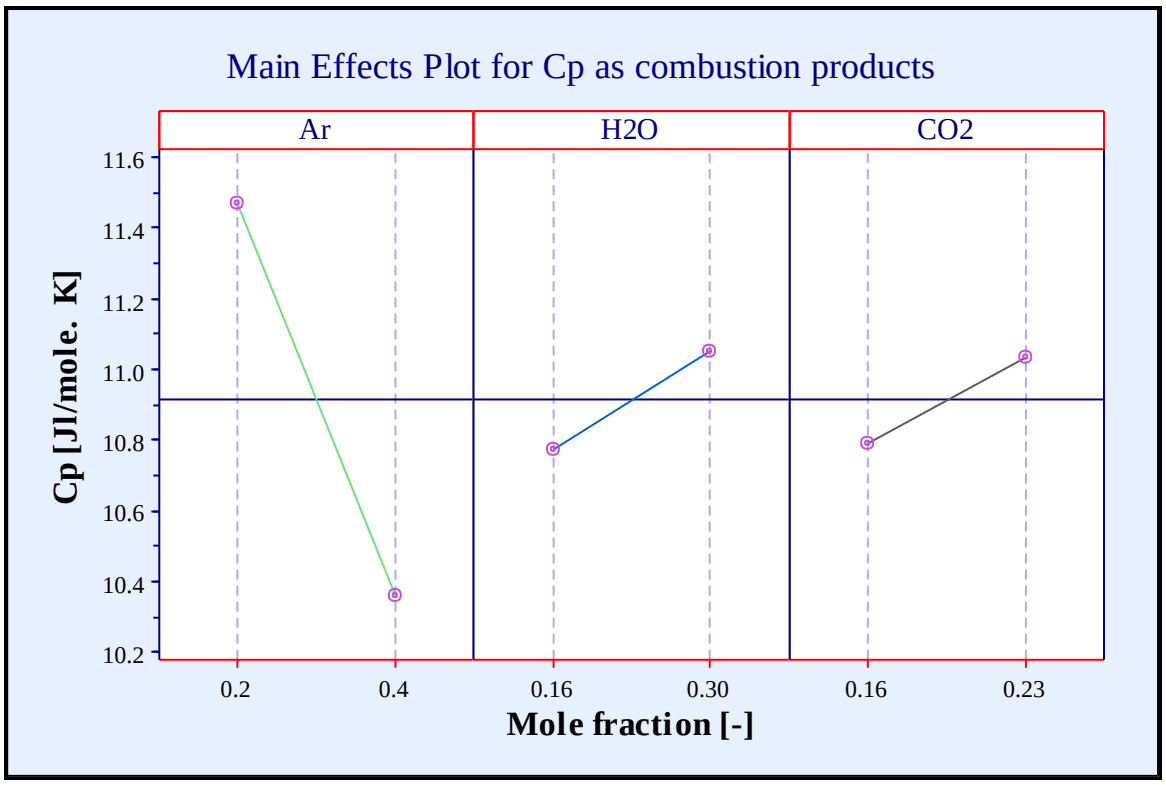

Figure 4.13 Main effects plot of heat capacity response towards each blend component

Figure 4.14, the main plot chart, shows the direction of the effect of each blend component on H_2O as a combustion product. It can be seen that an increase in the proportion of H_2O as a blend component correlates directly to a heightening of the mole fraction of water as a product.

This can be explained the fact that an increase in the amount of water in the combustion process should result in a direct increase in its concentration as water vapour in the combustion products. This is supported by the Pareto chart in Figure 4.9, which indicates that the proportion of H_2O as a blend component has the most significant impact on the resulting amount of H_2O as a combustion product. This significantly increased amount of water vapour could be used in a water recovery system (see Section 2.3.3).

It can also be seen in Figure 4.14 that an increased Ar concentration in the blend components has an inverse impact on water vapour concentration in the combustion products. This can be attributed to the fact that Ar, as an inert gas, does not interact with the combustion process. Thus, the remaining proportion of O_2, which usually interacts with N_2 in case of using air as a working fluid to create NO_x, helps to increase combustion temperature and this results in a reduced amount of water vapour in the combustor products [87, 112, 195].

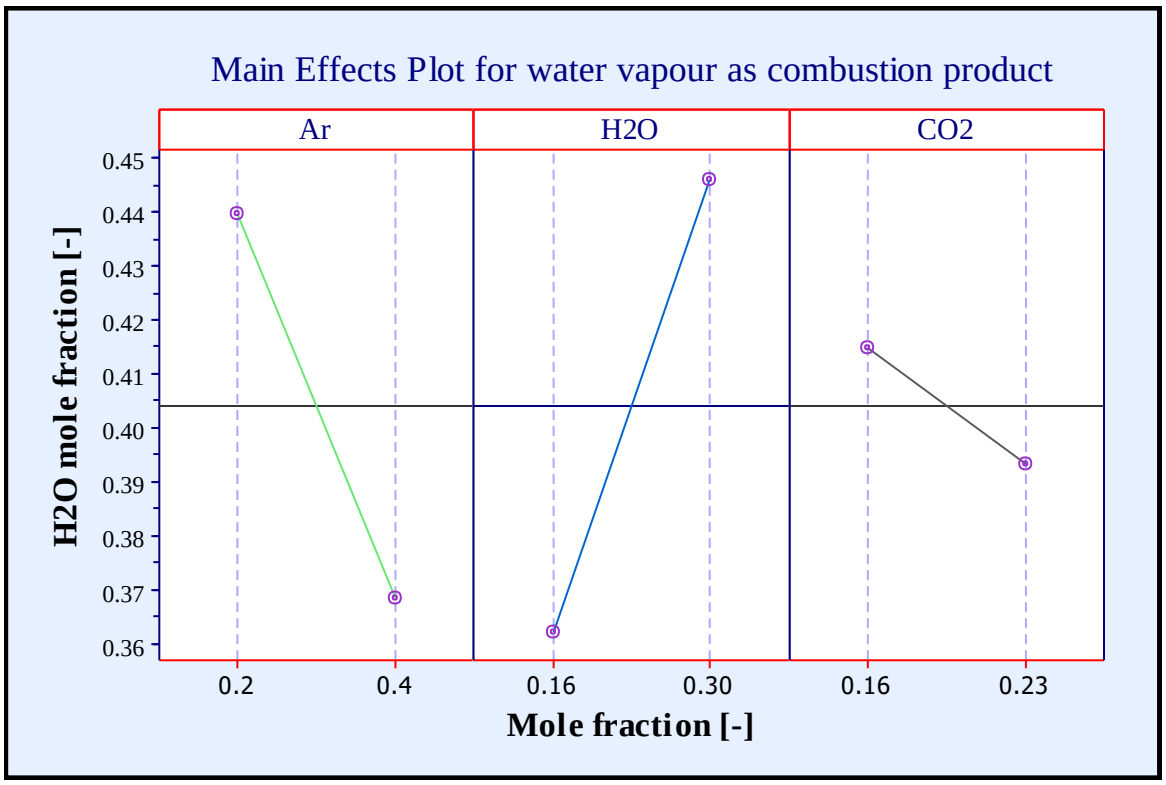

Figure 4.14 Main effects plot of response of H_2O as a product towards each blend component

Figure 4.15 illustrates how CO_2 as a blend component has a strong correlation to the mole fraction of the same gas in the combustion products. This figure shows that increased CO_2 concentration as a blend component has a positive impact on its level as a combustion product. An increase in this gas as a product occurs because the same amount of gas is produced in the recycling process as when it is used as a blend component.

However, this figure also shows that raising the proportion of Ar as a blend component decreases the amount of CO_2 present in the combustion products. This is likely to be due to

the fact that Ar is an inert gas and does not interact with the combustion process. As a result, the remaining amount of oxygen in the combustion chamber helps to complete the combustion process, which leads to a reduction in CO_2 products.

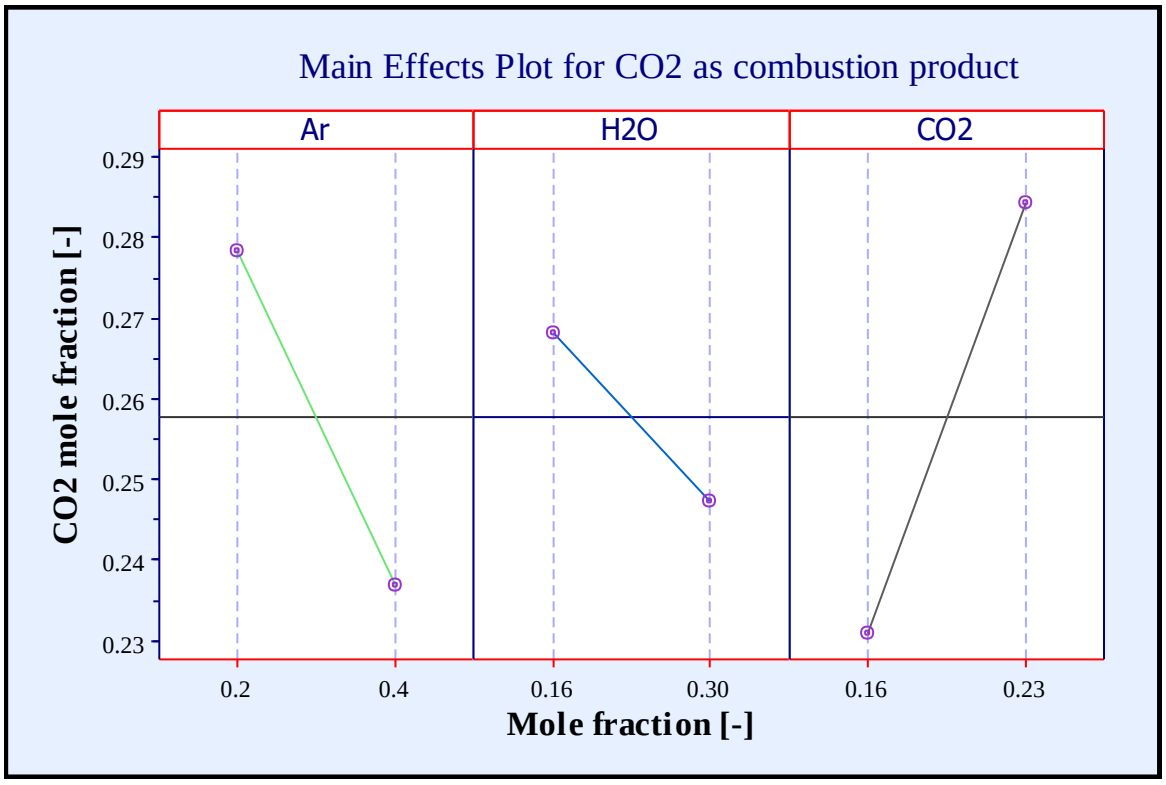

Figure 4.15 Main effect plot of response of CO_2 as a product towards each blend component

4.2.2.1 Analytical conclusions from DOE

Data on each blend component and its effect on specific combustion properties and products provided in the main effects' plots (see Figures 4.11 to 4.15) was analysed to ascertain the direction of these effects. This analytical data was linked to the individual Pareto chart for the same specific combustion property or product (see Figures 4.6 to 4.10) to indicate the magnitude of these positive or negative effects for each blend component.

Therefore, it was possible to show how the concentration of each component in the blend affects the reduction or increase in each thermodynamic characteristic or combustion product, along with the extent of this effect.

As an illustration of this process, data on the water as a blend component was analysed in the following way. Considering the main effects plot for combustion product outlet temperatures in Figure 4.11, it can be seen that all three blend components have a negative impact on this thermodynamic characteristic. The data from the Pareto chart in Figure 4.6 for this same property can then be considered. This figure shows that water has the largest magnitude of effect on combustion outlet temp of the three blend components.

Thus, by considering the two charts' data together, it can be clearly seen that an increase in water as a blend component leads to the biggest reduction in combustion product outlet temperature of all three blend components. Considering data from the main effects plot in Figure 4.12, it can be seen that both water and CO_2 as blend components have a negative impact on specific heat ratio.

This finding can then be linked to the data from Figure 4.7, where it is shown that water has a bigger impact on specific heat ratio than CO_2 as a blend component. Considering the data from the two chart types together, it can thus be clearly understood that increasing both H_2O and CO_2 as blend components by the same proportions results in water having a larger effect in reducing specific heat capacity.

Similarly, Figure 4.15 shows that both water and argon have a negative impact on CO_2 as a combustion product. Consideration of the Pareto chart for this combustion product in Figure 4.9 clearly shows that Ar has a larger effect than water on this combustion product. Considering the data from the two charts together, it can be clearly seen that increasing both Ar and H_2O as blend components by the same proportions results in water having a lower effect than Ar in reducing this combustion product.

If Figure 4.13 is considered, it can be seen that both water and CO_2 have a positive impact on heat capacity as a thermodynamic property. However, it is not immediately clear which

of these two blend components has a bigger positive impact on this thermodynamic property. Therefore, it is necessary to consider the data represented in the Pareto chart in Figure 4.8 to see that water has a more significant impact than CO_2 on this thermodynamic property.

Thus, it can be understood that increasing both water and CO_2 as blend components by the same proportions results in water causing a bigger increase in heat capacity of combustion products. In the same way, the main effects plot in Figure 4.14 indicates that water and Ar both have a significant impact on water vapour as a combustion product. It can also be seen that water impacts this combustion product in a positive direction while Ar impacts it in a negative direction. Considering this data together with that represented in the Pareto chart in Figure 4.9, it can be clearly seen that increasing both H_2O and Ar as blend components by the same proportions results in water having a larger effect in terms of increasing water vapour as a combustion product than Ar has in terms of reducing this combustion product.

The data from the DOE analysis has facilitated understanding of both the magnitude of the effect of each blend component on the combustion process and its products and the direction (either positive or negative) of these effects. This is essential information for the selection of the optimum blend because the goal is to select the blend which provides the best balance of these effects in terms of thermodynamic properties that directly affect the efficiency of the turbine, while also producing the necessary amounts of CO_2 and water vapour as combustion products, which can then be recycled in the proposed CARSOXY cycle.

4.2.3 **Combustion characteristics**

Identification of the optimum CARSOXY blend requires a deep knowledge of its thermodynamic properties through a combustion process. Moreover, a comprehensive understanding of its flame speed with combustion characteristics is needed.

Following these investigative goals, the Chemkin-Pro program initially tested the 16 blends at 288 K with atmospheric pressure and equivalence ratio $\phi = 1$ to find flame speed compared to air at the same running conditions. After this analysis, eight blends were rejected due to their flame speeds being too far from the reference value for flame speed, which was that of conventional air as a working fluid.

Thus, the following eight tabulated blends were selected because their flame speed values were around those of air as a working fluid. The flame characteristics of these eight blends were then simulated at 900 K with 10^6 Pa, which is similar to the operating conditions used by the Gaseq program to simulate conventional combustor operating conditions.

Table 4.3 Flame speed for selected blends at 10^5 and 10^6 Pa, with ϕ=1 compared with air

Pressure condition (Pa)	Flame speed (m/s)								
	Air	Eight optimum blends							
		27	58	79	109	33	26	18	6
10^5	0.431	0.218	0.312	0.453	0.384	0.217	0.203	0.201	0.204
10^6	0.151	0.797	0.127	0.212	0.178	0.723	0.640	0.650	0.676

A comparison was then made for the eight flame values against the one obtained from the reference. Equivalent running conditions were considered for this comparison approach. Further investigations were carried out for those blends that have flame speeds close to the reference, as shown in Table 4.3.

Out of the eight blends, the chosen blends for further investigation were 58 (25-23-19), 79 (24-19-19), and 109 (24-8-29) because these blends were shown to have flame speeds close

to those of air at the same running conditions of (10^5) and 10-bar (10^6) pressure. Blend 27 (30-24-16) was also included in this investigation, even though its flame speed descends to around half the reference value, due to the fact that its data for other parameters obtained from Gaseq, especially outlet temperature (see Appendix 2), was closer to the values for air. These four mixtures were then compared according to characteristics obtained from Chemkin-Pro software in both the PSR and PFR clusters.

Figure 4.16 shows that the temperatures of blend 58 are approximately equivalent to those produced when air is used as the conventional working fluid. Both blends 109 and 79 have temperatures around 100 degrees higher than the reference's values. Only blend 27 has product temperatures that are considerably – by approximately 150 degrees - lower than the reference.

Blend 58 has a higher steam component concentration compared to blends 79 and 109, which leads to these blends having a higher combustion temperature. Additionally, blend 27 has a similar steam concentration to blend 58 as a component of the proposed blend. Blend 27 also includes a high concentration of argon as a component, which is also likely to have an impact in terms of reducing combustion product temperature, as explained in the DOE tests in the previous section. As such, the combustion temperature using blend 27 has the lowest value of the three proposed blends and conventional air as a working fluid.

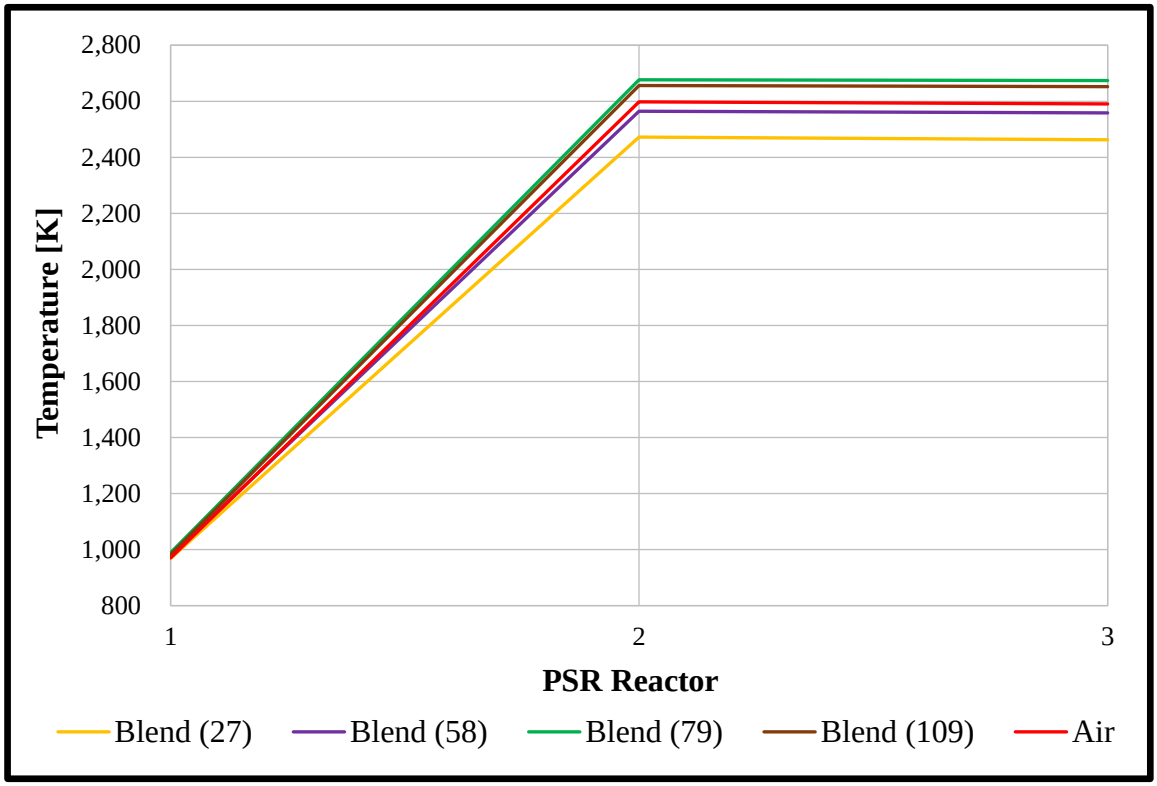

Figure 4.16 Product temperature at PSR, for selected blends compared with air

It is important to note that the flame speed value of blend 27 is very far from the value of air in both running conditions. Therefore, at this stage in the optimisation process, blend 27 could be considered much less likely to be proposed for use as an alternative working fluid to air in the combustion process, compared to the other blends investigated here.

Blend 58 also has a high concentration of CO_2 in the exhaust gases, which approximately matches the values of blend 79. These two blends produce around 20% more CO_2 in the exhaust gas than air does, as shown in Figure 4.17. This figure also illustrates that the maximum and minimum values of CO_2 products are produced by blends 109 and 27, respectively.

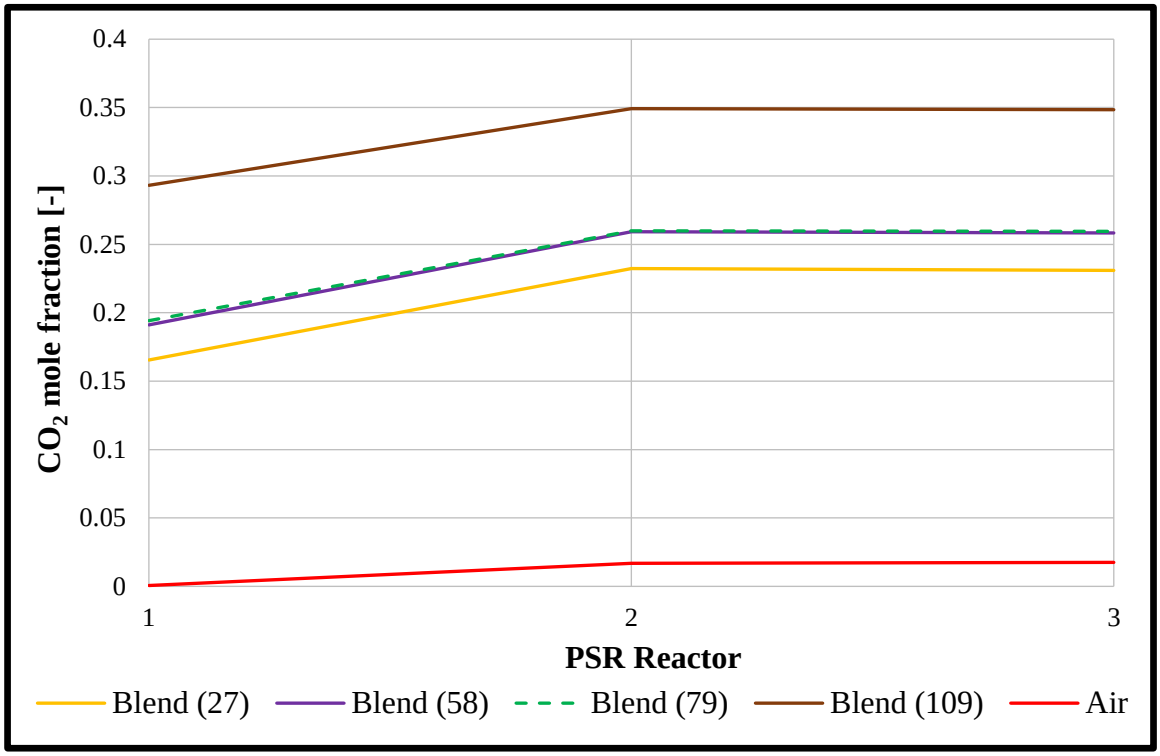

Figure 4.17 CO_2 in exhaust gas at PSR, for selected blends compared with air

These blends all have a higher proportion of CO_2 than air. Therefore, these blends as working fluids produce a higher percentage of CO_2 in their combustion products. It can be clearly seen that the increase in concentration of CO_2 as a blend component has the effect of increasing its level as a combustion product.

This further investigation of combustion characteristics using Chemkin-Pro supports the data in the previous section, which were obtained from the DOE using the Minitab program. This also further supports the novel concept of utilising these blend components in combination in an industrial gas combustor as a practical approach to be combined with CCS technology to recycle CO_2 in the combustion process and thus reduce emissions of this harmful gas from the industrial combustion process.

Figure 4.18 shows that blend 58 and blend 27 produce the highest values of H_2O vapour in the exhaust gases. These blends have mole fractions of water product that are about 30% higher than conventional air as a working fluid. In comparison with these blends, blend 79

produces approximately 5% less water, while water production for blend 109 is around 10% higher than the reference.

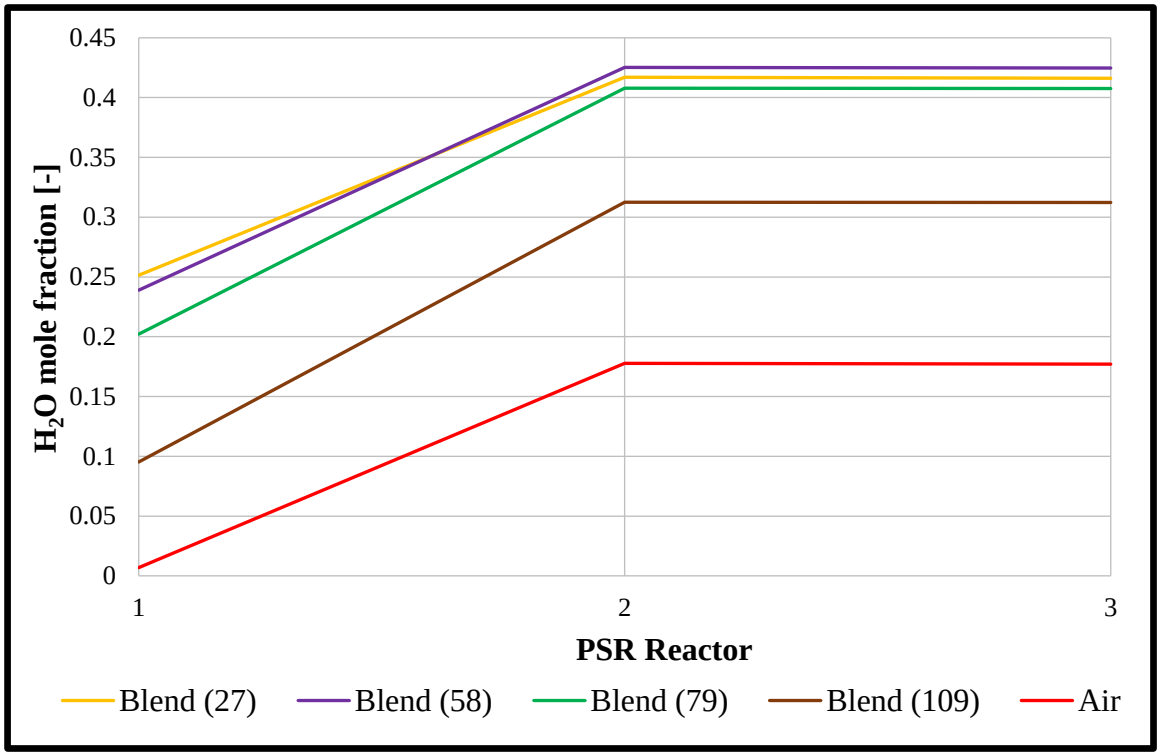

Figure 4.18 Water in exhaust gas at PSR, for selected blends compared with air

The blends all possess higher concentrations of H_2O than air. Therefore, as with CO_2, these blends as working fluids produce a higher percentage of water vapour in their combustion products. In this regard, the data gathered from Chemkin-Pro also support the data obtained from Minitab DOE. The fact that blend 58 has a higher steam concentration than blends 109 and 79 results in its significantly higher proportion of water vapour as a combustion product. At the next lowest levels to blend 58, blends 79 and 109 produce water vapour in the PSR reactor according to their proportion of steam as a blend component.

Compared to blend 27, blend 58 produces slightly more steam as a combustion product, even though both have a similar proportion of water vapour in their components. This could be due to the fact that combustion temperature when using blend 58 in the combustion process is approximately equivalent to the value of combustion temperature when using air. This

could result in operating conditions similar to those obtained from air to complete the combustion process. Therefore, this could potentially increase the amount of water vapour produced and convert hydrocarbons to water vapour, producing an increased proportion of steam as a combustion product when using blend 58.

This increased level of water vapour produced by the proposed blends supports the proposed use of steam as one component of the novel CARSOXY blend because it could be practically utilised in a water recovery system in the proposed gas turbine cycle to increase its efficiency compared with a conventional cycle.

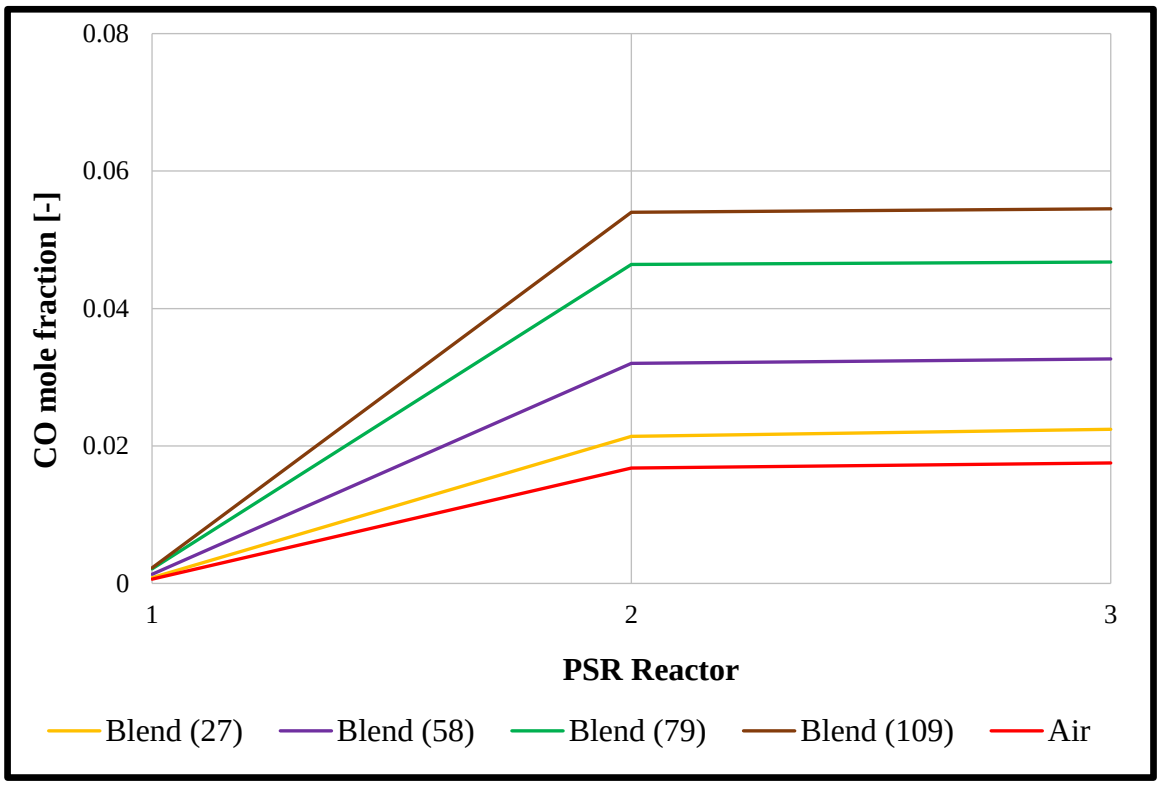

Figure 4.19 CO products at PSR, for selected blends compared with air

In terms of CO concentration as a product, blend 58 has a value 2% higher than air as the reference. Blend 109 has the highest CO products, while blend 79 is approximately 4% higher than the reference, as shown in Figure 4.19.

As shown above, using Blend 58 provides similar combustion temperatures to those produced when using air as a working fluid. This could lead to a more complete combustion process and reduce the amount of CO that is converted to CO_2, due to the more complete combustion process. Another factor that could potentially affect the combustion temperature is the CO_2 proportion as a blend component.

It can be seen that blend 58 has the same CO_2 concentration as a component to blend 79. However, blend 58 produces a lower proportion of CO than that produced by blend 79, which is likely to be due to its combustion temperature being similar to that when using air and resulting in a more complete combustion process. Despite the combustion temperature of blend 79 being almost equal to that of blend 109, CO as a combustion product when using blend 109 has the highest value out of the proposed blends, which can be explained by the fact that it has the highest concentration of CO_2 as a blend component.

Downstream of the reaction zone, the concentration of water remains high, resulting in a drop of around 40 K for the temperature of the hot gases of blend 58 (25-23-19), as shown in Figures 4.20 and 4.21. These figures also demonstrate that a blend such as 27 (30-24-16) can still have acceptable product values under the combustion process.

However, the considerable fall in the flame speed, in comparison with air under the same working conditions, leads to a higher propensity for blow off, whereby the concentration of water extinguishes the flame. These results match those of the PSR, which provides support for the validity of this investigative approach.

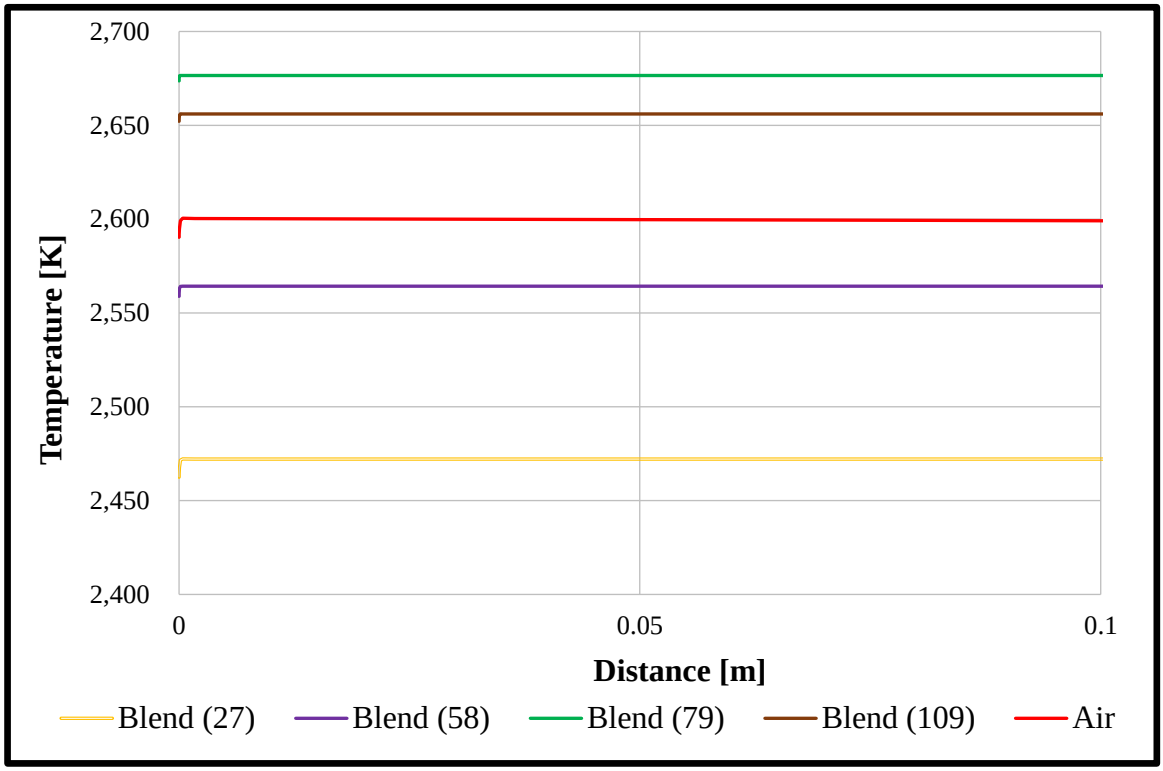

Figure 4.20 Outlet temperature at PFR

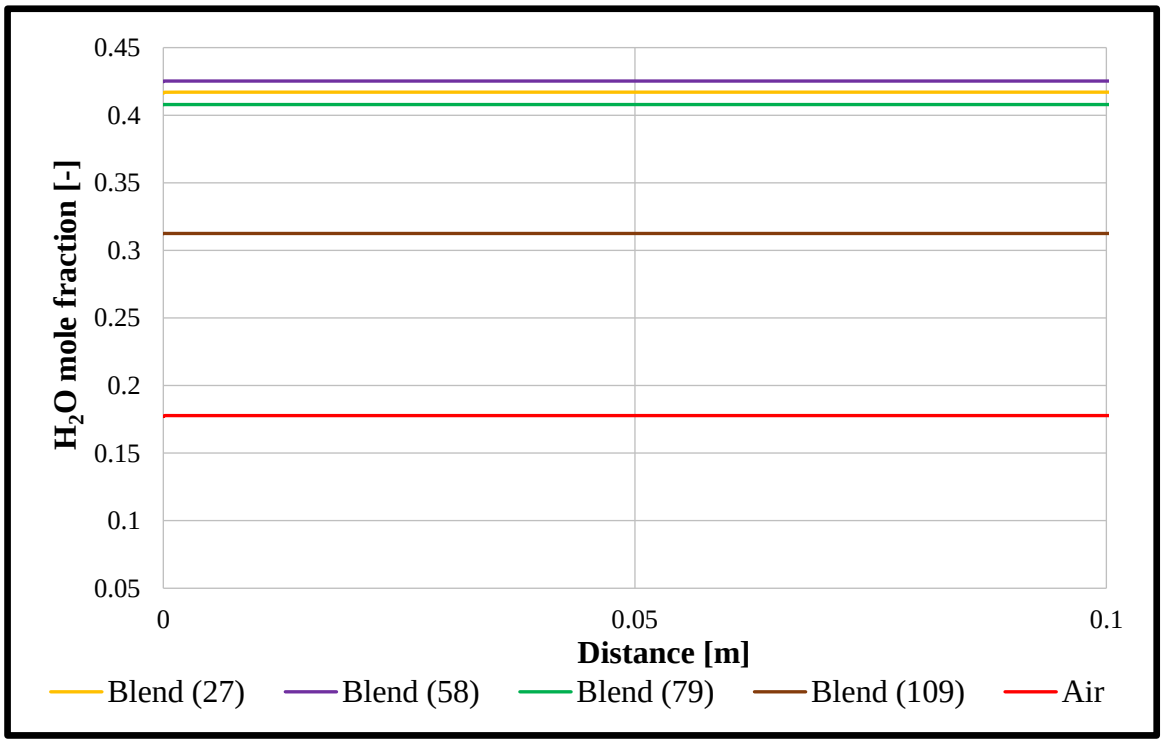

Figure 4.21 H_2O products at PFR

Figure 4.22 shows the mole fraction of unburned nitrogen in conventional air as a working fluid. This value is approximately three times higher than the unburned mole fraction of Ar

in all the selected blends. This results from nitrogen being a component of conventional air as a working fluid but not included in the components of the proposed blends. Thus, using the proposed blend should eliminate NOx emissions from the combustion process. This provides support for the idea of replacing nitrogen with this combination of blend components, while attempting to identify the best balance of these components to provide a feasible replacement for conventional air as a working fluid.

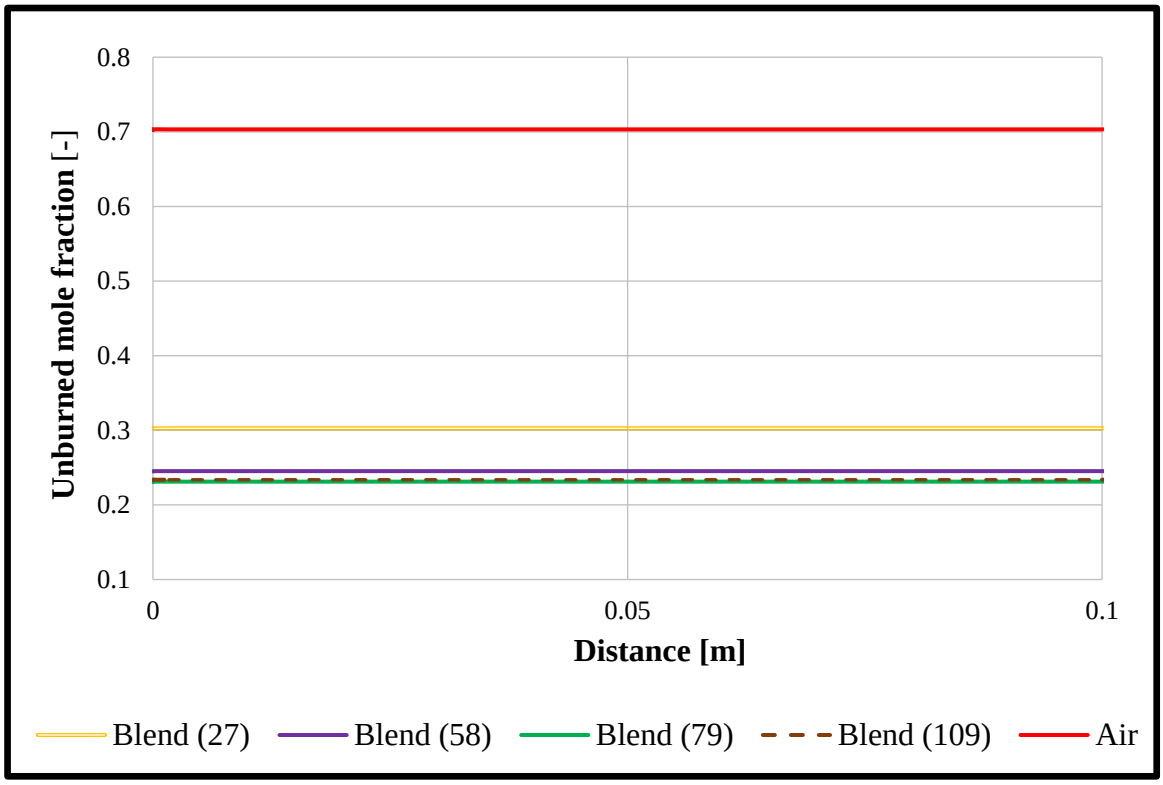

Figure 4.22 Unburned N_2 (for air), Ar (for all other blends) at PFR

The increase in the proportion of argon as a blend component has a direct effect on its concentration in the combustion products. Therefore, blend 27 produces the highest amount of Ar as a combustion product, and this amount as a combustion product is equivalent to its proportion as a blend component. Blend 58 produced the second highest result, as would be expected from its having the second highest proportion of Ar as a blend component. Blends 79 and 109 produced approximately the same level of Ar as a combustion product, which was the lowest level among these blends, as would be expected from their identical

proportions of Ar as a blend component, which are also the lowest concentrations among these blends. This figure shows that there is no unburned nitrogen for any of the selected blends, while the residual Ar could be recycled in the combustion process. Therefore, the products of NO_x are eliminated in all four blends, supporting the use of the blend to contribute to maintaining a clean atmosphere.

Analysis of the data in all of the preceding figures has clearly indicated that blend 58 (25-23-19) is the optimum blend and can be used as an alternative to air as a working fluid in the combustion process of industrial gas turbines, due to its possession of equivalent characteristics to those obtained from conventional air.

The outlet temperature produced by this blend approximately matches that obtained from the reference. This is important because it indicates that use of this blend as an alternative to air as a working fluid in existing industrial combustors should be feasible because modifications in temperature limit design are unnecessary. In addition, the mole fraction of CO_2 as combustion product was high compared with other blends. Such a comparatively high value of this product can be used in an oxy-combustion process, which is required in the proposed CARSOXY cycle to be used in the recirculation process for this technique.

The data indicated that the flame speed of the selected optimum blend is only slightly lower than that of the reference under the same operating conditions. This should mean that this blend provides at least the same combustion conditions in terms of providing ignition and flame stability as air as a working fluid, in comparison with other blends. This blend also provided the highest concentration of water vapour in combustion products, when compared to the other selected blends and air. This is a useful characteristic for the water recovery system in the proposed cycle.

In terms of the mole fraction of CO as a combustion product, blend 58 was located near the middle of the range for the selected blends. This comparatively low level indicates that this blend helps to complete the combustion process, leading to a reduction of harmful CO emissions. An important motivation for investigating whether the proposed blend could replace air as a working fluid in industrial combustors is to reduce the environmentally dangerous emissions that are currently produced by industrial gas turbines.

Although blend 109 was also a strong candidate for selection because it has very similar properties to those of blend 58, blend 58 was selected as the optimum blend because the value of blend 109's combustion product outlet temperatures was significantly higher than that of air, which could mean that modifications to TIT limits would be necessary, whereas these modifications would not be needed for blend 58 to be used as an alternative working fluid to air.

Thus, in the following section, a theoretical examination of the optimum indicated blend (58) as a working fluid in a real gas turbine is carried out to compare the turbine's performance when using the blend and when using conventional air.

4.3 The numerical simulation model

As outlined in Section 3.2, the calibrated computational model was used to examine the performance of an industrial gas turbine running with the novel blend in comparison with conventional air as a working fluid. Each of the seven cases in the following figures (Figures 4.23–4.29) represents a different set of running conditions in terms of mass flow rate and gas TIT used in the 3.9 MW Rolls Royce gas turbine. The working conditions were considered to be the same to calculate the parameters in Equations 3.2–3.8, particularly specific output power and turbine efficiency, and to compare the performance of the Rolls

Royce engine running with NG/air as a working fluid and blend 58 with an oxygen atmosphere combustion process using methane as a fuel.

4.3.1 Comparison of the optimum blend with NG/air

The results obtained from the numerical simulation show that heat provided by the CARSOXY blend with methane is approximately 5% higher than NG/air as a working fluid, as indicated in Figure 4.23. This additional supplied heat could help to complete the combustion process, which would improve its efficiency. A more complete combustion process results in fewer unburned hydrocarbons, which would also contribute to a reduction in emissions.

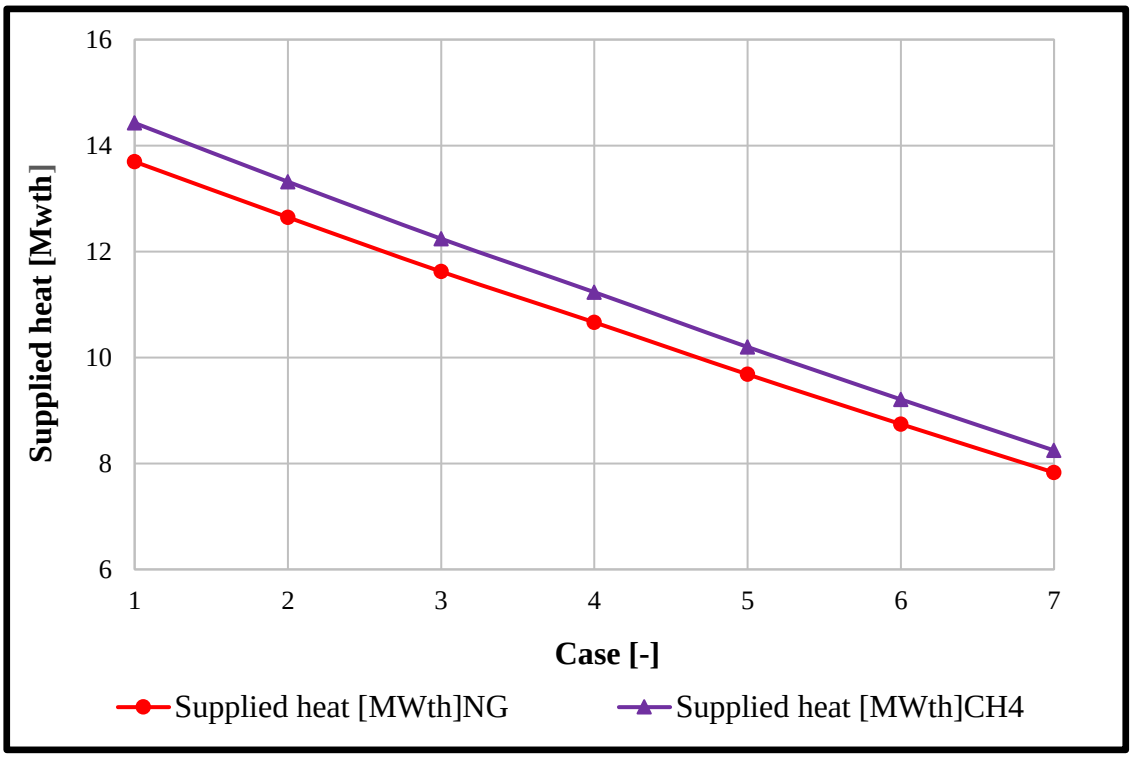

Figure 4.23 Supplied heat in gas turbine in comparative approach

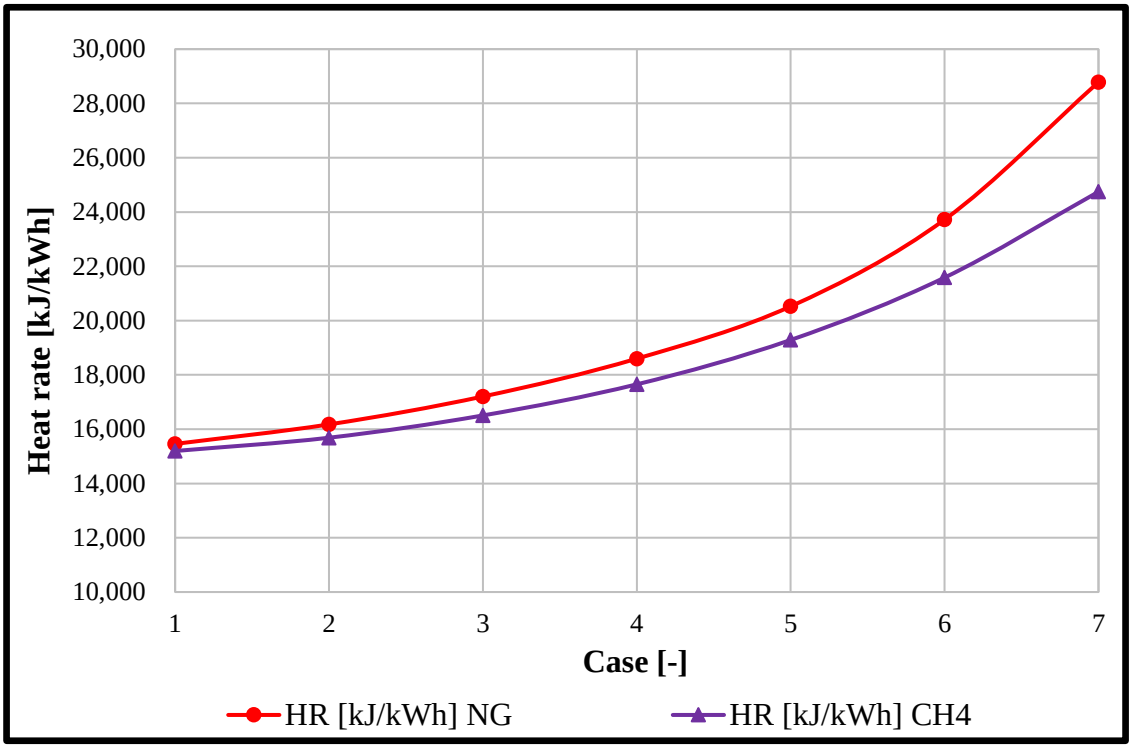

Figure 4.24 Heat rate of gas turbine in comparative approach

In terms of heat rate comparison, the optimum blend is 2–16% lower than NG/air, as shown in Figure 4.24.

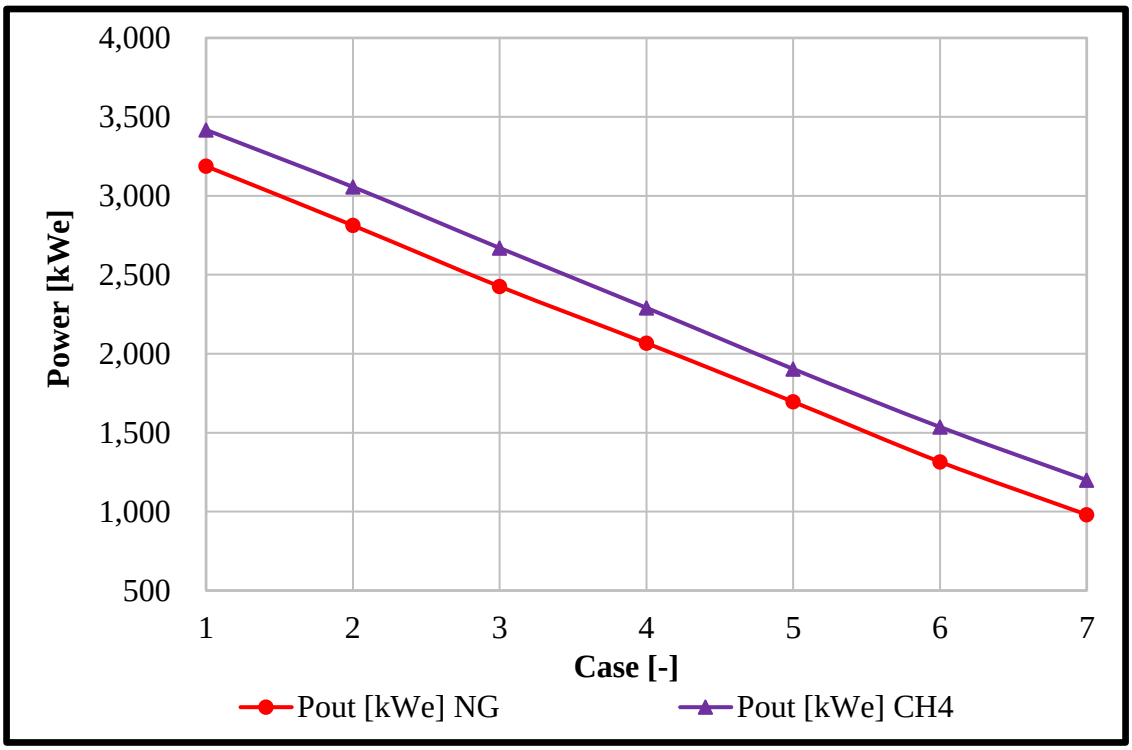

Figure 4.25 Output power of gas turbine in comparative approach

Figure 4.25 shows that the output power using the CARSOXY blend is 6–18% higher than in the case of using NG/air, due to the enhancement in the thermodynamic properties.

As a result, the overall efficiency of the turbine running with the optimum blend is 1.75–13.93% higher than when running under NG/air operating conditions, as illustrated in Figure 4.26. This indicates that the optimum blend 58 could be proposed as a replacement for air as a working fluid in the combustion process of a gas turbine. Additionally, CO_2 as a combustion product can be recirculated in the gas combustor to lessen its concentration in exhaust gases, thus contributing to protecting the environment.

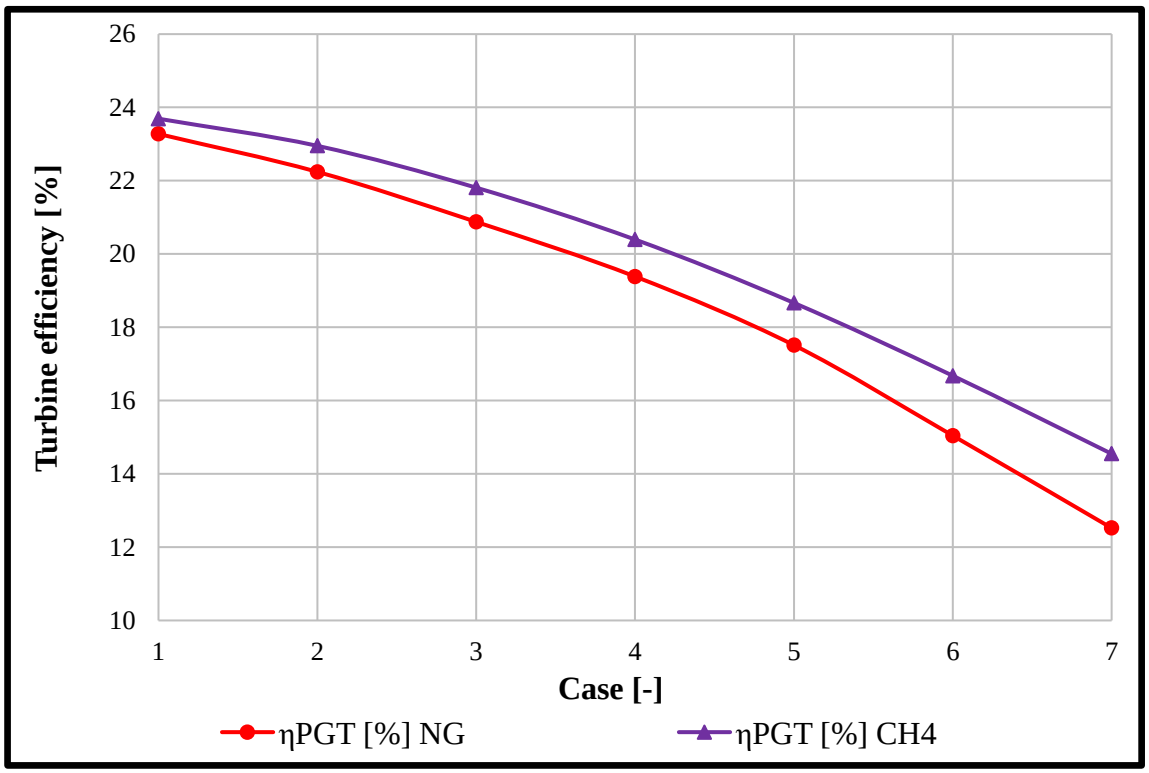

Figure 4.26 Gas turbine overall efficiency in comparative approach

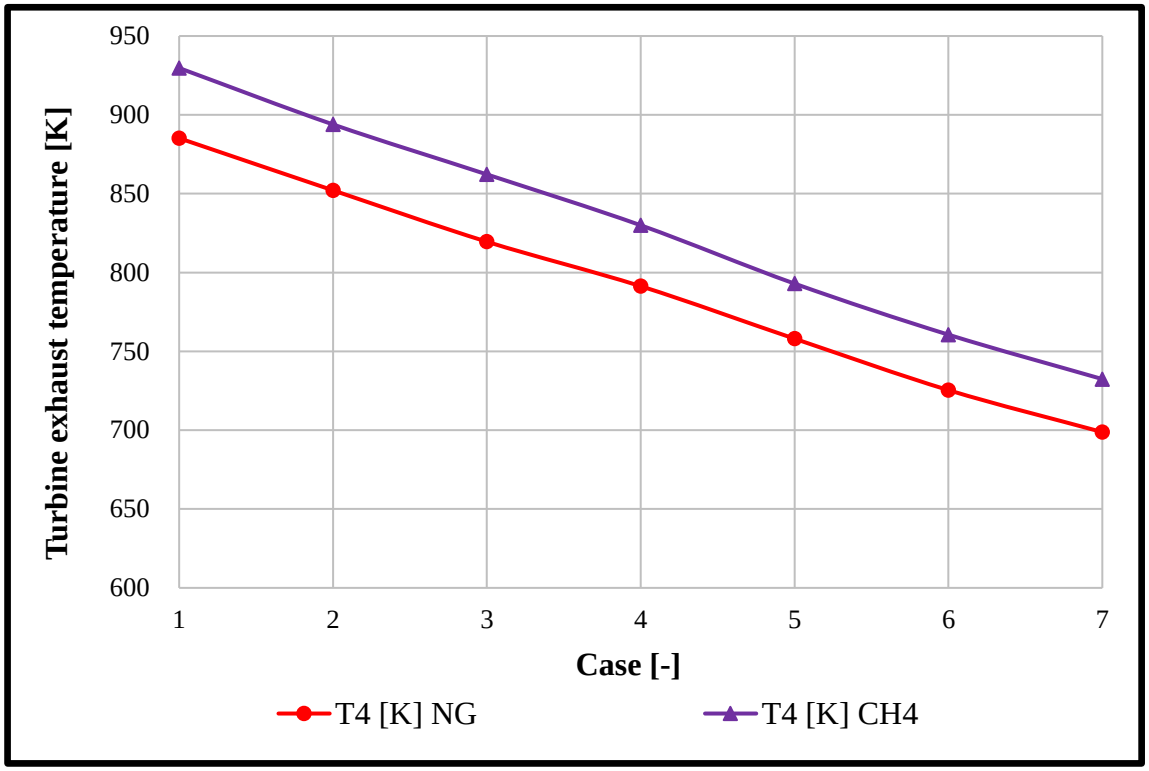

Figure 4.27 Exhaust temperature of gas turbine in comparative approach

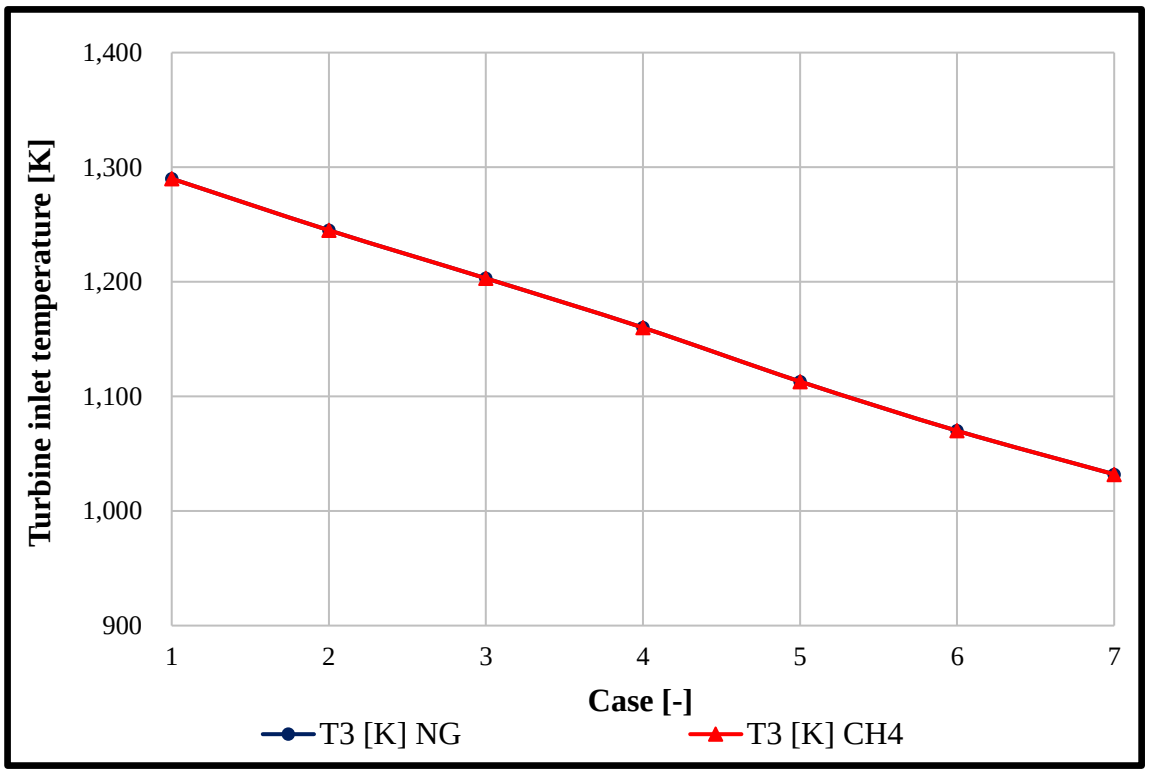

Figure 4.28 Inlet temperature of gas turbine in comparative approach

The temperature of the exhaust gas for the selected blend is greater than that obtained when using NG/air for the same inlet temperature, as shown in Figures 4.27 and 4.28, with a temperature difference of about 4.5%. In industrial processes, this temperature difference could be useful in heat recovery systems that can be utilised to produce water vapour. The steam from the humidification process can then be recirculated in the gas combustor as one component of the optimum blend.

The computational comparison approach using the new numerical model indicated that the specific output power produced by the Rolls Royce gas turbine running blend 58 with oxygen and methane as a reactant was between 219 kWe and 244 kWe higher than that produced by NG/air. The model also indicated that the efficiency of the turbine was improved by between approximately 2–14% using the indicated optimum blend in comparison with NG/air as a working fluid for the same inlet temperature.

Thus, per these results, the optimum indicated CARSOXY blend could feasibly replace air in the combustion process of the gas turbine in the proposed cycle. This supports this study's aim to establish the feasibility of use in terms of providing at least equivalent efficiency and output power to propose the novel CARSOXY blend as a practical replacement for air in industrial gas combustors and thus help reduce harmful pollutants emitted from power plants' gas turbines.

4.4 **Summary**

This chapter has focused on the integration of several computational approaches, which were employed to obtain data for analysis to indicate the optimum blend that could be used as a working fluid in a gas turbine combustor. A number of gas mixtures (comprising Ar, H_2O, and CO_2) were numerically generated utilising a pure domain of oxygen as a CARSOXY blend and methane as a fuel.

The final data resulting from an integrated empirical approach with a simulation model indicated that blend 58 (i.e., 25%Ar-23%H_2O-19%CO_2) has similar characteristics (e.g. thermodynamic properties and flame speed) to those obtained for conventional fuel with an air domain under equivalent operating conditions. The optimum CARSOXY blend also produces the highest mole fraction of water with a high proportion of CO_2 in the exhaust gas, with zero NO_x emissions. Consequently, water could be used in humidified injection while residual CO_2 might be captured and recycled in a combustion process.

The data obtained from the new numerical model showed that using the CARSOXY blend with methane as a fuel improved the industrial gas turbine's performance. Both the specific output work and turbine efficiency were enhanced in comparison with NG as fuel and air as a working fluid under the same running conditions. However, the heat consumption for this blend is around 5% higher than that of NG/air.

The next chapter will detail the use of Aspen Plus to examine the efficiency of the CARSOXY cycle.

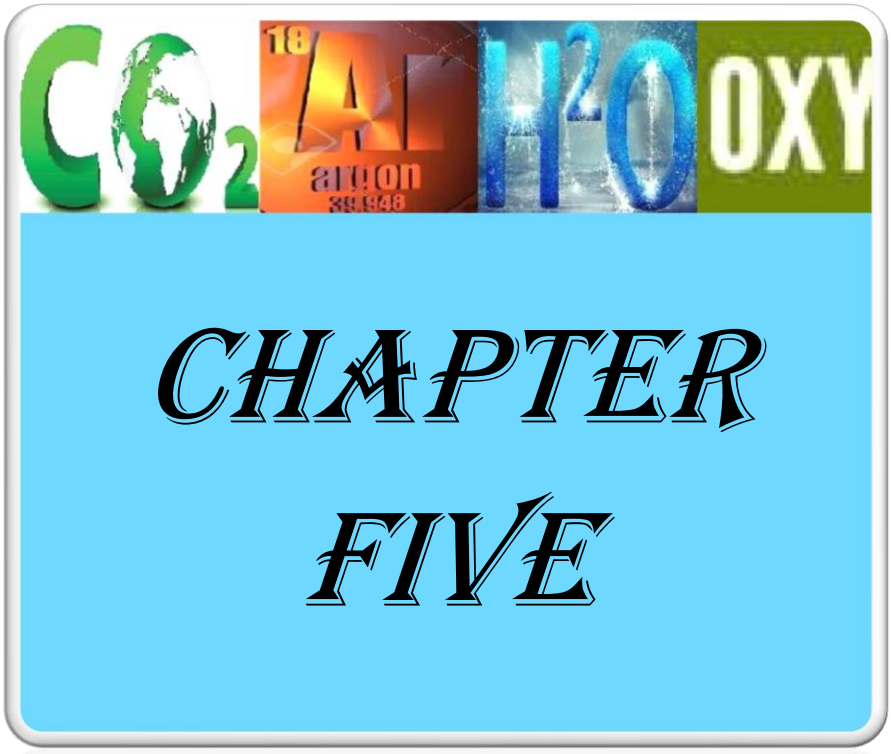

CHAPTER FIVE

Chapter 5 The efficiency of the CARSOXY cycle

This chapter details the theoretical investigation of the use of the proposed CARSOXY blend in an industrial gas turbine compared with a conventional air humidified cycle. The aims are to analyse theoretically modelled data on the effect of the novel proposed blend's use on cycle efficiency and exhaust gas products, with the purpose of providing further theoretical support for the previously discussed benefits of using the CARSOXY cycle in industrial gas turbines.

First, the process of setting up the Aspen Plus simulation procedure is described. Then, theoretical data comparing the use of CARSOXY with a conventional air humidified cycle in terms of cycle efficiency is provided and analysed. This is followed by presentation and discussion of data on cycle performance, compressor work and compressor outlet temperature. Next, data and analysis on TITs are given, followed by the presentation and discussion of CO, H_2, CO_2, H_2O and Ar products for CARSOXY against NO products for the air humidified cycle. After that, combustion product data is presented as a reference for the study's experimental work. Finally, a chapter summary is provided.

Briefly, cycle efficiency is found to be higher running with CARSOXY when compared to an air humidified cycle, TITs are shown to be lower along with CO and H_2 products, while CO_2 and H_2O products are shown to be higher, all of which broadly support the proposed use of the CARSOXY cycle from efficiency, economic and environmental standpoints.

5.1 Aspen Plus simulation procedure

The CARSOXY cycle that is used in this study, as mentioned in Chapter One (see Figure 1.21), basically consists of two compressors, two mixers, a water pump, an ASU, a stream splitter, a turbine and heat exchangers. In this cycle, the working fluid, which comprises O_2,

Ar and CO_2, is first compressed by Compressor 1. Then, the compressed blend is mixed in Mixer 1, with the lower portion of water vapour coming from a splitter to produce a humidified mixture that flows to the gas combustor. The higher portion of water vapour flows to Mixer 2 to be utilised for dilution of combustion products. The aim of the dilution process is to lessen the temperature of the combustion product to within an acceptable range for the turbine design [83]. A mixture that consists of a high proportion of CO_2 with a low concentration of Ar is compressed in Compressor 2 also to be used in Mixer 2 for the dilution process.

The diluted combustion stream then enters a turbine to produce work to generate electricity. Following that, the exhaust gas passes through the heat exchanger, known as the Recuperator, to exchange heat with pumped water to produce water vapour that is employed for humidification and dilution processes in the cycle. Water supplied to the cycle is pumped to a condenser, where it is initially heated by exhaust gas. The temperature of the exhaust gas reduces in the condenser, which helps to separate CO_2 and Ar from the exhaust gas so they can be recirculated in the compressors. CO_2 from any other industrial source could also be compressed in Compressor 2 of the modified EvGT cycle to be used for this dilution process. The temperature of the heated water exiting the Condenser increases in the Economiser due to heat exchange with the compressed mixture of CO_2 and Ar.

The CARSOXY cycle was modelled using Aspen Plus program v. 10 to simulate its performance. In this simulation model, the reactants were specified as follows: methane as fuel, CARSOXY or air as a working fluid and anticipated combustion products (CO_2, H_2O, NO_2, N_2O, H_2 and CO) were defined. The default equation of state for Aspen Plus is the Peng–Robinson equation of state, which was selected for fuel, CARSOXY and air. The Gibbs Reactor model was selected for the gas turbine combustor. This model uses the Gibbs free energy equation to calculate the equilibrium's composition [173, 179, 196]. Table 5.1 shows

the blocks selected for modelling both cycles with assumed efficiency values [174, 197]. Flowsheets for the modified unit using CARSOXY and humidified gas turbine cycles are sequentially illustrated in Figures 5.1 and 5.2.

Table 5.1 Definition of blocks

CARSOXY	Block	Definition	Isentropic efficiency	Mechanical efficiency
1	PUMP	Water pump	90%	99.89%
2	COMP1	(O_2, CO_2, Ar) Compressor	90%	99.89%
3	COMP2	(Ar, CO_2) Compressor	90%	99.89%
4	MIXR1	Combustion streams mixer	-	-
5	MIXR2	Dilution stream mixer	-	-
6	SSPLIT	Steam (Vapour) splitter	-	-
7	COMBSR	Combustor	-	-
8	TURBINE	Turbine	90%	99.89%
9	HX1	Exhaust gases heat exchanger	-	-
10	HX2	Water heat exchanger	-	-
11	VALVE	Fuel valve	-	-
Humidified	COMP1	Air compressor	90%	99.89%
	AIR-SPLITT	Air splitter	-	-

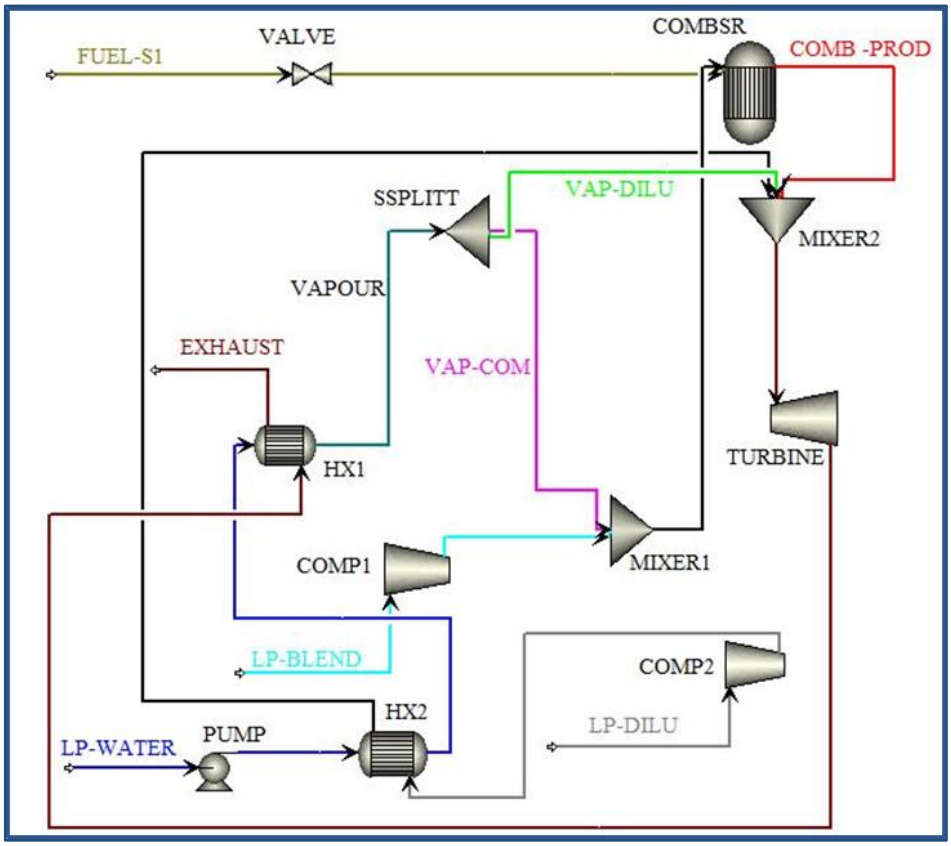

Figure 5.1 Flowsheet in Aspen Plus of CARSOXY cycle

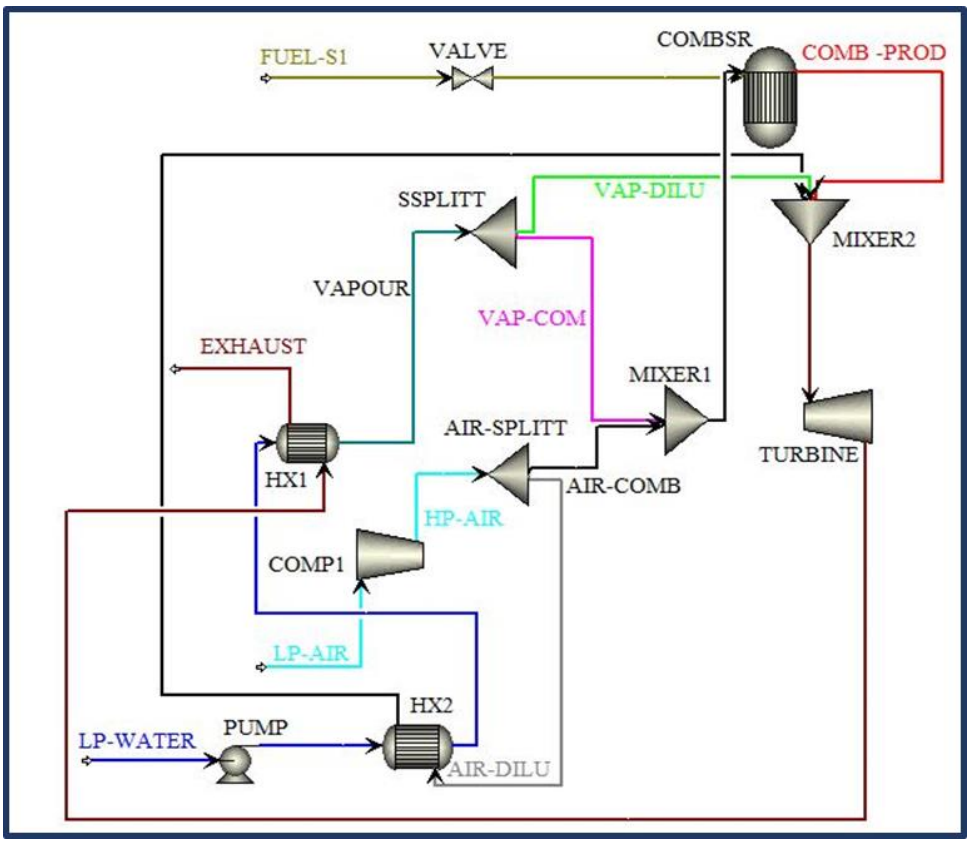

Figure 5.2 Flowsheet in Aspen Plus of humidified air cycle

Table 5.2 presents the required value of each parameter, inlet temperatures, the required input data for the streams, and their definition for the modified cycle and the humidified gas turbine cycle modelled using Aspen Plus.

Table 5.2 Input data required and stream definitions

	Inlet Temp, (K)	Stream	Definition	Component	Pressure (kPa)	Temp. (K)
1	293	LP-Water	Low-pressure water	H_2O	100	298
2	298	VAP-COM	Vapour for combustion	H_2O	1000	628
3	303	LP-BLEND	Low-pressure blend	O_2, CO_2, Ar	100	298
4	308	LP-DILU	Low-pressure dilution	CO_2, Ar	100	298
5	313	FUEL-S1	Fuel supply	CH_4	2000	298
6		VAP-DILU	Vapour for dilution	H_2O	-	-
7		VAP-COM	Vapour for combustion	H_2O	-	-
8		COM-PROD	Combustion products	-	-	-
1	293	LP-Water	Low-pressure water	H_2O	10	298
2	298	VAP-COM	Vapour for combustion	H_2O	1000	540
3	303	LP-AIR	Low-pressure air	O_2, N_2	100	298
4	308	FUEL-S1	Fuel supply	CH_4	2000	298
5	313	AIR-COMB	Air for combustion	O_2, N_2	-	-

A bespoke numerical model was also employed in this study to validate the results obtained using Aspen Plus. This numerical model has been calibrated elsewhere with experimental and industrial units. The equations provided in Chapter Three were sequentially employed in the mathematical model to calculate the required parameters, which were compressor work, compressor outlet temperature, heat capacity, specific output power and the efficiency of the turbine [113, 198]. The numerical model was used to validate the parameters that were calculated for both the CARSOXY cycle and the humidified cycle. Both the Aspen Plus model and the bespoke numerical model were run at the same specific operating conditions (298 k ambient temperature, 10-bar pressure and the same mass flow rate).

Relative errors for both cycles and the numerical model were between 2.5–3.57% for turbine output power. Meanwhile, for Mixer 1 and Mixer 2, the temperature relative errors were between 0.0–2.0 %. For the CARSOXY cycle, which included two compressors (Compressor 1 and Compressor 2), the relative errors for compressor work were between 2.5–3.1%. The relative errors for compressor work from the air humidified cycle, which included a single compressor, were 5.75% with Aspen Plus and the bespoke numerical model. It is believed that differences in the values of the specific heat and gas constants used in both codes may have led to the differences between the simulations.

These results demonstrate the improved efficiency in the novel cycle modelled using Aspen Plus, which supported the continuation of the study with the new blend. In addition, the results show that the modified cycle running with CARSOXY is one of the most reliable and practical solutions to improve the performance of the proposed cycle while contributing to protecting the global environment because it allows higher CO_2 flue gas concentrations, which can eventually be captured and recycled in the gas combustor. In addition, the proposed cycle ensures that NO_x is eliminated because CARSOXY does not include N_2.

5.2 Results and analysis

The CARSOXY cycle and the conventional air humidified cycle were run at different operating inlet temperatures (293, 298, 303, 308 and 313) at 10-bar pressure. Meanwhile, 3.117 kg/sec mass flow rate compositions entering the gas turbine were considered as operating conditions. The following equations were used to calculate cycle efficiency [199].

$$\eta = \frac{L_T - L_C}{FAR.H_u} * \eta_m \quad \text{Eq (5.1)}$$

$$FAR = \frac{\Delta H_{Reaction,25^0C}}{HHV} \quad \text{Eq (5.2)}$$

$$\Delta H_{Reaction,25^0C} = \sum \Delta H_{products} - \sum \Delta H_{reactant} \quad \text{Eq (5.3)}$$

Cycle efficiency was considerably higher running with CARSOXY as a working fluid and methane as a fuel than a conventional humidified air cycle in all cases, with a peak difference of around 10% observed at 293 K, with this figure then decreasing steadily to a difference of approximately 6% at the highest ambient temperature level, as shown in Figure 5.3. These results support the use of argon in the CARSOXY blend to improve cycle efficiency compared to air, as first proposed in Section 2.6.5.

This comparatively higher cycle efficiency is likely due to alternative gases used as working fluids, such as helium (as detailed in Section 2.3.4.2), having a higher specific heat ratio than air, leading to significant improvements in efficiency. As argon also has a higher specific heat ratio than air and is considered a better alternative than helium due to its higher molecular weight (see Section 2.3.4.3), it was expected that the CARSOXY blend would produce considerably higher cycle efficiency, as Figure 5.3 shows.

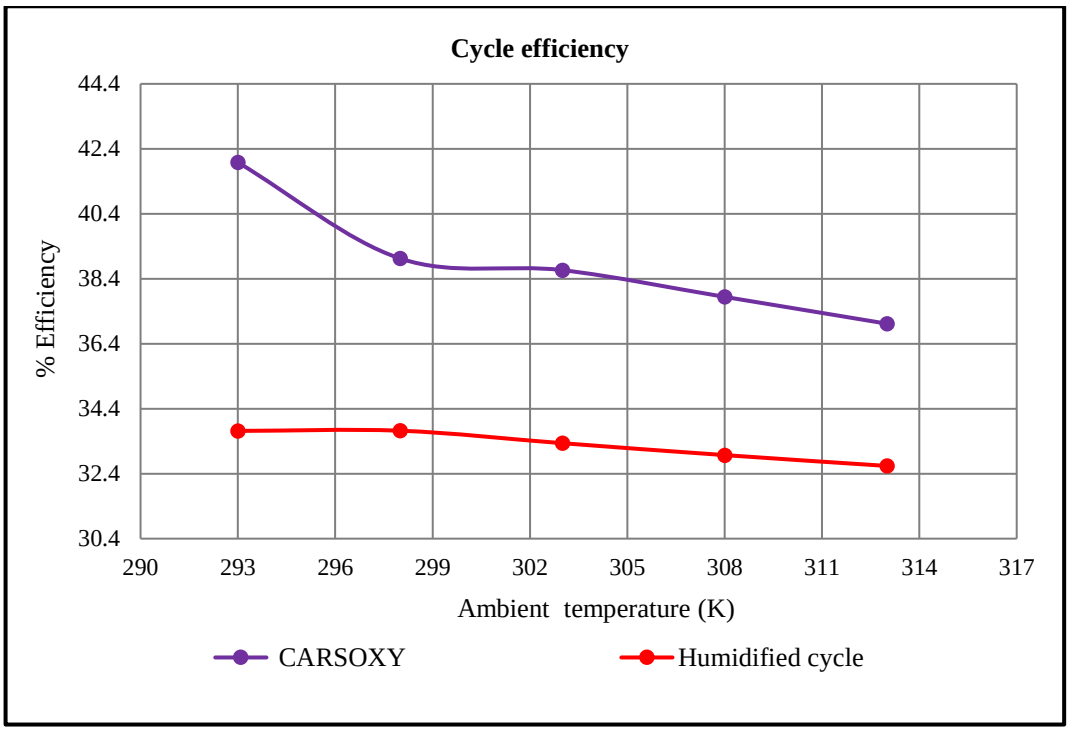

Figure 5.3 Efficiency comparison between CARSOXY and humidified air cycles

This result is also supported by the theoretical data produced using argon in an ideal gas turbine (see Section 2.6.5) where the higher efficiency produced was also attributed to argon's higher specific heat ratio than air. The data from this Aspen Plus simulation indicates that the CARSOXY blend could be practical for use in industrial gas turbines, as the efficiency gains provided could be used to offset the extra power consumption required by the ASU, thus overcoming this obstacle while maintaining cycle efficiency.

This higher efficiency can be achieved, as can be clearly seen in Figure 5.4, by TIT for the CARSOXY blend remaining lower throughout the cycle than for the air humidified cycle, with a peak difference of around 100 K at the lowest ambient temperature and a minimum difference of around 45 K at the highest ambient temperature level. This shows that efficiency remained higher for the CARSOXY blend even though the inlet temperature for CARSOXY was lower than for the air humidified cycle.

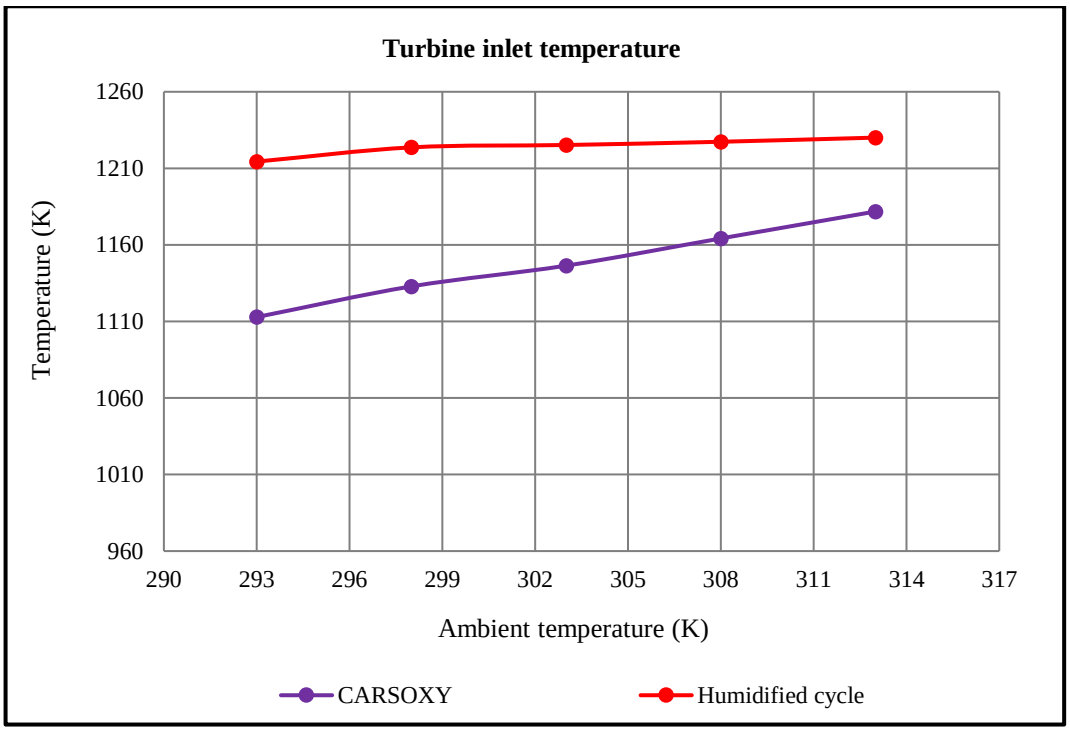

Figure 5.4 Turbine inlet temperature for CARSOXY and humidified air cycle

This is likely attributable to the fact that CO_2 is used for the dilution process instead of air when running with the CARSOXY blend, which adds additional support to the proposal to use the novel blend as a replacement for air in industrial gas turbines, as well as supporting the use of argon instead of other alternatives such as helium. This is because the comparatively low turbine inlet temperatures produced by CARSOXY are within the TIT limits of conventional gas turbines, which are not very heavy duty, and thus running with CARSOXY does not require the structural modifications needed to run with helium (see Section 2.3.4.2), making use of CARSOXY a potentially more practical alternative for replacing air in the power generation sector.

The conventional air humidified cycle's compressor work was also much higher in all cases than the figures for the CARSOXY cycle, rising slowly from just under 875 kW at 293 K to around 900 kW at the highest ambient temperature level of 313 K, as shown in Figure 5.5.

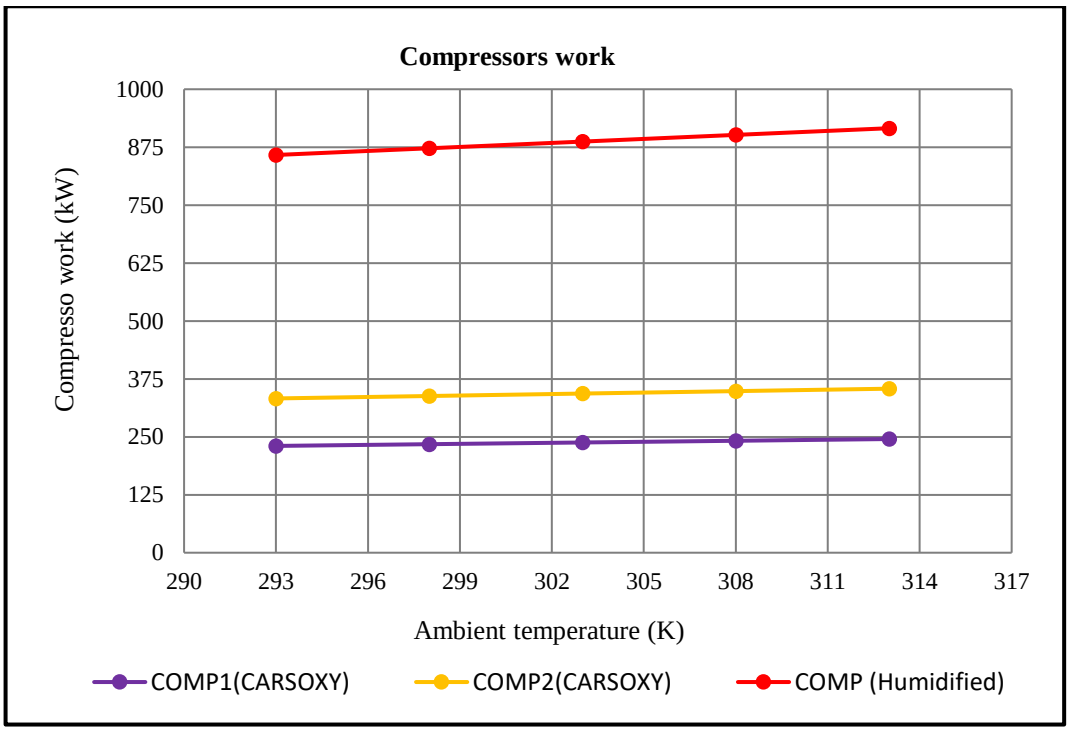

Figure 5.5 Compressors work required in CARSOXY and humidified air cycles

In the case of the CARSOXY blend, two compressors were used: Compressor 1, running with argon, oxygen and CO_2 and Compressor 2, running with a high concentration of CO_2 and a low proportion of argon for the dilution process. Work from Compressors 1 and 2 running with the CARSOXY blend was significantly lower than compressor work for the air humidified cycle, running from just under 375 kW to around 375 kW and from just under 250 kW to 250 kW, respectively. Thus, the combined work from both compressors running with CARSOXY remained considerably lower than the work produced by the compressor using the air humidified cycle.

These results could be explained by the fact that Compressors 1 and 2 for the CARSOXY blend were both running mixtures that are more condensed and as such have a higher density than air, which was running through a single compressor used for compressing air for the combustion and dilution processes. As well as supporting this study's proposed use of CARSOXY as a working fluid in industrial gas turbines, the fact that Compressor 2 could use recycled CO_2 from another industrial source, thus re-using a potential pollutant instead

of allowing it to be emitted directly into the atmosphere, contributes to the aim of helping to protect the global environment from further deterioration.

Further to the above, as shown in Figure 5.6, outlet temperature data for the two compressors used for the CARSOXY cycle shows the temperatures for Compressor 1 almost matched the values for the compressor used in the humidified air cycle, with both of these compressors recording values around 100 K higher than Compressor 2. Compressor 2's lower temperature is likely due to the fact that it compresses a high proportion of CO_2, which has the highest density of the CARSOXY blend components, thus requiring less work and producing lower temperatures.

These results support the proposed use of the CARSOXY cycle in industrial applications as the similar values recorded compared to the conventional air humidified cycle indicate that this novel approach could be used in conventional turbines without the need for expensive modifications or incorporation of additional units with specific design features.

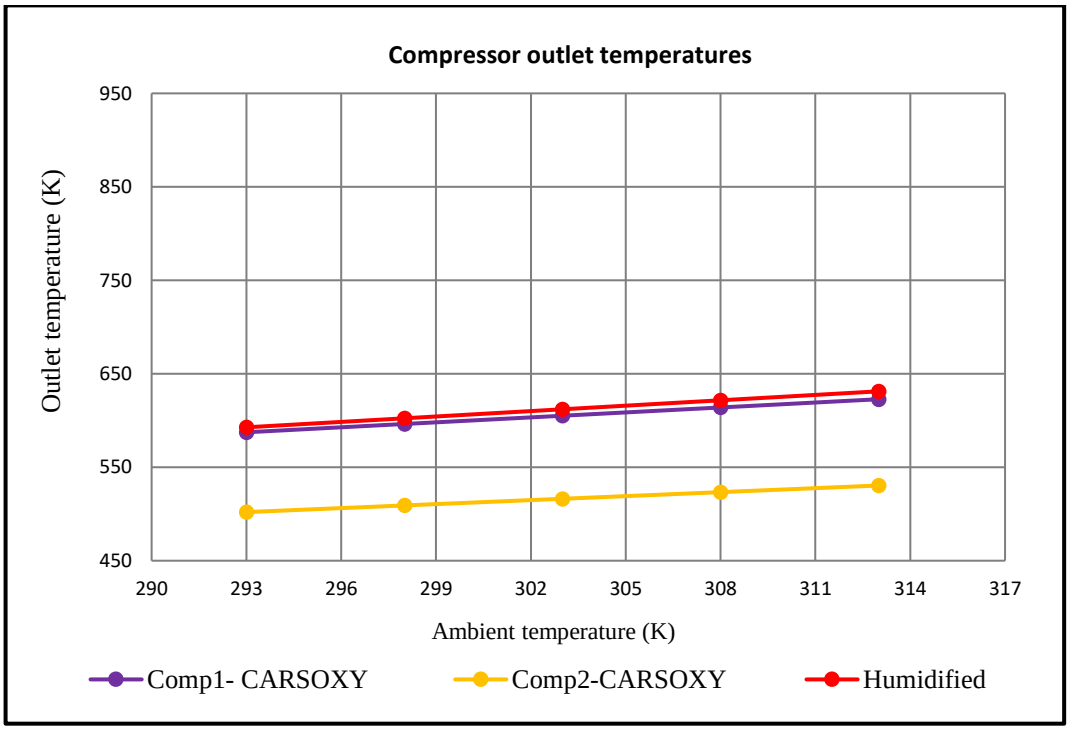

Figure 5.6 Compressor outlet temperatures for CARSOXY and humidified air cycles

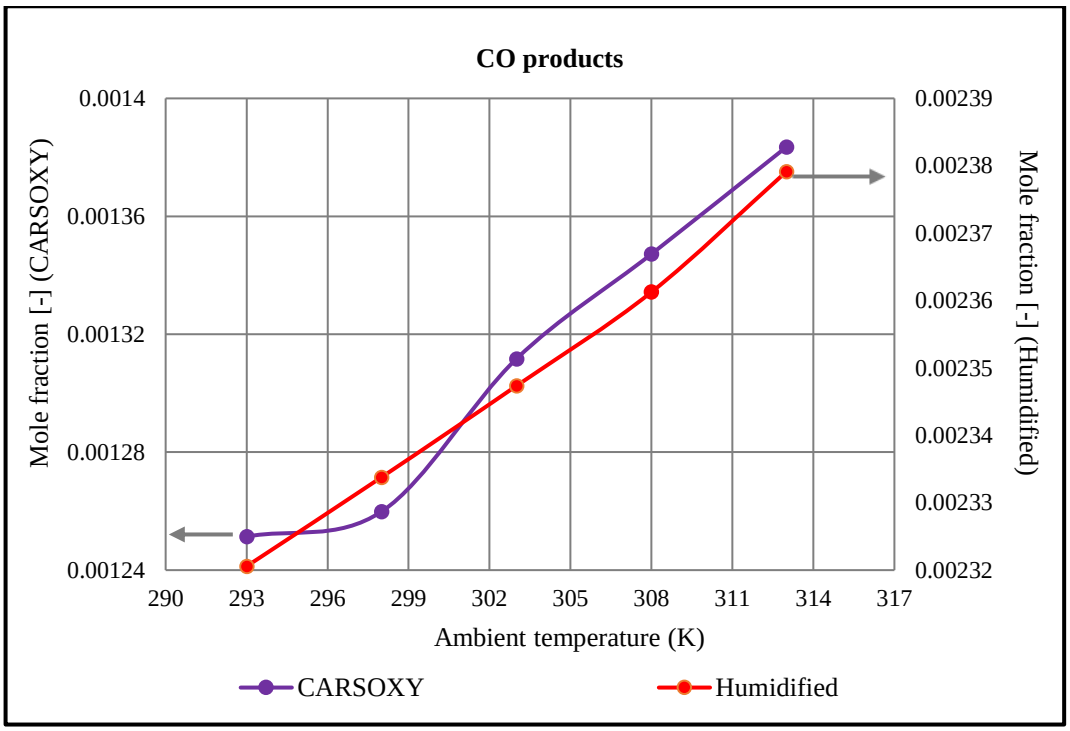

Figure 5.7 CO products from CARSOXY and humidified cycles

CO products for CARSOXY were slightly lower than those for the air humidified cycle throughout, ranging from 0.00125 to 0.00138 compared with 0.0232 to 0.00238, as can be seen in Figure 5.7. A probable explanation for these results is that, owing to its use of an enriched oxygen domain, the CARSOXY cycle completes the combustion process more thoroughly in comparison with air, especially in the secondary zone of the burner (see Section 2.3.1.3.2).

During this process, CO is converted to CO_2, which increases CO_2 levels in the exhaust gases [146] and is, as such, beneficial to the CO_2 recirculation process designed to be incorporated into the novel CARSOXY cycle.

Even though the CO products obtained from the Aspen Plus combustion process simulation running with CARSOXY were lower than CO concentrations in the exhaust produced from air as a working fluid, these values of CO are still considered high and they exceed the upper limit of the acceptable range for exhaust gases after the dilution process. This could be due to the use of the Gibbs Reactor as a gas turbine combustor in both investigative model cycles.

The resulting lower levels of CO, normally considered an unburned hydrocarbon, in the exhaust gases also provide support for the proposed use of CARSOXY in industrial gas turbines as reduction of NO_x, which is one of the features of CARSOXY, normally leads to an increase in CO product, with the inverse also being true. However, using CARSOXY eliminates NO_x from produced emissions while reducing CO product in comparison with air, thus providing a way to overcome the NO_x-CO emissions obstacle (see Section 1.8) and thus contribute to the protection of the global environment.

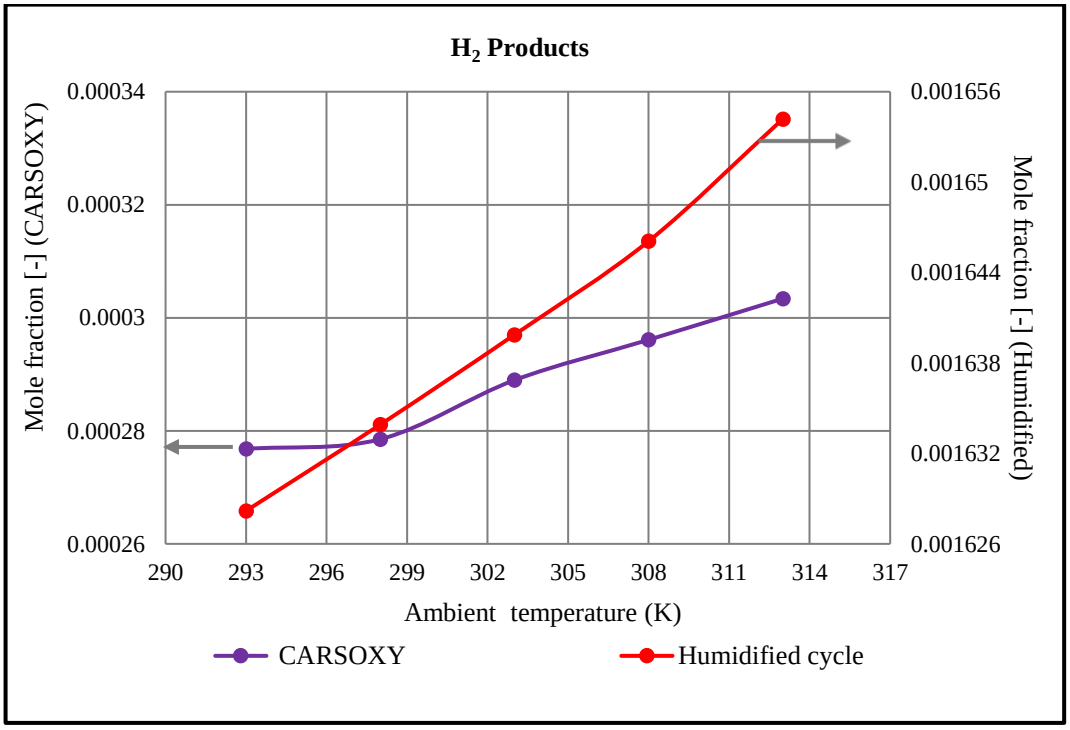

Figure 5.8 H_2 products produced from CARSOXY and humidified air cycles

With a similar pattern to Figure 5.7, H_2 products for CARSOXY remained lower than for the air humidified cycle, ranging from just below 0.00028 to just above 0.0003 compared with 0.001627 to 0.001655, as shown in Figure 5.8.

The probable explanation for this is also similar to that given above for CO. The completion of the combustion process allowed for by the CARSOXY cycle's use of an enriched oxygen domain also allows for almost complete burning of other products which are normally

considered unburned hydrocarbons, including H_2, thus providing the same potential environmental benefits outlined above regarding reduction of harmful emissions.

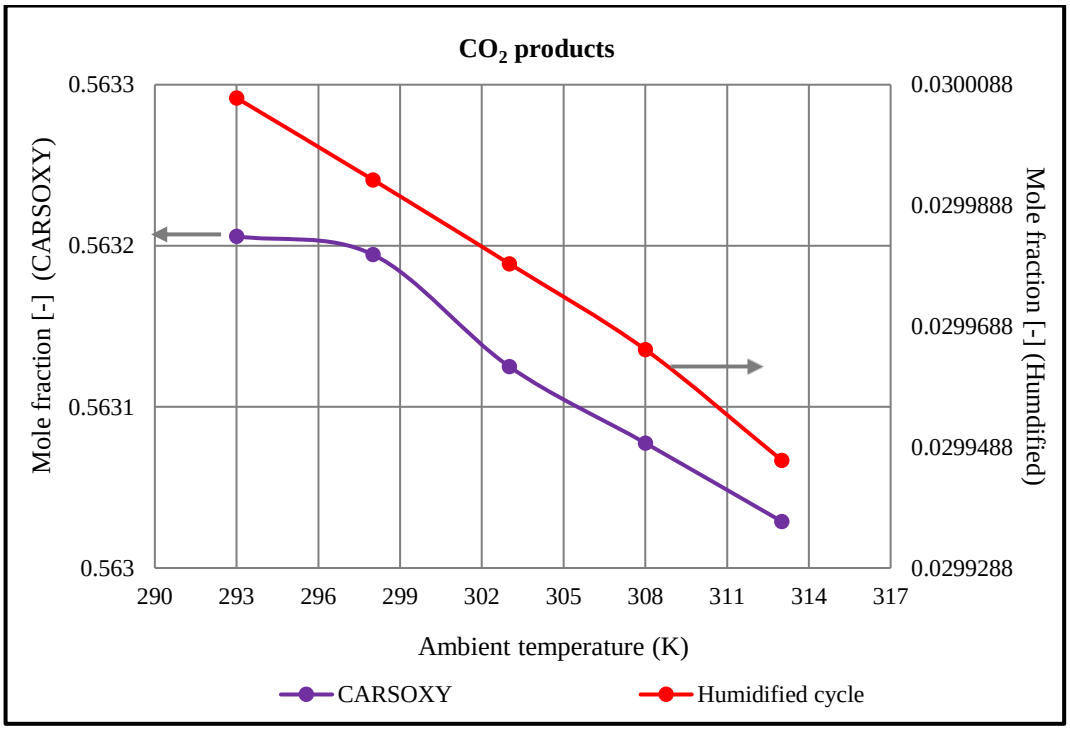

Figure 5.9 CO_2 emitted from CARSOXY and humidified cycles

Figure 5.9 shows that CO_2 products for the CARSOXY blend were much higher across the ambient temperature range than for the air humidified cycle, ranging from 0.5632 to just above 0.563 compared with 0.0300088 to just below 0.0299488.

This is likely to be due to the fact that the CARSOXY cycle uses CO_2 for dilution instead of air so there is more present in the system. As CO_2 is more condensed and, thus, has a higher density than air, it also reduces compressor work, as can be connected to the discussions regarding Figures 5.6 and 5.7. These results add further support to using the proposed CARSOXY cycle in industrial gas turbines as CO_2 is designed to be recycled in the cycle (see Section 2.2) so comparatively high levels of it are beneficial to the process. When coupled with the fact that the proposed system can use CO_2 products from other industrial sources to compensate for any lack of it within the system, the potential environmental

benefits of using CARSOXY to help reduce harmful emissions in industrial applications are clear.

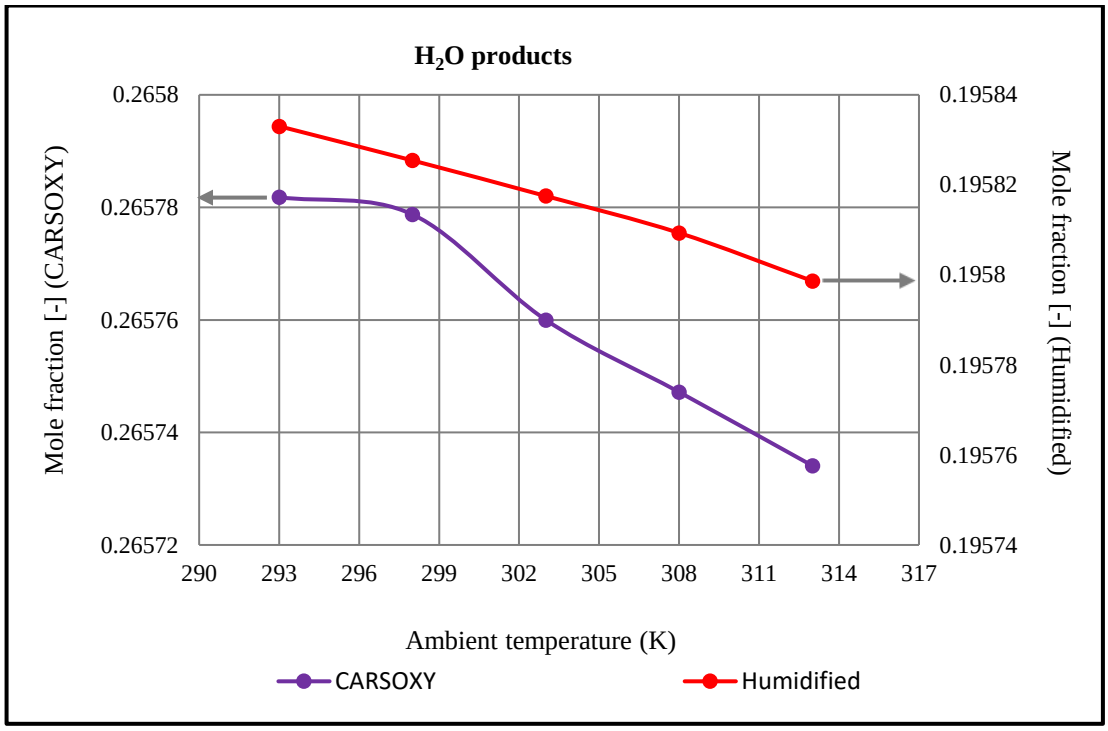

Figure 5.10 H_2O produced from CARSOXY and humidified air cycles

As can be seen in Figure 5.10, H_2O products for CARSOXY were slightly higher throughout than for the air humidified cycle, ranging from just over 0.26578 to just under 0.26574 compared with 0.19583 to 0.19581.

These results indicate that using the novel blend can be considered a practical solution for the provision of water recirculation for the humidification process as increased H_2O product levels help to condense water which can then be utilised in humidification and dilution processes in the cycle.

The above results related to exhaust products are critical as effective use of the CARSOXY cycle's proposed recirculation approach requires data on these products' concentrations. The following section focuses on combustor products.

5.3 Combustion products

The following figures represent data on the products directly after combustion without dilution, indicating the effects of the novel blend on emission reduction and providing useful references for the experimental work detailed in the next chapter.

Figure 5.11 shows that post-combustor CO products using the CARSOXY blend were lower than those for the cycle using air as a working fluid. The figures for CARSOXY rose steadily from a minimum level of just over 0.00306 at 293 K to just over 0.00342 at the highest ambient temperature level, while the values for the air humidified cycle began at just under 0.00615 and reached 0.0063 at 313 K.

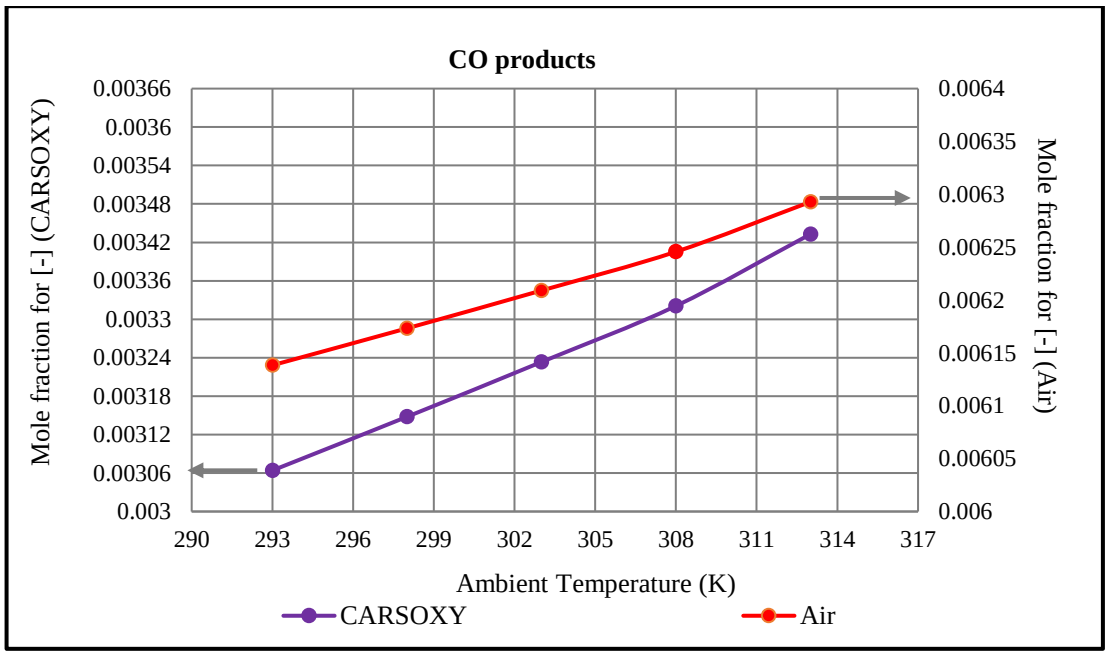

Figure 5.11 CO combustion products using CARSOXY and humidified air as working fluids

Figures for H_2 products after combustion were also considerably lower for the novel CARSOXY blend than for air, ranging from around 0.00068 to around 0.00075 compared with 0.00431 to just below 0.00438, as shown in Figure 5.12.

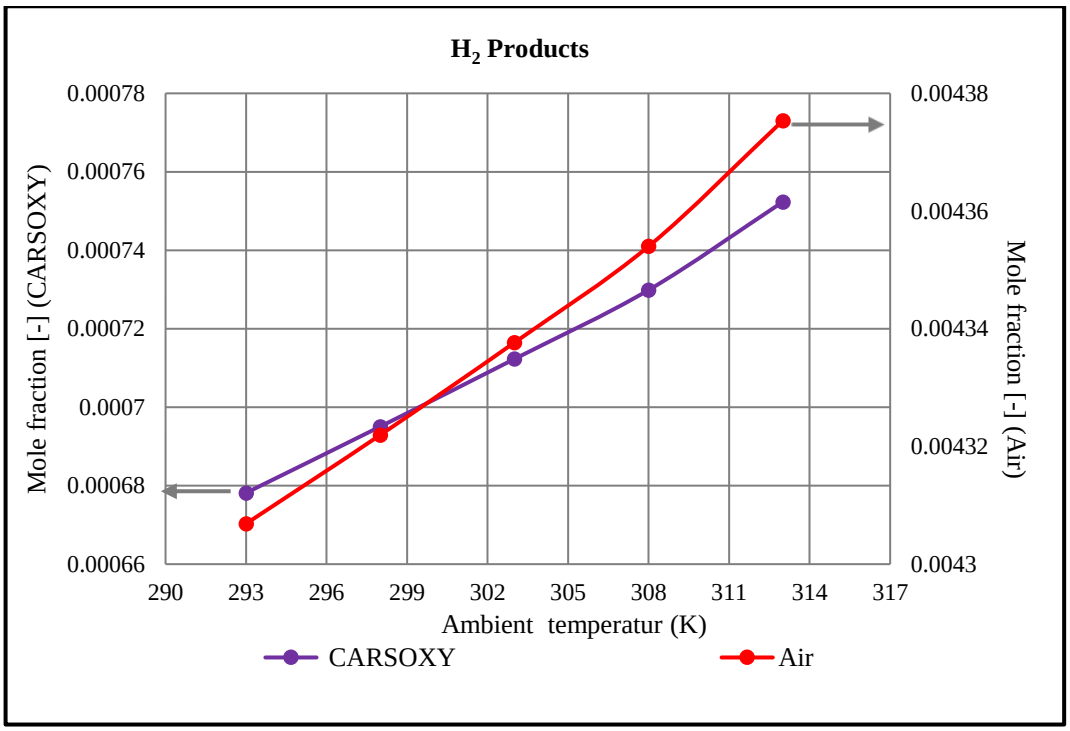

Figure 5.12 H_2 combustion products using CARSOXY and humidified air as working fluids

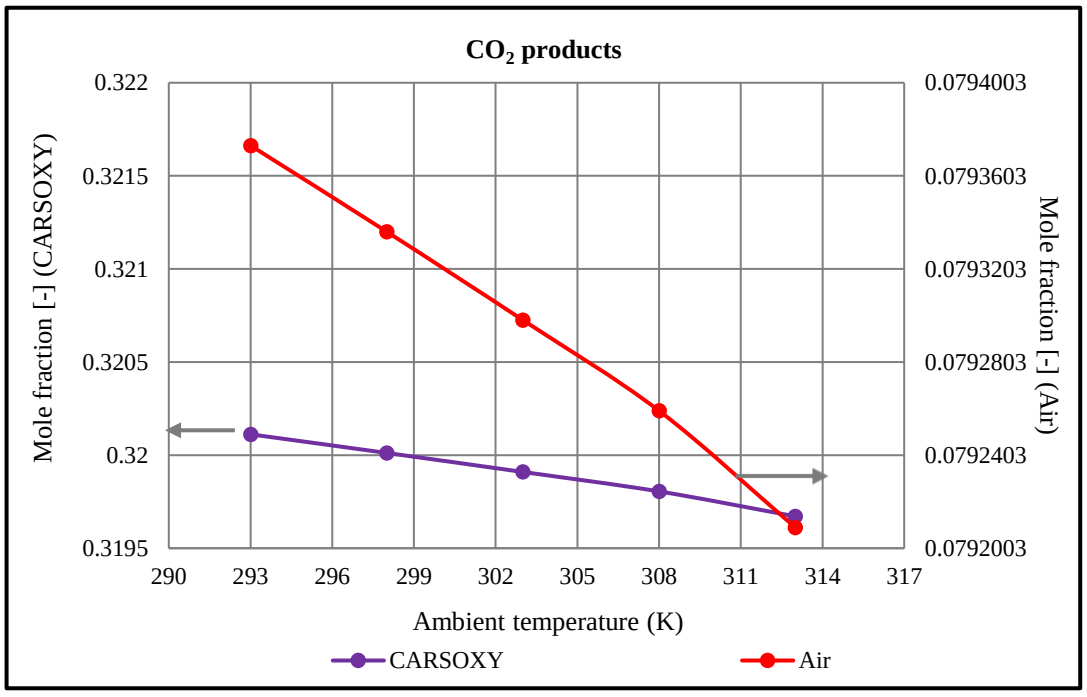

Figure 5.13 CO_2 combustion products using CARSOXY and humidified air as working fluids

As can be seen in Figure 5.13, CO_2 products following combustion for the CARSOXY blend were significantly higher than air humidified cycle products across the ambient temperature range. Figures for CARSOXY dropped slightly from 0.321 to around 0.3196 at 313 K, while

values for air began at just above 0.0793603 and fell to just above 0.0792003 at the highest ambient temperature level.

Figure 5.14 shows that post-combustor concentrations for H_2O products were also noticeably higher for CARSOXY than for air as a working fluid, ranging from 0.36069 to 0.36054 compared with just over 0.28344 to 0.28338.

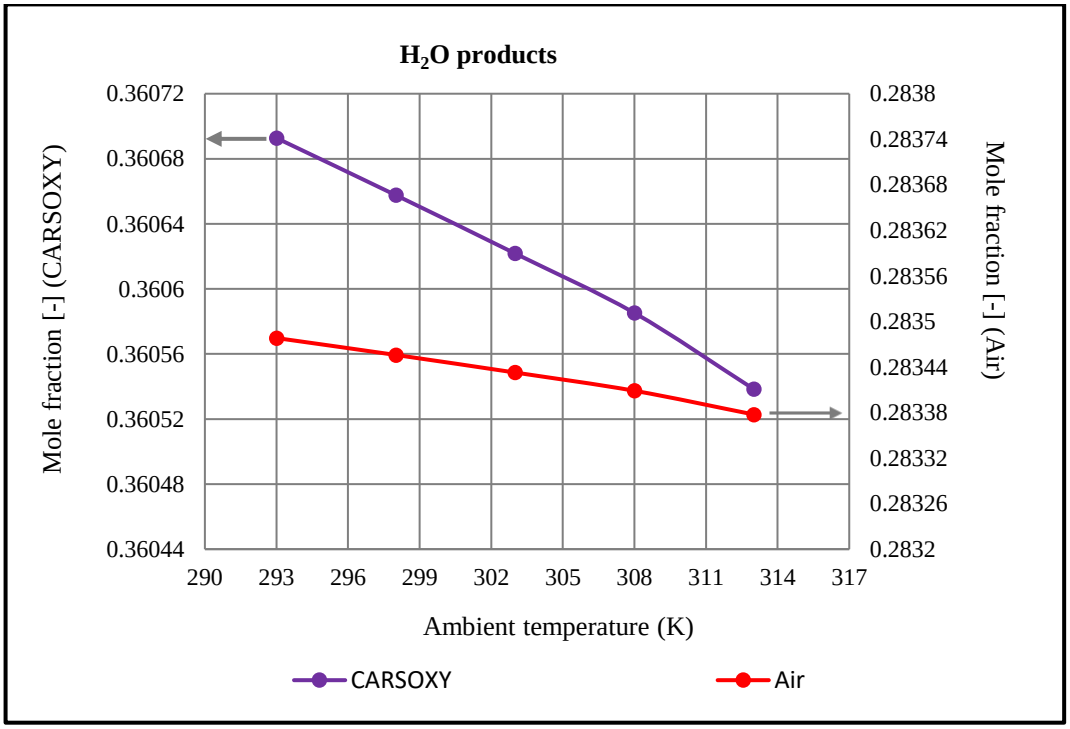

Figure 5.14 H_2O combustion products using CARSOXY and humidified air as working fluids

5.4 Summary

This chapter has focused on the use of Aspen Plus software to investigate theoretically whether the proposed CARSOXY blend provides improved cycle efficiency compared to a conventional air humidified cycle when used in an industrial gas turbine, as well as potential improvements in contributing to environmental protection.

The final data indicated that running with CARSOXY improves cycle efficiency, which could help overcome the power consumption requirement obstacles of using an ASU. Data

on compressor work and compressor outlet temperatures suggested that the CARSOXY blend could be used in industrial applications and achieve similar values to conventional systems, avoiding the need for costly modifications or additions while potentially providing efficiency and environmental benefits. Turbine inlet temperatures were shown to be lower than those for the air humidified cycle, even though cycle efficiency remained higher throughout, placing them within TIT limits and further highlighting CARSOXY's potential practical benefits as expensive turbine modifications can be avoided.

CO and H_2 products were seen to be lower for CARSOXY, indicating the potential environmental benefits of the proposed blend through reduction of harmful emissions while data on CO_2 levels in exhaust gases indicated that a high quantity of CO_2 would remain in the system - contributed to by the conversion of CO into CO_2 - a result that supports use of the proposed cycle as this remaining CO_2 could then be recycled in the cycle as per system design. H_2O product levels were also marginally higher for CARSOXY than air, indicating an increase in water in the system which could help with condensation for the cycle's humidification and dilution processes.

Data on combustion products, presented as a reference for the experimental work detailed in the following chapter, showed that CO and H_2 products were lower for CARSOXY than for air as a working fluid whereas both CO_2 and H_2O product levels were significantly higher for the blend than for air.

The next chapter will provide results and analysis from this study's experimental stage.

CHAPTER SIX

Chapter 6 Experimental work

This chapter focuses on experimental work using the blend consisting of Ar, CO_2 and O_2 to ignite a flame in a generic burner. The aim of this procedure is to compare the proposed blend with conventional air as a working fluid by measuring stability and emissions to examine whether the blend could be used as a more stable, lower-emitting replacement for air.

First, the experimental setup and procedures are briefly detailed. The collected experimental data is then presented, firstly concerning emissions and outlet temperature measurements then followed by heat release data and supported by description and analysis. Additionally, the usefulness of the data relative to the focus of this study is discussed. Finally, a summary of the significant results and analysis in this chapter is provided, along with consideration of relevant limitations of the experimental work and implications for future study.

Following the use of chemiluminescence to measure flame stability and a gas analyser to measure emission levels (see Section 3.7) for experimental comparison of the two working fluids, the experimental data indicates that the blend could be used to provide stable ignition in the combustion process and almost eliminates NO_x emissions in comparison with air as a working fluid. The data also shows a reduction in unburned hydrocarbon (H_2 and CO) emissions compared with air.

Thus, preliminary experimental data indicates that the proposed blend could be used to replace conventional air as a working fluid in industrial gas turbines, with improved stability of the flame and a reduction in harmful emissions.

6.1 Experimental setup and procedure

As mentioned in Chapter Three, a 20-kW generic burner rig was used with a HSC, as shown in Figure 6.1 (a and b), to capture chemiluminescence while a gas analyser, Testo 350XL, was employed to measure the emissions in the exhaust gases.

Chemiluminescent images were captured by the HSC at 500 fps and the light intensity gain was set at 3/10. These values were selected through pragmatic considerations to provide sufficient flame glare for capture while protecting the HSC from damage. Photron FASTCAM Viewer software (PFV version 3620) was used to capture and store the flame images. The images were taken approximately 1 m away from the flame, which simulated a gas turbine-type of the flame inside the quartz confinement cylinder. Chemiluminescence intensity was processed using MATLAB 2017-b (for code, see Appendix 3) and taken as a direct measure of heat release.

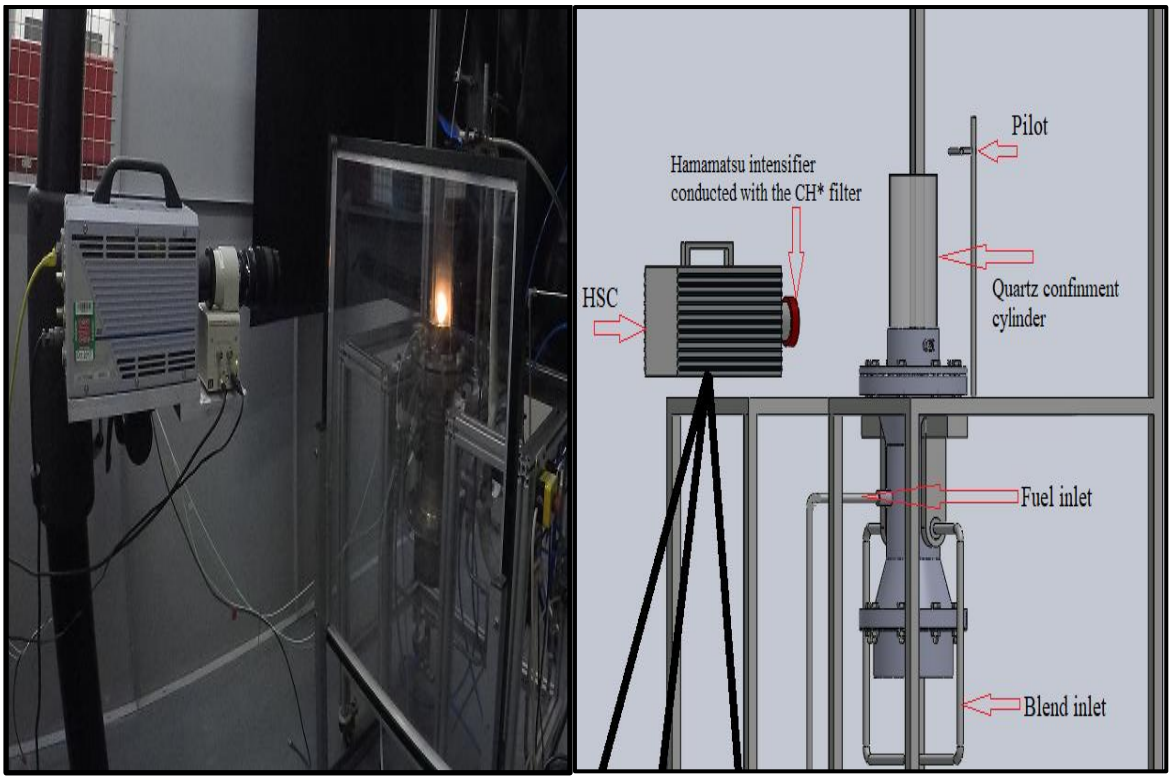

Figure 6.1 a) Actual generic burner, b) CH* filter attached with HSC to measure chemiluminescence

6.1.1 **Air investigation**

First, the pressure of methane fuel was set to 2-bar and the working fluid flowmeter valve was partially opened to provide sufficient air for ignition. The fuel flowmeter valve was then opened to achieve ignition and then set to the value of 0.111g/sec. Next, the pilot was set at a specific height that provided ignition while preventing system blowout (see Section 3.5.1.1). Next, the air flow rates were varied from 0.813g/sec. as a starting point up to blowout condition, in increments shown in Table 6.1 (see Appendix 4, Table 1 for readings in volumetric units), setting a constant power of 0.55 kw.

As shown in Appendix 4, Figure 1, three flow meters were connected to the burner. Two Platon flowmeters were used in combination or individually to supply and control working fluid, in both the case of air and the proposed blend. The flow range of the first flowmeter was 6–50 L/min (air @ATP) using a Platon NGX series glass tube with 2 L/min interval with an accuracy of ±1.25% FSD and an operating pressure of 18 bar. The flow range of the second flowmeter was 40–40 L/min (air @ATP) with 20 L/min interval.

The operating pressure was 10 bar using a TPX series plastic tube and the accuracy range was 5% FSD. All of the flowmeters were vertical with upward flow, so the reading is taken from the top of the float with a max temperature of 80 ^{o}C for the nitrile seals. Methane flows were supplied and regulated via a Platon flowmeter and Platon NGX series glass tube with a flow range of 0.4-2.8 L/min with 0.1L/min interval and an accuracy of ± 1.25% FSD [200].

At each specific mass flow rate of air, chemiluminescence was captured using the HSC with an attached Hamamatsu intensifier conducted with the CH* filter, recording with the PFV software. Exhaust gas emissions were also measured and recorded using the gas analyser over 60 seconds.

Table 6.1 Fuel/air composition

S/N	Air (g/sec)	Fuel (g/sec)	Equivalence ratio	Power (kW)
1	0	0.111	0	0.55
2	0.813	0.111	0.234	0.55
3	1.220	0.111	0.156	0.55
4	1.342	0.111	0.142	0.55
5	1.626	0.111	0.117	0.55
6	2.033	0.111	0.093	0.55
7	2.440	0.111	0.0781	0.55

6.1.2 **Correction factors of air flow meters**

The flowmeters that were used in the experimental work for a working fluid were calibrated specifically for air. Therefore, using these flowmeters for the blend would result in inaccurate experimental readings due to the density difference between air and the blend. Therefore, due to the density difference between air and the blend, another factor which needed to be considered was the calibration of the working fluid flowmeters for the experimental blend. The following equation calculated the accurate mass flow rates for the blend [201]:

$$q_{v2} = \sqrt{\frac{D_1}{D_2}} \times q_{v1} \qquad \text{Eq. (6.1)}$$

In order to allow comparison, power output was also kept at 0.55 kW for the proposed blend.

6.1.3 **Blend investigation**

In the case of the optimum blend investigation, a similar experimental procedure to that described in Section 6.1 was followed. In this case, a gas cylinder which contained a blend consisting of 0.32 O_2, 0.29CO_2 0.39 Ar was connected to the rig. It was not essential to include H_2O in this blend so it was not included due to time and resource limitations. Consequently, this blend was utilised to represent the novel CARSOXY blend in the experimental investigation to provide preliminary evidence of its effective use in the full combustion process.

Table 6.2 Fuel/blend composition

S/N	Proposed blend (g/sec)	Fuel (g/sec)	Equivalence ratio	Power (kW)
1	0	0.111	0	0.55
2	0.933	0.111	0.204	0.55
3	1.40	0.111	0.136	0.55
4	1.50	0.111	0.123	0.55
5	1.86	0.111	0.102	0.55
6	2.33	0.111	0.081	0.55
7	2.80	0.111	0.068	0.55
8	3.26	0.111	0.058	0.55
9	3.73	0.111	0.051	0.55

Table 6.2 shows the increasing values of the blend mass flow rates with their increments (see Appendix 4, Table 2 for readings in volumetric units). It can also be seen that the mass

flow rate of the blend did not reach blowout condition, even at the value of 3.73 g/sec. It must be emphasized that both working fluids were used under diffusive, non-premixed condition injection, as CARSOXY is expected to produce negligible NO_x and thus does not require a premixing process.

6.2 Results and discussion

6.2.1 Emission and outlet temperature measurements

The outlet temperature of the combustion products using both working fluids steadily increased with equivalence ratio values, as shown in Figure 6.2. A flame was provided with a range of low equivalence ratios, due to the fact that the combustion process was run in a diffusive mode. The graph also shows that the temperatures of the blend were higher than air at lower mass flow rates. The profile of the experimental outlet temperatures almost matched the theoretical data obtained from Gaseq (see Figure 4.1). The data shows that the blend temperatures were higher than predicted for conventional air at the highest value of the experiment. In the theoretical model, the outlet temperatures demonstrated similar behaviour to the experimental data at similarly low values of equivalence ratio.

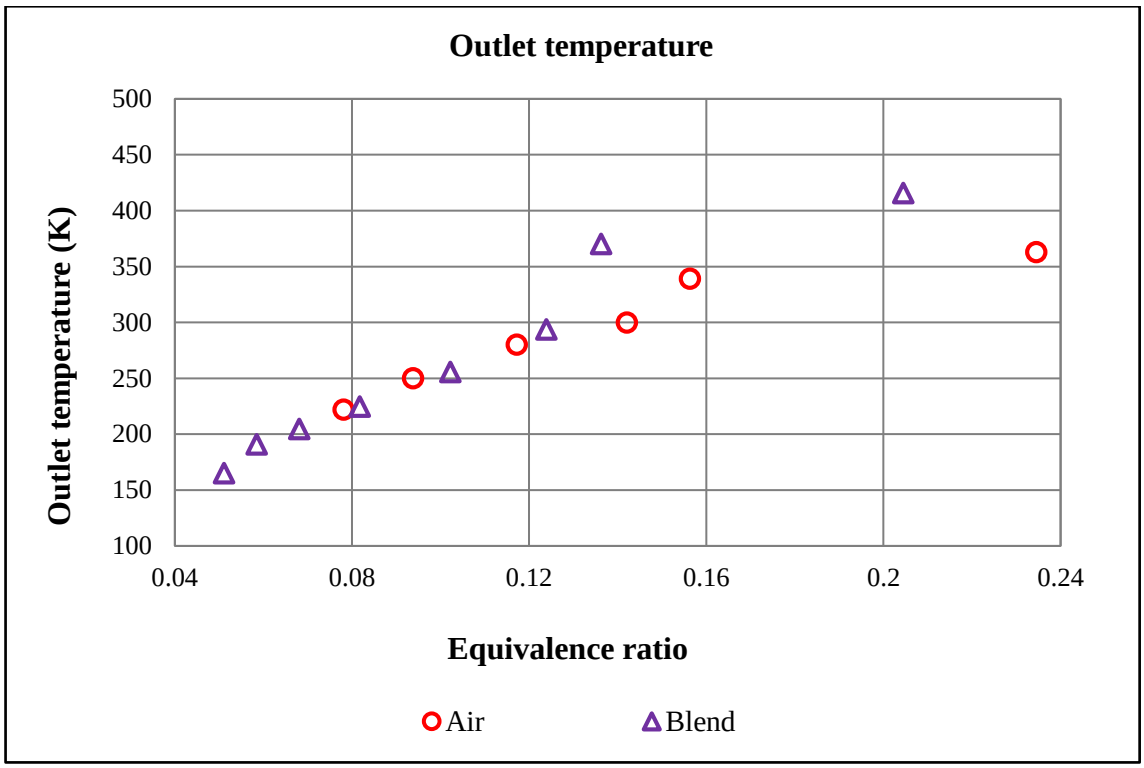

Figure 6.2 Product temperatures against equivalence ratio

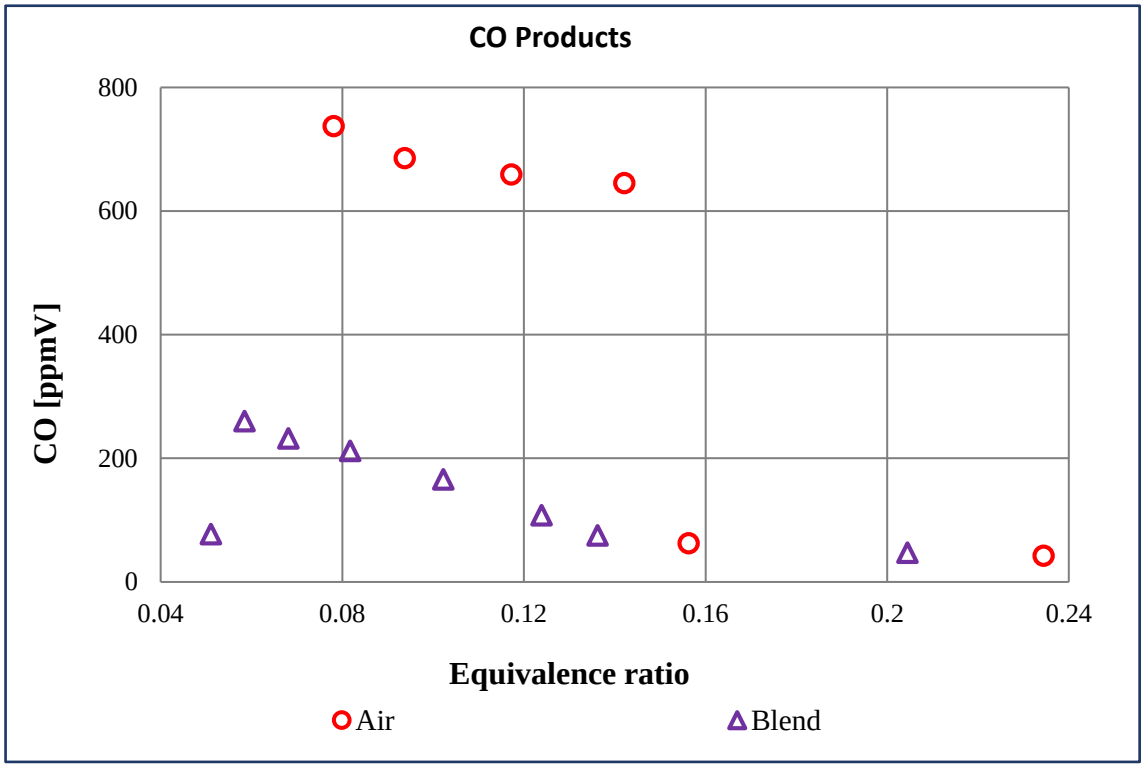

Figure 6.3 CO products against equivalence ratio

Figure 6.3 shows that the CO levels of exhaust gases using air and the blend as a working fluid had approximately the same value of around 50 ppm at higher equivalence ratio values. As the equivalence ratio dropped, CO products dramatically increased for air to reach around 750 ppm. In comparison, the level of CO in the exhaust increased gradually to around 240 ppm, which represents its highest value.

The experimental data for CO products shows similar trends compared to the Aspen results (see Figure 5.11) for the proposed blend produced lower CO product than air. As mentioned in Chapter 2, using the proposed blend as an oxidiser enhances the conversion of CO in the secondary zone to CO_2 by providing a high-concentration oxygen domain, leading to complete burning of CO products [195, 202].

However, the experimental burner was run through a diffusive mode in contrast to the Gibbs Reactor model, which was utilised in Aspen Plus as the gas turbine combustor model, where the chemical reaction equilibrium is numerically considered and does not simulate a diffusion burner. As a result, there were relative differences in the data gathered by the experimental tests compared to that obtained from the Aspen Plus model. Even though there was relative similarity in trends between the experimental and Aspen Plus data, utilising the Gibbs Reactor in the model produced a level of CO products that is considered to exceed the upper limit of the acceptable range for exhaust gases after the dilution process. This could be due to the type of combustor used in this model.

These results indicate that the blend produces lower CO emissions compared with air as a working fluid. Therefore, this blend could be used to replace air in industrial gas turbines to help reduce incomplete combustion, which will help protect the environment from deterioration.

Figures 6.4 and 6.5 show that the blend produced zero NO and NO_x at low equivalence ratios in comparison with air, which produced around 5 ppm of these products at the same equivalence ratio values. As the equivalence ratio increased, NO and NO_x products rose significantly for air as a working fluid. However, these products also increased slightly with rising equivalence ratio using the blend.

It was expected that NO and NO_x would not be produced at all using the blend as a working fluid because N_2 was not included in the novel blend composition. Although the experimental data nearly matched this expectation, the figures show the blend produced small levels of NO and NO_x products at a high equivalence ratio. One potential explanation is that the pilot flame produces these products and, due to the fact it was located near the gas analyser prop, it might have led to NO and NO_x products from pilot combustion being detected by the Testo 350 XL gas analyser. Another explanation might be an effect caused by the fact that the extractor was running during the experimental work. This could have resulted in N_2 in ambient air being sucked into the gas analyser through the prop, leading to these anomalous readings.

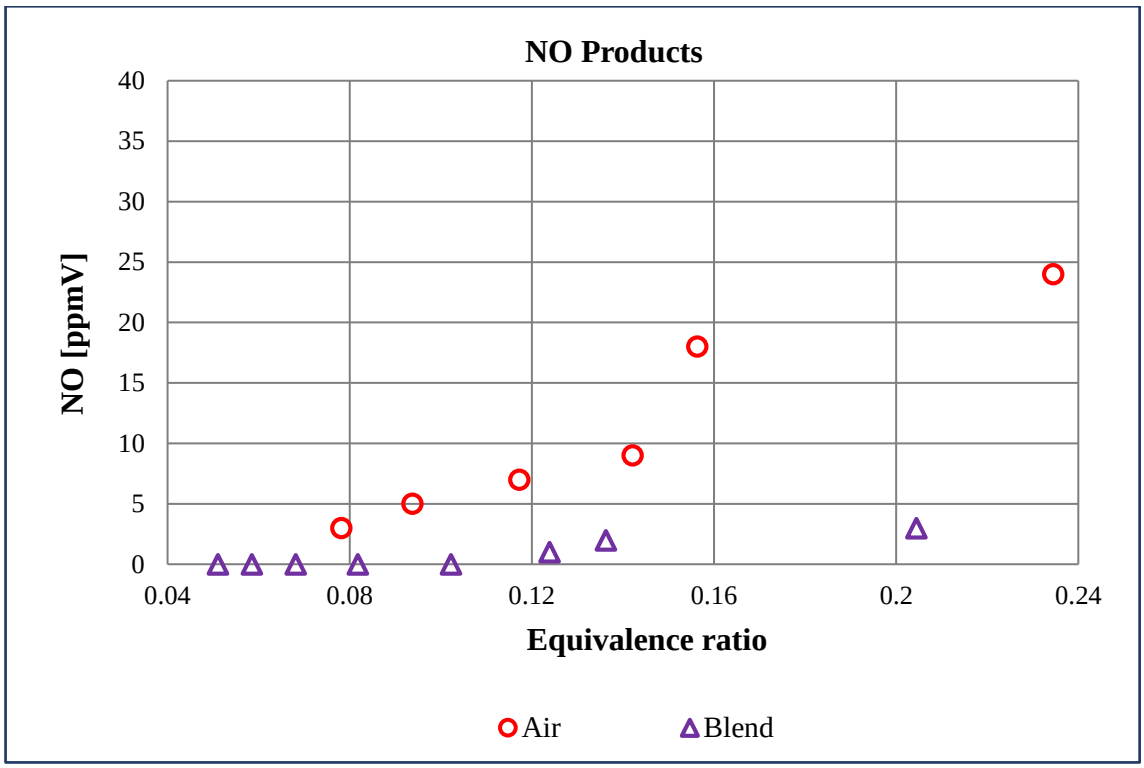

Figure 6.4 NO products against equivalence ratio

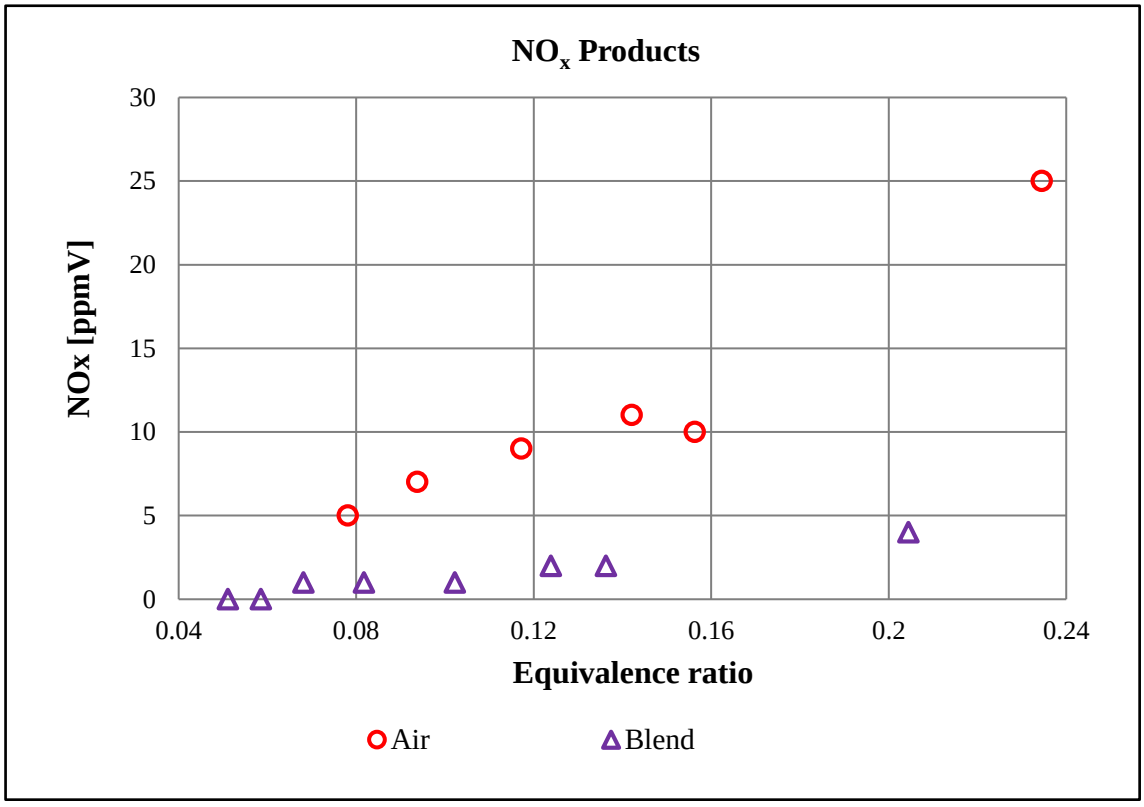

Figure 6.5 NO_x products against equivalence ratio

However, these results indicate that the blend eliminates NO and NO_x products during the combustion process in a generic burner. This also supports using the blend in industrial gas burners to replace air as a working fluid to reduce harmful anthropogenic gas emissions and contribute to keeping the environment clean.

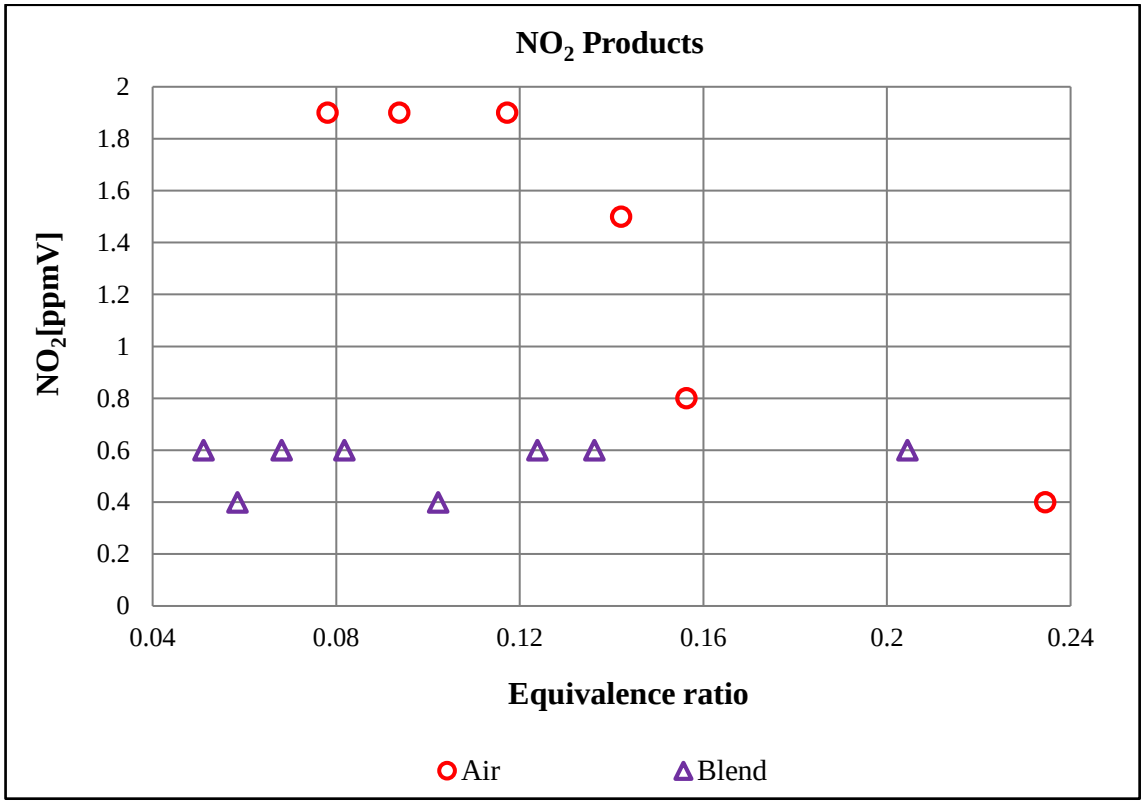

Figure 6.6 NO_2 products against equivalence ratio

Figure 6.6 shows that the NO_2 concentration in the exhaust gases using the blend as a working fluid were stable, with minor fluctuations, at 0.6 ppm across equivalence ratio values. In the case of using air as a working fluid, NO_2 products were about 1.4 ppm higher than in the case of the alterative blend from the minimum equivalence ratio up to 0.12, where it began to drop rapidly, reaching its lowest level of 0.4 at the highest analysed equivalence ratio.

As with NO_x, it was predicted that this product would be eliminated from the exhaust gas because N_2 was not included in the blend components. A possible explanation for this

unexpected reading is a similar systemic reason to the situation with NO_x, such as interference from the pilot flame or the extractor. The experimental results show that, while the blend did not fully eliminate NO_2, it did produce a low level of the product. This supports the use of this blend to reduce the emission levels of these polluting gases from gas combustors. These NO_x, N_2 and NO_2 products were fully eliminated in the Aspen Plus simulation model. This discrepancy can be explained by the fact that N_2 was not included in the blend compositions investigated using the Gibbs Reactor model running with CARSOXY as a working fluid. Therefore, these products were not included.

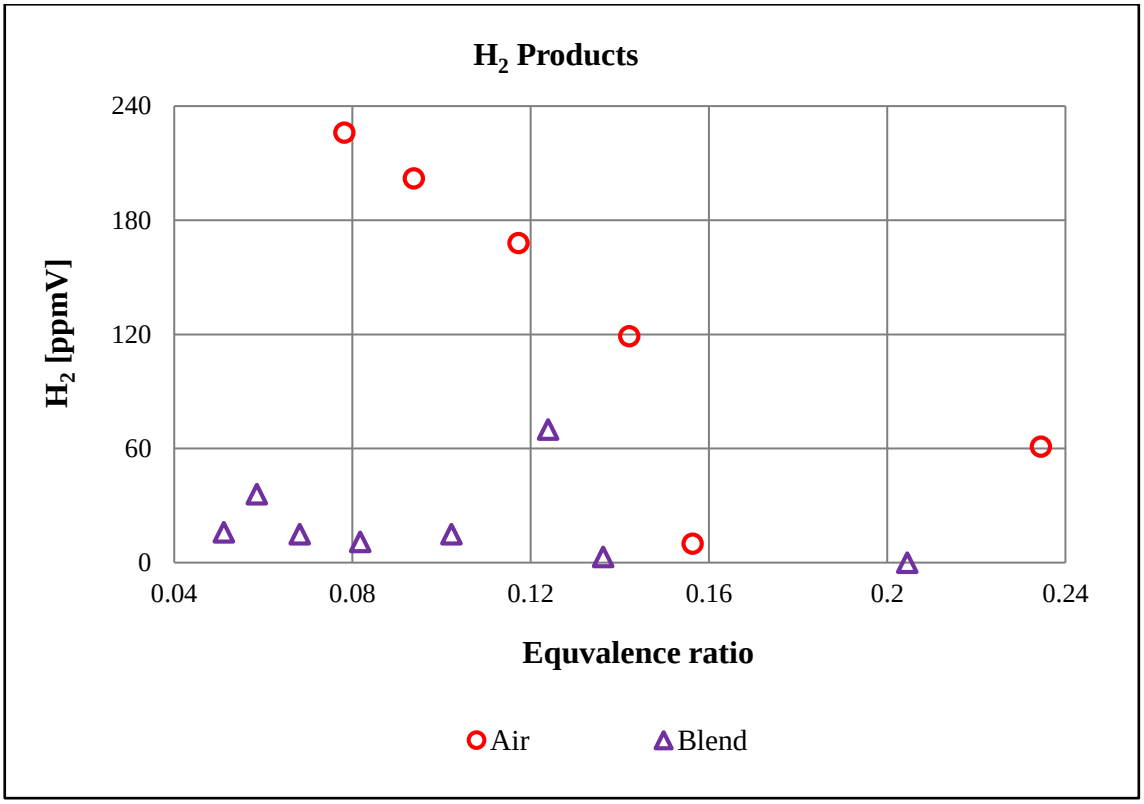

Figure 6.7 H_2 products against equivalence ratio

Figure 6.7 shows that the H_2 concentration in the exhaust gases using the blend as a working fluid remained low, at around 15 ppm with minor fluctuations, at the lowest equivalence ratios. After a brief spike, H_2 emission levels fell to zero past an equivalence ratio of 0.2. In the case of air, H_2 products were considerably higher as the equivalence ratio increased from its lowest level to around 0.14.

They then fell briefly to similarly low levels to those of the blend at 0.16, before rising again slightly at the highest equivalence ratio. As referenced in Chapter 2, the reduction of emitted H_2 products using the proposed blend in the combustion process can be explained due to the higher O_2 concentration in the blend compared to its normal value in air.

As shown in Figure 5.12, the concentrations of H_2 products after combustion were, similarly to experimental trends, lower for the novel CARSOXY blend than for air. The excess proportion of O_2 facilitates complete burning of H_2 and other unburned hydrocarbons in the secondary zone, which results in low levels of post-flame H_2 products [195, 202]. However, as previously mentioned, the differences between experimental and computational burner modes led to a relative difference in both results. The experimental and computational results show that using CARSOXY as an alternative working fluid could produce a lower percentage of H_2 compared with conventional air. This could indicate a high potential to recirculate the other products, CO_2 and Ar, in the proposed cycle.

6.3 **Heat release**

In the previous section, the data indicated that the novel blend reduced emissions compared to air as a working fluid in the combustion process of a gas turbine burner. Thus, use of this blend could contribute to protecting the environment from these harmful emissions. This section will attempt to demonstrate that the novel blend can feasibly replace air in a gas combustor while maintaining gas turbine reliability. There are several factors that impact flame stability in the combustion process of gas combustors and an unstable flame can lead to unreliability of gas turbines in industrial applications. As mentioned in Chapter 2 (Section 2.3), one of the measurements of flame stability is heat release oscillations.

A Photron FASTCAM APX-RS HSC with a Hamamatsu image intensifier coupled with a CH* filter installed was used to capture flame images using PFV software from the 20-kW

burner in the experimental work. Figures 6.8 and 6.9 show images of flame cases running with air and the proposed blend as working fluids, respectively.

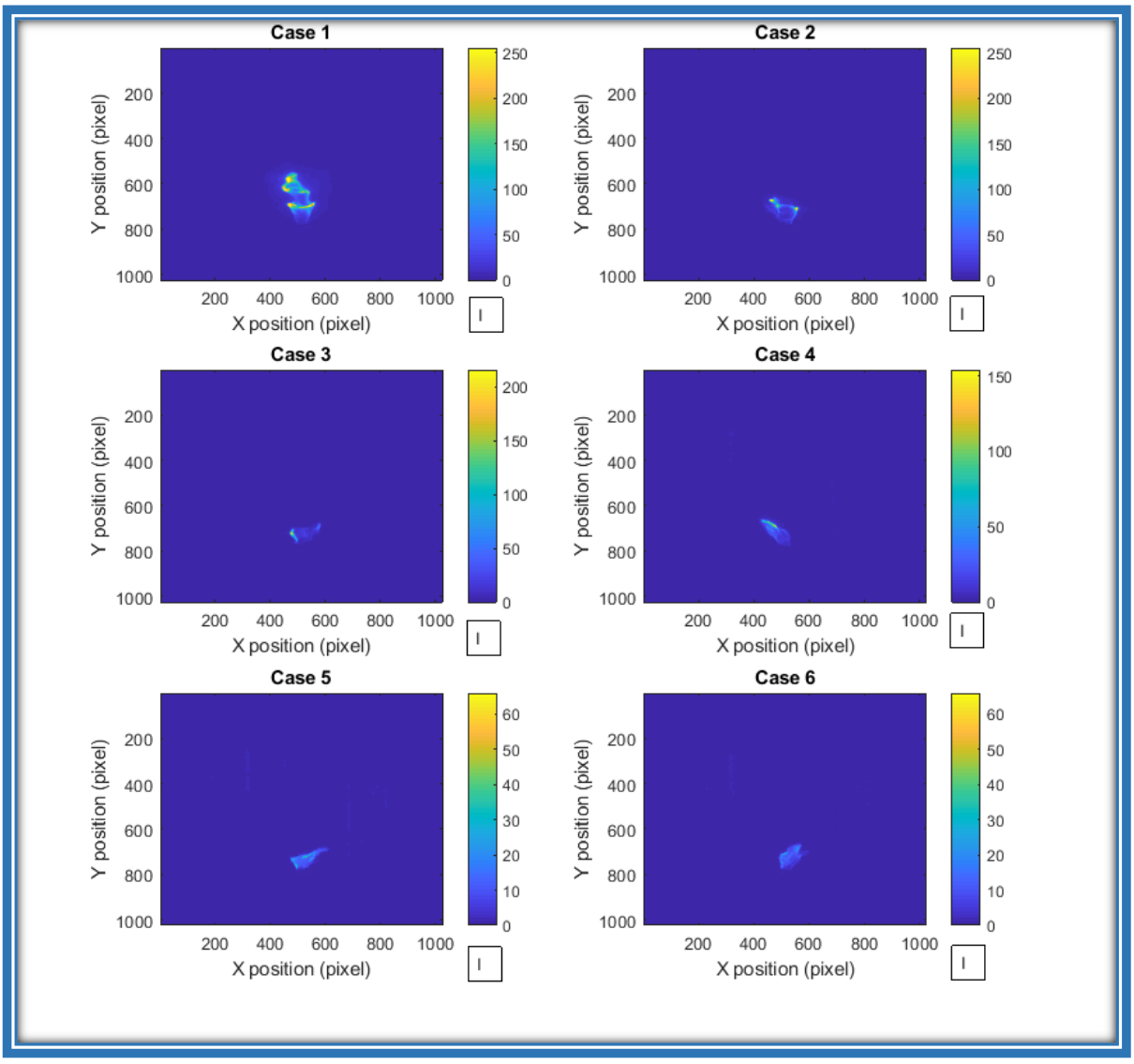

Figure 6.8 Flames running with air as a working fluid

Figure 6.8 shows that light intensity of the flame running with air decreased across the cases presented, while Figure 6.9 indicates that light intensity of the flame running with the blend remained at the same high magnitude across the cases presented.

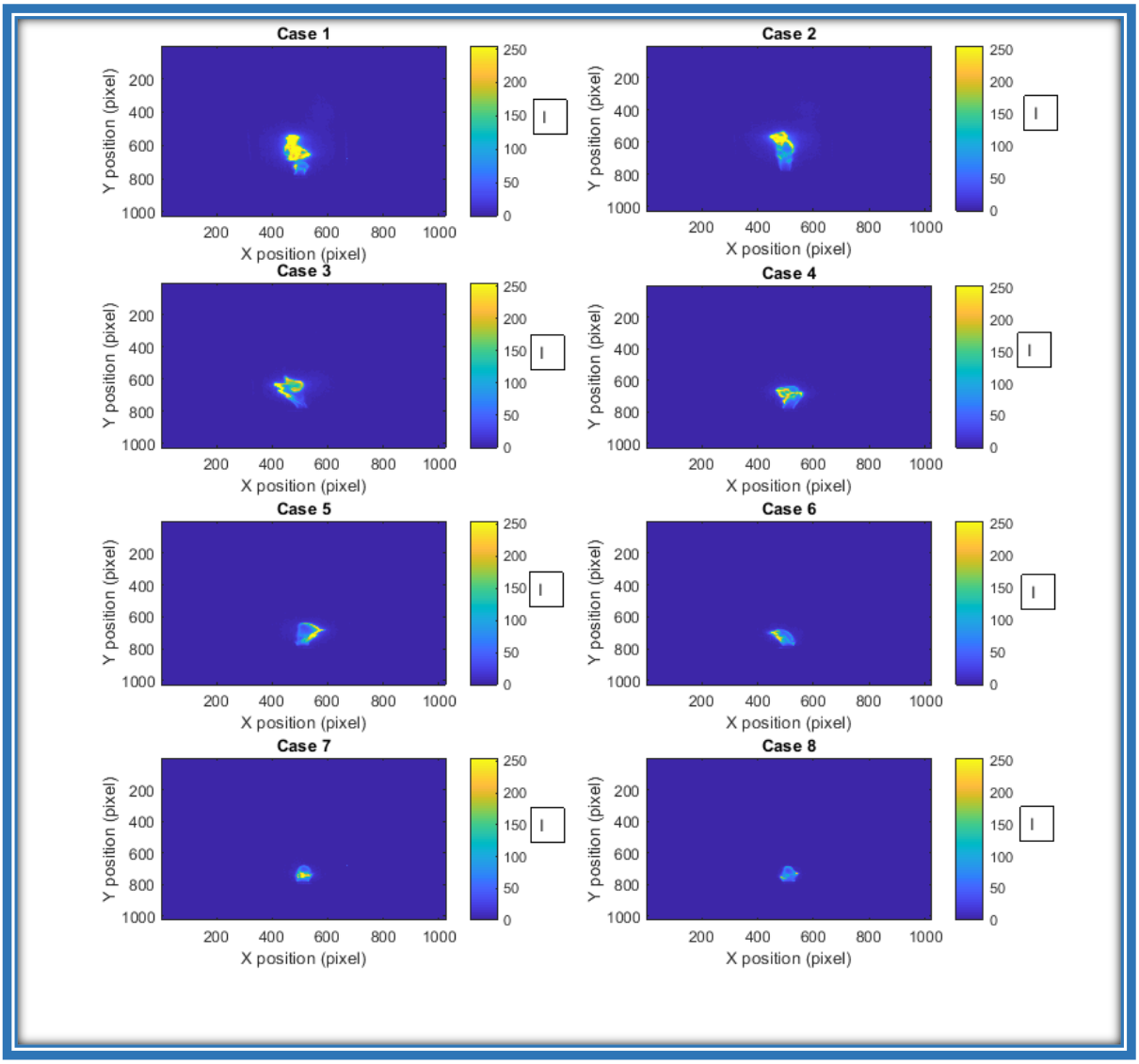

Figure 6.9 Flames running with blend as a working fluid

In this study, 100 flame chemiluminescence images each of the flame running with CARSOXY as a working fluid and of the flame running with air were captured. Each image consists of a number of pixels. The MATLAB code described in Appendix 3 applies Equation 6.2 (provided below)—where R, i, j *and* I are the number of images, horizontal, vertical pixels and light intensity measurements, respectively—to calculate heat release fluctuations, which equate to integral pixel intensity, referring to the summation of count values for each pixel within each image.

$$Q'_R = \sum_i^n \sum_j^m I \qquad \text{Eq. (6.2)}$$

Once Q'_R was obtained for the 100 images (i.e. $Q'_1, Q'_2, Q'_3 \ldots\ldots\ldots\ldots Q'_{R=100}$), the average value ($\bar{Q}$) was calculated using a separate Excel spreadsheet, as described in Equation 6.3.

$$\bar{Q} = \frac{\sum_R^{100} Q'_R}{(R = 100)} \qquad \text{Eq. (6.3)}$$

Finally, the $\left|Q'_R/\bar{Q}\right|$ was obtained for each image by dividing Equation 6.2 over Equation 6.3. Since the time frame is known for each image (0.0333 s), a Time -$\left|Q'_R/\bar{Q}\right|$ figure was plotted, as shown in Figures 6.10- 6.17.

Heat release from flame images and averages were calculated using 0.33-second time intervals at different mass flow rates, as shown in Appendix 4, Tables 2 and 3. These tables represent heat release comparisons between the two working fluids within a 3.3-second time period.

Figures 6.10 to 6.15 show that significantly more heat release ratios $\left|Q'_R/\bar{Q}\right|$ for the proposed blend were located within the range of 0.8 and 1.2—calculated as 0.2 added to the mean and subtracted from it following the standard deviation model—than the values for air over a similar time period. However, further statistical investigation is required to indicate whether these values of heat release for the proposed blend are closer to the mean than the values for air as a working fluid. This range of heat release magnitude is evidence that the novel blend provides a more stable flame than air as a working fluid at the different mass flow rate levels analysed.

As predicted (see Section 2.9), using diffusive injection running with a high concentration of oxygen in the working fluid extends the flammability limits, thus increasing flame

velocity. As a result, the diffusive flame with oxygen enrichment is more stable than the flame running with conventional air as a working fluid. The flame also anchors to the burner rim [146, 147].

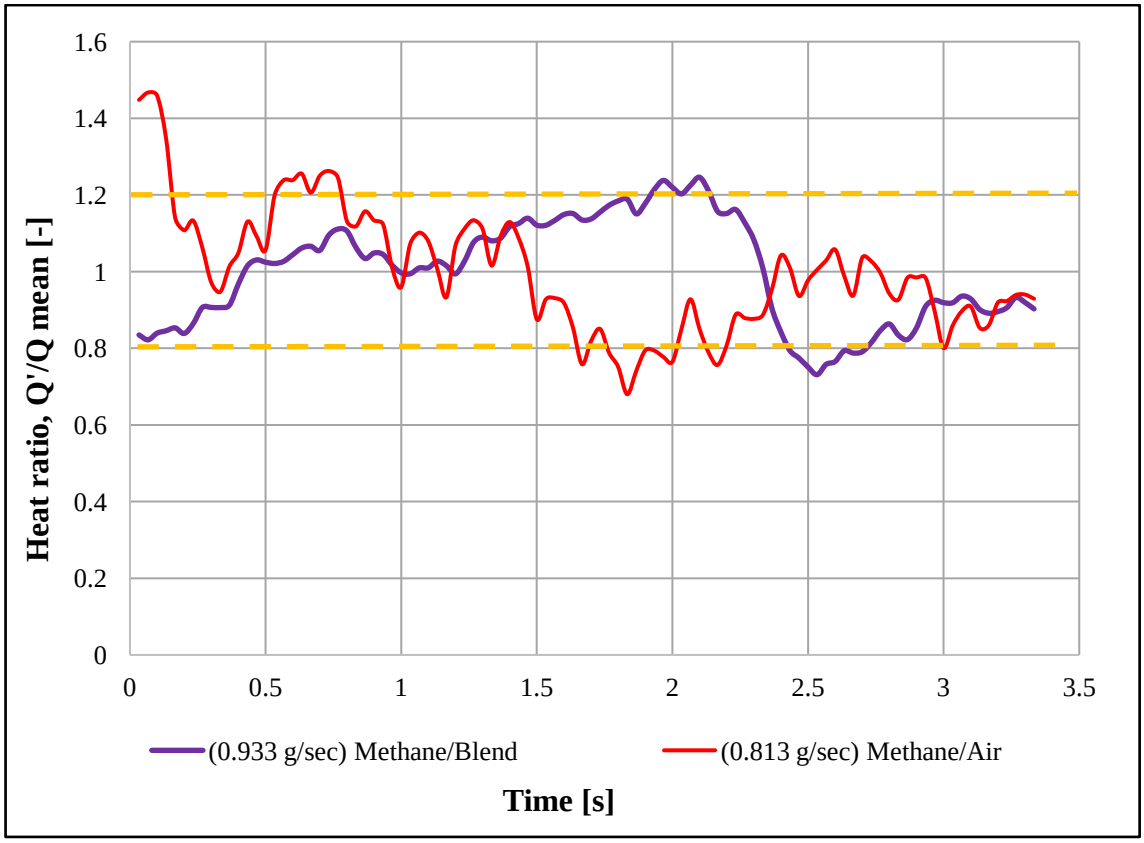

Figure 6.10 Heat release oscillation comparison [case 1 mass flow rate]

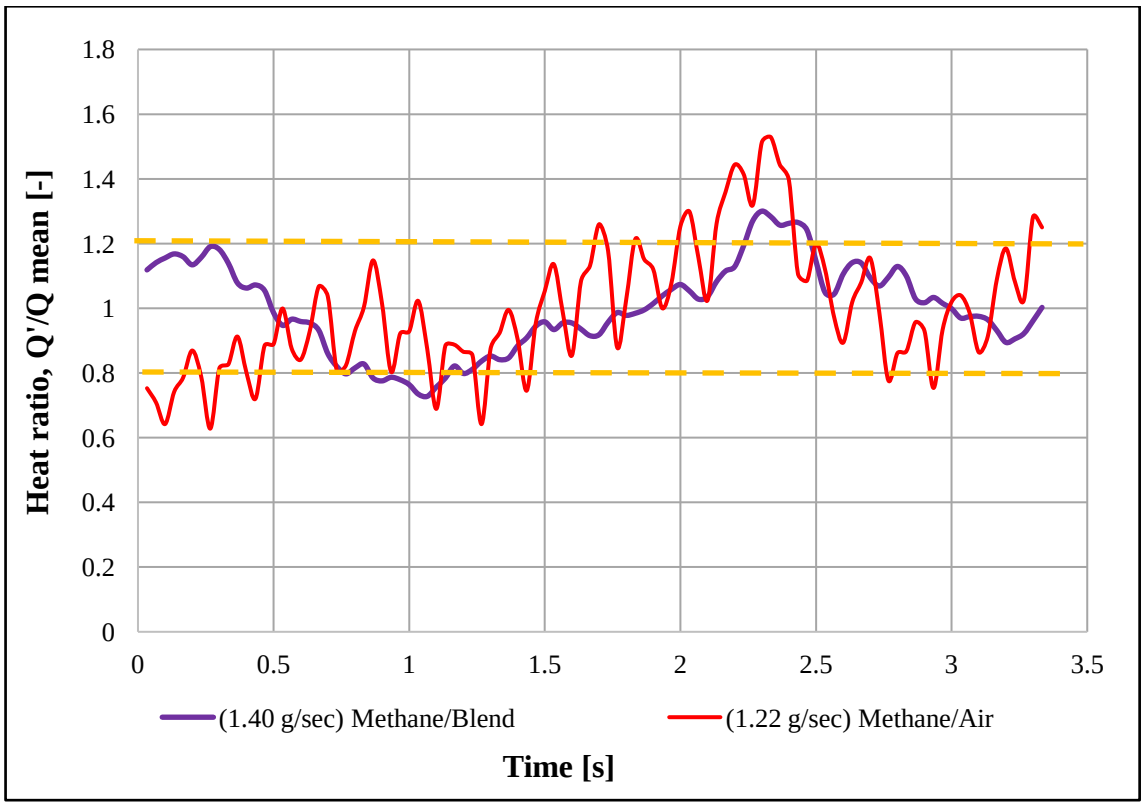

Figure 6.11 Heat release oscillation comparison [case 2 mass flow rate]

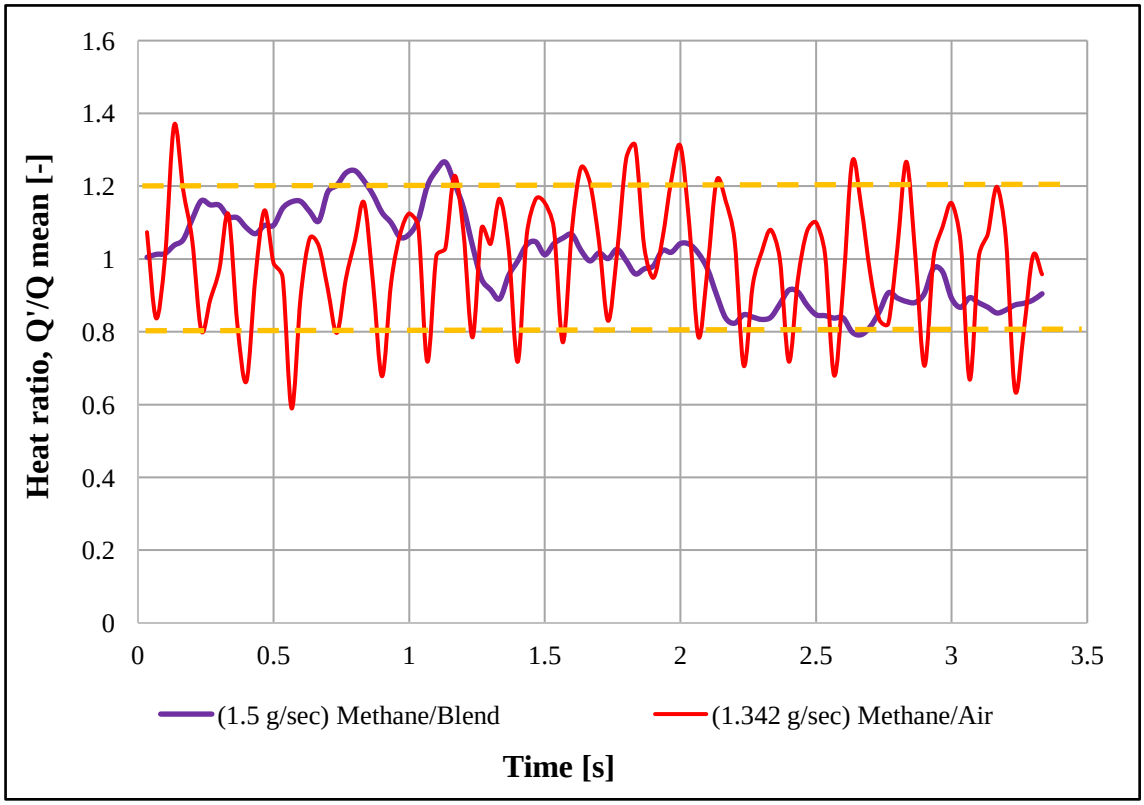

Figure 6.12 Heat release oscillation comparison [case 3 mass flow rate]

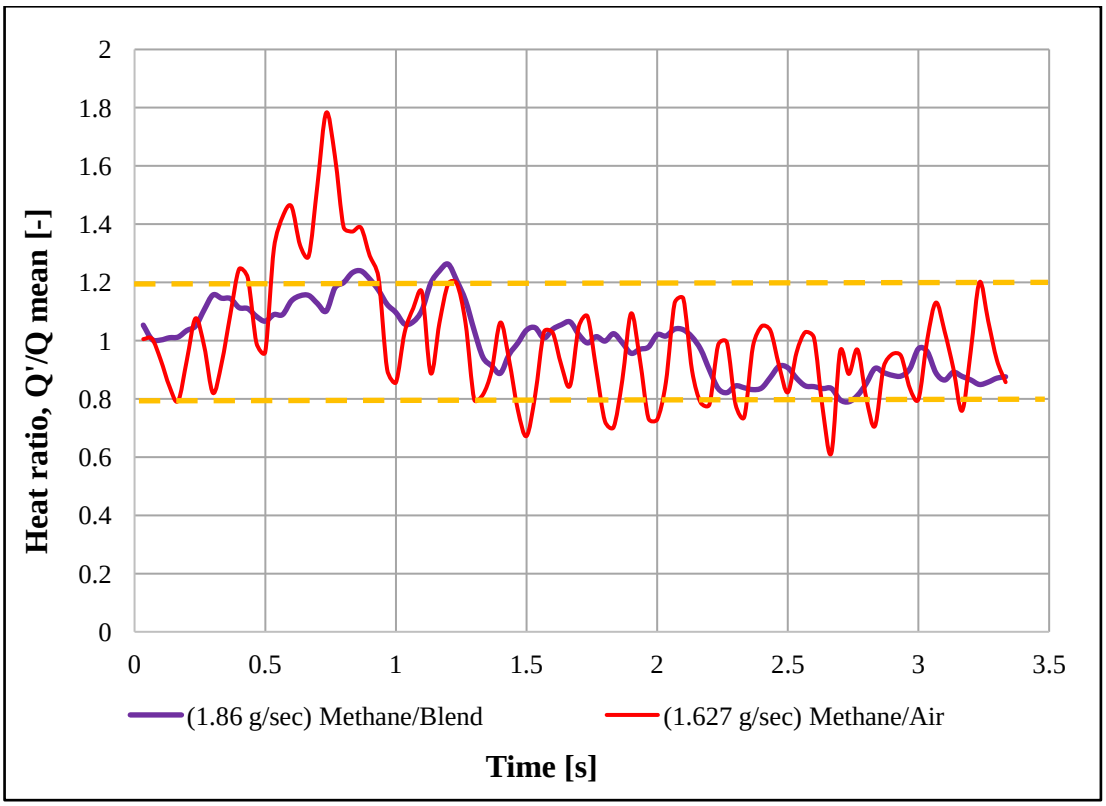

Figure 6.13 Heat release oscillation comparison [case 4 mass flow rate]

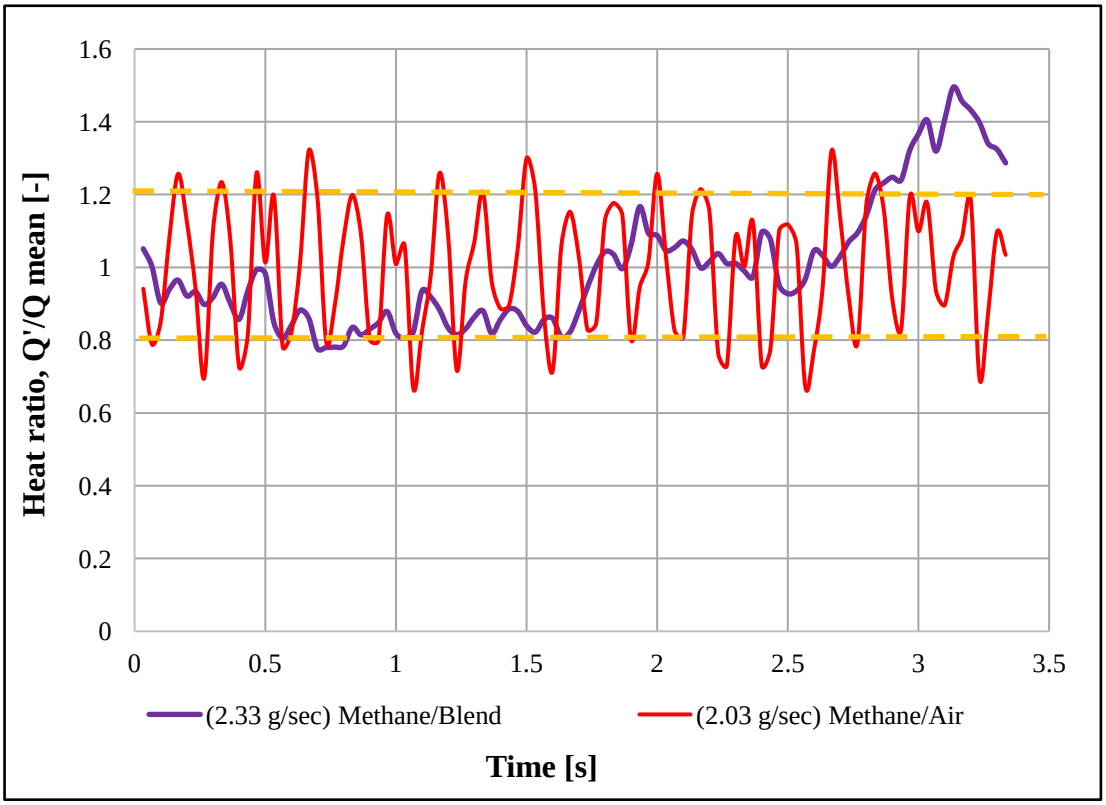

Figure 6.14 Heat release oscillation comparison [case 5 mass flow rate]

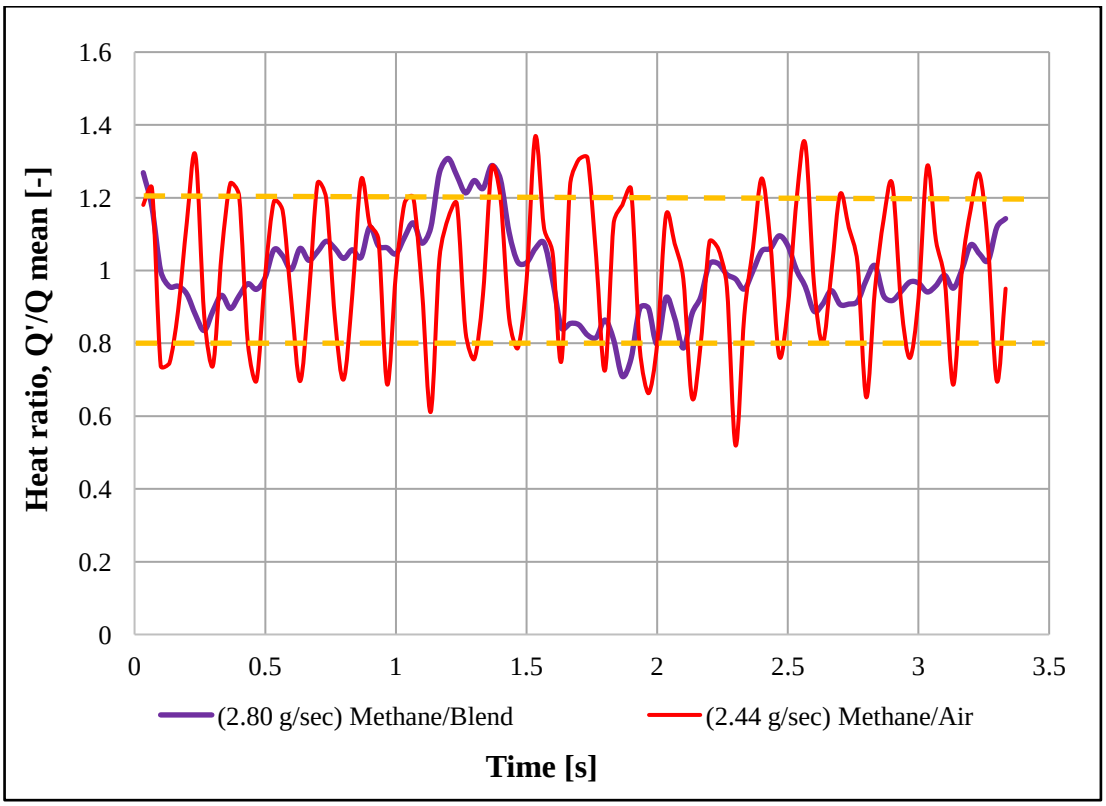

Figure 6.15 Heat release oscillation comparison [case 6 mass flow rate]

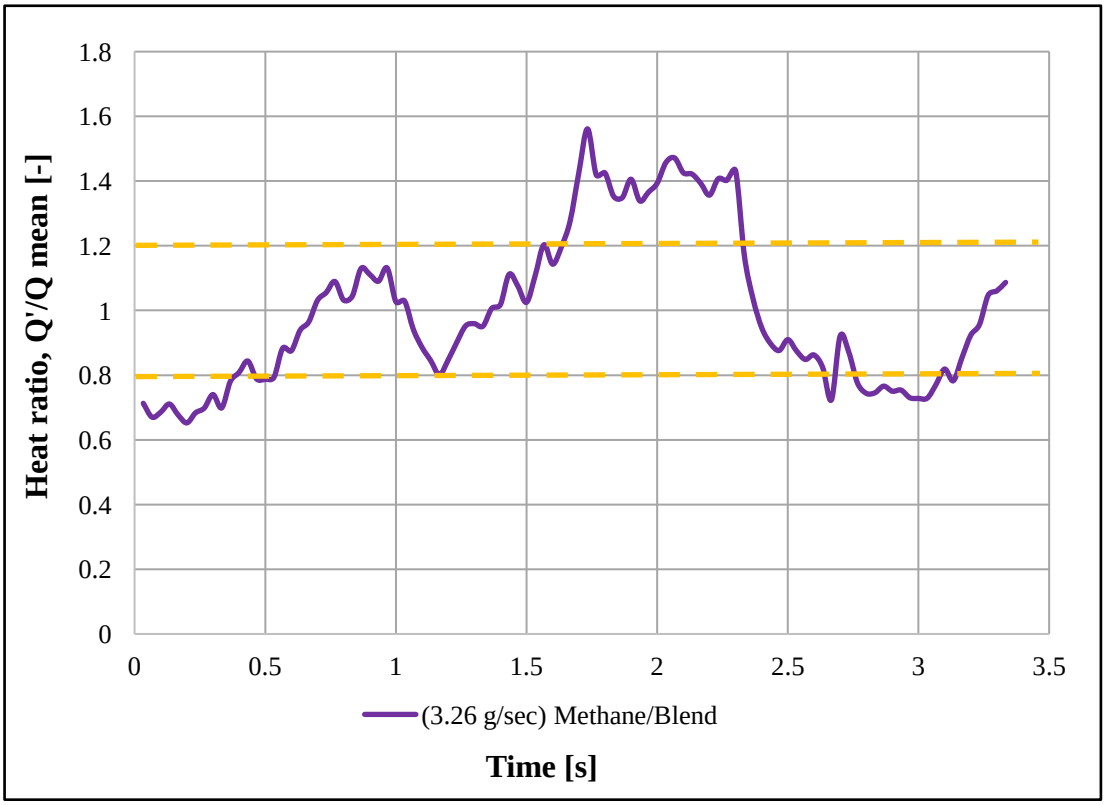

Figure 6.16 Heat release oscillations for the blend at 3.26 g/sec

The blowout limit was reached at the highest levels of mass flow rate for air. Therefore, Figures 6.16 and 6.17 show the heat release magnitude for only the novel blend at the equivalent mass flow rate levels of the working fluid.

Most of the heat release magnitude values shown in Figure 6.16 are within the stability range limit of 0.8 and 1.2, indicating a mostly stable flame at the higher mass flow rate of the novel blend as a working fluid in the combustion process.

However, it can be seen that the values of heat release exceeded the range limit between 1.5 and 2.5 sec, indicating an increasing instability in the flame. In contrast, Figure 6.17 shows more heat release values located inside these limits, indicating a high level of flame instability. It must be emphasized that running at such lean conditions is considered in gas turbines, thus more tests are needed at high-power levels and high equivalence ratios to reach fuller conclusions regarding the applicability of CARSOXY as a replacement for air.

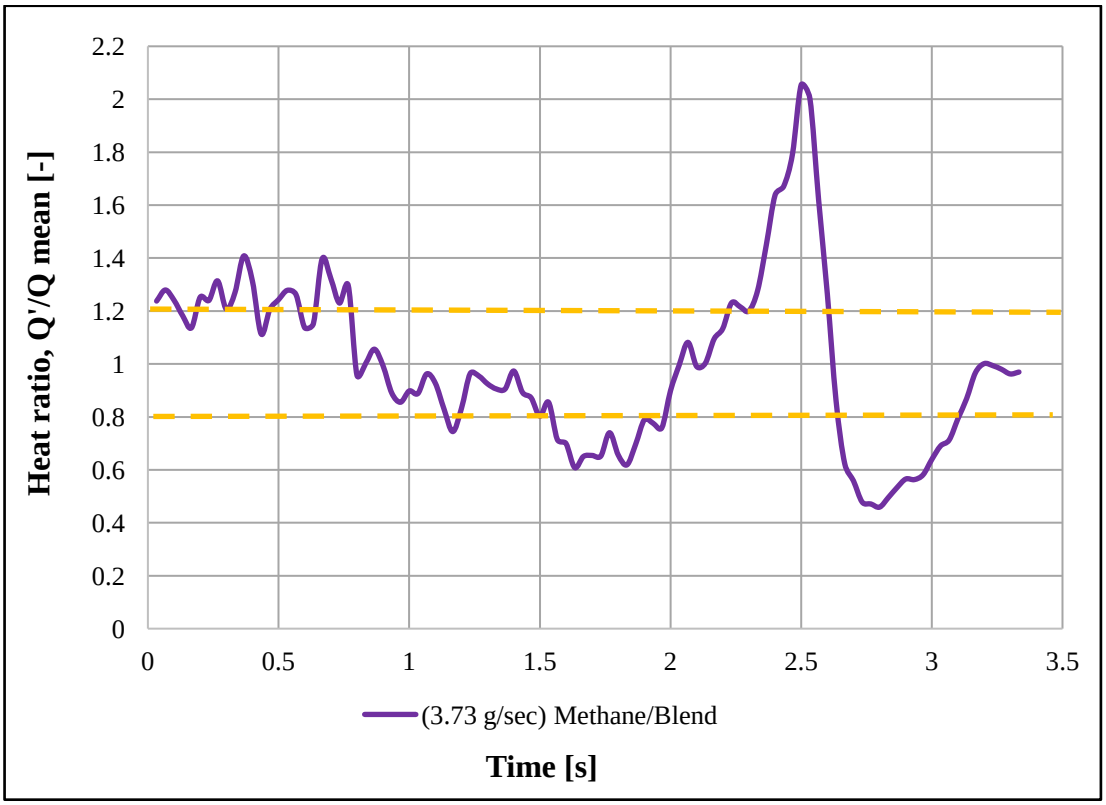

Figure 6.17 Heat release oscillations for the blend at 3.73 g/sec

6.4 **Summary**

A 20-kW generic burner experimental rig was set up to ascertain whether the proposed blend produced fewer harmful gas emissions and equal or better flame stability compared to conventional air as a working fluid. This enabled the feasibility of replacing air with the novel blend as a working fluid in industrial gas turbine combustors to be examined. Outlet temperature and CO, NO, NO_x and NO_2 emissions were measured using a Testo 350XL.

The results indicated that the novel blend not only produced useful outlet temperatures but also reduced or eliminated harmful emission levels, notably NOx, compared to air when used as working fluid. This demonstrates that the blend could be used as a more environmentally friendly alternative to air in industrial gas turbine combustors.

Chemiluminescence was observed and analysed using a HSC and MATLAB software. Subsequently, it was examined in terms of heat release oscillations to measure the flame stability of the blend compared to that of conventional air as a working fluid.

Overall, the results show that the proposed blend provided a consistently more stable flame, operating mostly within the statistical flame stability range of 0.8 to 1.2, indicating that the blend could be used as a practical alternative to air in industrial gas turbine combustors. Anomalous flame stability readings could be attributed to interference from external variables, such as the extractor or ambient temperature, which can be corrected in future experimental work.

Broadly, the experimental results are in line with the theoretical predictions made earlier in this study using Aspen Plus. It was predicted that the proposed blend would reduce or eliminate harmful gas emissions while ensuring at least equal stability to conventional air as a working fluid. The next step was to experimentally test the practical feasibility of using the proposed blend as an alternative to conventional air in an industrial gas turbine

combustor. The experimental results indicate that the theoretical predictions of reduced NO, NO_2 and NO_x emissions were mostly replicated in the experimental tests.

Although there were huge reductions, complete elimination of NO_x did not occur in all cases, which differed from the theoretically modelled predictions. Given that this discrepancy is likely attributable to external interference from the extractor or the pilot flame, it is unlikely to affect the validity of the results but should be considered in terms of further work. The unexpectedly high levels of CO, although also likely to be attributed to external variables, also require further exploration and explanation.

The heat release oscillation results also closely matched and, in fact, exceeded the theoretical predictions that the proposed blend would provide at least equal flame stability to that of conventional air. However, at higher mass flow rates, it was not possible to compare data between the blend and air as a working fluid due to the blowout limit being reached. Moreover, at the highest mass flow rate of 3.73 g/sec, flame stability when running the proposed blend was well outside the statistical flame stability range of 0.8 to 1.2. Therefore, further exploration of this trend should thus be considered in any future work.

Time and resource constraints should also be taken into account when considering the scope of this present experimental investigation. The limitations in terms of the time available for experimental work resulted in experimental limitations, such as the lack of the possibility to measure CO_2 emissions. Therefore, while providing supporting data to back up the theoretical hypothesis that the CARSOXY blend is a practically feasible and more environmentally-friendly alternative to conventional air as a working fluid, these results should be considered as preliminary supporting data.

CHAPTER SEVEN

Chapter 7 Conclusions and recommendations for future work

This chapter provides a brief summary of this thesis in terms of the background to gas turbine use and its connected environmental issues, the study's aims and objectives, its theoretical and experimental approaches, and the principal findings.

In the past few decades, the demand for electricity has continued to grow rapidly, leading to increased anthropogenic emissions that make a significant contribution to the problem of climate change. Currently, the majority of electricity demand still has to be met using fossil fuel-based gas turbines, which contribute to the problem of climate change due to their production of harmful CO_2 and NO_x emissions. Oxyfuel has been proposed as one innovative technique to solve the problem of reducing gas turbine emissions without replacing fossil fuels because it can recycle CO_2 in the combustion process while eliminating NO_x emissions. It has been proposed to combine oxyfuel with the concept of HGTs to reduce harmful emissions while maintaining system efficiency.

To address the issue of potential blowout due to the high amounts of water involved in using this combined concept, this study proposed a novel blend that could replace air as a working fluid in an industrial gas turbine combustor, which uses the combined concepts of the oxyfuel technique and the recycling of CO_2 in a humidified cycle while adding the inert gas argon to the combustion process to create a novel blend, CARSOXY, for use as an alternative working fluid to air in industrial gas turbines.

In this brief conclusion, this study's main theoretical and experimental findings are highlighted, along with a consideration of potential future work connected to this paper and its findings. A theoretical investigation employing the computational modelling software Gaseq, Minitab and Chemkin-Pro was carried out to indicate the optimum novel blend, consisting of Ar, CO_2 and H_2O with O_2, out of 120 potential blends. A bespoke numerical

model was also incorporated into the study to investigate the performance of the gas turbine in terms of heat production, output power and the efficiency of the gas turbine running with the novel blend, while Aspen Plus was used to investigate the proposed CARSOXY cycle to determine its performance and compare it with a conventional humidified gas turbine cycle.

Preliminary experimental work was then carried out to investigate the combustion process with methane as fuel and the indicated optimum blend as a working fluid in comparison with conventional air at the same operating conditions. This comparison was focused on the feasibility of the novel blend in terms of reducing emissions and flame stability. The key findings from this study's investigative work are outlined below.

7.1.1.1 **Theoretical outcomes**

- The use of Gaseq resulted in the creation of 120 blends consisting of Ar, CO_2, H_2O and O_2 as a working fluid in a combustion process for methane, with calculations for outlet temperature, thermodynamic properties and products, including H_2O and CO_2. Gaseq also calculated these properties and products for a combustion process that used air as a working fluid at the same operating conditions. The software also allowed air to be used as a reference for data obtained from the 120 blends.
- Empirical data was employed in the following step to compare the blends' characteristics, previously calculated using Gaseq, to those obtained from air. This resulted in the selection of the 16 best blends with the closest values of properties and products to those of air.
- Minitab software was also used in this study as a tool for the DOE approach to clarify the correlation between each component of the investigative blends and each thermodynamic property and product. Results showed that an increasing proportion of argon significantly heightens the specific heat ratio as a thermodynamic property

while decreasing outlet temperature. Increasing both H_2O and CO_2 as components of these blends reduces outlet temperature and specific heat ratio.

- Chemkin-Pro was employed in the next step to determine the flame characteristics for the 16 selected blends, subsequently further narrowed down to eight blends, in order to compare flame speeds to those obtained from air under the same running conditions. Results showed that blends 58, 79 and 109 had flame speeds that were closest to those of air.
- The optimum relative proportions of the novel blend gas components were identified as belonging to: blend 58 (i.e., 25%AR-23%H_2O-19%CO_2). This blend has approximately equivalent outlet temperatures and thermodynamic properties to air as a working fluid in the combustion process. Consequently, the novel blend could be proposed as a replacement for air in gas combustors to help contribute to protecting the global environment.
- The efficiency of the gas turbine running with the optimum novel CARSOXY blend/methane as fuel was up to 13.9% higher than when running with NG/air as a working fluid in all operating conditions of varying mass flow rates. As a result, the optimum blend could be used as a working fluid in the proposed CARSOXY cycle that recirculates CO_2 products in the combustion process.
- The exhaust temperature data produced using CARSOXY, obtained from the bespoke simulation model, showed higher levels than for air as a working fluid. This could be beneficial for heat recovery systems utilised in the proposed cycle to produce water vapour.
- Aspen Plus results also demonstrated a significant increase in cycle efficiency compared to a conventional air humidified cycle, with lower combined compressor work, similar compressor outlet temperatures to conventional systems, suggesting no necessity for expensive modifications or additions and lower turbine inlet

temperatures – also indicating no need for costly system modifications as they remained within TIT limits – even with increased cycle efficiency.

- Exhaust product data from Aspen Plus showed that CO and H_2 products were lower for CARSOXY than for the air humidified cycle, supporting the potential environmental benefits of its use in terms of reducing harmful emissions. CO_2 and H_2O products were both higher, contributing to recirculation and humidification and dilution processes as per the cycle's design. Relatively high NO levels found for the air humidified cycle reinforced the comparative environmental benefits of using CARSOXY for industrial applications.

7.1.2 Experimental outcomes

- Blend product temperatures were higher than air at lower mass flow rates of the working fluid. These results closely matched the profile from the theoretical data and they indicate that using the CARSOXY blend within the proposed cycle could benefit industrial gas turbine performance because the high product temperatures can be utilised in heat recovery systems.
- CO levels of exhaust gases using air and the blend as a working fluid had approximately the same value at higher equivalence ratio values. However, at lower equivalence ratios, CO products rose dramatically for air while they only rose a small amount for the proposed blend.
- The blend produced zero NO and NO_x at low equivalence ratios, rising to small amounts at higher equivalence ratios. NO_2 was produced at consistently low levels across the equivalence ratios. All cases were considerably lower than the figures for air, indicating that the use of this blend in industrial gas turbines could contribute to reducing harmful anthropogenic emissions. The small amounts of NO, NO_x and NO_2

produced by the blend could be attributed to interference from outside variables, such as the pilot flame or the extractor.

- H_2 concentration values in the exhaust gases using the blend as a working fluid were considerably lower overall than those for air. The likely explanation for this is the higher O_2 concentration in the blend compared to its normal value in air, leading to complete combustion of the fuel. Such low levels of H_2 could be beneficial as they indicate a high potential to recirculate CO_2 and Ar in the proposed cycle.
- Significantly more of the heat release values for the blend were located within the optimal flame stability range than the values for air over a similar time period. These experimental results are evidence that the novel blend provides a more stable flame than air as a working fluid across a range of different mass flow rate levels.
- At the highest mass flow rate levels, heat release magnitude values for the blend began to move from the optimum flame stability range, indicating increased instability which requires examination by further assessment at high equivalence ratios and power outputs.

7.2 **Overall conclusion**

This thesis proposed a novel approach to replacing air as a working fluid in an industrial gas turbine combustor, combining CCS integrated with OF techniques with the inert gas argon. The proposed CARSOXY blend was found to have similar thermodynamic properties to conventional air while reducing harmful emissions.

In terms of industrial gas turbine performance, the proposed blend could be used instead of air because it has been shown numerically to have higher efficiency. From the point of view of feasibility, experimental work indicated that the proposed blend eliminates NOx from combustion products and reduces harmful emissions. The flame when running with de-

humidified CARSOXY was shown to be more stable, which also supports the practical applicability of this novel idea to gas turbines.

Thus, this study has revealed that its novel concept could be used to help working gas turbines produce energy in a more environmentally-friendly way while continuing to use conventional NG.

7.3 Recommendations for future work

There are various aspects of this research that lend themselves to future work due to one, or a combination, of the following reasons: limitations in terms of time, limitations in terms of resources, the emergence of potential new avenues of interest as the work progressed and data was collected. An expansion of this study's investigations and work to replicate, or improve, results can, therefore, be considered useful and desirable.

7.3.1 Experimental recommendations

The following are recommended as possible focuses for future experimental investigations:

- The experimental burner could be run with gradual mass flow rate increments up to higher power levels, closer to what the burner really produces. This study's experimental work ran at 1 litre per minute at 0.55kw power. More optimal parameters would be incremental increases from 1 to 15 litres at 7.5kw power. In this way, a more complete flame map with a greater stability range could be produced, which would increase the validity of experimental results.
- The Testo 350 XL exhaust gas analyser should be calibrated for measuring CO_2 products as it was not possible to do this as part of this study. Collecting data on CO_2 would give an indication as to its concentration in the combustion products. These figures could then be cross-checked against the theoretical data, allowing for the

calculation of the percentage of CO_2 which could be recirculated in the combustion process.

- Phase-resolved Planar Laser-Induced Fluorescence (PLIF) could be used to provide structural data for the flame characteristics and emissions spectroscopy with a higher degree of accuracy.
- A Photo Multiplier Tube (PMT) device could be utilised to measure heat release from the combustion process. This study used a HSC with an attached CH* filter to capture chemiluminescent flame images, which were then processed using MATLAB code to provide the heat release ratio. Data obtained with the PMT device could give a more precise indication of flame stability.
- Flames produced from other types of fuels, such as hydrogen and CARSOXY as a working fluid, could be investigated. This would allow data comparison with this study, where the flame was produced using methane/CARSOXY, which could lead to improved analysis of flame characteristics.
- A steam generator could be employed to add water vapour to the combustion process. This was not possible as part of this study's experimental work—a blend of CO_2, argon and O_2 was utilised to approximate the proposed system. Use of a steam generator would allow the flow rate of the proportion of steam at blowout condition to be measured, thus providing more accurate data with higher engine performance.

7.3.2 **Theoretical recommendations**

The following recommendations are made for future numerically-based theoretical investigations:

- It is recommended that the ASU be modelled to feed the CARSOXY cycle with oxygen and the inert gas argon. As discussed in Chapter 2, the ASU plays a significant role in power consumption, which may directly affect the overall

efficiency of the cycle. Therefore, including the ASU in the proposed CARSOXY cycle and its theoretical modelling could provide a more complete picture of predicted cycle efficiency.

- A techno-economic comparative study of the proposed cycle and a conventional humidified air cycle is also recommended. Such a study could provide practical data on the economic feasibility of the proposed cycle running with the novel CARSOXY blend by examining the technical aspects of both cycles, together with their financial costs and benefits.

References

[1] V. Smil, *Energy at the crossroads: global perspectives and uncertainties*: MIT press, 2005.

[2] N. Unies, "World Population Prospects. Key Findings and Advanced Tables. The 2015 Revision," ESA/P/WP. 241, New York2015.

[3] EIA, "International Energy Outlook 2016," 2016.

[4] Y. Bayar and H. A. Özel, "Electricity consumption and economic growth in emerging economies," *Journal of Knowledge Management, Economics and Information Technology,* vol. 4, pp. 1-18, 2014.

[5] V. Arora and J. Lieskovsky, "Electricity use as an indicator of US economic activity," 2016.

[6] WEC, "World Energy Resources: 2013 Survey," 2013.

[7] IEA, "World OutlookEnergy 2015," 2015.

[8] V. C. Nelson and K. L. Starcher, *Introduction to renewable energy*: CRC press, 2015.

[9] A. Labouret and M. Villoz, *Solar photovoltaic energy* vol. 9: IET, 2010.

[10] M. H. Ali, *Wind energy systems: solutions for power quality and stabilization*: CRC Press, 2012.

[11] IRENA, "Tidal Energy Technology Brief," June 2014.

[12] S. Currie, *Hydropower*: ReferencePoint Press, 2011.

[13] R. Ren21, "Global status report," *Renewable Energy Policy Network for the 21st Century, Paris, France,* 2010.

[14] V. Smil, *Energy transitions: history, requirements, prospects*: ABC-CLIO, 2010.

[15] J. K. Casper, *Fossil fuels and pollution: the future of air quality*: Infobase Publishing, 2010.

[16] P. Breeze, *Gas-turbine Power Generation*: Academic Press, 2016.

[17] A. Demirbas, "Methane Gas Hydrate: Springer Science & Business Media," *London, England,* 2010.

[18] IEA, "World Energy outlook " 2009.

[19] IEA, *Fossil FIel-fired Power Generation*: OECD/IEA, 2007, 2007.

[20] EIA, "Annual Energy Outlook 2015: With Projections to 2040," April 2015.

[21] R. T. Harman, *Gas Turbine Engineering: Applications, Cycles and Characteristics*, 1981.

[22] T. Giampaolo, "Gas turbine handbook principles and practices, 2006," ed: The Fairmont Press Inc., USA.

[23] C. Soares, *Gas turbines: a handbook of air, land and sea applications*: Butterworth-Heinemann, 2011.

[24] R. Farmer, "Gas Turbine World 2012 GTW Handbook," ed: Pequuot Publishing Inc, 2011.

[25] A. C. Yunus and A. B. Michael, "Thermodynamics: An engineering approach," *McGraw-Hill, New York,* 2006.

[26] C. Borgnakke and R. E. Sonntag, *Fundamentals of thermodynamics*: Wiley Global Education, 2016.

[27] O. Singh, *Applied Thermodynamics 3rd Edition*: Digital Designs, 2003.

[28] R. Pavri and G. D. Moore, "Gas turbine emissions and control," *General Electric Report No. GER-4211,* 2001.

[29] M. P. Boyce, *Gas turbine engineering handbook*: Elsevier, 2011.

[30] G.-M. Choi and M. Katsuki, "Advanced low NOx combustion using highly preheated air," *Energy Conversion and Management,* vol. 42, pp. 639-652, 2001.

[31] M. M. Schorr and J. Chalfin, "Gas Turbine NOx Emissions Approaching Zero—Is It Worth the Price?," *General Electric Power Generation, Report No. GER,* vol. 4172, 1999.

[32] R. Hendricks, D. Shouse, and W. Roquemore, "Water injected turbomachinery," 2005.

[33] N. Docquier and S. Candel, "Combustion control and sensors: a review," *Progress in energy and combustion science,* vol. 28, pp. 107-150, 2002.

[34] W. W. Hay, *Experimenting on a small planet: A History of Scientific Discoveries, a Future of Climate Change and Global Warming*, Second ed.: Springer Science & Business Media, 2016.

[35] IPCC, "Climate Change 2014–Impacts, Adaptation and Vulnerability: Regional Aspects," Cambridge University Press 1107058163, 2014.

[36] R. K. Pachauri, M. R. Allen, V. R. Barros, J. Broome, W. Cramer, R. Christ, *et al.*, *Climate change 2014: synthesis report. Contribution of Working Groups I, II and III to the fifth assessment report of the Intergovernmental Panel on Climate Change*: IPCC, 2014.

[37] IPCC, "Climate change 2007- The physical science basis: Working Group I Contribution to the Fourth Assessment Report of the IPCC," 2007.

[38] M. L. Parry, O. F. Canziani, J. P. Palutikof, P. J. van der Linden, and C. E. Hanson, "IPCC, 2007: climate change 2007: impacts, adaptation and vulnerability. Contribution of working group II to the fourth assessment report of the intergovernmental panel on climate change," ed: Cambridge University Press, Cambridge, 2007.

[39] BBC. (2017). *'Physical and human causes of climate change'*. Available: http://www.bbc.co.uk/education/guides/z3bbb9q/revision/3

[40] IEA, "CO_2 Emissions From Fuel Combustion IEA Statistics," 2013.

[41] P. Breeze, *Power generation technologies*: Newnes, 2014.

[42] IPCC, "IPOC Change - Climate change, 2014," 2014.

[43] Y. Schreuder, *The Corporate Greenhouse: Climate Change Policy in a Globalizing World*: Zed Books Ltd., 2013.

[44] IEA, "World Energy Investment Outlook, Special Report," 2014.

[45] WEC, "World Energy Resources-2016 - Executive summary," 2016.

[46] WEC, "World Energy Trilemma, Priority actions on climate change and how to balance the trilemma," 2015.

[47] WEC, "World Energy Trilemma | 2016, Defining measures to Accelerate the Energy Transition," 2016.

[48] IEA, "Technology Roadmap Carbon Capture and Storage," 2013.

[49] R. Stanger, T. Wall, R. Spörl, M. Paneru, S. Grathwohl, M. Weidmann, *et al.*, "Oxyfuel combustion for CO2 capture in power plants," *International Journal of Greenhouse Gas Control*, vol. 40, pp. 55-125, 2015.

[50] T. F. Wall, "Combustion processes for carbon capture," *Proceedings of the combustion institute*, vol. 31, pp. 31-47, 2007.

[51] K. Goto, K. Yogo, and T. Higashii, "A review of efficiency penalty in a coal-fired power plant with post-combustion CO2 capture," *Applied Energy*, vol. 111, pp. 710-720, 2013.

[52] G. Richards, K. Casleton, and B. Chorpening, "CO2 and H2O diluted oxy-fuel combustion for zero-emission power," *Proceedings of the Institution of Mechanical Engineers, Part A: Journal of Power and Energy*, vol. 219, pp. 121-126, 2005.

[53] P. Chiesa and S. Consonni, "Natural gas-fired combined cycles with low CO2 emissions," *Transactions of the ASME-A-Engineering for Gas Turbines and Power*, vol. 122, pp. 429-436, 2000.

[54] S. G. c. Göke, Katharina Krüger, Oliver Paschereit, Christian O, "Computational and experimental study of premixed combustion at ultra wet conditions," in *ASME Turbo Expo 2010: Power for Land, Sea, and Air*, 2010, pp. 1125-1135.

[55] K. Al-Attab and Z. Zainal, "Externally fired gas turbine technology: A review," *Applied Energy*, vol. 138, pp. 474-487, 2015.

[56] J. Lee, J. Campbell, and D. Wright, "Closed-cycle gas turbine working fluids," *Journal of Engineering for Power*, vol. 103, pp. 220-228, 1981.

[57] K. Saha, *The Earth's Atmosphere: Its Physics and Dynamics*: Springer Science & Business Media, 2008.

[58] Q. Liu, L. Wu, R. Jackstell, and M. Beller, "Using carbon dioxide as a building block in organic synthesis," *Nature communications*, vol. 6, 2015.

[59] W. Wang, S. Wang, X. Ma, and J. Gong, "Recent advances in catalytic hydrogenation of carbon dioxide," *Chemical Society Reviews*, vol. 40, pp. 3703-3727, 2011.

[60] N. MacDowell, N. Florin, A. Buchard, J. Hallett, A. Galindo, G. Jackson, *et al.*, "An overview of CO 2 capture technologies," *Energy & Environmental Science*, vol. 3, pp. 1645-1669, 2010.

[61] B. Metz, O. Davidson, H. De Coninck, M. Loos, and L. Meyer, "Carbon dioxide capture and storage," 2005.

[62] C. DEEC, "Roadmap: Supporting deployment of Carbon Capture and Storage in the UK," *UK Department of Energy and Climate Change*, 2012.

[63] IEA, "Technology roadmap, carbon capture and storage," *IEA Papers*, 2009.

[64] S.-Y. Lee and S.-J. Park, "A review on solid adsorbents for carbon dioxide capture," *Journal of Industrial and Engineering Chemistry*, vol. 23, pp. 1-11, 2015.

[65] M. L. Szulczewski, C. W. MacMinn, H. J. Herzog, and R. Juanes, "Lifetime of carbon capture and storage as a climate-change mitigation technology," *Proceedings of the National Academy of Sciences*, vol. 109, pp. 5185-5189, 2012.

[66] M. E. Boot-Handford, J. C. Abanades, E. J. Anthony, M. J. Blunt, S. Brandani, N. Mac Dowell, *et al.*, "Carbon capture and storage update," *Energy & Environmental Science*, vol. 7, pp. 130-189, 2014.

[67] Z.-A. Chen, Q. Li, L.-C. Liu, X. Zhang, L. Kuang, L. Jia, *et al.*, "A large national survey of public perceptions of CCS technology in China," *Applied Energy*, vol. 158, pp. 366-377, 2015.

[68] W. De Paepe, M. M. Carrero, S. Giorgetti, A. Parente, S. Bram, and F. Contino, "Exhaust Gas Recirculation on Humidified Flexible Micro Gas Turbines for Carbon Capture Applications," in *ASME Turbo Expo 2016: Turbomachinery Technical Conference and Exposition*, 2016, pp. V003T06A011-V003T06A011.

[69] J. Wang, L. Huang, R. Yang, Z. Zhang, J. Wu, Y. Gao, *et al.*, "Recent advances in solid sorbents for CO 2 capture and new development trends," *Energy & Environmental Science*, vol. 7, pp. 3478-3518, 2014.

[70] A. Korre, Z. Nie, and S. Durucan, "Life cycle modelling of fossil fuel power generation with post-combustion CO 2 capture," *International Journal of Greenhouse Gas Control*, vol. 4, pp. 289-300, 2010.

[71] M. A. Habib, M. A. Nemitallah, P. Ahmed, M. H. Sharqawy, H. M. Badr, I. Muhammad, *et al.*, "Experimental analysis of oxygen-methane combustion inside a gas turbine reactor under various operating conditions," *Energy*, vol. 86, pp. 105-114, 2015.

[72] D. Berstad, R. Anantharaman, and K. Jordal, "Post-combustion CO2 capture from a natural gas combined cycle by CaO/CaCO3 looping," *International Journal of Greenhouse Gas Control*, vol. 11, pp. 25-33, 2012.

[73] B. Najmi and O. Bolland, "Operability of Integrated Gasification Combined Cycle Power Plant with SEWGS Technology for Pre-combustion CO 2 Capture," *Energy Procedia*, vol. 63, pp. 1986-1995, 2014.

[74] M. Kawabata, O. Kurata, N. Iki, A. Tsutsumi, and H. Furutani, "System modeling of exergy recuperated IGCC system with pre-and post-combustion CO 2 capture," *Applied Thermal Engineering*, vol. 54, pp. 310-318, 2013.

[75] C. Kunze and H. Spliethoff, "Assessment of oxy-fuel, pre-and post-combustion-based carbon capture for future IGCC plants," *Applied Energy*, vol. 94, pp. 109-116, 2012.

[76] R. Priddle, "World energy outlook 2002," *International Energy Agency, IEA/OECD, Paris*, 2002.

[77] S. H. Higuchi, Shigeo Araki, Hidefumi Marushima, Shinya, "A Study of Performance on Advanced Humid Air Turbine Systems," *日本ガスタービン学会誌*, vol. 34, pp. 54-61, 2006.

[78] M. Bartlett, "Developing humidified gas turbine cycles," 2002.

[79] T. C. Lieuwen and V. Yang, *Gas turbine emissions* vol. 38: Cambridge university press, 2013.

[80] F. Xing, A. Kumar, Y. Huang, S. Chan, C. Ruan, S. Gu, *et al.*, "Flameless combustion with liquid fuel: A review focusing on fundamentals and gas turbine application," *Applied energy*, vol. 193, pp. 28-51, 2017.

[81] A. H. Lefebvre and D. R. Ballal, *Gas turbine combustion: alternative fuels and emissions*: CRC press, 2010.

[82] E. Benini, *PROGRESS IN GAS TURBINE PERFORMANCE*: InTech, 2013.

[83] A. Razak, *Industrial gas turbines: performance and operability*: Elsevier, 2007.

[84] G. Scheffknecht, L. Al-Makhadmeh, U. Schnell, and J. Maier, "Oxy-fuel coal combustion—A review of the current state-of-the-art," *International Journal of Greenhouse Gas Control*, vol. 5, pp. S16-S35, 2011.

[85] C. Liu, G. Chen, N. Sipöcz, M. Assadi, and X.-S. Bai, "Characteristics of oxy-fuel combustion in gas turbines," *Applied Energy,* vol. 89, pp. 387-394, 2012.

[86] Stanger, Rohan Wall, Terry Spörl, Reinhold Paneru, Manoj Grathwohl, Simon Weidmann, *et al.*, "Oxyfuel combustion for CO_2 capture in power plants," *International Journal of Greenhouse Gas Control,* vol. 40, pp. 55-125, 2015.

[87] M. A. Habib, M. Nemitallah, and R. Ben-Mansour, "Recent development in oxy-combustion technology and its applications to gas turbine combustors and ITM reactors," *Energy & Fuels,* vol. 27, pp. 2-19, 2012.

[88] D. R. Vinson, "Air separation control technology," *Computers & Chemical Engineering,* vol. 30, pp. 1436-1446, 2006.

[89] S. G. Sundkvist, A. Dahlquist, J. Janczewski, M. Sjödin, M. Bysveen, M. Ditaranto, *et al.*, "Concept for a combustion system in oxyfuel gas turbine combined cycles," *Journal of Engineering for Gas Turbines and Power,* vol. 136, p. 101513, 2014.

[90] B. Belaissaoui, Y. Le Moullec, H. Hagi, and E. Favre, "Energy efficiency of oxygen enriched air production technologies: Cryogeny vs membranes," *Separation and Purification Technology,* vol. 125, pp. 142-150, 2014.

[91] T. Burdyny and H. Struchtrup, "Hybrid membrane/cryogenic separation of oxygen from air for use in the oxy-fuel process," *Energy,* vol. 35, pp. 1884-1897, 2010.

[92] M. Aneke and M. Wang, "Potential for improving the energy efficiency of cryogenic air separation unit (ASU) using binary heat recovery cycles," *Applied Thermal Engineering,* vol. 81, pp. 223-231, 2015.

[93] R. Castillo, "Thermodynamic analysis of a hard coal oxyfuel power plant with high temperature three-end membrane for air separation," *Applied Energy,* vol. 88, pp. 1480-1493, 2011.

[94] J. Kotowicz and A. Balicki, "Enhancing the overall efficiency of a lignite-fired oxyfuel power plant with CFB boiler and membrane-based air separation unit," *Energy Conversion and Management,* vol. 80, pp. 20-31, 2014.

[95] T. L. Saleman, G. K. Li, T. E. Rufford, P. L. Stanwix, K. I. Chan, S. H. Huang, *et al.*, "Capture of low grade methane from nitrogen gas using dual-reflux pressure swing adsorption," *Chemical Engineering Journal,* vol. 281, pp. 739-748, 2015.

[96] W. Castle, "Air separation and liquefaction: recent developments and prospects for the beginning of the new millennium," *International Journal of Refrigeration,* vol. 25, pp. 158-172, 2002.

[97] C. A. Grande, "Advances in pressure swing adsorption for gas separation," *ISRN Chemical Engineering,* vol. 2012, 2012.

[98] Y. Wang and N. Lior, "Performance analysis of combined humidified gas turbine power generation and multi-effect thermal vapor compression desalination systems—Part 1: The desalination unit and its combination with a steam-injected gas turbine power system," *Desalination,* vol. 196, pp. 84-104, 2006.

[99] J. Cleeton, R. Kavanagh, and G. Parks, "Blade cooling optimisation in humid-air and steam-injected gas turbines," *Applied Thermal Engineering,* vol. 29, pp. 3274-3283, 2009.

[100] Y. Hui, Y. Wang, and S. Weng, "Experimental investigation of pressurized packing saturator for humid air turbine cycle," *Applied Thermal Engineering,* vol. 62, pp. 513-519, 2014.

[101] K. Göckeler, O. Krüger, and C. O. Paschereit, "Laminar Burning Velocities and Emissions of Hydrogen–Methane-Air–Steam Mixtures," *Journal of Engineering for Gas Turbines and Power,* vol. 137, p. 031503, 2015.

[102] Y. Hu, H. Li, and J. Yan, "Integration of evaporative gas turbine with oxy-fuel combustion for carbon dioxide capture," *International Journal of Green Energy,* vol. 7, pp. 615-631, 2010.

[103] M. Jonsson and J. Yan, "Humidified gas turbines—a review of proposed and implemented cycles," *Energy,* vol. 30, pp. 1013-1078, 2005.

[104] Y. Wang and N. Lior, "Performance analysis of combined humidified gas turbine power generation and multi-effect thermal vapor compression desalination systems," in *ASME 2005 International Mechanical Engineering Congress and Exposition*, 2005, pp. pp. 523-539.

[105] O. Olumayegun, M. Wang, and G. Kelsall, "Closed-cycle gas turbine for power generation: A state-of-the-art review," *Fuel,* vol. 180, pp. 694-717, 2016.

[106] R. Allam, S. Martin, B. Forrest, J. Fetvedt, X. Lu, D. Freed, *et al.*, "Demonstration of the Allam Cycle: an update on the development status of a high efficiency supercritical carbon dioxide power process employing full carbon capture," *Energy Procedia,* vol. 114, pp. 5948-5966, 2017.

[107] R. Allam, M. R. Palmer, G. W. Brown, J. Fetvedt, D. Freed, H. Nomoto, *et al.*, "High efficiency and low cost of electricity generation from fossil fuels while eliminating atmospheric emissions, including carbon dioxide," *Energy Procedia,* vol. 37, pp. 1135-1149, 2013.

[108] R. Allam, J. Fetvedt, B. Forrest, and D. Freed, "The Oxy-Fuel, Supercritical CO_2 Allam Cycle: New Cycle Developments to Produce Even Lower-Cost Electricity From Fossil Fuels Without Atmospheric Emissions," in *ASME Turbo Expo 2014: Turbine Technical Conference and Exposition*, 2014, pp. V03BT36A016-V03BT36A016.

[109] H. C. No, J. H. Kim, and H. M. Kim, "A review of helium gas turbine technology for high-temperature gas-cooled reactors," *Nuclear Engineering and Technology,* vol. 39, pp. 21-30, 2007.

[110] J. Wang and Y. Gu, "Parametric studies on different gas turbine cycles for a high temperature gas-cooled reactor," *Nuclear Engineering and Design,* vol. 235, pp. 1761-1772, 2005.

[111] C. F. McDonald, "Helium turbomachinery operating experience from gas turbine power plants and test facilities," *Applied Thermal Engineering,* vol. 44, pp. 108-142, 2012.

[112] C. M. Invernizzi, "Prospects of Mixtures as Working Fluids in Real-Gas Brayton Cycles," *Energies,* vol. 10, p. 1649, 1981.

[113] A. Al-Doboon, M. Gutesa, A. Valera-Medina, N. Syred, J.-H. Ng, and C. T. Chong, "CO 2-argon-steam oxy-fuel (CARSOXY) combustion for CCS inert gas atmospheres in gas turbines," *Applied Thermal Engineering,* vol. 122, pp. 350-358, 2017.

[114] P. D. Ronney, *Premixed-gas flames*: Academic Press, New York, 2001.

[115] K.-J. Nogenmyr, P. Petersson, X.-S. Bai, C. Fureby, R. Collin, A. Lantz, *et al.*, "Structure and stabilization mechanism of a stratified premixed low swirl flame," *Proceedings of the Combustion Institute,* vol. 33, pp. 1567-1574, 2011.

[116] S. McAllister, Jyh-Yuan and A. C. Fernandez-Pello, "Non-premixed Flames (Diffusion Flames)," in *Fundamentals of Combustion Processes.* , ed: Springer, New York, NY, 2011, pp. 139-154.

[117] Y. Nada, K. Matsumoto, and S. Noda, "Liftoff heights of turbulent non-premixed flames in co-flows diluted by CO2/N2," *Combustion and Flame,* vol. 161, pp. 2890-2903, 2014.

[118] X. Zhu, X. Xia, and P. Zhang, "Near-field flow stability of buoyant methane/air inverse diffusion flames," *Combustion and Flame,* vol. 191, pp. 66-75, 2018.

[119] T. Zhang, Q. Guo, X. Song, Z. Zhou, and G. Yu, "The chemiluminescence and structure properties of normal/inverse diffusion Flames," *Journal of Spectroscopy,* vol. 2013, 2012.

[120] F. Escudero, A. Fuentes, J.-L. Consalvi, F. Liu, and R. Demarco, "Unified behavior of soot production and radiative heat transfer in ethylene, propane and butane axisymmetric laminar diffusion flames at different oxygen indices," *Fuel,* vol. 183, pp. 668-679, 2016.

[121] Y. Jung, K. C. Oh, C. Bae, and H. D. Shin, "The effect of oxygen enrichment on incipient soot particles in inverse diffusion flames," *Fuel,* vol. 102, pp. 199-207, 2012.

[122] M. Kholghy, M. Saffaripour, C. Yip, and M. J. Thomson, "The evolution of soot morphology in a laminar coflow diffusion flame of a surrogate for Jet A-1," *Combustion and Flame,* vol. 160, pp. 2119-2130, 2013.

[123] P. D. Teini, D. M. Karwat, and A. Atreya, "The effect of CO2/H2O on the formation of soot particles in the homogeneous environment of a rapid compression facility," *Combustion and Flame,* vol. 159, pp. 1090-1099, 2012.

[124] H. Xu, F. Liu, S. Sun, Y. Zhao, S. Meng, and W. Tang, "Effects of H2O and CO2 diluted oxidizer on the structure and shape of laminar coflow syngas diffusion flames," *Combustion and Flame,* vol. 177, pp. 67-78, 2017.

[125] B. Kumfer, S. Skeen, and R. Axelbaum, "Soot inception limits in laminar diffusion flames with application to oxy–fuel combustion," *Combustion and Flame,* vol. 154, pp. 546-556, 2008.

[126] G. Krieger, A. Campos, M. Takehara, F. A. Da Cunha, and C. G. Veras, "Numerical simulation of oxy-fuel combustion for gas turbine applications," *Applied Thermal Engineering,* vol. 78, pp. 471-481, 2015.

[127] C. Eichler and T. Sattelmayer, "Premixed flame flashback in wall boundary layers studied by long-distance micro-PIV," *Experiments in fluids,* vol. 52, pp. 347-360, 2012.

[128] T. Sattelmayer, C. Mayer, and J. Sangl, "Interaction of flame flashback mechanisms in premixed hydrogen-air swirl flames," *Journal of Engineering for Gas Turbines and Power,* vol. 138, p. 011503, 2016.

[129] P. Basu, C. Kefa, and L. Jestin, *Boilers and burners: design and theory*: Springer Science & Business Media, 2012.

[130] N. Syred, "A review of oscillation mechanisms and the role of the precessing vortex core (PVC) in swirl combustion systems," *Progress in Energy and Combustion Science,* vol. 32, pp. 93-161, 2006.

[131] A. Valera-Medina, N. Syred, P. Kay, and A. Griffiths, "Central recirculation zone analysis in an unconfined tangential swirl burner with varying degrees of premixing," *Experiments in Fluids,* vol. 50, pp. 1611-1623, 2011.

[132] D. G. Lilley, "Swirl flows in combustion: a review," *AIAA journal,* vol. 15, pp. 1063-1078, 1977.

[133] N. Syred and J. Beer, "Combustion in swirling flows: a review," *Combustion and flame,* vol. 23, pp. 143-201, 1974.

[134] H. Gotoda, H. Nikimoto, T. Miyano, and S. Tachibana, "Dynamic properties of combustion instability in a lean premixed gas-turbine combustor," *Chaos: An Interdisciplinary Journal of Nonlinear Science,* vol. 21, p. 013124, 2011.

[135] Y. Huang and V. Yang, "Dynamics and stability of lean-premixed swirl-stabilized combustion," *Progress in energy and combustion science,* vol. 35, pp. 293-364, 2009.

[136] J. Janicka, A. Sadiki, M. Schäfer, and C. Heeger, *Flow and Combustion in Advanced Gas Turbine Combustors* vol. 102: Springer Science & Business Media, 2012.

[137] R. Giezendanner, O. Keck, P. Weigand, W. Meier, U. Meier, W. Stricker, *et al.*, "Periodic combustion instabilities in a swirl burner studied by phase-locked planar laser-induced fluorescence," *Combustion Science and technology,* vol. 175, pp. 721-741, 2003.

[138] T. C. Lieuwen and V. Yang, *Combustion instabilities in gas turbine engines: operational experience, fundamental mechanisms, and modeling*: American Institute of Aeronautics and Astronautics, 2005.

[139] K. S. Kedia and A. F. Ghoniem, "The blow-off mechanism of a bluff-body stabilized laminar premixed flame," *Combustion and Flame,* vol. 162, pp. 1304-1315, 2015.

[140] N. Syred, A. Giles, J. Lewis, M. Abdulsada, A. V. Medina, R. Marsh, *et al.*, "Effect of inlet and outlet configurations on blow-off and flashback with premixed combustion for methane and a high hydrogen content fuel in a generic swirl burner," *Applied Energy,* vol. 116, pp. 288-296, 2014.

[141] A. Giusti and E. Mastorakos, "Detailed chemistry LES/CMC simulation of a swirling ethanol spray flame approaching blow-off," *Proceedings of the Combustion Institute,* vol. 36, pp. 2625-2632, 2017.

[142] N. Peters and F. A. Williams, "Liftoff characteristics of turbulent jet diffusion flames," *AIAA Journal,* vol. 21, pp. 423-429, 1983.

[143] S. Ghosal and L. Vervisch, "Stability diagram for lift-off and blowout of a round jet laminar diffusion flame," *Combustion and Flame,* vol. 124, pp. 646-655, 2001.

[144] A. Palacios, D. Bradley, and M. Lawes, "Blow-off velocities of jet flames," 2016.

[145] Y. Wu, "Flame Lift-Off and Blow-Out Stability Limits and Their Application in Gas Burners," *Handbook of Combustion: Online,* pp. 121-140, 2010.

[146] N. Merlo, T. Boushaki, C. Chauveau, S. p. de Persis, L. Pillier, B. Sarh, *et al.*, "Experimental study of oxygen enrichment effects on turbulent non-premixed swirling flames," *Energy & Fuels,* vol. 27, pp. 6191-6197, 2013.

[147] H. Zaidaoui, T. Boushaki, J. Sautet, C. Chauveau, B. Sarh, and I. Gökalp, "Effects of CO2 Dilution and O2 Enrichment on Non-premixed Turbulent CH4-Air Flames in a Swirl Burner," *Combustion Science and Technology,* vol. 190, pp. 784-802, 2018.

[148] J. Oh and D. Noh, "Lifted flame behavior of a non-premixed oxy-methane jet in a lab-scale slot burner," *Fuel,* vol. 103, pp. 862-868, 2013.

[149] O. Singh, *Applied thermodynamics*: New Age International, 2003.

[150] C. Morley. (2005). *Gaseq: a chemical equilibrium program for Windows. Ver. 0.79.* Available: http://www.gaseq.co.uk/

[151] A. Valera-Medina, R. Marsh, J. Runyon, D. Pugh, P. Beasley, T. Hughes, *et al.*, "Ammonia–methane combustion in tangential swirl burners for gas turbine power generation," *Applied Energy,* vol. 185, pp. 1362-1371, 2017.

[152] U. Stopper, W. Meier, R. Sadanandan, M. Stöhr, M. Aigner, and G. Bulat, "Experimental study of industrial gas turbine flames including quantification of pressure influence on flow field, fuel/air premixing and flame shape," *Combustion and Flame,* vol. 160, pp. 2103-2118, 2013.

[153] P.-A. Glaude, B. Sirjean, R. Fournet, R. Bounaceur, M. Vierling, P. Montagne, *et al.*, "Combustion and oxidation kinetics of alternative gas turbines fuels," in *ASME Turbo Expo 2014: Turbine Technical Conference and Exposition*, 2014, pp. V03AT03A001-V03AT03A001.

[154] H. K. Kayadelen and Y. Ust, "Prediction of equilibrium products and thermodynamic properties in H2O injected combustion for CαHβOγNδ type fuels," *Fuel*, vol. 113, pp. 389-401, 2013.

[155] L. Chen, Z. Zhang, W. Gong, and Z. Liang, "Quantifying the effects of fuel compositions on GDI-derived particle emissions using the optimal mixture design of experiments," *Fuel*, vol. 154, pp. 252-260, 2015.

[156] R. Evans, W. Dawes, and Q. Zhang, "Application of design of experiment to a gas turbine cascade test cell," in *ASME Turbo Expo 2013: Turbine Technical Conference and Exposition*, 2013, pp. V06BT43A008-V06BT43A008.

[157] I. J. Esfahani and C. Yoo, "Feasibility study and performance assessment for the integration of a steam-injected gas turbine and thermal desalination system," *Desalination*, vol. 332, pp. 18-32, 2014.

[158] ReactionDesign:SanDiego, *ANSYS Chemkin Theory Manual 17.0 (15151)*, 2015.

[159] M. Li, Y. Tong, M. Thern, and J. Klingmann, "Investigation of methane oxy-fuel combustion in a swirl-stabilised gas turbine model combustor," *Energies*, vol. 10, p. 648, 2017.

[160] W. Qian, M. Zhu, and S. Li, "A Kinetics Study on the NOx Emissions of Axially Staged Combustion System for Gas Turbine Applications."

[161] V. Prakash, *Parametric Emission Prediction Model in Gas Turbines with Exhaust Gas Recirculation*, 2017.

[162] M. Chmielewski, S. Fulara, and M. Gieras, "Theoretical studies of variable geometry: hot section of the miniature jet engine," *Journal of KONES*, vol. 23, 2016.

[163] H. Li, A. ElKady, and A. Evulet, "Effect of exhaust gas recirculation on NOx formation in premixed combustion system," in *47th AIAA Aerospace Sciences Meeting Including The New Horizons Forum and Aerospace Exposition*, 2009, p. 226.

[164] L. Rosentsvit, Y. Levy, V. Erenburg, V. Sherbaum, V. Ovcharenko, B. Chudnovsky, *et al.*, "Extension of the combustion stability range in dry low NOx lean premixed gas turbine combustor using a fuel rich annular pilot burner," *Journal of Engineering for Gas Turbines and Power*, vol. 136, p. 051509, 2014.

[165] A. Akbari, V. McDonell, and S. Samuelsen, "Study of NOx from different natural gas and hydrogen fuel compositions in combustion applications," in *8th US National Combustion Meeting, Salt Lake City, Utah*, 2013.

[166] M. Evans, *MINITAB Manual*. United States of America W.H. Freeman and Company, 2009.

[167] L. Minitab. (2019). *Minitab® 18 Support*. Available: www.minitab.com

[168] L. Minitab, *Minitab® 17 ,Getting Started with Minitab 17*, 2016.

[169] M. G. Božo, A. Valera-Medina, N. Syred, and P. J. Bowen, "Fuel quality impact analysis for practical implementation of corn COB gasification gas in conventional gas turbine power plants," *Biomass and Bioenergy*, vol. 122, pp. 221-230, 2019.

[170] S. S. Aji, Y. S. Kim, K. Y. Ahn, and Y. D. Lee, "Life-Cycle Cost Minimization of Gas Turbine Power Cycles for Distributed Power Generation Using Sequential Quadratic Programming Method," *Energies*, vol. 11, p. 3511, 2018.

[171] AspenPlus. (2009). *Aspen Technology*. Available: https://www.aspentech.com/

[172] AspenPlus, *Building and Running a Process Model Version 10.*: Aspen Technology, Inc., 1981—1999.

[173] R. Canepa, M. Wang, C. Biliyok, and A. Satta, "Thermodynamic analysis of combined cycle gas turbine power plant with post-combustion CO2 capture and exhaust gas recirculation," *Proceedings of the Institution of Mechanical Engineers, Part E: Journal of Process Mechanical Engineering*, vol. 227, pp. 89-105, 2013.

[174] J.-M. Amann, M. Kanniche, and C. Bouallou, "Natural gas combined cycle power plant modified into an O2/CO2 cycle for CO2 capture," *Energy Conversion and Management*, vol. 50, pp. 510-521, 2009.

[175] A. A. JMing Pan, Mona Gharaie, Simon Perry, Nan Zhang, Igor Bulatov, Robin Smith, "Optimal Design Technologies for Integration of Combined Cycle Gas Turbine Power Plant with CO2 Capture," *Chemical Engineering Transactions*, vol. 39, pp. 1441-1446, 2014.

[176] J. Hong, G. Chaudhry, J. Brisson, R. Field, M. Gazzino, and A. F. Ghoniem, "Analysis of oxy-fuel combustion power cycle utilizing a pressurized coal combustor," *Energy*, vol. 34, pp. 1332-1340, 2009.

[177] A. M. Al Menhali, A. A. Al Marzooqi, A. R. S. Alameri, A. M. Al Ameri, and Z. E. Dadach, "Simulation of the Effects of Turbine Exhaust Recirculation on the Composition of Flue Gas for A CO^ sub 2^ Capture Unit," *Journal of Chemical Engineering & Process Technology*, vol. 5, p. 1, 2014.

[178] A. A. Ming Pan, Mona Gharaie, Simon Perry, Nan Zhang, Igor Bulatov, and Robin Smith, "Optimal Design Technologies for Integration of Combined Cycle Gas Turbine Power Plant with CO2 Capture," *CHEMICAL ENGINEERING TRANSACTIONS*, vol. 39, pp. 1441-1446, 2014.

[179] P. Kuchonthara, S. Bhattacharya, and A. Tsutsumi, "Combinations of solid oxide fuel cell and several enhanced gas turbine cycles," *Journal of Power Sources*, vol. 124, pp. 65-75, 2003.

[180] W. Cai, X. Li, F. Li, and L. Ma, "Numerical and experimental validation of a three-dimensional combustion diagnostic based on tomographic chemiluminescence," *Optics express*, vol. 21, pp. 7050-7064, 2013.

[181] V. Nori and J. Seitzman, "Evaluation of chemiluminescence as a combustion diagnostic under varying operating conditions," in *46th AIAA Aerospace Sciences Meeting and Exhibit*, 2008, p. 953.

[182] J. Ballester and T. García-Armingol, "Diagnostic techniques for the monitoring and control of practical flames," *Progress in Energy and Combustion Science*, vol. 36, pp. 375-411, 2010.

[183] Y. Jin, Y. Song, X. Qu, Z. Li, Y. Ji, and A. He, "Three-dimensional dynamic measurements of CH* and C2* concentrations in flame using simultaneous chemiluminescence tomography," *Optics express*, vol. 25, pp. 4640-4654, 2017.

[184] T. García-Armingol, Y. Hardalupas, A. Taylor, and J. Ballester, "Effect of local flame properties on chemiluminescence-based stoichiometry measurement," *Experimental Thermal and Fluid Science*, vol. 53, pp. 93-103, 2014.

[185] M. De Leo, A. Saveliev, L. A. Kennedy, and S. A. Zelepouga, "OH and CH luminescence in opposed flow methane oxy-flames," *Combustion and Flame*, vol. 149, pp. 435-447, 2007.

[186] T. Shimizu, F. A. Williams, and A. Frassoldati, "Concentrations of nitric oxide in laminar counterflow methane/air diffusion flames," *Journal of propulsion and power*, vol. 21, pp. 1019-1028, 2005.

[187] E. Dunlea, S. Herndon, D. Nelson, R. Volkamer, F. San Martini, P. Sheehy, *et al.*, "Evaluation of nitrogen dioxide chemiluminescence monitors in a polluted urban environment," *Atmospheric Chemistry and Physics*, vol. 7, pp. 2691-2704, 2007.

[188] R. J. Tidona, A. A. Nizami, and N. P. Cernansky, "Reducing interference effects in the chemiluminescent measurement of nitric oxides from combustion systems," *JAPCA*, vol. 38, pp. 806-811, 1988.

[189] PHOTRONLIMITED. (2006). *FASTCAM-APX RS Hardware Manual* Available: http://www.highspeedimaging.com/media/photron_manuals/FASTCAM-APX_RS_HW_Manual.pdf

[190] HAMAMATSUPHOTONISOURBUSINESS. (2019). *Copyright © Hamamatsu Photonics K.K. All Rights Reserved.* Available: https://www.hamamatsu.com/eu/en/product/type/C9546-03/index.html

[191] J. Runyon, "Gas turbine fuel flexibility: pressurized swirl flame stability, thermoacoustics, and emissions," Cardiff University, 2017.

[192] T. S. C. KGaA. (2018). *Instruction manual test350 M/XL*. Available: https://static-int.testo.com/media/4f/63/12fa44a894ea/testo-350-M-XL-Instruction-Manual.pdf

[193] İ. Çelikten, E. Mutlu, and H. Solmaz, "Variation of performance and emission characteristics of a diesel engine fueled with diesel, rapeseed oil and hazelnut oil methyl ester blends," *Renewable Energy*, vol. 48, pp. 122-126, 2012.

[194] A. B. Koc and M. Abdullah, "Performance and NOx emissions of a diesel engine fueled with biodiesel-diesel-water nanoemulsions," *Fuel Processing Technology*, vol. 109, pp. 70-77, 2013.

[195] A. O. Said and A. K. Gupta, "Oxygen Enriched Air Effects on Combustion, Emission, and Distributed Reaction," *Journal of Energy Resources Technology*, vol. 137, p. 042203, 2015.

[196] A. Ong'Iro, V. Ugursal, A. Al Taweel, and D. Blamire, "Simulation of combined cycle power plants using the ASPEN PLUS shell," *Heat Recovery Systems and CHP*, vol. 15, pp. 105-113, 1995.

[197] H. Yang, D. Kang, J. Ahn, and T. Kim, "Evaluation of design performance of the semi-closed oxy-fuel combustion combined cycle," *Journal of Engineering for Gas Turbines and Power*, vol. 134, p. 111702, 2012.

[198] N. Syred, M. V. Gutesha, A. Doboon, A. Valera-Medina, and P. J. Bowen, "CARSOXY (CO2-Argon-Steam-OxyFuel) Combustion in Gas Turbines for CCS Systems," in *55th AIAA Aerospace Sciences Meeting*, 2017, p. 1608.

[199] I. Glassman, R. A. Yetter, and N. G. Glumac, *Combustion*: Academic press, 2014.

[200] CTPLATONSAS. (2004). © *CT PLATON*. Available: http://www.ctplaton.com/uploads/pdf/En/deb_ng_lg.pdf

[201] D. P. G. Rollmann. *Calculation of correction factors for variable area flow meters at deviating working conditions.* Available: https://www.kt-flow.de/fileadmin/kirchnerundtochter/physikalische_grundlagen/korrekturfaktorenberechnung_en_2.3.pdf

[202] N. Merlo, T. Boushaki, C. Chauveau, S. De Persis, L. Pillier, B. Sarh, *et al.*, "Combustion characteristics of methane–oxygen enhanced air turbulent non-premixed swirling flames," *Experimental thermal and fluid science*, vol. 56, pp. 53-60, 2014.

APPENDIX 1

Specific heats

The specific heat of a substance is defined as the amount of heat required for changing the temperature of the unit mass of a substance by one degree. This unit change in temperature may occur under a condition where pressure is maintained constant, which is called specific heat at constant pressure, denoted as (C_p). In contrast, specific heat at a constant volume is a heat value with heat interaction under constant volume conditions, denoted as (C_v).

Mathematically, the heat interaction causing ΔT temperature change in m mass of a substance can be given as:

For isochoric conditions (constant volume process)

$$Q_v = m.C_v.\Delta T \equiv C_v = \frac{Q_v}{m.\Delta T} \qquad \text{Eq. (1)}$$

For isobaric conditions (constant pressure process)

$$Q_v = m.C_p.\Delta T \equiv C_p = \frac{Q_p}{m.\Delta T} \qquad \text{Eq. (2)}$$

To obtain specific heat values, substituting $m = 1, \quad \Delta T = 1$

$C_v = Q_v$ and $C_p = Q_p$

The specific heat at constant volume can also be given as the partial derivative of internal energy with respect to temperature at constant volume.

Thus,

$$C_v = \left(\frac{\partial u}{\partial T}\right)_v \equiv C_v = \left(\frac{du}{dT}\right)_v \equiv C_v.dT = du \quad \text{Eq. (3)}$$

In addition, from the first law of thermodynamics, on a unit mass basis

$$dq = du + pdv \quad \text{Eq. (4)}$$

At constant volume, $dv = 0$

$$dq = du \text{ or } dq = C_v.dT = du \quad \text{Eq. (5)}$$

$$C_v = \frac{dq}{dT} \quad \text{Eq. (6)}$$

Specific heat at constant pressure can be given as a partial derivative of enthalpy with respect to temperature at constant pressure.

$$C_p = \left(\frac{\partial h}{\partial T}\right)_p \equiv C_p = \left(\frac{dh}{dT}\right)_p \quad \text{Eq. (7)}$$

$$C_p.dT = dh \quad \text{Eq. (8)}$$

From the definition of enthalpy, on a unit mass basis

$$h = u + pv \equiv dh = du + vdp + pdv \quad \text{Eq. (9)}$$

At constant pressure $dp = 0$

$$dh = du + pdv \quad \text{Eq. (10)}$$

Substitution of the first law of thermodynamics

$$dq = du + pdv \equiv dq = dh$$

$$dh = dq \equiv dq = C_p.dT = dh \qquad \text{Eq. (11)}$$

$$C_p = \frac{dq}{dT} \qquad \text{Eq. (12)}$$

To establish the relationship between C_v and C_p

From the enthalpy definition, on a unit mass basis

$$h = u + pv \qquad \text{Eq. (13)}$$

For ideal gas $pv = RT$ Eq. (14)

R is a gas constant for a specific gas

$$h = u + RT$$

Taking a derivative

$$dh = du + RdT \qquad \text{Eq. (15)}$$

$$dh = C_p.dT; \qquad du = C_v.dT$$

Substituting dh and du

$$C_p.dT = C_v.dT + R.dT \qquad \text{Eq. (16)}$$

$$C_p = C_v + R \quad \equiv \quad C_p - C_v = R \qquad \text{Eq. (17)}$$

$$C_v\left(\frac{C_p}{C_v} - 1\right) = R \quad \equiv C_v(\gamma - 1) = R$$

$$C_v = \frac{R}{(\gamma - 1)} \qquad \text{Eq. (18)}$$

Differences of specific heats at constant pressure and volume is equal to the gas constant for an ideal gas.

The ratio of specific heats at constant pressure and constant volume can be given as

$$\gamma = \frac{C_p}{C_v} \qquad \text{Eq. (19)}$$

Therefore, combining the above two relations of C_p and C_v gives

$$C_p = \gamma . C_v$$

$$C_p = \frac{\gamma . R}{(\gamma - 1)}$$

$$\frac{C_p}{R} = \frac{\gamma}{(\gamma - 1)} \equiv \frac{R}{C_p} = \frac{(\gamma - 1)}{\gamma} \qquad \text{Eq. (20)}$$

Modelling Gas turbine power plant

For isentropic processes 1-2 and 2-3, discussed in Chapter One (Section 1.6)

$$T_2 = T_1 \left(\frac{P_2}{P_1}\right)^{\frac{(\gamma-1)}{\gamma}} , T_4 = T_3 \left(\frac{P_4}{P_3}\right)^{\frac{(\gamma-1)}{\gamma}} \equiv T_3 \left(\frac{P_1}{P_2}\right)^{\frac{(\gamma-1)}{\gamma}} \qquad \text{Eq. (21)}$$

$$\frac{T_2}{T_1} = \left(\frac{P_2}{P_1}\right)^{\frac{(\gamma-1)}{\gamma}} \; and \; \frac{T_3}{T_4} = \left(\frac{P_2}{P_1}\right)^{\frac{(\gamma-1)}{\gamma}}$$

Whereas

$\frac{P_2}{P_1}$ is a compressor ratio, let the pressure ratio be $\frac{P_2}{P_1} = r$.

$$\frac{T_2}{T_1} = (r)^{\frac{(\gamma-1)}{\gamma}} \equiv \qquad \frac{T_3}{T_4} = (r)^{\frac{(\gamma-1)}{\gamma}}$$

Specific work output for turbine

Both compressor and turbine work can be expressed as the following equations

$$W_C = m_1.(h_2 - h_1) \quad \text{Eq. (22)}$$

$$W_T = m_3.(h_3 - h_4) \quad \text{Eq. (23)}$$

For air standard analysis, $m_1 = m_3$, whereas in an actual cycle $m_1 = 1$

$$w_T = \{(h_3 - h_4)\}$$

$$w_T = c_{p_{3-4}}\{(T_3 - T_4)\} \quad \text{Eq. (24)}$$

$$w_T = c_{p_{3-4}}.T_3\left\{\left(1 - \frac{T_4}{T_3}\right)\right\} = c_{p_{3-4}}.T_3\left\{1 - \left(\frac{P_1}{P_2}\right)^{\frac{(\gamma-1)}{\gamma}}\right\}$$

$$w_T = c_{p_{3-4}}.T_3\left\{1 - \left(\frac{P_1}{P_2}\right)^{\left(\frac{R}{C_p}\right)}\right\}$$

$$w_T = c_{p\ gas-air(3-4)}.T_3\left(1 - \left(\frac{P_1}{P_2}\right)^{\eta_{pT}\cdot\frac{Rgas}{Cp_{gas-air(3-4)}}}\right) \quad \text{Eq. (25)}$$

The expansion of the working fluid in the gas turbine is considered an expansion of the combustion gases from the turbine inlet to its outlet and is also treated as an adiabatic process. The expansion of specific work of combustion products relative to the compressor inlet air mass flow is calculated by the equation:

$$L_{iT} = \bar{c}_{p_g}{}^{(3-4)} \cdot T_{Tin} \cdot \left(1 - \Pi_T{}^{\eta_p \cdot \frac{R_g}{\bar{c}_{p_g}{}^{(3-4)}}}\right) \quad \text{Eq. (26)}$$

or

$$w_T = c_{p_{3-4}} . T_1 \left\{ \left(\frac{T_3}{T_1} - \frac{T_4}{T_1} \right) \right\}$$ Eq. (27)

$$w_T = c_{p_{3-4}} . T_1 \left\{ \left(\frac{T_3}{T_1} \right) \left(1 - \frac{T_4 . T_1}{T_3 . T_1} \right) \right\}$$

$$w_T = c_{p_{3-4}} . T_1 \left\{ \left(\frac{T_3}{T_1} \right) \left(1 - \frac{T_4}{T_3} \right) \right\}$$

$$\frac{T_3}{T_4} = (r)^{\frac{(\gamma-1)}{\gamma}} \equiv \frac{T_4}{T_3} = \frac{1}{(r)^{\frac{(\gamma-1)}{\gamma}}}$$

$$w_T = c_{p_{3-4}} . T_1 \left\{ t. \left(1 - \frac{1}{(r)^{\frac{(\gamma-1)}{\gamma}}} \right) \right\}$$

$$T_3 = T_4 . (r)^{\frac{(\gamma-1)}{\gamma}}$$ Eq. (28)

Specific work output for compressor

$$w_c = \{(h_2 - h_1)\}$$ Eq. (29)

$$w_c = c_{p_{1-2}} \{(T_2 - T_1)\}$$

$$w_c = c_{p_{1-2}} . T_1 \left\{ \left(\frac{T_2}{T_1} - 1 \right) \right\}$$

$$\frac{T_2}{T_1} = (r)^{\frac{(\gamma-1)}{\gamma}} \equiv T_2 = T_1 . (r)^{\frac{(\gamma-1)}{\gamma}}$$

$$w_c = c_{p_{1-2}} . T_1 \left\{ \left((r)^{\frac{(\gamma-1)}{\gamma}} - 1 \right) \right\}$$

$$L_c = c_{p\ air\ (1-2)} . T_1 \left((r)^{\frac{1}{\eta pc} . \frac{R_{air}}{Cp_{air(1-2)}}} - 1 \right)$$ Eq. (30)

APPENDIX 2

(Generated blends)

Best Blends Matrix (1-10)

Case	Ar [Mole fraction]	H_2O [Mole fraction]	CO_2 [Mole fraction]	T(K)		C_p [J/mole. K]		Gamma [C_p/C_v]		H_2O [Mole fraction]		CO_2 [Mole fraction]	
Air				2596.4		41.766		1.249		0.177607		0.076828	
1	0.18	0.27	0.26	- -	-2.05324	+++	2.81549	- - -	-3.03226	+++	3.255084	+++	2.580272
2	0.19	0.27	0.24	- -	-1.91581	+++	2.560364	- - -	-2.83871	+++	3.246857	++	2.395942
3	0.21	0.27	0.22	- -	-1.77474	++	2.303721	- - -	-2.58065	+++	3.23811	++	2.21203
4	0.24	0.27	0.19	- -	-1.55722	++	1.921033	- -	-2.19355	+++	3.223901	++	1.937109
5	0.26	0.27	0.18	-	-1.40705	++	1.664389	- -	-1.93548	+++	3.213615	++	1.754585
6	0.27	0.27	0.17	-	-1.3306	++	1.536826	- -	-1.80645	+++	3.208202	++	1.663588
7	0.22	0.25	0.23	- -	-1.75381	++	2.221716	- - -	-2.51613	+++	3.025049	++	2.294857
8	0.14	0.27	0.29	- -	-2.31991	+++	3.327259	- - -	-3.48387	+++	3.270146	++	2.949944
9	0.10	0.27	0.33	- - -	-2.57565	++++	3.837509	- - - -	-3.87097	+++	3.283582	+++	3.320628
10	0.21	0.21	0.34	- - - -	-4	+++	2.501139	- - -	-2.77419	++	2.239361	+++	3.28539

Matrix (11-20)

Case	Ar [Mole fraction]	H_2O [Mole fraction]	CO_2 [Mole fraction]	T(K)		C_p [J/mole. K]		Gamma [C_p/C_v]		H_2O [Mole fraction]		CO_2 [Mole fraction]	
Air				2596.4		41.766		1.249		0.177607		0.076828	
11	0.13	0.30	0.21	-	-0.59067	+++	3.287775	- - -	-3.41935	++++	3.979126	++	2.184792
12	0.14	0.29	0.23	-	-0.90557	+++	3.143508	- - -	-3.35484	++++	3.75651	++	2.290166
13	0.17	0.27	0.23	-	-1.28328	+++	2.801822	- - -	-3.03226	+++	3.443409	++	2.333058
14	0.18	0.26	0.24	- -	-1.57634	+++	2.683371	- - -	-2.90323	+++	3.255143	++	2.422687
15	0.20	0.25	0.25	- -	-1.8603	+++	2.569476	- - -	-2.83871	+++	3.078183	+++	2.505535
16	0.24	0.24	0.24	- -	-2.0678	++	2.044039	- -	-2.32258	+++	2.821391	++	2.353365
17	0.23	0.23	0.26	- -	-2.46826	++	2.192863	- -	-2.45161	+++	2.676441	+++	2.601098
18	0.28	0.25	0.17	-	-1.34699	+	1.372817	- -	-1.67742	+++	2.95298	++	1.725813
19	0.21	0.26	0.22	-	-1.23322	++	2.353834	- - -	-2.64516	+++	3.220837	++	2.177311
20	0.23	0.24	0.22	-	-1.49078	++	2.031891	- -	-2.32258	+++	2.99454	++	2.152574

Matrix (21-30)

Case	Ar [Mole fraction]	H_2O [Mole fraction]	CO_2 [Mole fraction]	T(K)		C_p [J/mole. K]		Gamma		H_2O [Mole fraction]		CO_2 [Mole fraction]	
Air				2596.4		41.766		1.249		0.177607		0.076828	
21	0.14	0.26	0.29	- -	-2.14334	+++	3.292331	- - -	-3.41935	+++	3.250567	+++	2.913511
22	0.15	0.24	0.31	- - -	-2.52742	+++	3.208808	- - -	-3.35484	+++	2.931539	+++	3.122993
23	0.17	0.24	0.29	- -	-2.22435	+++	2.918755	- - -	-3.16129	+++	2.900713	+++	2.906911
24	0.18	0.25	0.28	- -	-2.41001	+++	2.844343	- - -	-3.09677	+++	2.984799	+++	2.827542
25	0.21	0.23	0.27	- -	-2.15882	++	2.485953	- - -	-2.77419	+++	2.809372	+++	2.667945
26	0.34	0.23	0.15	-	-1.32787	+	0.646925	-	-0.83871	+++	2.635406	+	1.456478
27	0.30	0.24	0.16	-	-1.10489	+	1.090357	-	-1.35484	+++	2.8762	++	1.558469
28	0.24	0.21	0.30	- - -	-3.43572	++	2.077449	- -	-2.3871	++	2.297844	+++	2.891454
29	0.21	0.22	0.30	- - -	-2.71399	++	2.484434	- - -	-2.77419	+++	2.549628	+++	2.911618
30	0.21	0.23	0.28	- -	-2.39181	++	2.46773	- - -	-2.70968	+++	2.69463	+++	2.76361

Matrix (31-40)

Case	Ar [Mole fraction]	H_2O [Mole fraction]	CO_2 [Mole fraction]	T(K)		C_p [J/mole. K]		Gamma [C_p/C_v]		H_2O [Mole fraction]		CO_2 [Mole fraction]	
Air				2596.4		41.766		1.249		0.177607		0.076828	
31	0.25	0.22	0.25	- -	-2.18339	++	1.92407	- -	-2.19355	+++	2.54375	++	2.471438
32	0.24	0.22	0.24	- -	-1.90853	++	2.009112	- -	-2.32258	+++	2.692575	++	2.393743
33	0.29	0.23	0.18	-	-1.17497	+	1.319666	- -	-1.6129	+++	2.820453	++	1.754949
34	0.26	0.23	0.21	-	-1.40523	++	1.708428	- -	-2	+++	2.836087	++	2.031753
35	0.20	0.24	0.26	- -	-1.69829	+++	2.540623	- - -	-2.77419	+++	2.94652	+++	2.549847
36	0.12	0.23	0.36	- - -	-2.63026	++++	3.703872	- - - -	-3.80645	+++	2.815167	++++	3.546977
37	0.19	0.23	0.29	- -	-2.21433	+++	2.724374	- - -	-2.96774	+++	2.751423	+++	2.873023
38	0.20	0.23	0.26	- -	-1.80387	+++	2.578588	- - -	-2.83871	+++	2.906613	+++	2.61682
39	0.22	0.26	0.28	- - -	-2.34812	++	2.369021	- - -	-2.64516	+++	2.591591	+++	2.759667
40	0.23	0.22	0.27	- -	-2.31627	++	2.164009	- -	-2.45161	+++	2.550177	+++	2.645379

Matrix (41-50)

Case	Ar [Mole fraction]	H_2O [Mole fraction]	CO_2 [Mole fraction]	T(K)		C_p [J/mole. K]		Gamma [C_p/C_v]		H_2O [Mole fraction]		CO_2 [Mole fraction]	
Air				2596.4		41.766		1.249		0.177607		0.076828	
41	0.16	0.27	0.20	0	-0.05097	+++	2.89142	- - -	-3.09677	++++	3.670529	++	2.038512
42	0.17	0.25	0.23	-	-0.62708	+++	2.856492	- - -	-3.09677	+++	3.361153	++	2.318495
43	0.26	0.21	0.23	- -	-1.60364	++	1.716021	- -	-2	+++	2.550935	++	2.251773
44	0.20	0.22	0.26	- -	-1.53447	+++	2.508732	- - -	-2.77419	+++	2.810008	+++	2.594824
45	0.20	0.22	0.27	- -	-1.74835	+++	2.587699	- - -	-2.83871	+++	2.732077	+++	2.729836
46	0.13	0.24	0.31	- -	-1.86212	++++	3.501898	- - - -	-3.6129	+++	3.037971	+++	3.152231
47	0.17	0.22	0.31	- -	-2.26894	+++	2.96735	- - -	-3.16129	+++	2.692258	+++	3.082048
48	0.15	0.21	0.34	- - -	-2.68669	+++	3.307517	- - -	-3.48387	+++	2.585984	+++	3.438696
49	0.22	0.18	0.18	- -	-1.57816	++	1.693242	- -	-2	+++	2.654088	++	2.165362
50	0.09	0.24	0.34	- -	-1.92856	++++	4	- - - -	-4	+++	3.142855	+++	3.424013

Matrix (51-60)

Case	Ar [Mole fraction]	H_2O [Mole fraction]	CO_2 [Mole fraction]	T(K)		C_p [J/mole. K]		Gamma [C_p/C_v]		H_2O [Mole fraction]		CO_2 [Mole fraction]	
Air				2596.4		41.766		1.249		0.177607		0.076828	
51	0.11	0.21	0.14	+	0.626915	+++	2.864085	- - -	-3.09677	++++	3.847689	++	1.754428
52	0.16	0.26	0.19	0	0.33081	+++	2.735004	- - -	-2.96774	++++	3.615124	++	1.89339
53	0.13	0.27	0.26	- -	-1.58544	+++	3.231587	- - -	-3.41935	+++	2.776027	+++	3.103148
54	0.16	0.20	0.33	- -	-2.06962	+++	3.166287	- - -	-3.35484	+++	2.532155	+++	3.2927
55	0.20	0.22	0.26	-	-1.07031	+++	2.580106	- - -	-2.83871	+++	2.837738	+++	2.554732
56	0.19	0.19	0.34	- - -	-2.59477	+++	2.917236	- - -	-3.16129	++	2.235379	+++	3.393298
57	0.19	0.21	0.27	-	-1.29511	+++	2.666667	- - -	-2.90323	+++	2.756897	+++	2.69916
58	0.25	0.23	0.19	0	-0.26576	++	1.79347	- -	-2.06452	+++	2.974111	++	1.827968
59	0.26	0.20	0.227	-	-1.14039	++	1.743356	- -	-2.06452	+++	2.563387	++	2.197277
60	0.26	0.20	0.22	-	-1.29238	++	2.013667	- - -	-2.32258	+++	2.573551	++	2.390243

Matrix (61-70)

Case	Ar [Mole fraction]	H_2O [Mole fraction]	CO_2 [Mole fraction]	T(K)		C_p [J/mole. K]		Gamma [C_p/C_v]		H_2O [Mole fraction]		CO_2 [Mole fraction]	
Air				2596.4		41.766		1.249		0.177607		0.076828	
61	0.11	0.19	0.38	- -	-2.11149	++++	3.905847	- - - -	-3.93548	+++	2.486279	++++	3.822135
62	0.14	0.20	0.31	-	-1.12765	+++	3.347001	- - -	-3.48387	+++	2.804524	+++	3.089298
63	0.15	0.19	0.33	- -	-1.63458	+++	3.281701	- - -	-3.41935	+++	2.549257	+++	3.293957
64	0.17	0.19	0.31	-	-1.49261	+++	2.999241	- - -	-3.22581	+++	2.540542	+++	3.091121
65	0.19	0.19	0.29	-	-1.3479	+++	2.716781	- - -	-2.96774	+++	2.531306	+++	2.888689
66	0.20	0.18	0.30	- -	-1.63549	+++	2.604404	- - -	-2.83871	++	2.373822	+++	2.961217
67	0.21	0.18	0.32	- -	-2.11786	+++	2.57555	- - -	-2.83871	++	2.158348	+++	3.151305
68	0.21	0.16	0.36	- - -	-2.94972	+++	2.67426	- - -	-2.90323	++	1.839785	++++	3.535572
69	0.25	0.18	0.27	- -	-1.63458	++	1.975702	- -	-2.25806	++	2.210936	++	2.652608
70	0.26	0.17	0.26	- -	-1.70557	++	1.807137	- -	-2.12903	++	2.137613	+++	2.598426

Matrix (71-80)

Case	Ar [Mole fraction]	H_2O [Mole fraction]	CO_2 [Mole fraction]	T(K)		C_p [J/mole. K]		Gamma [C_p/C_v]		H_2O [Mole fraction]		CO_2 [Mole fraction]	
Air				2596.4		41.766		1.249		0.177607		0.076828	
71	0.13	0.19	0.32	-	-0.881	++++	3.550494	- - - -	-3.67742	+++	2.745025	+++	3.220676
72	0.14	0.18	0.36	- -	-1.61274	++++	3.548975	- - - -	-3.67742	++	2.406484	++++	3.561458
73	0.15	0.17	0.36	- -	-1.89033	+++	3.403189	- - - -	-3.54839	++	2.248403	++++	3.611217
74	0.18	0.16	0.36	- -	-2.22708	+++	3.069096	- - -	-3.29032	++	2.026775	++++	3.582773
75	0.20	0.17	0.32	- -	-1.68464	+++	2.652999	- - -	-2.90323	++	2.155321	+++	3.14499
76	0.23	0.17	0.27	- -	-1.10216	++	2.198937	- - -	-2.51613	++	2.286473	+++	2.67387
77	0.27	0.14	0.27	-	-1.3752	++	1.712984	- -	-2	++	1.842778	+++	2.68585
78	0.18	0.16	0.34	-	-1.37793	+++	3.020501	- - -	-3.22581	++	2.158416	+++	3.340668
79	0.24	0.19	0.19	+	0.613624	++	1.854214	- -	-2.12903	+++	2.763722	++	1.834647
80	0.12	0.22	0.25	0	0.351486	+++	3.333333	- - -	-3.48387	+++	3.326451	++	2.458931

Matrix (81-90)

Case	Ar [Mole fraction]	H_2O [Mole fraction]	CO_2 [Mole fraction]	T(K)		C_p		Gamma [C_p/C_v]		H_2O [Mole fraction]		CO_2 [Mole fraction]	
Air				2596.4		41.766		1.249		0.177607		0.076828	
81	0.10	0.10	0.10	++++	4	++	2.180714	- -	-2.45161	+++	2.926054	+	0.996985
82	0.08	0.08	0.26	++	2.334133	+++	3.230068	- - -	-3.41935	+++	2.521466	++	2.370551
83	0.07	0.07	0.37	+	1.046336	++++	3.981777	- - - -	-4	++	2.07279	++++	3.511802
84	0.10	0.06	0.41	0	0.178697	++++	3.937737	- - - -	-3.93548	++	1.642943	++++	3.999997
85	0.19	0.08	0.20	++	2.472217	++	1.887623	- -	-2.19355	++	2.197966	++	1.751629
86	0.16	0.07	0.33	+	0.905298	+++	2.90205	- - -	-3.09677	++	1.755522	+++	3.084654
87	0.22	0.06	0.32	0	0.470371	++	2.305239	- - -	-2.58065	+	1.429529	+++	3.029725
88	0.23	0.05	0.34	0	-0.0182	++	2.343204	- - -	-2.64516	+	1.234159	+++	3.291281
89	0.24	0.06	0.38	-	-1.19408	++	2.405467	- - -	-2.70968	+	0.982471	++++	3.686186
90	0.14	0.11	0.28	+	1.190327	+++	3.009871	- - -	-3.22581	++	2.348961	+++	2.6864

Matrix (91-100)

Case	Ar [Mole fraction]	H_2O [Mole fraction]	CO_2 [Mole fraction]	T(K)		C_p [J/mole. K]		Gamma [C_p/C_v]		H_2O [Mole fraction]		CO_2 [Mole fraction]	
Air				2596.4		41.766		1.249		0.177607		0.076828	
91	0.02	0.21	0.10	++++	3.568027	+++	3.318147	- - -	-3.48387	++++	4.000016	+	1.090621
92	0.10	0.17	0.17	++	2.507661	+++	2.908125	- - -	-3.09677	+++	3.305704	++	1.628619
93	0.14	0.14	0.27	+	1.016061	+++	3.088838	- - -	-3.29032	+++	2.563212	+++	2.640512
94	0.20	0.11	0.31	00	0.005907	+++	2.654518	- - -	-2.90323	++	1.934308	+++	3.023524
95	0.16	0.12	0.33	00	0.002954	+++	3.061503	- - -	-3.29032	++	2.029877	+++	3.222132
96	0.19	0.12	0.31	0	0.141776	+++	2.710706	- - -	-2.96774	++	2.014654	+++	2.976287
97	0.19	0.13	0.32	-	-0.58157	+++	2.76082	- - -	-3.03226	++	1.967385	+++	3.170401
98	0.20	0.09	0.39	--	-1.59636	+++	2.970387	- - -	-3.16129	+	1.398914	++++	3.842573
99	0.16	0.11	0.35	0	-0.243	+++	3.167806	- - -	-3.35484	++	1.95505	+++	3.38488
100	0.16	0.13	0.19	++	2.246262	++	2.364465	- - -	-2.64516	+++	2.690654	++	1.780402

Matrix (101-110)

se	Ar [Mole fraction]	H_2O [Mole fraction]	CO_2 [Mole fraction]	T(K)		C_p [J/mole. K]		Gamma [C_p/C_v]		H_2O [Mole fraction]		CO_2 [Mole fraction]	
Air				2596.4		41.766		1.249		0.177607		0.076828	
101	0.19	0.13	0.09	+++	3.489754	++	1.573273	- -	-1.87097	+++	2.8236	+	0.891962
102	0.10	0.14	0.10	++++	3.740078	++	2.359909	- - -	-2.64516	+++	3.216595	+	0.99825
103	0.19	0.12	0.19	++	2.263984	++	2.024298	- -	-2.32258	++	2.444714	++	1.732705
104	0.18	0.10	0.24	++	1.709433	++	2.379651	- - -	-2.64516	++	2.288573	++	2.199236
105	0.22	0.10	0.22	++	1.552151	++	1.870919	- -	-2.19355	++	2.073485	++	2.072411
106	0.25	0.11	0.13	+++	2.700388	+	1.110099	-	-1.35484	++	2.343878	+	1.151
107	0.18	0.08	0.36	0	-0.28942	+++	2.965831	- - -	-3.16129	++	1.516764	+++	3.552603
108	0.29	0.10	0.14	++	2.220417	+	0.856492	-	-1.09677	++	2.06675	+	1.303047
109	0.24	0.08	0.29	0	0.45708	++	2.025816	- -	-2.32258	++	1.618589	+++	2.731086
110	0.2	0.08	0.40	-	-1.43254	+++	2.938497	- - -	-3.16129	+	1.22721	++++	3.910814

Matrix (110-120)

Case	Ar [Mole fraction]	H_2O [Mole fraction]	CO_2 [Mole fraction]	T(K)		C_p [J/mole. K]		Gamma [C_p/C_v]		H_2O [Mole fraction]		CO_2 [Mole fraction]	
Air				2596.4		41.766		1.249		0.177607		0.076828	
111	0.03	0.20	0.20	++	2.180543	++++	3.840547	- - - -	-3.87097	++++	3.758031	++	1.985563
112	0.09	0.18	0.24	+	1.479786	+++	3.470008	- - - -	-3.6129	+++	3.222867	++	2.317865
113	0.17	0.17	0.17	++	1.768507	++	2.317388	- - -	-2.58065	+++	3.010375	++	1.679261
114	0.15	0.15	0.30	0	0.33081	+++	3.138952	- - -	-3.35484	++	2.478792	+++	2.898812
115	0.19	0.16	0.21	+	1.17482	++	2.369021	- - -	-2.64516	+++	2.71311	++	2.056267
116	0.17	0.13	0.34	-	-0.73811	+++	3.078208	- - -	-3.29032	++	1.978642	+++	3.396197
117	0.21	0.14	0.26	0	0.341148	++	2.306758	- - -	-2.58065	++	2.261862	+++	2.510626
118	0.22	0.13	0.30	0	-0.42048	++	2.441913	- - -	-2.70968	++	1.955427	+++	2.945307
119	0.26	0.11	0.32	- -	-1.51354	++	2.030372	- -	-2.32258	++	1.449847	+++	3.173996
120	0.26	0.10	0.37	- - -	-2.65392	++	2.118451	- -	-2.3871	+	1.079477	++++	3.623613

APPENDIX 3

(MATLAB CODE)

```
sum=0;

for x=1:100
    number=num2str(x);
    sort_file='.png';
    figure=[number,sort_file];
    picture1=imread(figure);
    support1=im2double(picture1);
    sum(x)=0;

    i=0; j=0;
        for i=20:1024
            for j=20:1024
                sum(x)=sum(x)+support1(i,j);
            end
        end
    sum(x)
    picture1=0;
    support1=0;
end
```

APPENDIX 4

(Experimental work)

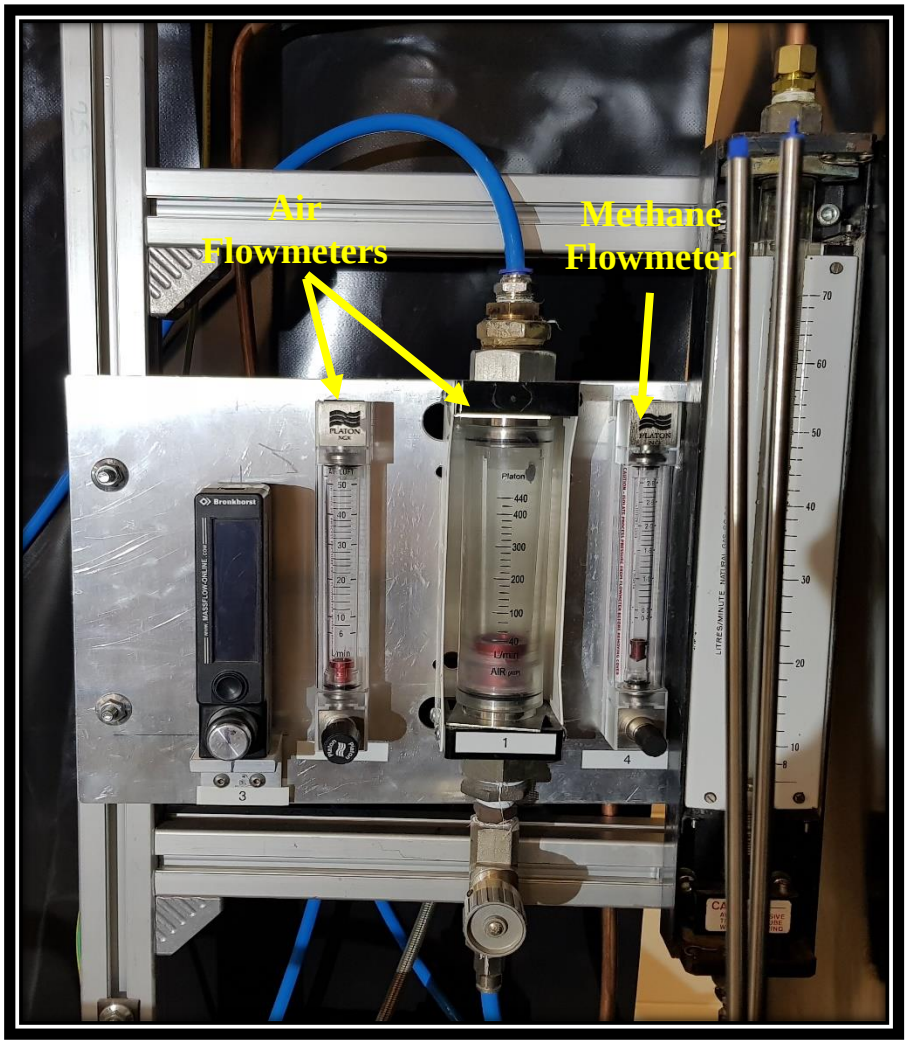

Figure 1. Air and methane flowmeters installed in 20-kW generic burner

Table 0. Fuel/air composition cases, Fuel/ proposed blend composition cases (Volumetric unit)

S/N	Air investigation (Cases)		Proposed blend investigation (Cases)	
	Air (l/min)	Fuel (l/min)	Proposed blend (l/min)	Fuel (l/min)
1	0	1	0	1
2	40	1	34.8	1
3	60	1	52.2	1
4	66	1	57.5	1
5	80	1	69.7	1
6	100	1	87.1	1
7	120	1	104.5	1
8	-	-	121.99	1
9	-	-	139.4	1

Table 0. Heat release oscillations for air

Case 1			Air = 0.813g/sec				Power = 0.55 kW			
S/N	1	2	3	4	5	6	7	8	9	10
Heat (Q')	10146.7	9991.6	10202.8	10278.4	10370.4	10192.7	10506.03	11015.6	11019.2	11014.3
Mean Heat value (Q)	10473.8	10473.81	10473.81	10473.81	10473.81	10473.81	10473.81	10473.81	10473.81	10473.81
Heat ratio [Q'/Q]	0.9687	0.9539	0.9741	0.9813	0.9901	0.9731	1.003	1.051	1.052	1.051
Time	0.0333	0.0666	0.1	0.1333	0.1666	0.2	0.2333	0.2666	0.3	0.3333
Case 2			Air = 1.22 g/sec				Power = 0.55 kW			
S/N	1	2	3	4	5	6	7	8	9	10
Heat (Q')	11008.7	11230.8	11373.8	11496	11410.3	11164	11390.8	11717.9	11630.5	11211.2
Mean Heat value (Q)	11363.45	11363.45	11363.45	11363.45	11363.45	11363.45	11363.45	11363.45	11363.45	11363.45
Heat ratio [Q'/Q]	0.968785	0.988329	1.00	1.017	1.004	0.98245	1.002	1.031	1.023	0.9866

Time	0.0333	0.0666	0.1	0.1333	0.1666	0.2	0.2333	0.2666	0.3	0.3333
Case 3			Air = 1.342 g/sec				Power = 0.55 kW			
S/N	1	2	3	4	5	6	7	8	9	10
Heat (Q')	7533.97	7592.9	7610.8	7779.5	7894.0	8316.8	8697.3	8612.3	8604	8369.6
Mean Heat value (Q)	8101.152	8101.152	8101.152	8101.152	8101.152	8101.152	8101.152	8101.152	8101.152	8101.152
Heat ratio [Q/Q]	0.9299	0.9372	0.9394	0.9394	0.9744	1.026	1.073	1.063	1.062	1.033
Time	0.0333	0.0666	0.1	0.1333	0.1666	0.2	0.2333	0.2666	0.3	0.3333
Case 4			Air = 1.626 g/sec				Power = 0.55 kW			
S/N	1	2	3	4	5	6	7	8	9	10
Heat (Q')	7918.1	7549.2	7533.9	7592.9	7610.8	7779.5	7894	8316.8	8697.3	8612.3
Mean Heat value (Q))	7950.534	7950.534	7950.534	7950.534	7950.534	7950.534	7950.534	7950.534	7950.534	7950.534
Heat ratio [Q'/Q]	0.9959	0.9495	0.9476	0.9550	0.9572	0.9784	0.9929	1.046	1.093	1.083
Time	0.0333	0.0666	0.1	0.1333	0.1666	0.2	0.2333	0.2666	0.3	0.3333
Case 5			Air = 2.033 g/sec				Power = 0.55 kW			
S/N	1	2	3	4	5	6	7	8	9	10
Heat (Q)	4896.9	4667.3	4202.8	4378.1	4495	4292.8	4347.9	4183.6	4274.3	4443.1
Mean Heat value (Q)	4418.232	4418.232	4418.232	4418.232	4418.232	4418.232	4418.232	4418.232	4418.232	4418.232
Heat ratio [Q'/Q]	1.108	1.056	0.951	0.990	1.017	0.971	0.984	0.946	0.967	1.005
Time	0.0333	0.0666	0.1	0.1333	0.1666	0.2	0.2333	0.2666	0.3	0.3333
Case 6			Air = 2.44 g/sec				Power = 0.55 kW			
S/N	1	2	3	4	5	6	7	8	9	10
Heat (Q')	4654	4304.1	3663.2	3506.6	3509.8	3430.8	3220.3	3063.1	3261.3	3418.1
Mean Heat value (Q)	3603.1	3603.1	3603.1	3603.1	3603.1	3603.1	3603.1	3603.1	3603.1	3603.1
Heat ratio [Q'/Q]	1.2916	1.1945	1.0166	0.9732	0.974	0.9521	0.8937	0.8501	0.9051	0.9486
Time	0.0333	0.0666	0.1	0.1333	0.1666	0.2	0.2333	0.2666	0.3	0.3333

Table 3. Heat release oscillation for blend

Case 1			Blend = 0.933 g/sec				Power = 0.55 kW			
S/N	1	2	3	4	5	6	7	8	9	10
Heat (Q')	9413.2	11429.7	11368.6	10487.3	8884.9	8630	8825.2	8278.6	7566.3	7381.1
Mean Heat value (Q)	9413.24	9413.24	9413.24	9413.24	9413.24	9413.24	9413.24	9413.24	9413.24	9413.24
Heat ratio [Q'/Q]	1.1983	1.2142	1.2077	1.1141	0.9438	0.9167	0.9375	0.8794	0.8037	0.7841
Time	0.0333	0.0666	0.1	0.1333	0.1666	0.2	0.2333	0.2666	0.3	0.3333
Case 2			Blend = 1.4 g/sec				Power = 0.55 kW			
S/N	1	2	3	4	5	6	7	8	9	10
Heat (Q')	2707.9	2548.7	2309.4	2666.2	2826.7	3127.1	2834.4	2258.8	2929	2973.4
Mean Heat value (Q)	2718.25	2718.25	2718.25	2718.25	2718.25	2718.25	2718.25	2718.25	2718.25	2718.25
Heat ratio [Q'/Q]	0.9962	0.9376	0.8496	0.9808	1.0399	1.1504	1.0427	0.8310	2051.396	1.0939
Time	0.0333	0.0666	0.1	0.1333	0.1666	0.2	0.2333	0.2666	0.3	0.3333
Case 3			Blend = 1.5 g/sec				Power = 0.55 kW			
S/N	1	2	3	4	5	6	7	8	9	10
Heat (Q')	2268.1	1768.6	2126.6	2888.9	2512.7	2220.6	1696.9	1876.9	2051.3	2371.3
Mean Heat value (Q)	2178.22	2178.22	2178.22	2178.22	2178.22	2178.22	2178.22	2178.22	2178.22	2178.22
Heat ratio [Q/Q]	1.0412	0.8119	0.9763	1.326	1.1535	1.0194	0.7790	0.8616	0.9417	1.0886
Time	0.0333	0.0666	0.1	0.1333	0.1666	0.2	0.2333	0.2666	0.3	0.3333
Case 4			Blend = 1.86 g/sec				Power = 0.55 kW			
S/N	1	2	3	4	5	6	7	8	9	10
Heat (Q')	7918.1	7549.2	7533.9	7592.9	7610.8	7779.5	7894	8316.8	8697.3	8612.3
Mean Heat value (Q)	2404.6	2404.6	2404.6	2404.6	2404.6	2404.6	2404.6	2404.6	2404.6	2404.6
Heat ratio [Q'/Q]	1.079	1.0802	1.0028	0.9053	0.8513	1.0015	1.1557	1.0517	0.8806	0.9914
Time	0.0333	0.0666	0.1	0.1333	0.1666	0.2	0.2333	0.2666	0.3	0.3333
Case 5			Blend = 2.33 g/sec				Power = 0.55 kW			

S/N	1	2	3	4	5	6	7	8	9	10
Heat (Q')	2594.8	2597.6	2411.4	2177	2047	2408	2779.2	2529	2117.7	2384.1
Mean Heat value (Q)	2404.6	2404.6	2404.6	2404.6	2404.6	2404.6	2404.6	2404.6	2404.6	2404.6
Heat ratio [Q'/Q]	1.0790	1.0802	1.0028	0.9053	0.8513	1.0015	1.1557	1.0517	0.8806	0.9914
Time	0.0333	0.0666	0.1	0.1333	0.1666	0.2	0.2333	0.2666	0.3	0.3333
Case 6			Blend = 2.83 g/sec				Power = 0.55 kW			
S/N	1	2	3	4	5	6	7	8	9	10
Heat (Q')	11280.3	11429.7	11368.6	10487.3	8884.9	8630	8825.2	8278.6	7566.3	7381.1
Mean Heat value (Q)	9413.24	9413.24	9413.24	9413.24	9413.24	9413.24	9413.27	9413.27	9413.24	9413.24
Heat ratio [Q'/Q]	1.1983	1.2142	1.2077	1.114	0.9438	0.9167	0.9375	0.8794	0.8037	0.7841
Time	0.0333	0.0666	0.1	0.1333	0.1666	0.2	0.2333	0.2666	0.3	0.3333
Case 7			Blend = 3.26 g/sec				Power = 0.55 kW			
S/N	1	2	3	4	5	6	7	8	9	10
Heat (Q')	2007.4	1887	1929.8	2001	1906	1837.2	1924.4	1965.7	2083.4	1967.3
Mean Heat value (Q)	1950.9	1950.9	1950.9	1950.9	1950.9	1950.9	1950.9	1950.9	1950.9	1950.9
Heat ratio [Q'/Q]	1.0289	0.9672	0.9891	1.0256	0.9769	0.9417	0.9864	1.0075	1.0679	1.0084
Time	0.0333	0.0666	0.1	0.1333	0.1666	0.2	0.2333	0.2666	0.3	0.3333
Case 8			Blend = 3.72 g/sec				Power = 0.55 kW			
S/N	1	2	3	4	5	6	7	8	9	10
Heat (Q')	1974.1	2040.8	1979.2	1884.9	1812.9	1997.7	1977.7	2096	1925.6	2026.1
Mean Heat value (Q)	1971.5	1971.5	1971.5	1971.5	1971.5	1971.5	1971.5	1971.5	1971.5	1971.5
Heat ratio [Q'/Q]	1.00131	1.0351	1.0039	0.9560	0.9195	1.0132	1.0031	1.0631	0.9767	1.0276
Time	0.0333	0.0666	0.1	0.1333	0.1666	0.2	0.2333	0.2666	0.3	0.3333

APPENDIX 5

(Published Paper)

Applied Thermal Engineering 122 (2017) 350–358

Contents lists available at ScienceDirect

Applied Thermal Engineering

journal homepage: www.elsevier.com/locate/apthermeng

Research Paper

CO_2-argon-steam oxy-fuel (CARSOXY) combustion for CCS inert gas atmospheres in gas turbines

Ali Al-Doboon [a,b,*], Milana Gutesa [c], Agustin Valera-Medina [a], Nick Syred [a], Jo-Han Ng [d,e,f], Cheng Tung Chong [e]

[a] Cardiff School of Engineering, Queen's Buildings, 14-17 The Parade, Cardiff, Wales CF24 3AA, UK
[b] Basra University, Basra, Iraq
[c] University of Novi Sad, Serbia
[d] Energy Technology Research Group, University of Southampton, UK
[e] UTM Centre for Low Carbon Transport in Cooperation with Imperial College London, Universiti Teknologi Malaysia, 81310 Skudai Johor, Malaysia
[f] University of Southampton Malaysia Campus, 79200 Iskandar Puteri, Malaysia

HIGHLIGHTS

- Integration of CCS system, oxy-fuel combustion in Humidified Gas Turbines.
- Optimum CARSOXY blend proposed for gas turbine combustors.
- CO_2 concentration increased for further capture and NOx eliminated.
- Numerical model successfully used with optimum blend.

ARTICLE INFO

Article history:
Received 12 December 2016
Revised 14 April 2017
Accepted 7 May 2017
Available online 9 May 2017

Keywords:
Inert gases
Gas turbine cycle
Carbon capture and storage
Oxy-fuel combustion

ABSTRACT

CO_2 emitted from gas turbines in power plants is considered a major contributor to the global environmental damage. Carbon Capture and Storage (CCS) integrated with oxy-fuel (OF) combustion is an advanced and innovative approach that may be used in turbines to reduce these emissions. This method is based on CO_2 recycling, however the obstacle to using this recirculation approach in gas turbines is reduction in their performance and reliability.

This paper attempts to address the problem in a novel way by investigating theoretically a number of blends that can overcome the performance and reliability issues of pure CO_2. These blends, comprising of argon, H_2O and CO_2, can be used as a working fluid with oxygen and methane as reactants. Additionally, a numerical model for an industrial gas turbine is employed. The aim is to find the optimum blend for complete NO_x elimination with a recirculation of products. This study uses 0-D chemical kinetic software (Gaseq), an empirical selection approach with design of experiments and, 1-D chemical kinetic software (CHEMKIN-PRO).

Results identify the optimum blend which is numerically assessed in an industrial gas turbine that has been experimentally correlated. The efficiency of this turbine running the selected blend is 1.75–13.93% higher than when running with natural gas/air conditions. This shows the promising use of this blend for a future high efficiency CCS-Oxyfuel approach in gas turbine combustors.

1. Introduction

Increasing demand for energy production from fossil fuel-fired electrical plants significantly raises anthropogenic emissions of CO_2, with its inherent consequences for climate change [1]. The dependency on gas turbines in the power sector has been vastly increasing because of their versatility in covering a wide range of energy load demands [2]. In gas-turbine combustors, different advanced technologies have been investigated to mitigate CO_2 emissions and other pollutants to maintain a clean environment [3].

Carbon Capture and Storage (CCS) has been proposed as one of the most innovative technologies utilised to mitigate emitted CO_2

* Corresponding author at: Cardiff School of Engineering, Cardiff University, CF24 3AA, Basra University, Basra, Iraq.
E-mail address: Al-DoboonAl@cardiff.ac.uk (A. Al-Doboon).

http://dx.doi.org/10.1016/j.applthermaleng.2017.05.032
1359-4311/

Nomenclature

G_i^o	molar free energy at the atmospheric pressure of species *i* [J/mole]
x_i	equilibrium number of moles of species i
G	Gibbs free energy [J]
nSp	species n
p	pressure [Pa]
T	temperature [K]
R	universal gas constant [J/mole K]
c_p	specific heat at constant pressure [kJ/kg K]
h_{fuel}	specific enthalpy of fuel at combustion chamber inlet [kJ/kg]
L_T	gas turbine specific work [kJ/kg]
L_c	specific work of compression [kJ/kg]
LHV	lower heating value [kJ/kg]
T_0	ambient temperature [K]
T_1	inlet compressor temperature [K]
r_{air}	cooling air mass flow and compressor inlet mass flow ratio
ϕ	equivalence ratio [–]
η_{CC}	efficiency of a combustion chamber
η_{pC}	polytropic efficiency of a compressor
η_{pT}	polytropic efficiency of a turbine
η_m	mechanical efficiency
Π_C	compressor pressure ratio
Π_T	turbine pressure ratio
M	cooling air distribution factor
q_{in}	amount of input heat [kJ/kg]
$\bar{c}p_{gas-air(3-4)}$	averaged value of gas specific heat through the expansion [kJ/kg K]
$\bar{c}p_{air(1-2)}$	averaged value of air specific heat through the compression [kJ/kg K]
T_2	outlet compressor temperature [K]
T_{3t}	inlet turbine temperature [K]
η_{GT}	gas turbine plant efficiency

from fossil-fueled power generation stations [4]. Basically, CCS is an approach through which CO_2 is captured from large industrial sources, such as gas turbines in power plants, and deposited securely into safe locations, such as subterranean sites, to protect the global environment [5]. Oxyfuel (OF) combustion is a promising technique which can be combined with CCS to enhance the combustion efficiency for the power cycle [6]. This technique involves burning hydrocarbon in a highly-diluted atmosphere at near-stoichiometric conditions, leading to high chamber temperatures. Consequently, a portion of the CO_2 from the flue gas is employed in a recirculation process to control combustor temperature. The remaining CO_2 can be treated for further applications [7].

A drawback of the recirculation of CO_2 in gas-turbine combustors is a reduction in both overall efficiency and generated output power [8]. Practically, the cycle performance can be improved by about 15% through employing a humidified working fluid in a combustor [9]. In Humid Air Turbines (HAT), the efficiency and output power are enhanced by humidifying the compressed air [10]. The Evaporative Gas Turbines (EvGt) cycle, representing one of the configurations of the HAT cycles, was integrated with oxyfuel combustion. The aim was to improve the performance of the cycle while reducing emitted NO_x, in comparison with a combined cycle [11]. However, this enhancement in turbine performance is limited because water injection into a combustion process increases blowout propensity. This can lead to a shutdown of the system [12].

To avoid this issue, it is proposed in this study to add another gas with CO_2-H_2O mixture in a gas combustor using an EvGt cycle. This should enhance the efficiency by improving thermodynamic properties of the working fluid such as, specific heat ratio (γ). Thus, equivalent power and efficiency to that of a conventional cycle should be produced.

Moreover, a novel approach is suggested in this paper to use a combination of concepts which not only integrate CCS technologies with oxyfuel combustion and EvGT cycle, but also add to the working fluid inert gases (i.e. Argon) to the mixture of CO_2 and water, thus improving the thermodynamic properties of such a blend. The aim of this investigation is to find the optimum gas blend that can replace air as a working fluid. Argon is used in these blends due to its higher specific heat ratio and because of its relatively high concentration in the atmosphere. Thus, gas turbines using the suggested blend could produce higher efficiency than that of a conventional air cycle. The blend of Argon-CO_2-H_2O in a pure domain of oxygen heightens the improvement in the cycle efficiency and reduces flame blowout. Meanwhile, a CO_2 recirculation approach can be utilised in gas turbines to maintain a clean environment.

This paper theoretically investigates a considerable number of Co_2, ARgon and Steam with OXYfuel combustion (CARSOXY) blends. The goal is to discover the blend that has similar thermodynamic properties to air while recycling CO_2 and emitting zero NO_x. The proposed cycle for this technology is depicted in Fig. 1. A mathematical program is used to calculate the generated output power and the efficiency of an industrial gas turbine running the optimum blend with oxygen and methane, compared with Natural Gas (NG)/air.

2. Setup

The investigation process included four steps used to detect the optimum blend that has similar thermodynamic characteristics to air as a working fluid. This optimum blend can be used in a combustion process for gas turbines to generate equivalent power to that of current cycles while reducing emissions and pollutants.

This process was started using a 0-D chemical kinetic software (Gaseq). This program is based on a method of complex balance at specified pressure, which was defined by Sanford Gordon and Bonnie J. McBridge for NASA [13]. Eq. (1) shows the Gibbs free energy equation for n species which is used to calculate the products:

$$\frac{G}{RT} = \sum_{i=1}^{nSp}\left(\frac{x_i G_i^o}{RT} + x_i \ln\frac{x_i}{\sum x_i} + x_i \ln p\right) \quad (1)$$

First, Gaseq was utilised to generate 120 blends of argon, H_2O and CO_2 in an oxygen atmosphere with methane as a fuel at 10 bar and 900 K, which may be considered to be industrial operation conditions. Simultaneously, the properties of the products for each blend, such as outlet temperature, γ and heat capacity (c_p), were calculated. Moreover, the mole fractions were determined for both CO_2 and water vapor as products. An adiabatic process was considered for the combustion chamber. Each blend was represented by its number and an acronym (X. Y. and Z) in which "X" stands for the molar fraction of argon, "Y" for H_2O and "Z" for CO_2. The remaining fractions were used for oxygen and methane at a range of equivalence ratios which is between 0.67–1.00.

Second, empirical data obtained from the Gaseq program was used to compare each blend with a reference, which was a conven-

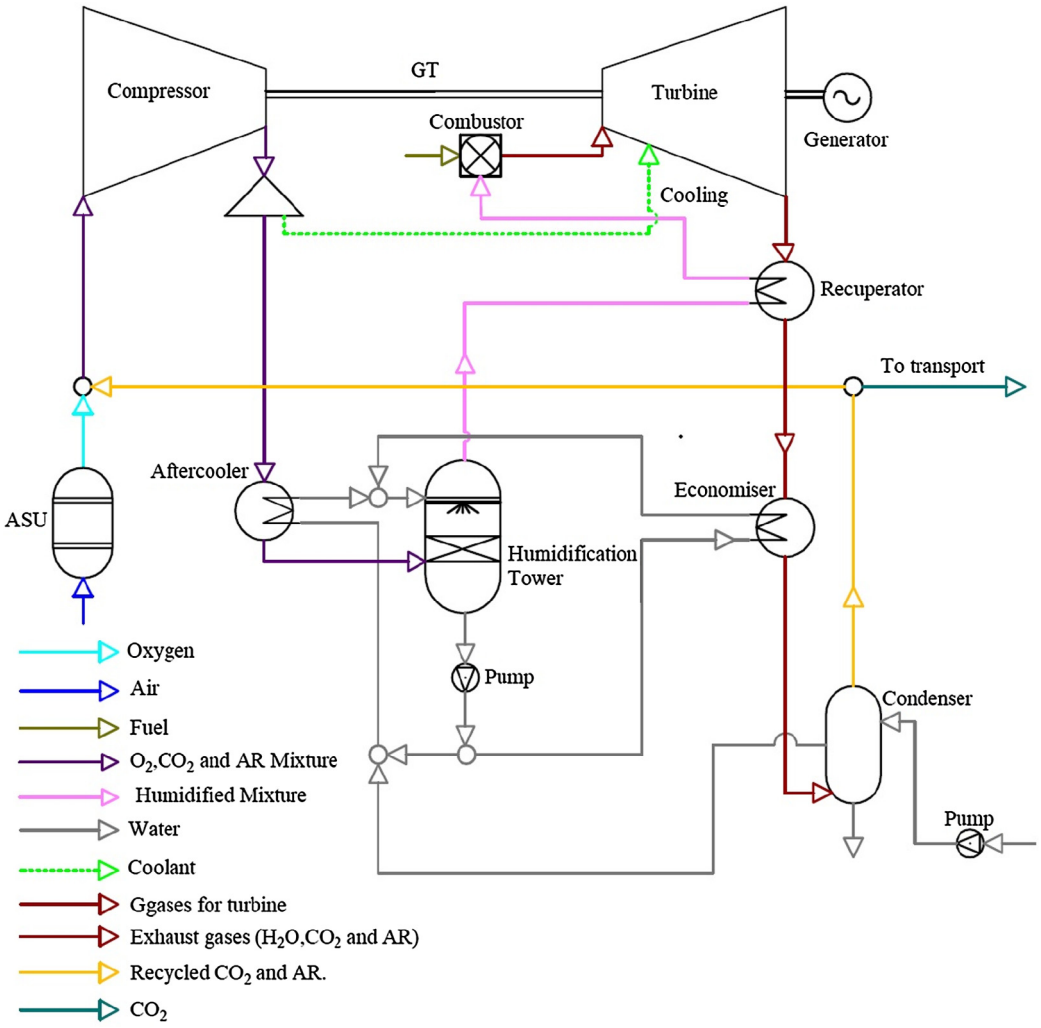

Fig. 1. Schematic diagram of the proposed cycle.

tional air-fuel mixture. Through this process, four equivalent intervals were used to divide between the greatest and the smallest value for each property of these blends. Every interval with a value higher than the reference was signed (+), whereas (−) identified those lower than the reference.

At this stage, a Design of Experiment (DOE) was devised to provide a minimal number of experimental layouts. Minitab software was employed as a tool for DOE, by applying a two-level full factorial design due to the number of inputs. Therefore, there were eight combinations of these blends' components, showing the correlation between them and their products. As such, reliable conclusions can be proposed through matrices obtained by following this systematic procedure [14]. At the same time, the expense and effort of traditional experiments can be saved. Numerically, the DOE approach was implemented for quantifying the individual and interactive effects between the blends' components, represented by argon, H_2O and CO_2 against both the products' properties and the mole fractions for both CO_2 and H_2O calculated by the Gaseq program, according to the design of the experimental matrix.

The final inspection in this procedure was to employ the CHEMKIN-PRO program, applying the GRI-Mech 3.0 chemical kinetics reaction mechanism, to give reliable results by providing different critical species for the one-dimensional combustor model [15]. This model was used to determine flame characteristics for the final selected blends in a combustion process of a gas turbine. These mixtures were simulated through two clusters. The first cluster is called the Perfectly Stirred Reactor (PSR), consisting of the following three distinct zones: a mixing zone in which fuel is partially premixed, a flame region connecting directly to the previous zone, and the Central Recirculation Zone (CRZ), where the products of the combustion process are recirculated. The second cluster uses a Plug Flow Reactor (PFR) for post-flame operation along a 0.1 m duct.

3. Results and discussion

3.1. 0-D Chemical reaction analysis

The thermodynamic properties were calculated for each blend using the Gaseq program. In addition, a conventional methane-air mixture was used as a reference. These properties for products, including temperature, γ, c_p, with H_2O and CO_2 as products, were selected for blends against a range of equivalence ratios, as shown in the following Figs. 2 and 3.

The outlet temperatures for blend 58 (25-23-19) almost matched those obtained for the methane-air mixture, as shown in Fig. 2(a). In addition, other blends are either higher at around 100 degrees – blend 79 (24-19-19) and blend 109 (24-8-29) – or

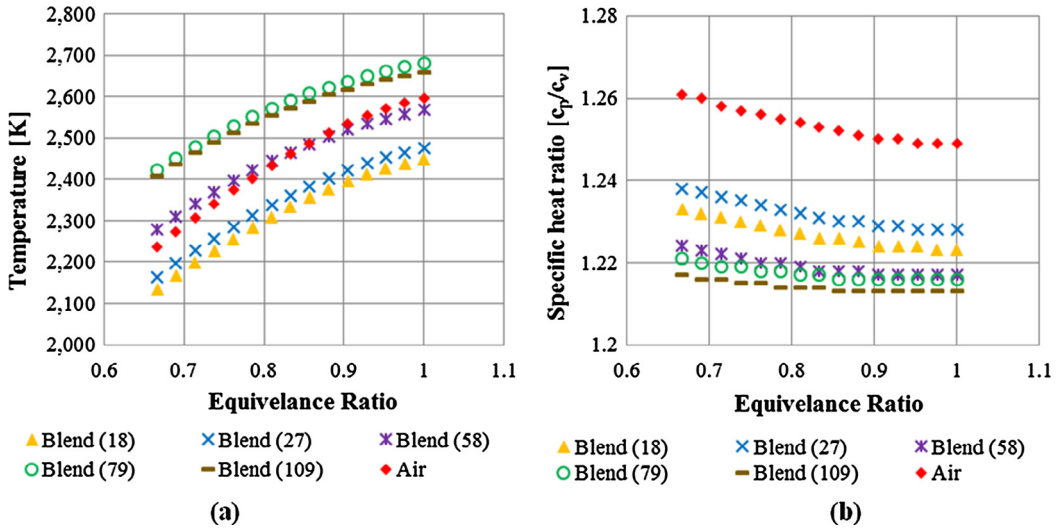

Fig. 2. Products of temperature and specific heat ratio for blends compared to air.

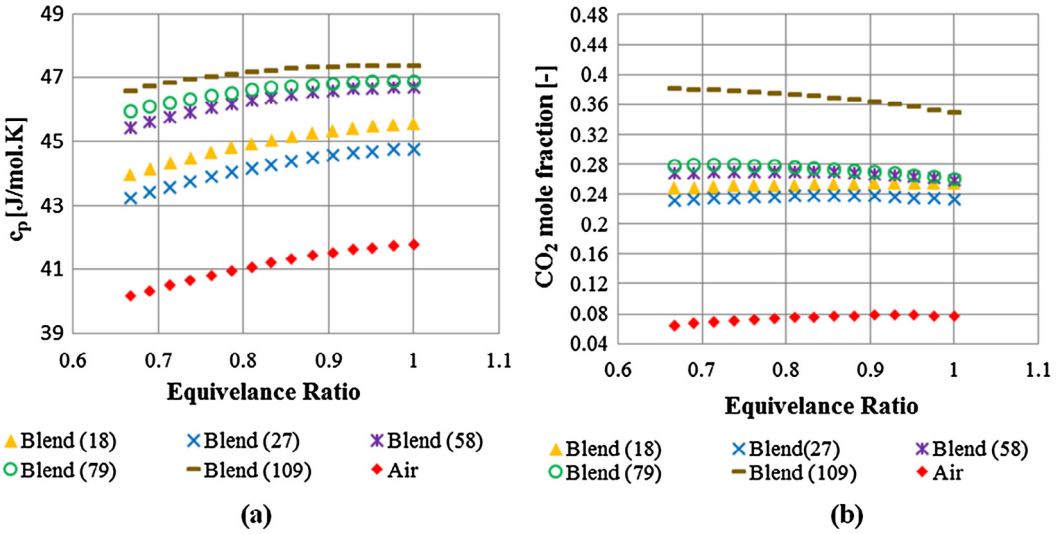

Fig. 3. Products of heat capacity and CO_2 for blends compared to air.

lower with an approximately similar range to the reference. Regarding specific heat ratio, the results indicate that this property is only about 2–4% below that obtained from air. Blend 58 (25-23-19) is nearly in the middle of this group, as shown in Fig. 2(b).

Moreover, heat capacity increases for all mixtures in comparison with air as a working fluid, as shown in Fig. 3(a), enhancing power output generation. Additionally, Fig. 3(b) indicates that the concentration of CO_2 products rises by around 40% compared with air. These mole fractions might enable mitigation of a portion of CO_2 emissions by condensing the water in the exhaust gas. The remainder of the CO_2 and inert gas in the exhaust would have to be recirculated in the OF combustion process.

The matrix shown in Table 1 was created using empirical data utilising results obtained from the Gaseq program. In this matrix, each thermodynamic property and the mole fraction of products for all of the generated blends were compared with their equivalent produced from the methane-air mixture used as a reference. As such, the eight blends tabulated represent the optimum blends out of all 120 cases. In the following Table 1, column 1 represents the blend's number, columns 2–4 indicate sequentially the mole fractions of Ar, H_2O and CO_2 while columns 5–7 represent the thermodynamic properties for these blends and the last two columns, 8 and 9, signify the mole fractions for both water and CO_2 products.

3.2. DOE analysis

Data provided by the DOE method shows whether thermodynamic properties with H_2O and CO_2 products were either affected positively or negatively by individual or interacting blend components. As illustrated in Fig. 4(a), outlet temperature responds inversely towards Ar, H_2O and CO_2. Fig. 4(b) illustrates that increased Ar correlates with increased specific heat ratio value, producing higher efficiency, while this property reacts inversely with both H_2O and CO_2.

3.3. Combustion characteristics

The Chemkin-PRO program initially tested the eight tabulated blends at 288 K with atmospheric pressure and equivalence ratio = 1. The flame characteristics of these mixtures were then simulated at industrial conditions similar to those of a gas turbine combustor, i.e. 10^6 Pa. Subsequently, a comparison was made for

Table 1
The optimum selected blends, using empirical data.

Blend	Ar [Mole fraction]	H_2O [Mole fraction]	CO_2 [Mole fraction]	T (K)	c_p [J/mole K]	Gamma [c_p/c_v]	H_2O [Mole fraction]	CO_2 [Mole fraction]
Air				2596.4	41.766	1.249	0.177	0.076
6	0.271	0.271	0.171	–	++	– –	+++	++
18	0.287	0.251	0.179	–	+	– –	+++	++
26	0.343	0.231	0.154	–	+	–	+++	+
27	0.307	0.244	0.162	–	+	–	+++	++
33	0.292	0.237	0.182	–	+	– –	+++	++
58	0.251	0.230	0.188	0	++	– –	+++	++
79	0.239	0.191	0.191	+	++	– –	+++	++
109	0.242	0.084	0.290	0	++	– –	++	+++

0: Same as reference; +: Greater than reference; ++: Considerably greater than reference; +++: Far greater than reference; –: Lower than reference; – –: Considerably lower than reference; – – –: Far lower than reference.

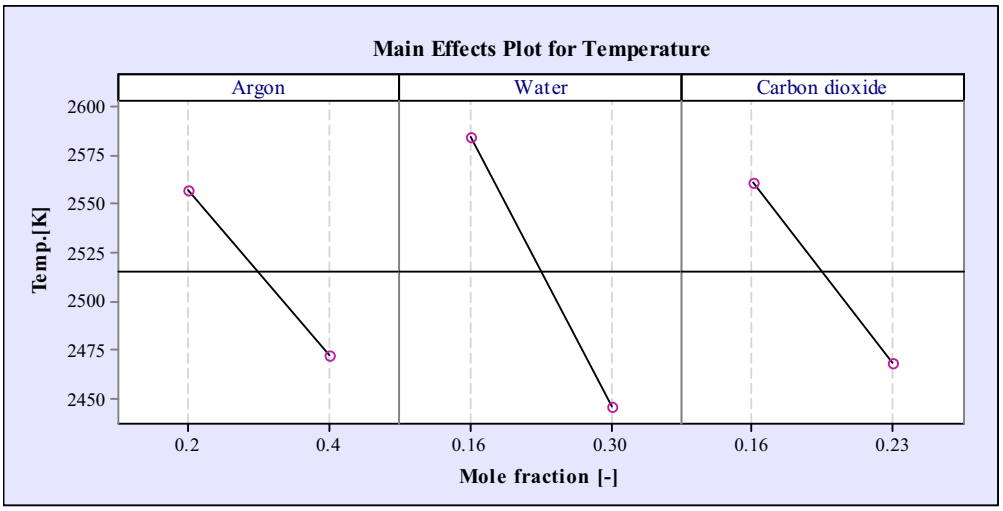

(a)

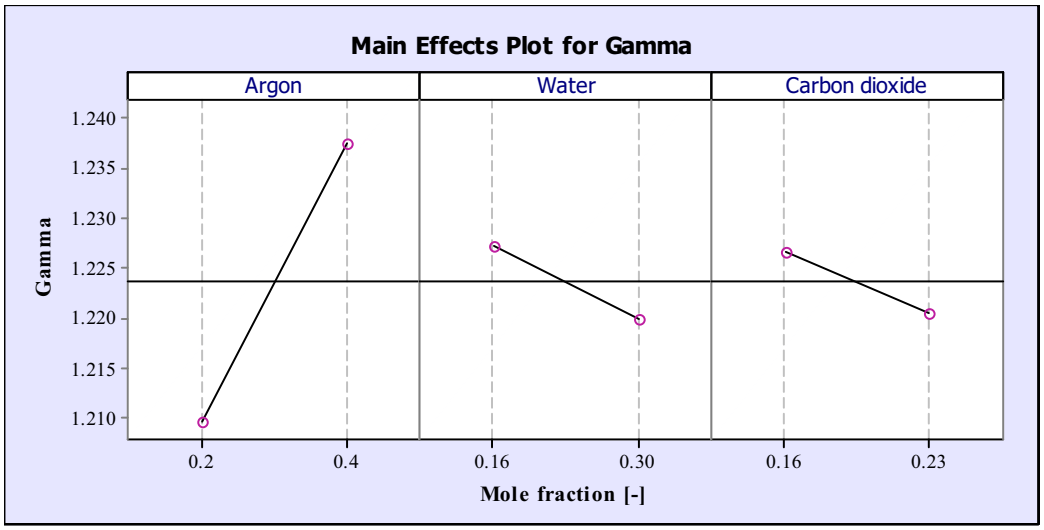

(b)

Fig. 4. Temperature and specific heat ratio response towards Ar, H_2O and CO_2.

the eight flame values against the one obtained from the reference under the equivalent running conditions, for further investigations of those that have flame speeds close to the reference, as shown in Table 2.

Out of the eight blends, the chosen blends for further analysis were 58 (25-23-19), 79 (24-19-19), and 109 (24-8-29). Blend 27 (30-24-16) was also investigated, although its flame speed descends to around half the reference value. These four mixtures were compared according to characteristics obtained from the 1-D simulation approach in both the PSR and PFR clusters. Fig. 5(a) shows that the temperatures of blend 58 (25-23-19) are approximately equivalent to those produced by the current air cycle. Moreover,

Table 2
Flame speed for selected blends with methane at 10^5 and 10^6 Pa, and $\phi = 1$.

Pressure condition (Pa)	Flame speed (m/s)								
	Pure methane	8 Optimum blends							
		27	58	79	109	33	26	18	6
10^5	0.431	0.218	0.312	0.453	0.384	0.217	0.203	0.201	0.204
10^6	0.151	0.797	0.127	0.212	0.178	0.723	0.640	0.650	0.676

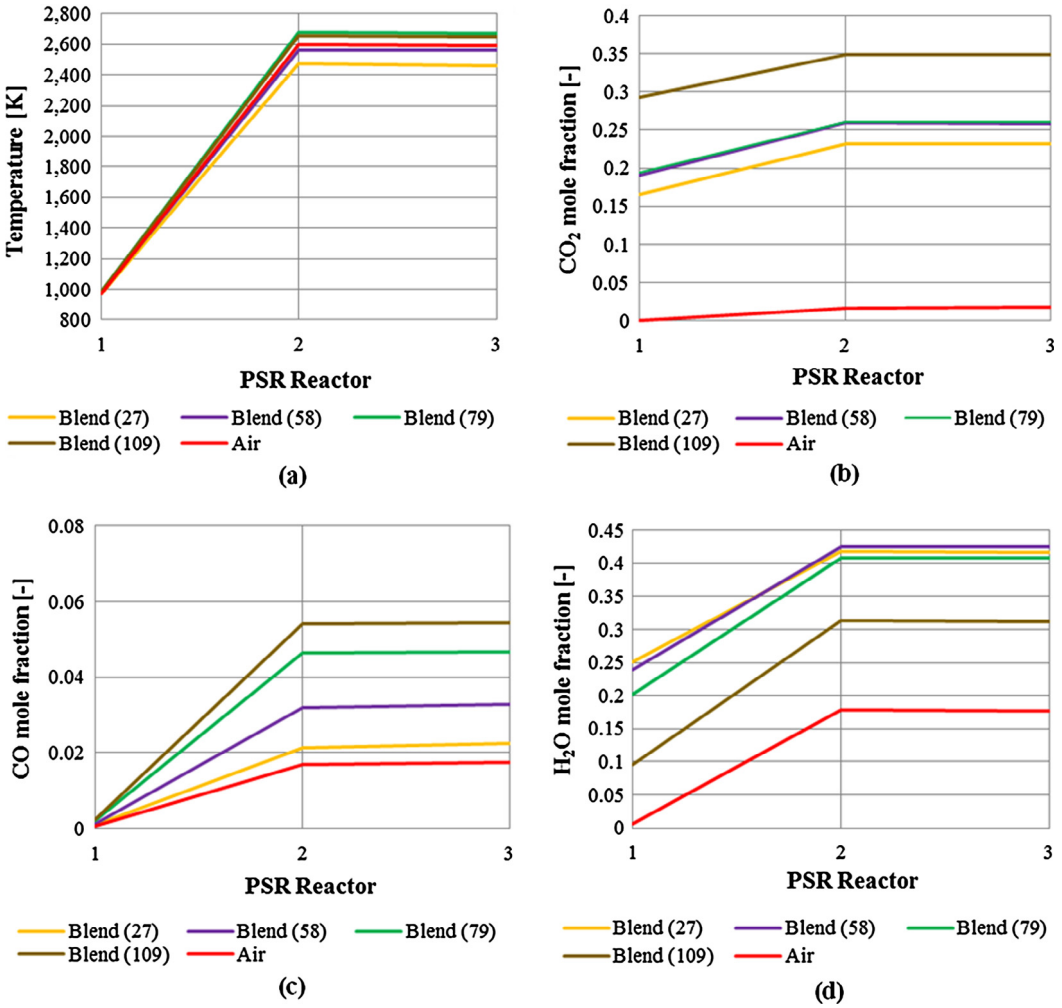

Fig. 5. Temperature and mole fractions of CO_2, CO and H_2O in a PSR.

CO_2 concentration is elevated in the exhaust gas for this blend with the highest mole fractions of water vapor, for the recovery process and about 1.5 times more CO than conventional fuel as shown in Fig. 5(b) –(d).

Downstream of the reaction zone, the concentration of water remains high, resulting in a drop of ~40 K for the temperature of the exhaust gas for blend 58 (25-23-19), as shown in Fig. 6 (a) and (b). This figure also demonstrates that a blend, such as 27 (30-24-16), can still have acceptable product values under the combustion process. However, the considerable fall in the flame speed to 0.79 m/s leads to a higher propensity for blowoff. As such, a definition of the optimum CARSOXY blend requires a deep knowledge of its thermodynamic properties in a combustor and a comprehensive understanding of its flame and combustion characteristics. Thus, further research is required to demonstrate that the optimum blend, 58 (25-23-19), can be used under real gas turbine operating conditions.

4. Industrial gas turbine model for comparison

A simulation model was proposed for calculating the performance of a 3.9 MW Rolls-Royce Allison 501-KB5 industrial gas turbine. This model was used to calculate the generated power and the efficiency working with NG/air. Then, the results were correlated to those obtained from a real turbine running at equivalent fuel-air mixture under design (100% load) and off – design (90–10%) operating regimes [16]. This model for the gas turbine was utilised for comparing the optimum CARSOXY blend with oxygen/methane as reactants to NG/air running under stoichiometric working conditions.

In this numerical model, Eq. (2) was used to calculate the specific compression work. Then, the outlet temperature for the compressed air was determined by employing Eq. (3). After that, the heat capacity was ascertained from Eq. (4). Next, b, which represents the fuel/air mass flow rate ratio, was determined from Eq.

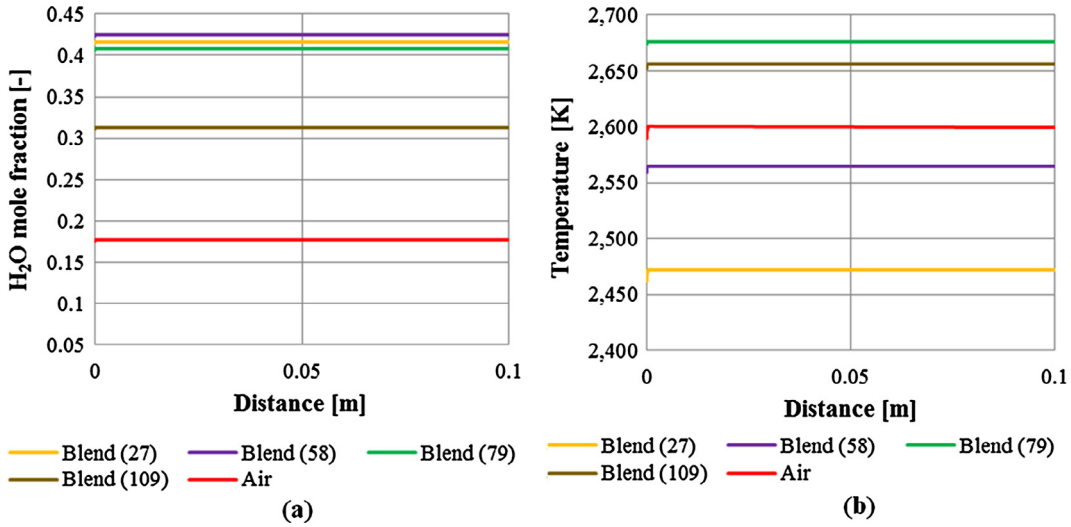

Fig. 6. Mole fraction of H_2O and temperature in a PFR.

(5). Following that, Eq. (6) was utilised for calculating the specific work for the industrial turbine. Finally, both heat supplied and the efficiency of the gas turbine were sequentially determined using Eqs. (7) and (8).

$$L_c = \bar{c}_{p_{air(1-2)}} \cdot T_1 \left(\Pi_C^{\frac{1}{\eta_{pc}} \frac{R_{air}}{\bar{c}_{p_{air(1-2)}}}} - 1 \right) \tag{2}$$

$$T_2 = T_1 \cdot \Pi_C^{\frac{1}{\eta_{pc}} \frac{R_{air}}{\bar{c}_{p_{air(1-2)}}}} \tag{3}$$

$$\frac{c_p(T)}{R} = \sum_{K=1}^{12} C_k \cdot \left(\frac{T}{1000} \right)^{k-6} \tag{4}$$

$$b = \frac{\dot{m}_{fuel}}{\dot{m}_2} = \frac{\bar{c}_{p_{gas(0-3)}} \cdot (T_{3t} - T_0) - \bar{c}_{p_{air(0-2)}} \cdot (T_{2t} - T_0)}{\eta_{CC} \cdot (LHV + h_{fuel}) - \bar{c}_{p_{gas(0-3)}} \cdot (T_{3t} - T_0)} \tag{5}$$

$$L_T = \bar{c}_{p_{gas-air(3-4)}} \cdot \frac{(1 - r_{air}) \cdot (1 + b) \cdot T_3 + r_{air} \cdot M \cdot T_2}{(1 - r_{air}) \cdot (1 + b) + r_{air}} \cdot \left(1 - \Pi_T^{\eta_{pT} \cdot \frac{R_{gas-air(3-4)}}{\bar{c}_{p_{gas-air(3-4)}}}} \right) \tag{6}$$

$$q_{in} = \frac{1}{\eta_{CC}} \cdot (1 - r_{air}) \times \left[(1 + b) \cdot \bar{c}_{p_{gas-air(0-2)}} \cdot (T_{3t} - T_0) - \bar{c}_{p_{air(0-2)}} \cdot (T_{2t} - T_0) - b \cdot h_{fuel} \right] \tag{7}$$

$$\eta_{GT} = \frac{L_T \cdot \eta_m - L_C}{q_{in}} \tag{8}$$

5. Numerical results

The results show that the relative error for the power calculated by the mathematical model and the value of the real turbine was 0.22% while the relative error for the efficiency was 0.07%. Thus, the curves of these parameters approximately match, as shown in Fig. 7(a) and (b).

The numerical model was employed to test the performance of the same turbine running on blend 58 (25-23-19) with oxygen and methane as reactants. Then, NG/air results running in the same turbine were compared to those obtained from the blend. Both cases used stoichiometric conditions in each of the seven different cases presented in Fig. 8.

The specific output power produced by the 3.9 MW Rolls-Royce turbine working running the 58 CARSOXY blend is 219–244 kWe

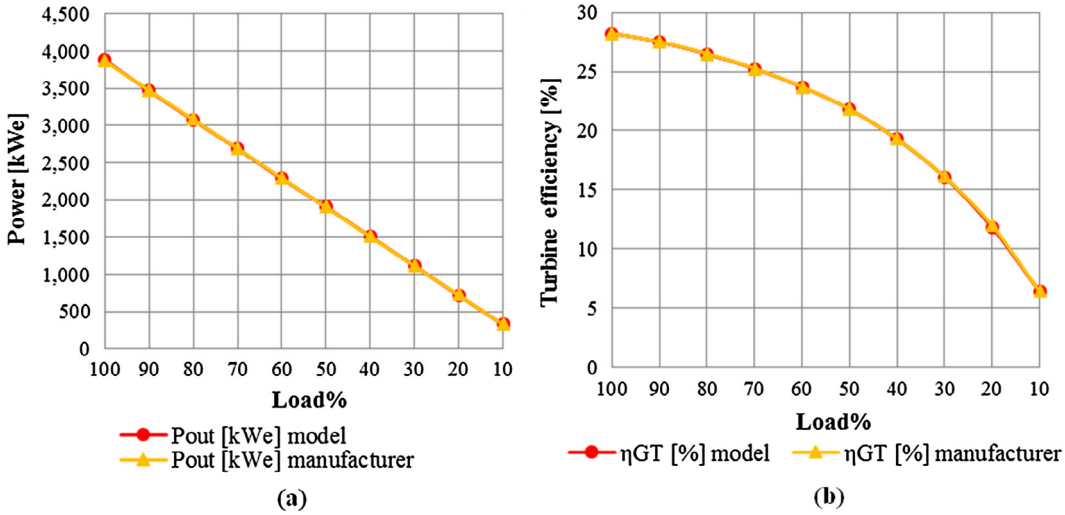

Fig. 7. Validation of power produced and efficiency.

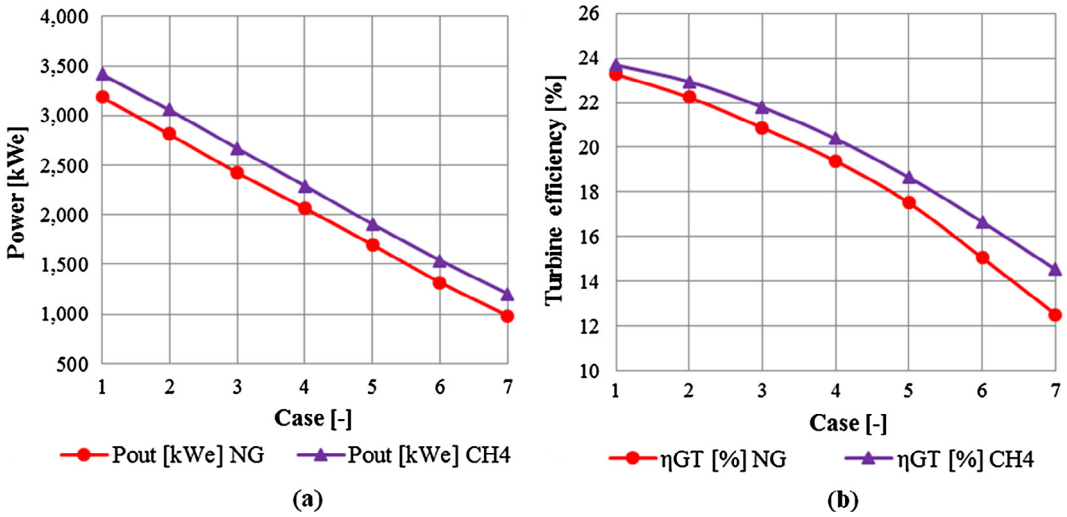

Fig. 8. The power produced and efficiency of the gas turbine working with CARSOXY blend for different mass flow rate cases compared to similar conditions for NG/air.

higher than the values obtained using NG/air, as shown in Fig. 8(a). Moreover, the efficiency of this industrial turbine working with CARSOXY is 1.75%–13.93% higher than that produced by NG/air. This comparison with NG/air as a working fluid is shown in Fig. 8(b).

6. Conclusion

This paper proposes a novel investigation for a combination of concepts, which were CCS technology integrated with oxy-fuel combustion and utilising steam with inert gas injections. The aim was to find an optimum CARSOXY blend that can be used instead of air as a working fluid. A mixture, consisting of 25%Ar-23%H_2O-19%CO_2, has almost equivalent thermodynamic properties and flame speeds to air which was used as a reference.

As a result, the optimum blend could replace air in a combustion process in the EvGT cycles. Using CARSOXY blend 58 has improved outlet temperature and specific heat ratio, which leads to generating higher output power and efficiency than that of a conventional air cycle. The specific output power produced by the industrial Rolls-Royce gas turbine running blend 58 with methane and oxygen as reactant is between 219–244 kWe higher than that produced by NG/air. The efficiency of the turbine has also been improved by 1.75–13.93% using the optimum blend in comparison with NG/air as working fluid.

Additionally, this optimum CARSOXY blend has potential for producing efficient and powerful CCS-Oxyfuel combustion in gas turbines to maintain a clean environment. Employing this blend in gas combustors also mitigates emissions by recirculating CO_2 products in a combustion process and eliminates NO_x, since N_2 is not used.

Recommendations

Future work is recommended to employ a diffusive injection method to test the CARSOXY blend since no premixed combustion is needed. This experimental work could be carried out to ascertain the combustion characteristics of the optimum blend under actual operation conditions.

Acknowledgments

Ali Al-Doboon would like to express his gratitude to the Ministry of Higher Education and Scientific Research represented by the Iraqi cultural attaché in London for supporting his PhD in this field.

References

[1] C.-C. Cormos, Evaluation of reactive absorption and adsorption systems for post-combustion CO_2 capture applied to iron and steel industry, Appl. Therm. Eng. 105 (2016) 56–64, http://dx.doi.org/10.1016/j.applthermaleng.2016.05.149.
[2] G. Kim, Y.D. Lee, C.H. Sohn, K.W. Choi, H.S. Kim, Experimental investigation on combustion and emission characteristics of a premixed flame in a gas-turbine combustor with a vortex generator, Appl. Therm. Eng. 77 (2015) 57–64, http://dx.doi.org/10.1016/j.applthermaleng.2014.11.073.
[3] H. Li, M. Ditaranto, D. Berstad, Technologies for increasing CO_2 concentration in exhaust gas from natural gas-fired power production with post-combustion, amine-based CO_2 capture, Energy 36 (2) (2011) 1124–1133, http://dx.doi.org/10.1016/j.energy.2010.11.037.
[4] R. Canepa, M. Wang, Techno-economic analysis of a CO_2 capture plant integrated with a commercial scale combined cycle gas turbine (CCGT) power plant, Appl. Therm. Eng. 74 (2015) 10–19, http://dx.doi.org/10.1016/j.applthermaleng.2014.01.014.
[5] H. Saboori, R. Hemmati, Considering carbon capture and storage in electricity generation expansion planning, IEEE Transact. Sustain. Energy 7 (4) (2016) 1371–1378, http://dx.doi.org/10.1109/TSTE.2016.2547911.
[6] G. Krieger, A. Campos, M. Takehara, F.A. Da Cunha, C.G. Veras, Numerical simulation of oxy-fuel combustion for gas turbine applications, Appl. Therm. Eng. 78 (2015) 471–481, http://dx.doi.org/10.1016/j.applthermaleng.2015.01.001.
[7] F.C. Barba, G.M.-D. Sánchez, B.S. Seguí, H.G. Darabkhani, E.J. Anthony, A technical evaluation, performance analysis and risk assessment of multiple novel oxy-turbine power cycles with complete CO_2 capture, J. Clean. Prod. 133 (2016) 971–985, http://dx.doi.org/10.1016/j.jclepro.2016.05.189.
[8] W. De Paepe, M.M. Carrero, S. Giorgetti, A. Parente, S. Bram, F. Contino, Exhaust Gas Recirculation on Humidified Flexible Micro Gas Turbines for Carbon Capture Applications, in ASME Turbo Expo, 2016: Turbomachinery Technical Conference and Exposition. American Society of Mechanical Engineers, 2016.
[9] H.K. Kayadelen, Y. Ust, Prediction of equilibrium products and thermodynamic properties in H_2O injected combustion for CαHβOγNδ type fuels, Fuel 113 (2013) 389–401, http://dx.doi.org/10.1016/j.fuel.2013.05.095.
[10] Y. Hui, Y. Wang, S. Weng, Experimental investigation of pressurized packing saturator for humid air turbine cycle, Appl. Therm. Eng. 62 (2) (2014) 513–519, http://dx.doi.org/10.1016/j.applthermaleng.2013.09.050.
[11] Y. Hu, H. Li, J. Yan, Integration of evaporative gas turbine with oxy-fuel combustion for carbon dioxide capture, Int. J. Green Energy 7 (6) (2010) 615–663, http://dx.doi.org/10.1080/15435075.2010.529405.
[12] K. Göckeler, O. Krüger, C.O. Paschereit, Laminar burning velocities and emissions of hydrogen–methane–air–steam mixtures, J. Eng. Gas Turbines Power 137 (3) (2015) 031503, http://dx.doi.org/10.1115/1.4028460.

[13] C. Morley, Gaseq: A Chemical Equilibrium Program for Windows, version 0.79, 2010. Available at: <http://www.c.morley.dsl.pipex.com/>.
[14] M. Inc. Getting Started with Minitab 17, 2014. Available at: <http://www.minitab.com/uploadefiles/documents/getting-started/Minitab17_Getting started-en.pdf>.
[15] R. CHEMKIN-PRO. 15112, Reaction Design, 2011. Available at: <http://www.ems.psu.edu/~radovic/ChemKin_Tutorial_2-3-7.pdf>.
[16] G. Milana, The Numerical Simulation of Gas Turbine Facility for Biomass Gasification Gas Application (Ph.D. thesis), University of Novi Sad, Serbia, 2016.